UNIVERSIDADE FEDERAL DO RIO DE JANEIRO

CENTRO DE CIÊNCIAS DA SAÚDE

PROGRAMA DE PÓS-GRADUAÇÃO EM BIOTECNOLOGIA VEGETAL E BIOPROCESSOS

TARCISIO NASCIMENTO CORREA

NANOTECNOLOGIA SUSTENTÁVEL: SIMULAÇÃO DE BIOPROCESSO E ANÁLISE ECONÔMICA DA PRODUÇÃO DE MAGNETOSSOMOS EM ESCALA INDUSTRIAL E DESENVOLVIMENTO DE FERRAMENTA PARA TRATAMENTO DE EFLUENTES

RIO DE JANEIRO

2021

Tarcísio Nascimento Correa

NANOTECNOLOGIA SUSTENTÁVEL: SIMULAÇÃO DE BIOPROCESSO E ANÁLISE ECONÔMICA DA PRODUÇÃO DE MAGNETOSSOMOS EM ESCALA INDUSTRIAL E DESENVOLVIMENTO DE FERRAMENTA PARA TRATAMENTO DE EFLUENTES

Tese de Doutorado apresentada ao Programa de Pós-graduação em Biotecnologia Vegetal e Bioprocessos da Universidade Federal do Rio de Janeiro - UFRJ, como parte dos requisitos necessários à obtenção do título de Doutor em Biotecnologia Vegetal e Bioprocessos.

Orientadora: Fernanda de Ávila Abreu

Rio de Janeiro

2021

CIP - Catalogação na Publicação

CC824n

Correa, Tarcisio Nascimento
Nanotecnologia Sustentável: Simulação de bioprocesso e análise econômica da produção de magnetossomos em escala industrial e desenvolvimento de ferramenta para tratamento de efluentes / Tarcisio Nascimento Correa. -- Rio de Janeiro, 2021.
210 f.

Orientadora: Fernanda de Ávila Abreu.
Tese (doutorado) - Universidade Federal do Rio de Janeiro, Decania do Centro de Ciências da Saude, Programa de Pós-Graduação em Biotecnologia Vegetal, 2021.

1. bactérias magnetotáticas. 2. magnetossomos. 3. nanopartículas magnéticas. 4. avaliação técnico econômica. 5. produção limpa. I. Abreu, Fernanda de Ávila, orient. II. Título.

Elaborado pelo Sistema de Geração Automática da UFRJ com os dados fornecidos pelo(a) autor(a), sob a responsabilidade de Miguel Romeu Amorim Neto - CRB-7/6283.

Universidade Federal do Rio de Janeiro
Centro de Ciências da Saúde

Coordenação de Pós-Graduação em Biotecnologia Vegetal e Bioprocessos

ATA DO EXAME DE DEFESA DE TESE DE DOUTORADO DE TARCÍSIO NASCIMENTO CORREA, COMO PARTE DOS REQUISITOS NECESSÁRIOS À OBTENÇÃO DO GRAU DE DOUTOR EM CIÊNCIAS (BIOTECNOLOGIA VEGETAL E BIOPROCESSOS).

Aos vinte e um dias do mês de setembro do ano de dois mil e vinte e um, às 09 horas, reuniu-se via videoconferência, a Banca Examinadora abaixo discriminada, para avaliação da Tese de Doutorado do aluno **Tarcísio Nascimento Correa**, intitulada*:* "Nanotecnologia Sustentável: simulação de bioprocesso e análise econômica da produção de magnetossomos em escala industrial e desenvolvimento de ferramenta para tratamento de efluentes" desenvolvida sob a orientação da **Profª. Fernanda de Ávila Abreu.** A apresentação feita pelo candidato foi acompanhada da arguição pelos componentes da Banca. Em seguida, esta se reuniu para sua avaliação e a tese foi (**A**) (inserir letra apropriada).

A) Aprovado;
B) Aprovado com pequenas modificações* a serem combinadas com o Presidente da Banca dentro de um mês;
C) Não aprovado ainda, é necessária a apresentação das modificações/correções* em uma nova versão do documento para o Presidente da Banca e uma carta do Presidente com prazo de máximo 3 meses para ser aprovada; se não reprovada
D) Não aprovado ainda, é necessária uma nova apresentação*, oral e escrita, para a mesma ou nova banca examinadora dentro de um prazo combinado com a comissão do Programa.
E) Reprovado, razões da reprovação* escritas no espaço destinado.

*As modificações/correções/razões para reprovação precisam ser discriminadas e o Presidente da Banca e o(a) aluno(a) precisam estar cientes.

E, para constar, foi lavrada a presente ata que vai devidamente assinada pelo coordenador, pelos membros da Comissão Examinadora e pela orientadora do aluno. O aluno deve ficar com uma cópia da ata e a outra deve ser entregue para a secretaria do PBV pelo Presidente da Banca.

Rio de Janeiro, 21 de setembro de 2021.

Universidade Federal do Rio de Janeiro
Centro de Ciências da Saúde

Coordenação de Pós-Graduação em Biotecnologia Vegetal e Bioprocessos

ATA DO EXAME DE DEFESA DE TESE DE DOUTORADO DE TARCÍSIO NASCIMENTO CORREA, COMO PARTE DOS REQUISITOS NECESSÁRIOS À OBTENÇÃO DO GRAU DE DOUTOR EM CIÊNCIAS (BIOTECNOLOGIA VEGETAL E BIOPROCESSOS).

_____
Drª. Fernanda de Ávila Abreu – Coordenadora

_____
Andrew Macrae– UFRJ

_____
Alex Prast - UFRJ

_____
Dirlei Nico- UFRJ

_____
Ana Maria Mazotto - UFRJ

_____
Roberto Tarazi - UFRJ

_____
Drª. Fernanda de Ávila Abreu (Orientadora)

_____
Tarcísio Nascimento Correa (Doutorando)

LISTA DE MODIFICAÇÕES, CORREÇÕES OU RAZÕES PARA REPROVAÇÕES:

Ciente,

_____
Presidente da Banca

Ciente,

_____
Aluno(a)

Centro de Ciências da Saúde – Bloco K
Sala K2-032 – 2º andar – Cidade Universitária
CEP: 21941-590 – Rio de Janeiro – RJ – Brasil
Tel: 3938-6676 - E-mail: pbv@ccsdecania.ufrj.br

Dedico este trabalho às centenas de milhares de
vidas encerradas em vão nesta pandemia

AGRADECIMENTOS

À minha orientadora Fernanda de Ávila Abreu, por ter confiado na minha "criatividade" e apostado na diversificação da pesquisa realizada pelo grupo, o que permitiu a realização da presente tese.

Ao Programa de Pós-Graduação Biotecnologia Vegetal e Bioprocessos, pela oportunidade de realizar o Doutorado nesta área com que tanto me identifico.

Ao Instituto de Microbiologia Paulo de Góes, por disponibilizar o espaço e a estrutura para esta pesquisa e por incentivar a minha qualificação profissional.

Aos colegas do Laboratório de Biologia Celular e Magnetotaxia, pelas amizades que se formaram a partir do excelente convívio, pelo apoio mútuo no dia-a-dia da pesquisa e por aturarem as minhas bagunças.

À Unidade de Microscopia Multiusuário Padrón-Lins, pelo uso de toda infraestrutura relacionada à parte de microscopia.

À minha mãe, Márcia, pelos sacrifícios realizados a vida inteira para que eu pudesse ter a melhor criação.

Às agências de fomento CAPES, FAPERJ e CNPq pelo suporte financeiro.

“Quando pessoas viram coisas, cabeças viram degraus”

Emicida

Resumo

Correa, Tarcísio Nascimento. Nanotecnologia sustentável: simulação de bioprocesso e análise econômica da produção de magnetossomos em escala industrial e desenvolvimento de ferramenta para tratamento de efluentes. Tese (Doutorado em Ciências – Biotecnologia Vegetal e Bioprocessos) – Decania do Centro de Ciências da Saúde, Universidade Federal do Rio de Janeiro, 2021.

A nanotecnologia é um mercado bilionário, cujo valor deve se aproximar de US$ 300 bilhões ainda nesta década. Uma parte importante desse mercado é constituído pelos produtos baseados em nanopartículas magnéticas (NPMs), que são utilizadas em aplicações inovadoras, como formulação de medicamentos, fabricação de sensores e tratamento de águas e efluentes, entre outras. Atualmente, a maioria dos produtos nanomagéticos reportados é proveniente de processos químicos de síntese, tais como a coprecipitação e a termodecomposição. Entretanto, as aplicações tecnológicas podem se beneficiar das características físico-químicas de NPMs biogênicas. Dentre essas, as mais promissoras são aquelas sintetizadas por bactérias magnetotáticas (BMTs) na forma de organelas denominadas magnetossomos. As nanopartículas magnéticas de origem bacteriana (NMOBs) apresentam uma menor dispersão de forma e tamanho se comparada à maioria das nanopartículas sintéticas. Além disso, as NMOBs são constituídas por um cristal de magnetita com monodomínio magnético e uma membrana biológica que confere uma alta estabilidade coloidal e facilita a inserção de moléculas funcionais. Apesar dessas vantagens, as NMOBs ainda não são produzidas em escalas industriais, principalmente devido ao seu baixo rendimento em cultura e à complexidade dos bioprocessos que utilizam BMTs. Neste sentido, a primeira parte do presente trabalho de doutorado contemplou a simulação do bioprocesso e a avaliação econômica da produção em escala industrial de NMOBs. O estudo teve como foco a comparação da performance econômica de dois modos de operação – batelada alimentada e cultivo semicontínuo – da fermentação industrial de *Magnetospirillum gryphiswaldense* cepa MSR-1 para a obtenção de NMOBs. A avaliação técnico-econômica forneceu dados sobre a viabilidade no fornecimento das NMOBs para aplicações tecnológicas. Na análise final, o custo-base de produção das NMOBs (US$ 10-11 mil/kg magnetita) foi de 2,5 a 53 vezes maior do que para a produção química de NMPs sintéticas. Esta diferença resulta principalmente dos custos operacionais indiretos, que representam 76-79% dos custos totais de fabricação. Os custos de produção e os preços estipulados para venda são influenciados significativamente por parâmetros operacionais (ex.: rendimentos de magnetita), mas minimamente alterados por fatores econômicos externos, como os gastos de compra em materiais. Ainda assim, a forte discrepância entre os custos de produção e os preços de venda de NPMs sintéticas disponíveis comercialmente (US$ 11-40 mil/g) faz com que a comercialização de NMOBs seja economicamente promissora. A venda de NMOBs por valores superiores aos preços mínimos de venda (US$ 21-120/g) pode reduzir o tempo de retorno do investimento e maximizar

os lucros. A segunda parte deste trabalho teve como objetivo a aplicação de NMOBs obtidas de *Magnetovibrio blakemorei* cepa MV-1^{T} na degradação do corante azul de metila. Os experimentos demonstraram eficiências de descolorização de até 100% em 10 minutos de reação na ausência e na presença de peróxido de hidrogênio. Além disso, por meio da recuperação magnética, as NMOBs puderam ser reutilizadas e mantiveram até 75% de sua atividade após 4 ciclos. Dessa forma, os NMOBs são potenciais ferramentas no tratamento de efluentes contendo corantes, como é o caso da indústria têxtil. Devido às características das NMOBs, incluindo sua maior atividade na degradação do corante e produção mais limpa, os custos superiores da produção microbiana de NPMs em relação aos processos químicos tornam-se justificáveis.

Palavras-chave: bactérias magnetotáticas, magnetossomos, nanopartículas magnéticas, biominerais, avaliação técnico-econômica, simulação de processo, produção limpa.

Abstract

Correa, Tarcísio Nascimento. Nanotecnologia sustentável: simulação de bioprocesso e análise econômica da produção de magnetossomos em escala industrial e desenvolvimento de ferramenta para tratamento de efluentes. Tese (Doutorado em Ciências – Biotecnologia Vegetal e Bioprocessos) – Decania do Centro de Ciências da Saúde, Universidade Federal do Rio de Janeiro, 2021.

Nanotechnology is a billion-dollar market, with a value that is expected to approach $300 billion later this decade. An important part of this market is made up of products based on magnetic nanoparticles (MNPs), which are used in innovative applications, such as biomedicine, sensor manufacturing and water/wastewater treatment, among others. Currently, most of the reported nanomagnetic products are yielded from chemical syntheses, such as co-precipitation and thermal decomposition. However, technological applications can benefit from the physical-chemical characteristics of biogenic MNPs. Among those, the most promising are those synthesized by magnetotactic bacteria (MTBs) in the form of organelles called magnetosomes. Bacterial-derived magnetic nanoparticles (BMNs) have a smaller dispersion in shape and size compared to most synthetic nanoparticles. In addition, BMNs consist of a magnetite crystal with a single magnetic domain and a biological membrane that provides high colloidal stability and facilitates the insertion of functional molecules. Despite the advantages, BMNs are still not produced on industrial scales, mainly due to the low culture yields and the complexity of controls necessary to the bioprocesses using MTB. In this sense, the first part of the present doctoral work included a bioprocess simulation and an economic evaluation of the industrial-scale production of BMNs. The study focused on the comparison between the economic performance of two modes of operation – fed-batch and semi-continuous cultivation – of the industrial fermentation of *Magnetospirillum gryphiswaldense* strain MSR-1 to obtain BMNs. The techno-economic assessment provided data on the feasibility of suppling BMNs for technology applications. In the final analysis, the base-case manufacturing cost of BMNs (US$10-11 thousand/kg magnetite) was 2.5 to 53 times higher than the production of synthetic MNPs. This difference mainly derives from indirect costs, which represent 76-79% of total manufacturing costs. Production costs and stipulated selling prices are influenced by operational parameters (e.g. magnetite yields), but only slightly changed by external economic factors, such as material purchase expenditures. Still, a strong discrepancy between production costs and sales prices of competitive commercially available MNPs (US$11-40k/g) makes the commercialization of BMNs economically promising. Selling BMNs at prices exceeding the minimum selling prices ($21-120/g) can abbreviate payback times and maximize profits. The second part of this work aimed at the application of BMNs obtained from *Magnetovibrio blakemorei* strain MV-1^T for the degradation of methyl blue dye. The experiments showed decolorization efficiencies of up to 100% within 10 min reactions, in the presence and absence of hydrogen peroxide. Moreover, by using magnetic collection,

BMNs were reused and retained up to 75% activity of after 4 cycles. Thus, NMOBs are potential tools in the treatment of effluents containing dyes, as is the case in the textile industry. Due to the characteristics of BMNs, including their higher dye degradation activity and cleaner production, the higher costs of microbial production of NPMs compared to chemical processes become justifiable.

Keywords: magnetotactic bacteria, magnetosomes, magnetic nanoparticles, biominerals, techno-economic assessment, process simulation, clean production.

Lista de abreviaturas

ATE	Avaliação técnico-econômica
BMTs	Bactérias magnetotáticas
CSM	Coluna de separação magnética
LPS	Lipopolissacarídeo
NMOBs	Nanopartículas magnéticas de origem bacteriana
NPMs	Nanopartículas magnéticas
OMS	Organização Mundial da Saúde
SDS	Dodecilsulfato de sódio

Lista de tabelas

Tabela 1. Sumário dos cultivos de BMTs em biorreatores de descritos na literatura e seus respectivos valores de produção e produtividade..... 23

Lista de figuras

Figura 1. Número de produtos nanotecnológicos registrados na *Nanotechnology Products Database* (statnano.com) categorizados de acordo com o setor industrial. Figura de autoria própria elaborada com dados disponíveis na base citada..... 15

Figura 2. Representação gráfica das reações envolvidas nos métodos clássicos de síntese de nanopartículas magnéticas: coprecipitação (A) e termodecomposição (B). Figura de autoria própria elaborada com base na revisão de Wu et al., 2016. 15

Figura 3. Diversidade morfológica de BMTs: microscopia óptica em contraste interferencial diferencial de espirilos (A) e cocos (B); imagens de microscopia eletrônica de varredura de um procarioto multicelular magnetotático (C) e de transmissão em alta resolução de um vibrião magnetotático (D). Note a presença da cadeia de magnetossomos indicada por M e do flagelo indicado por F. Imagens retiradas do acervo do Laboratório de Biologia Celular e Magnetotaxia. 18

Figura 4. Diversidade morfológica dos BMs produzidos por diferentes BMTs: (A) prismático alongado, (B) cubooctaédricos e (C) anisotrópicos em "ponta de lança". Em B, nota-se a presença da membrana, indicada pela ponta de seta. Imagens retiradas do acervo do Laboratório de Biologia Celular e Magnetotaxia..... 20

Figura 5. Microscopia eletrônica de transmissão (A), representação tridimensional (B) e representação estrutural (C) da nanoformulação desenvolvida pelo nosso grupo de pesquisa (Correa et al., 2021), constituída de anfotericina B conjugada a NMOBs por meio de adsorção mediada por poli-L-lisina. Em B, nota-se a presença de uma membrana espessa, indicada pela ponta de seta, devido à ligação das moléculas de fármaco e do agente de ligação. Imagem adaptada de Correa et al. (2021)..... 21

Figura 6. Exemplo de um processo proposto para produção em massa e isolamento de NMOBs com base nos trabalhos de Guo et al. (2011) e Rosenfeldt et al. (2021). Os NMOBs extraídos ao final do processo retêm a membrana (indicada por **m**), permitindo uma dispersibilidade coloidal estável e facilitando as aplicações pretendidas. Figura de autoria própria. As imagens de microscopia foram retiradas do acervo do Laboratório de Biologia Celular e Magnetotaxia..... 29

Figura 7. Resultados da busca na base *Web of Science* utilizando a palavra-chave '*techno-economic assessment*' nos campos título, resumo e palavras-chave: número de publicações ao longo dos últimos 15 anos (A) e categorização nas áreas do conhecimento (B). Figura de autoria própria elaborada com dados extraídos de busca. 31

Sumário

1. Introdução 14

1.1. Nanotecnologia e indústria 14

1.2. Nanopartículas magnéticas 14

1.3. Bactérias magnetotáticas 17

1.4. Nanopartículas magnéticas biogênicas 19

1.5. Produção de NMOBs em biorreator 22

1.6. Extração de NMOBs 27

1.7. Justificativa 30

2. Objetivos 32

2.1. Objetivos gerais 32

2.2. Objetivos específicos 32

3. Metodologia 33

3.1. Capacidade de produção 33

3.2. Base do projeto 33

3.3. *Software* de modelagem e simulação 33

3.4. Dados e cálculos econômicos 34

3.5. Seção de inoculação 34

3.6. Seção de fermentação 34

3.7. Seção de recuperação de NMOBs 34

3.8. Análises de sensibilidade 35

3.9. Culturas bacterianas 35

3.10. Lise de células bacterianas e extração de NMOBs 35

3.11. Remoção de membrana 35

3.12. Preparação de NPMs sintéticas 36

3.13. Microscopia eletrônica de transmissão 36

3.14. Ensaios de remoção de azul de metila 36

3.15. Reutilização e extravasamento de ferro 36

4. Artigos 37

4.1. *Why does not nanotechnology go green? Bioprocess simulation and economics for bacterial-origin magnetite nanoparticles.* 37

4.2. *Bacterial-origin magnetic nanoparticles for decolorization of methyl blue dye* 49

5. Considerações finais 63

6. Referências 64

7. Anexos 70

Introdução

1.1. Nanotecnologia e indústria

Enquanto a nanociência é definida como o campo do conhecimento dedicado ao estudo de materiais de dimensões nanométricas, a nanotecnologia constitui-se na manipulação e fabricação de dispositivos com esta característica (Askeland & Wright, 2016). Apesar de registros históricos revelarem que materiais nanométricos têm sido utilizados há séculos, notadamente em objetos vítreos da Roma Antiga, a expansão da nanotecnologia ocorre, sobretudo, a partir do final do século XX com o estabelecimento de indústrias de circuitos integrados e processadores e de nanomateriais de carbono – como nanotubos e grafeno (Bayda et al., 2020). Projeções econômicas indicam que o mercado global de nanotecnologia deve atingir, até 2028, o valor de US$ 291 bilhões com uma taxa anual de crescimento de 18% (Emergen Research, 2021).

Atualmente, os setores industriais com o maior número de produtos nanotecnológicos registrados são a indústria de sensores, materiais de construção e produtos dermatológicos (Figura 1). Recentemente, a aplicação da nanotecnologia nos setores farmacêuticos e de tratamento de águas e efluentes também têm se refletido em um número expressivo de novas tecnologias (Figura 1), muitas das quais se baseiam em nanopartículas magnéticas (NPMs) (Ali et al., 2021). Dentro destes setores, a utilização de NPMs destaca-se no desenvolvimento de produtos inovadores, tais como adsorventes e catalisadores para a remoção de poluentes orgânicos (Jain et al., 2021) e formulações de agentes diagnósticos e terapêuticos para o câncer e outras patologias (Kudr et al., 2017). Além desses produtos, diferentes tipos de NPMs têm sido aplicados na agricultura, geração de energia, recuperação de recursos naturais, desenvolvimento de sensores, entre outras aplicações (Ali et al., 2021).

1.2. Nanopartículas magnéticas

A variedade de aplicações reportadas para as NPMs se deve à combinação de suas dimensões nanométricas (1-100 nm) e ao magnetismo próprio destes materiais (Yang et al., 2017). A maioria das NPMs descritas é composta de óxidos de ferro sendo a magnetita (Fe_3O_4) a mais comum (Ali et al., 2021). Devido à versatilidade das aplicações de NPMs, inúmeros métodos físicos, químicos e biológicos foram desenvolvidos para a síntese

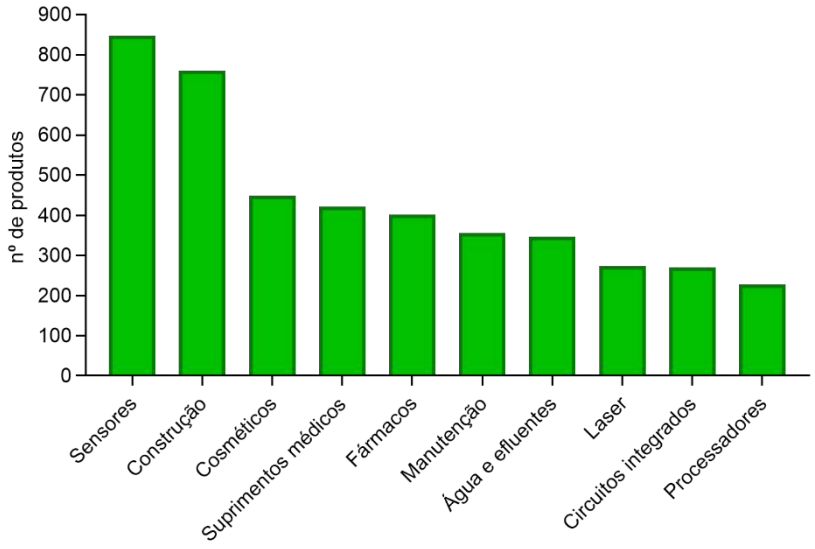

Figura 1. Número de produtos nanotecnológicos registrados na *Nanotechnology Products Database* (statnano.com) categorizados de acordo com o setor industrial. Figura de autoria própria elaborada com dados disponíveis na base citada.

destes materiais (Ali et al., 2021, Figura 2). Neste trabalho, daremos destaque aos processos biológicos e aos principais métodos químicos de fabricação.

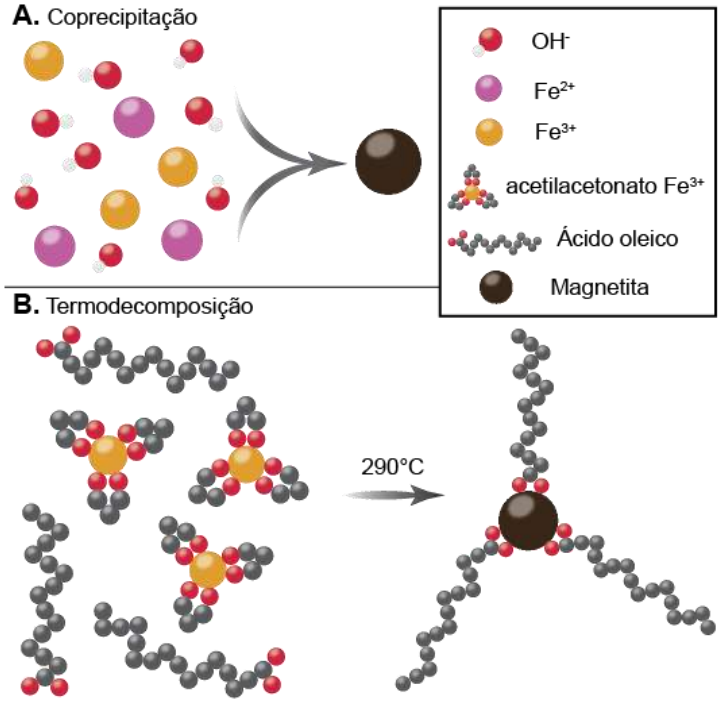

Figura 2. Representação gráfica das reações envolvidas nos métodos clássicos de síntese de nanopartículas magnéticas: coprecipitação (A) e termodecomposição (B). Figura de autoria própria elaborada com base na revisão de Wu et al., 2016.

Na síntese química, a coprecipitação (Figura 2.A) é o método mais simples e disponível para a obtenção de NPMs (Simeonidis et al., 2016). Este método baseia-se na precipitação de cátions de Fe^{3+} e Fe^{2+}, na proporção molar de 2:1, em meio alcalino (pH

> 10) (Simeonidis et al., 2016). Devido à facilidade de execução, a coprecipitação é o método de síntese para a maioria das aplicações de NPMs reportadas na literatura (Wallyn et al., 2019). Entretanto, as nanopartículas produzidas neste tipo de síntese costumam apresentar forma e tamanhos irregulares (Augusto et al., 2020). Para a obtenção de nanopartículas cujas propriedades são mais controladas, frequentemente são utilizados métodos baseados em solventes orgânicos, como a termodecomposição (Wu et al., 2016). A termodecomposição (Figura 2.B) ocorre quando há formação de magnetita em alta temperatura (> 200°C) a partir de um complexo orgânico de Fe^{3+} disperso em solvente apropriado (Park et al., 2004). A porção orgânica deste complexo geralmente é aniônica, sendo as mais comuns os íons oleato e acetilacetonato (Wu et al., 2016). Durante o processo, ocorre a decomposição da porção orgânica, simultaneamente à redução parcial do Fe^{3+} e consequente formação dos cristais de magnetita (Park et al., 2004). Uma vez que a superfície da magnetita formada é estabilizada pelo complexante aniônico, os cristais tendem a apresentar formas e tamanhos mais uniformes, em comparação à coprecipitação (Kim et al., 2009). Apesar destas vantagens, a demanda de grandes quantidades de solventes orgânicos e a necessidade de múltiplas etapas para a síntese das nanopartículas são inconvenientes relacionados à termodecomposição (Wu et al., 2016). Uma alternativa disponível a este método é a síntese hidrotérmica, que consiste na precipitação alcalina de Fe^{3+}/Fe^{2+} em altas temperaturas (>200 °C), também na presença de estabilizantes orgânicos aniônicos (Wallyn et al., 2019). As nanopartículas oriundas deste método possuem características físicas intermediárias àquelas obtidas por coprecipitação e termodecomposição (Wallyn et al., 2019).

Como discutido anteriormente, uma das aplicações mais promissoras para NPMs é a sua aplicação no tratamento de poluentes presentes em águas residuais. Para a maioria desses trabalhos, utilizaram-se NPMs fabricadas por coprecipitação aditivada com extratos vegetais para um melhor controle de forma e tamanho (Mondal et al., 2020). Como exemplo, nanopartículas de óxido (Fe_xO_y) e oxohidróxido de Fe ($Fe_xO_y(OH)_z$) fabricadas a partir do extrato de chá verde foram aplicadas como catalisadores da reação de Fenton para a degradação dos corantes azul de metileno e alaranjado de metila (Shahwan et al., 2011). Nesse tipo de reação, são gerados radicais hidroxila (OH·) a partir de peróxido de hidrogênio (H_2O_2) na presença de íons Fe^{2+} e Fe^{3+} (Pignatello et al., 2006). Devido à sua alta instabilidade química, os radicais OH· promovem reações intensas de oxidação de moléculas orgânicas. No trabalho de Shahwan e colaboradores (2011), as

nanopartículas (40-60 nm) catalisaram a degradação de quase 100% dos corantes testados a 200 mg/L durante um tempo de reação de 6 h. Em outro trabalho, nanopartículas de óxido de ferro foram sintetizadas utilizando extratos aquosos de folhas de diferentes espécies vegetais (Wang et al., 2014). As NPMs foram, então, aplicadas como catalisadores de reação de Fenton para a degradação de corantes azólico *Acid black* e as eficiências de remoção atingidas foram próximas de 100% (Wang et al., 2014). Juntamente à decolorização, o mesmo tratamento também removeu 87% da carga de carbono orgânico total das amostras tratadas. A utilização de nanocatalisadores magnéticos para este fim é vantajosa devido à fácil recuperação destas nanopartículas por concentração magnética. A recuperação do catalisador torna o processo de tratamento de efluentes mais econômico, uma vez que o mesmo pode ser reutilizado em diversas reações.

Apesar das melhorias realizadas nos métodos químicos e da comprovada eficiência em aplicações ambientais de NPMs sintéticas (Ali et al., 2021), NPMs de origem microbiana são distintas quanto às suas características físico-químicas devido ao controle inerente aos processos biológicos (Grasso et al., 2020). Adicionalmente, processos microbianos, em geral, apresentam menor impacto ambiental em comparação a processos químicos por envolverem apenas reagentes biocompatíveis e condições amenas de temperatura e pressão (Coelho & Ribeiro, 2016).

1.3. Bactérias magnetotáticas

O grupo de microrganismos que constitui a principal fonte de nanomateriais magnéticos são as bactérias magnetotáticas (BMTs) (Vargas et al., 2018). As BMTs compreendem um grupo diverso de procariotos aquáticos Gram-negativos com a capacidade de se orientar ao longo das linhas de um campo magnético (Abreu et al., 2020). A orientação magnética passiva da bactéria e a natação ativa através de propulsão flagelar são conjuntamente definidas como magnetotaxia (Abreu et al., 2020). A magnetotaxia confere caráter de locomoção unidirecional por ambientes quimicamente estratificados na coluna d'água e/ou sedimentos. As BMTs nadam ativamente em busca da interface óxica-anóxica na qual a força próton-motiva é máxima (Abreu et al., 2020). A maioria das BMTs é descrita como microaerófilas e/ou anaeróbias (Abreu et al., 2020).

A combinação de estudos morfológicos e filogenéticos tem ajudado a compreender a complexa diversidade encontrada nas comunidades de BMTs (Lin et al.,

2014). Observações de amostras ambientais através de microscopia de luz e eletrônica já revelaram morfologias dos tipos cocos, espirilos, vibriões, bacilos e multicelulares (Lefèvre & Bazylinski, 2013; Figura 3). Análises filogenéticas já confirmaram a existência de representantes procarióticos magnetotáticos nos filos Proteobacteria (classes Alpha-, Beta-, Gamma-, Delta-, e Etaproteobacteria), Nitrospirae e Omnitrophica (Lin et al., 2018; Abreu et al., 2020). Através de mineração de genoma, também já foram identificados representantes de BMTs na classe Zetaproteobacteria e nos filos Plantomycetes e Latescibacteria (Lin et al., 2018). Além da diversidade morfológica e taxonômica, a distribuição destes organismos é ubíqua, sendo encontrados em ambientes aquáticos, como mares, lagoas, estuários e sedimentos marinhos (Lin et al., 2014). A esta característica se soma produção de NPMs com características controladas, o que gera um grande potencial em biotecnologia, que ainda é pouco explorado (Vargas et al., 2018).

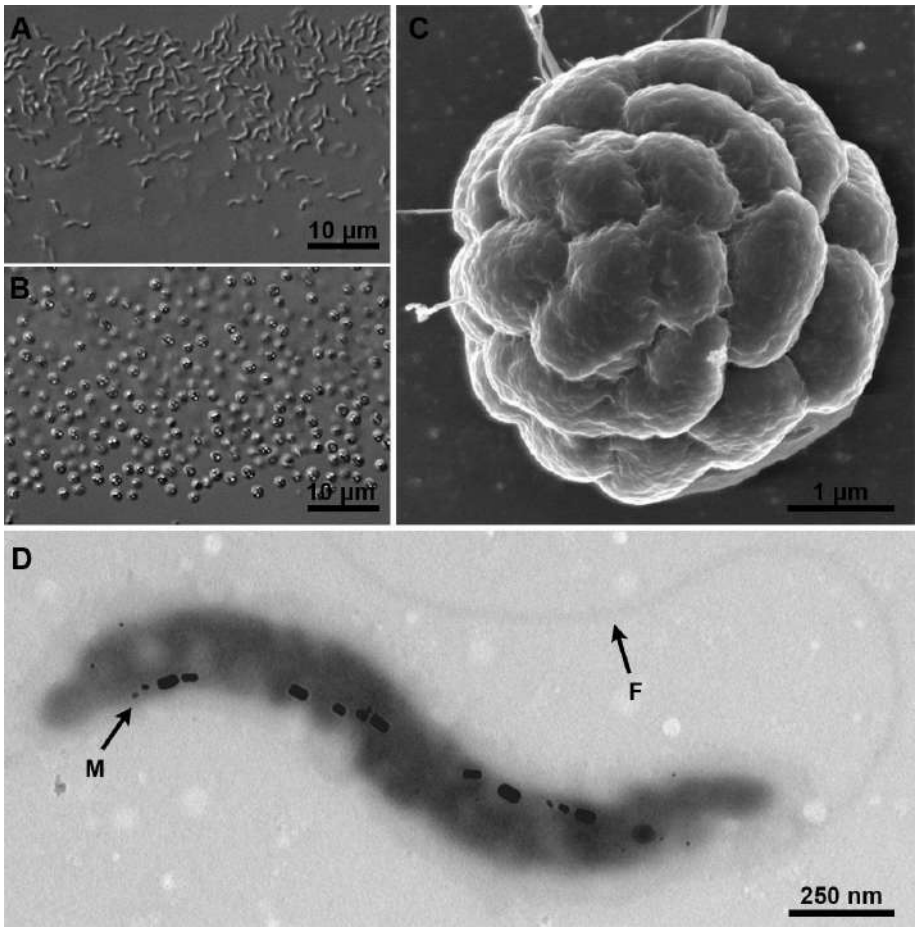

Figura 3. Diversidade morfológica de BMTs: microscopia óptica em contraste interferencial diferencial de espirilos (A) e cocos (B); imagens de microscopia eletrônica de varredura de um procarioto multicelular magnetotático (C) e de transmissão em alta resolução de um vibrião magnetotático (D). Note a presença da cadeia de magnetossomos indicada por M e do flagelo indicado por F. Imagens retiradas do acervo do Laboratório de Biologia Celular e Magnetotaxia.

1.4. Nanopartículas magnéticas biogênicas

As NPMs produzidas pelas BMTs são denominadas magnetossomos e encontram-se organizadas em uma ou mais cadeias no citoplasma bacteriano. Os magnetossomos são compostos por um cristal magnético constituído por mineral de ferro, envolto por uma membrana fosfolipídica (Bazylinski & Frankel, 2004). Assim como nas NPMs sintéticas, a constituição mineral dos magnetossomos presentes na maioria das espécies cultivadas de BMTs, e de todos aqueles já utilizados em aplicações tecnológicas, é de magnetita. Entretanto, algumas espécies de BMTs também são capazes de produzir magnetossomos de greigita (Fe_3S_4). A morfologia dos cristais de magnetossomos tende a ser única em uma espécie particular, sendo as três principais morfologias de cristais de magnetita encontradas a cuboctaédrica, prismática alongada e anisotrópica em forma de "ponta de lança" (Lower & Bazylinski, 2013; Figura 4). O processo de síntese dos magnetossomos é altamente controlado por uma complexa maquinaria proteica, codificada por genes específicos (Correa et al., 2020). O controle genético do processo de formação dos magnetossomos permite que essas estruturas tenham propriedades superiores às encontradas em partículas de óxido de ferro sintetizadas por métodos químicos (Correa et al., 2020). As propriedades que são otimizadas durante os processos bioquímicos de síntese incluem tamanho e forma controlados e pureza química (Vargas et al., 2018). Uma vez que as dimensões se encontram predominantemente na faixa de 20 a 100 nm, a maioria dos cristais de magnetossomos apresentam um monodomínio magnético estável (Amor et al., 2020). Como exemplo, magnetossomos produzidos por *Magnetovibrio blakemorei* cepa MV-1^T possuem morfologia prismática alongada e comprimento médio de 53,0 ± 10,9 nm enquanto as de *Magnetospirillum gryphiswaldense* cepa MSR-1 são cuboctaédricos com comprimento médio de 32,5 ± 10,0 nm (Sparks et al., 1990; Faivre et al., 2008; Posfái et al., 2013). A presença da membrana biológica envolvendo cada

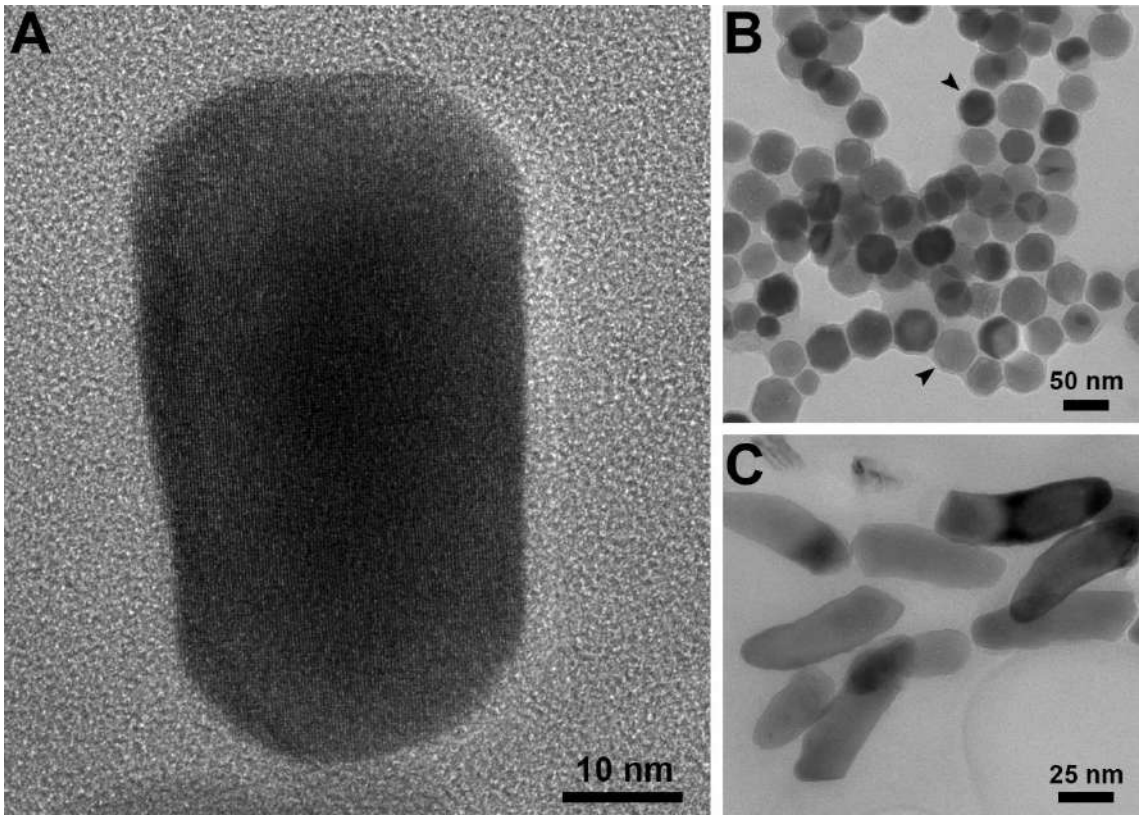

Figura 4. Diversidade morfológica dos BMs produzidos por diferentes BMTs: (A) prismático alongado, (B) cuboctaédricos e (C) anisotrópicos em "ponta de lança". Em B, nota-se a presença da membrana, indicada pela ponta de seta. Imagens retiradas do acervo do Laboratório de Biologia Celular e Magnetotaxia.

nanocristal magnético confere estabilidade coloidal às suspensões aquosas de magnetossomos após a sua extração das células de BMTs, além de conter proteínas inseridas, que fornecem grupos funcionais para a associação química de substâncias funcionais (Alphandéry, 2014).

Assim sendo, a química de superfície dos magnetossomos favorece a sua aplicação como nanoferramentas inovadoras, em consonância com as características físicas dos cristais de magnetita. Por convenção, denominaremos nanopartículas magnéticas de origem bacteriana (NMOBs) os magnetossomos obtidos de BMTs para aplicações tecnológicas. Recentemente, uma nanoformulação magnética resultante da associação entre NMOBs extraídas de *Mv. blakemorei* cepa MV-1^{T} e o fármaco anfotericina B (Figura 5) foi desenvolvida pelo nosso grupo de pesquisa (Correa et al., 2021). A base da nanoformulação foi o complexo obtido através da interação eletrostática entre a NMOB, cuja superfície é carregada negativamente, e o polipeptídio catiônico poli-L-lisina. A funcionalização da nanopartícula ocorreu através de ligações de hidrogênio entre o recobrimento catiônico e moléculas de anfotericina B. A nanoformulação obtida

apresentou um alto carregamento de fármaco (52 µg de anfotericina B por 100 µg de NMOBs) e ainda foi capaz de liberar aproximadamente 54% do fármaco associado em meio aquoso em resposta à aplicação de um campo magnético alternado por 60 min. Outras aplicações recentemente descritas para NMOBs incluem: remoção de aflatoxina de óleo vegetal por um complexo imunomagnético formado por NMOBs e anticorpos policlonais (Pi et al., 2017); aplicação como agentes de contraste no imageamento por ressonância magnética (Nan et al., 2021); transfecção magnética de genes para células hepáticas (Yang et al., 2020); e construção de um sensor biomagnético para a detecção de *Listeria monocytogenes* em amostras de alimentos (Sannigrahi et al., 2020).

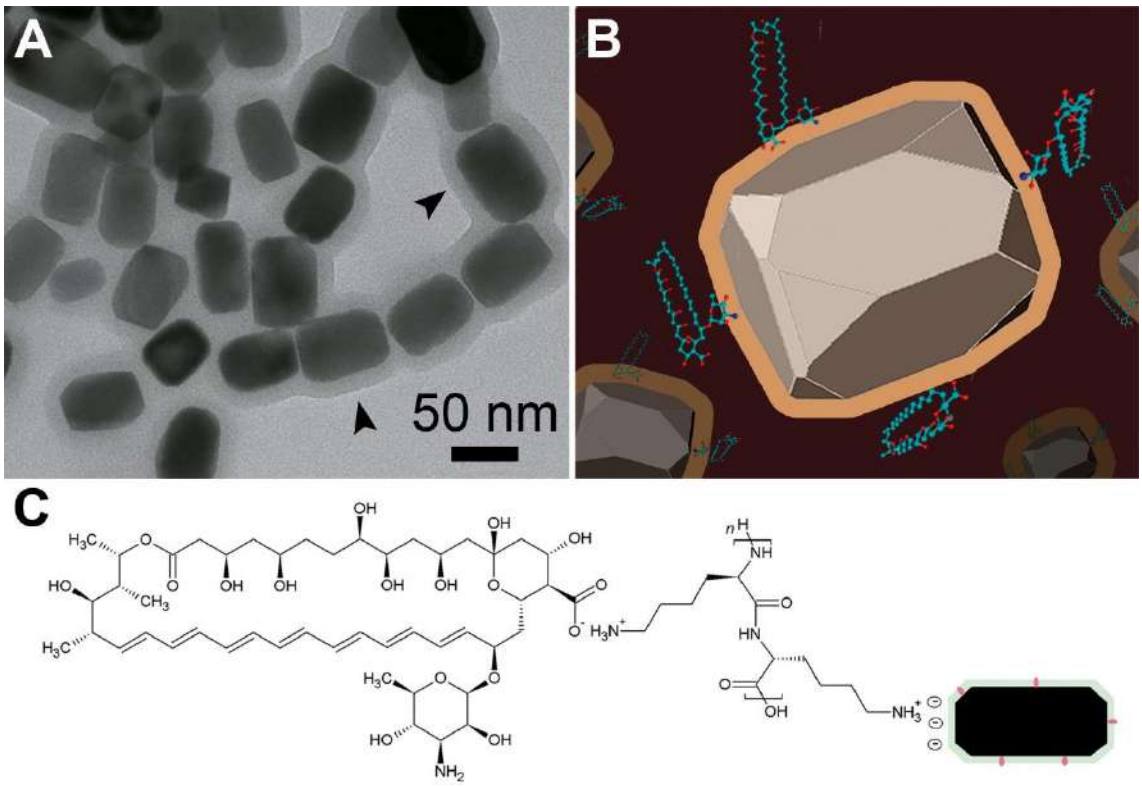

Figura 5. Microscopia eletrônica de transmissão (A), representação tridimensional (B) e representação estrutural (C) da nanoformulação desenvolvida pelo nosso grupo de pesquisa (Correa et al., 2021), constituída de anfotericina B conjugada a NMOBs por meio de adsorção mediada por poli-L-lisina. Em B, nota-se a presença de uma membrana espessa, indicada pela ponta de seta, devido à ligação das moléculas de fármaco e do agente de ligação. Imagem adaptada de Correa et al. (2021)

Apesar da maioria dos trabalhos de aplicação das NMOBs serem voltados a aplicações biomédicas, estas nanoestruturas também possuem um grande potencial a ser explorado em remediação ambiental. Ginet e colaboradores (2011) produziram uma NMOBs recombinante associada a uma paraoxonase por meio da expressão do gene *opd* de *Flavobacterium* sp. fusionado ao gene que codifica para a proteína transmembrana MamC em *Magnetospirillum magneticum* cepa AMB-1. O nanossistema foi capaz de

catalisar a degradação de etil-paraoxon, um pesticida organofosforado mundialmente utilizado, com uma atividade de aproximadamente 50% àquela da paraoxonase livre (Ginet et al., 2011). O nanocatalisador foi reutilizado por 6 ciclos, mantendo uma atividade catalítica acima de 90% na última utilização (Ginet et al., 2011). Deste modo, é evidente que NMOBs são plataformas promissoras para utilização na degradação catalítica de poluentes e, portanto, no tratamento de efluentes industriais. A membrana que envolve estas nanopartículas contem proteínas inseridas cujas funções e aplicabilidades ainda não foram exploradas (Alphandéry, 2014; Correa et al., 2020). Possivelmente, algumas dessas proteínas possuem atividade de oxidorredução uma vez que o processo de biomineralização envolve etapas de oxidação ou redução dos íons de ferro (Correa et al., 2020). Sendo assim, a atividade intrínseca dessas proteínas pode ser aproveitada na degradação de poluentes orgânicos, sem modificações funcionais de membrana.

1.5. Produção de NMOBs em biorreator

Embora o isolamento e a manutenção de culturas puras de BMTs sejam corriqueiramente realizados em escala laboratorial, a aplicação de NMOBs em tecnologia depende do cultivo em larga escala destes microrganismos. Neste sentido, vários estudos analisaram e otimizaram o crescimento de BMTs em fermentadores e obtiveram valores de produção significativamente diferentes de acordo com as estratégias de cultivo (Tabela 1). Essas estratégias incluíam modificações nos meios de cultivo, ajustes nas condições físico-químicas de cultura e regimes especializados de alimentação e injeção de oxigênio. No entanto, conforme evidenciado na Tabela 1, a condução de cultivo mais comum para BMTs em biorreatores é a batelada alimentada, na qual os nutrientes necessários ao crescimento e à formação de magnetossomos são suplementados ao longo do tempo de cultivo (McNeil & Harvey, 2008).

Tabela 1. Sumário dos cultivos de BMTs em biorreatores descritos na literatura e seus respectivos valores de produção e produtividade.

Espécie / cepa	Condução do cultivo	Produção* (mg/L)	Produtividade* (mg/L/dia)	Referência
Magnetospirillum magneticum / AMB-1	B.A.	9	3,7	Yang et al., 2001
Magnetospirillum gryphiswaldense / MSR-1	B.S.	7,9	6,3	Heyen & Schuler, 2003
	B.A.	58,4	--	Liu et al., 2008
	B.A.	41,7	16,7	Sun et al., 2008
	B.A.	83,2	55,49	Liu et al., 2010
	B.A.	356,5	178,26	Zhang et al., 2011
	S.C.	168,3	83,5	Zhang et al., 2011
	B.A.	139	47,0	Fernández-Castané et al., 2018
	B.A.	8-10	3,8-4,8	Berny et al., 2020
Magnetospirillum sp. / ME-1	B.A.	120	58,7	Ke et al., 2018
Magnetovibrio blakemorei / MV-1^T	B.S.	22,4	5,6	Silva et al., 2013
	B.A.	26	3,2	Silva et al., 2013
	B.A.	32,5	16,3	Correa, 2019
	C.C.	27,1	22,7	Correa, 2019

(*) A produtividade e a produção são expressas em relação à magnetita. B.A = batelada alimentada; B.S. = batelada simples; S.C. = semicontínuo; C.C. = cultivo contínuo.

Heyen & Schuler (2003) mostraram que baixas tensões de oxigênio (0,25 a 2 mbar) são mais favoráveis à formação de magnetossomos em cepas do gênero *Magnetospirillum*. Neste mesmo trabalho, foi demonstrado que a espécie *Ms. gryphiswaldense* cepa MSR-1 apresenta um crescimento mais acelerado em tensões de oxigênios mais elevadas embora suas células produzam um menor número de magnetossomos nesta condição. Entretanto, quando as células foram submetidas a uma redução na tensão de oxigênio de 20 para 2 mbar, o magnetismo celular, que era indetectável durante e fase exponencial de crescimento, aumentou acentuadamente. Essa descoberta se tornou referência para outros trabalhos sobre o cultivo de BMTs, nos quais

se busca manter a concentrações de oxigênio suficientes para o crescimento celular, sem impedir a produção de magnetita (Basit et al., 2020). Nesse sentido, uma estratégia utilizada em culturas é a aeração com baixo fluxo de ar com aumento gradativo da rotação do rotor do fermentador quando a concentração de oxigênio cai abaixo de um limiar pré-estabelecido (Sun et al., 2008). Nestes casos, a agitação intensifica a transferência de massa gás-líquido em uma taxa que é determinada pelo consumo de oxigênio - e, portanto, pelo crescimento celular. Esta aeração controlada por um mecanismo de *feedback* evita oscilações na concentração de oxigênio e mantém a atividade de produção de magnetita.

Durante o cultivo da cepa MSR-1 (Sun et al., 2008) em batelada alimentada com lactato, o oxigênio no meio foi esgotado durante a fase exponencial de crescimento pela respiração bacteriana, estabelecendo-se uma condição anaeróbica. Após o esgotamento do oxigênio, uma estratégia de *feedback* foi iniciada para manter uma vazão baixa de oxigênio, suficiente para o crescimento celular em microaerofilia e produção de magnetossomos.

Outra estratégia para o crescimento de BMTs é a batelada alimentada responsiva ao pH (Liu et al., 2010; Zhang et al., 2011; Fernández-Castané et al., 2018). Essa estratégia consiste na introdução da maior parte da fonte de carbono na forma de ácidos orgânicos (geralmente ácido lático) e totalidade do ferro a ser consumido através de meios de alimentação. Devido à natureza ácida do ácido lático (pKa = 3,86) e suas altas concentrações em solução (50-200 g/L), o pH dos meios de alimentação fica em torno de 2,7-3,7. O consumo de nutrientes pelas cepas de *Magnetospirillum* levam a um aumento no pH da cultura. Automaticamente, esse aumento de pH desencadeia uma resposta pelo sistema de monitoramento do fermentador, que ativa a bomba de alimentação e ajusta o pH para 6,8-7,0, através da adição do meio de alimentação. Consequentemente, o pH é corrigido ao passo em que são suplementados os nutrientes, incluindo fontes de carbono e ferro. O primeiro relato de tal estratégia (Liu et al., 2010) foi usado para cultivar a cepa MSR-1 em um biorreator de 7,5 L. A principal razão para o desenvolvimento de tal estratégia foi a observação de que altas concentrações de lactato inibiam o crescimento celular (Liu et al., 2010). Sendo assim, a suplementação de um meio de controle de pH contendo uma fonte de carbono altamente concentrada durante o cultivo evitou o estresse celular e, ainda, foi capaz de sustentar o crescimento bacteriano. O uso da mesma estratégia em um fermentador de 42 L resultou em alta densidade celular e rápido

crescimento da cepa MSR-1, juntamente com produção de 83 mg/L e produtividade de 55,5 mg/L/dia de magnetita.

A alimentação responsiva ao pH, desenvolvida por Liu et al. (2010), foi a base para os cultivos em batelada alimentada publicados em vários outros trabalhos (Zhang et al., 2011; Fernández-Castané et al., 2018; Ke et al., 2018). Fernández-Castané e colaboradores (2018) compararam diferentes concentrações de ácido lático (fonte de carbono) e nitrato de sódio (aceptor final de elétrons) no meio de alimentação. Os resultados da otimização do processo sugeriram que a maior concentração de nitrato testada (25 g/L) na alimentação levou a uma maior densidade celular. No entanto, a concentração de ácido lático, embora diretamente proporcional à produção de magnetita, foi inversamente proporcional ao crescimento celular. Dos diferentes experimentos de crescimento realizados, os melhores resultados foram uma massa celular seca de 4,2 g/L de biomassa e uma produção de magnetita de 139 mg/L alcançada em 71 h de cultivo.

Os maiores valores de produção (356,5 mg/L) e produtividade (178,26 mg/L/dia) de magnetita no cultivo de BMTs foram obtidos por Zhang e colaboradores (2011) em um biorreator de 42 L. A composição do meio de alimentação era ligeiramente diferente em relação aos estudos anteriores, uma vez que se buscou substituir as fontes de carbono e nitrogênio. A substituição do lactato de sódio pelo ácido lático e do cloreto de amônio pela amônia reduziu o potencial osmótico da solução – devido à menor concentração de íons Na^+ e Cl^- – fator causador do estresse celular bacteriano. Outra novidade nesse estudo foi a estratégia de fermentação semicontínua em duas etapas. No primeiro estágio, as células foram cultivadas em um biorreator de 7,5 L com 5 L de meio até o final do crescimento exponencial por 30 h. Nesse ponto, 4,5 L do meio gasto foram coletados do vaso do reator. Em seguida, 4,5 L de meio fresco foram adicionados aos 0,5 L restantes e o segundo estágio de cultivo foi iniciado. Embora a produção e a produtividade tenham sido menores do que a estratégia anterior, o processo semicontínuo possibilitou o cultivo de um volume maior de cultura sem o tempo ocioso necessário para lavagem dos vasos, propagação de inóculos, esterilização e inoculação.

Além dos rendimentos, as características das NMOBs obtidas também podem ser moduladas pelo meio no qual foram produzidas. Por exemplo, Li & Pan (2012) compararam os efeitos da agitação e da presença de oxigênio em cultivos de 48 h da espécie *Ms. magneticum* cepa AMB-1. Esses experimentos revelaram uma diminuição significativa no comprimento médio dos magnetossomos (de 41,5 ± 15 para 33,0 ± 8,5

nm) e no fator de forma (razão largura/comprimento), aumentando de 0,78 ± 0,12 para 0,89 ± 0,08 nm, quando as células foram cultivadas sob anaerobiose estática e aerobiose com uma agitação de 120 rpm, respectivamente. As condições também afetaram o rendimento da cultura, pois as células em anaerobiose produziram 12 ± 5 magnetossomos em média, mas apenas 7 ± 4 quando cultivadas em aerobiose agitada.

Nosso grupo de pesquisa otimizou o cultivo de *Mv. blakemorei* cepa MV-1^T, gerando um dos poucos trabalhos publicados no qual a célula cultivada em biorreator não pertence ao gênero *Magnetospirillum* (Silva et al., 2013). O melhoramento do cultivo de *Mv. blakemorei* cepa MV-1^T é interessante porque a maior área de superfície das NMOBs prismáticas presumivelmente apresenta mais sítios de ligação disponíveis para moléculas funcionais do que NMOBs cuboctaédricas. No cultivo, a cepa MV-1^T pode utilizar diversos compostos como doadores de elétrons e fontes de carbono, tanto em microaerobiose quanto em anaerobiose com óxidos de nitrogênio (Bazylinski et al., 2013). No entanto, as células MV-1^T produzem um número maior de magnetossomos quando crescidas anaerobicamente utilizando N_2O como o aceptor final de elétrons. A partir dessa propriedade metabólica, o trabalho de Silva et al. (2013) relata a otimização da produção de magnetossomos pela cepa MV-1^T por meio de um planejamento experimental. Os experimentos testados envolveram múltiplas modificações no meio líquido estabelecido anteriormente (Bazylinski et al., 2013), no qual a fonte de Fe^{2+} é o sulfato ferroso ($FeSO_4$). Como resultado, uma composição otimizada foi determinada para o meio de cultivo da cepa MV-1^T no biorreator. Utilizando-se esse meio, a produção máxima de magnetita obtida em um volume de 5 litros foi de 22,4 mg/L em 96 h, aproximadamente 3 vezes maior do que no meio inicial. Entretanto, a produtividade de magnetita diminuiu de 5,6 mg/L/dia às 96 h para 3,2 mg/L/dia em 192 h.

Posteriormente, uma nova estratégia de cultivo em batelada alimentada foi desenhada com suplementações de Fe^{2+}, e N_2O, a 0,5 L/min por 30 min (Correa, 2019). As suplementações foram feitas a cada 24 h, com início na fase exponencial, para que suas concentrações iniciais fossem restabelecidas. A produção de magnetita, cujo máximo valor foi atingido em 72 h (24,5 mg/L – Tabela 1), diminuiu nos intervalos posteriores devido à diminuição na produção de magnetossomos por célula. Esta diminuição foi relacionada ao estado fisiológico no qual ocorre a perda da capacidade de magnetossomos nas células cultivadas devido a deleções gênicas (Schübbe et al., 2003) inerentes às fases estacionária e de declínio do crescimento celular (Ullrich et al., 2005).

Na tentativa de se sustentar o crescimento e a produtividade por períodos mais longos, foi desenvolvida uma estratégia de cultivo contínuo (Correa, 2019). Entre o início do cultivo e o ponto de 72 h, o cultivo ocorreu como uma batelada simples e a densidade celular e a produção de magnetita atingiram valores ligeiramente inferiores aos reportados por Silva e colaboradores (21,8 mg/L) (Silva et al., 2013). Em 72 h, foram iniciadas a entrada de meio fresco e a saída de meio contendo crescimento celular a uma vazão de 70 mL/h. Com isso, conseguiu-se manter a produção em 27,1 mg/L e a produtividade em 22,7 mg/L/dia até 120 h. A manutenção de condições de fase exponencial por um tempo estendido evitou a fase estacionária e, consequentemente, preveniu o aumento na proporção de células não magnéticas.

1.6. Extração de NMOBs

Nas indústrias biotecnológicas, o isolamento de produtos intracelulares pode demandar etapas adicionais não exigidas pelas moléculas secretadas extracelularmente. Para NMOBs, métodos de extração química e física têm sido empregados como etapas a jusante ao cultivo em biorreator. A extração química pode ser realizada por incubação com NaOH e dodecilsulfato de sódio (SDS) (Cypriano et al., 2019). Embora a extração química dispense a necessidade de equipamentos especializados, altas concentrações de NaOH podem causar danos à estrutura da membrana das NMOBs relacionados à desnaturação de proteínas e saponificação de fosfolipídios. Detergentes, como o SDS e o Triton, também devem ser usados com cautela para esse fim, pois também podem remover parcial ou totalmente os componentes da membrana (Yoshino et al., 2008).

A lise celular por tratamento ultrassônico é um dos exemplos mais difundidos de métodos físicos de isolamento de bioprodutos intracelulares (de Carvalho et al., 2017). O mecanismo de lise baseia-se na formação de cavidades devido à incidência de ondas de alta frequência nas estruturas celulares. Essas cavidades liberam energia mecânica que, por sua vez, desintegra fisicamente os componentes celulares. A lise ultrassônica tem sido aplicada em diferentes trabalhos para isolamento de NMOBs (Vargas et al., 2018; Cypriano et al., 2019, Correa et al., 2021). Porém, a escalabilidade desta operação é difícil devido ao alto consumo de energia (de Carvalho et al., 2017) e risco ocupacional - as ondas sonoras liberadas podem prejudicar a audição e fazem necessário o uso de equipamentos de proteção acústica.

Provavelmente, um dos maiores desafios da produção de produtos bacterianos é garantir a ausência da endotoxina lipopolissacarídica (LPS) (Mamat et al., 2015). As endotoxinas são os principais componentes pirogênicos e sua presença em produtos farmacêuticos invalida sua comercialização e uso (OMS, 2019). Em um cenário de produção de NMOBs em escalas piloto ou industrial, o controle rigoroso da contaminação por LPS será necessário, especialmente porque todas as BMTs conhecidas são Gram-negativas (Abreu et al., 2020). Apesar de as vesículas onde se formam os magnetossomos serem derivadas da membrana interna da célula interna, fragmentos da membrana externa de LPS ainda podem permanecer adsorvidos às NMOBs durante a lise celular.

Entretanto, é reportado que procedimentos de extração física por lise celular em alta pressão, como prensas francesas ou homogeneizadores de alta pressão, eliminam adequadamente a contaminação pirogênica (Mandawala et al., 2017). A lise de alta pressão é comum na indústria e pode ser ampliada como uma seção a jusante do cultivo de biorreator de BMTs. Guo e colaboradores (2011) desenvolveram um processo de várias etapas em larga escala para extração de NMOBs. O processo compreendeu um homogeneizador de alta pressão, para rompimento celular, uma coluna de separação magnética (CSM) e um tratamento ultrassônico de baixa energia com solução de ureia, para a remoção dos restos celulares. Nesse caso, a CSM era um cilindro preenchido com esferas milimétricas de aço. Durante a eluição do lisado celular magnético, ímãs permanentes foram afixados externamente na coluna, permitindo que as NMOBs se ligassem às esferas magnetizados. A técnica permitiu a recuperação de 300 mg de NMOBs a partir de uma cultura de 6 L de *Ms. gryphiswaldense* cepa MSR-1. O conceito da CSM também foi fundamental na padronização do isolamento de NMOBs proposta por Rosenfeldt e colaboradores (2021). Esse trabalho relata uma sequência de procedimentos para a extração de NMOBs que consiste na homogeneização em alta pressão de células da cepa MSR-1 derivadas de uma cultura de 10 L, seguida pela eluição do extrato celular por meio de uma CSM e um procedimento final de ultracentrifugação (Figura 6). A CSM foi fornecida pelo fabricante e o meio de ligação consistia em uma matriz de fibra ferromagnética. Apesar de um rendimento NMOBs final de cerca de 60% da quantidade estimada no extrato celular, a contaminação por *debris* celulares foi reduzida para apenas 0,3%.

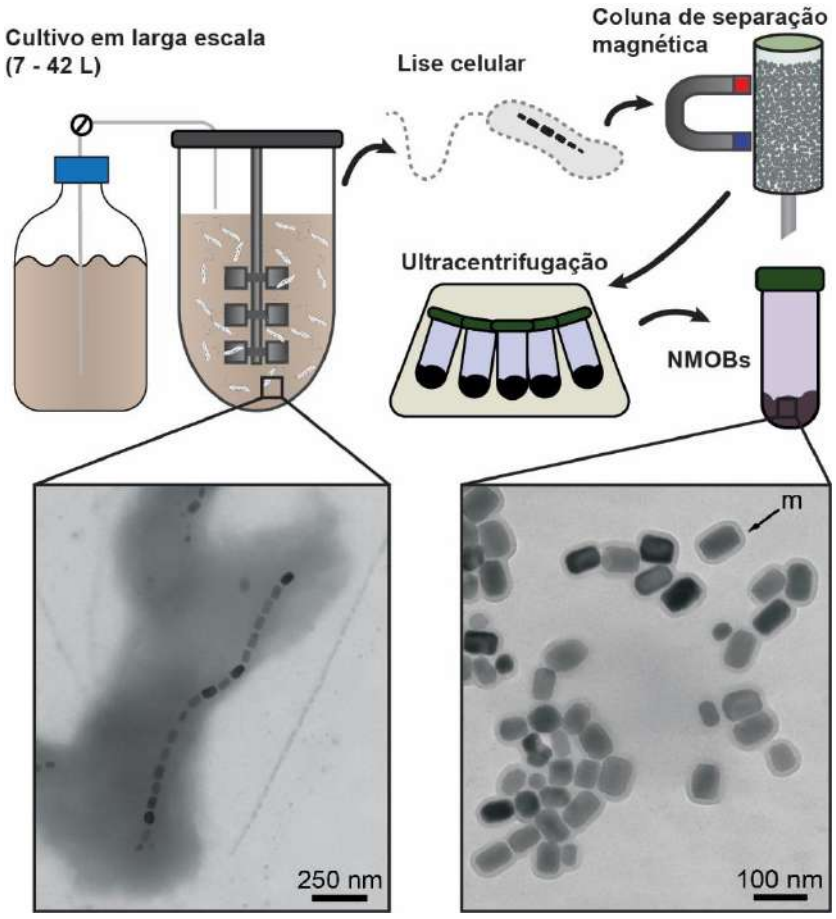

Figura 6. Exemplo de um processo proposto para produção em massa e isolamento de NMOBs com base nos trabalhos de Guo et al. (2011) e Rosenfeldt et al. (2021). Os NMOBs extraídos ao final do processo retêm a membrana (indicada por **m**), permitindo uma dispersibilidade coloidal estável e facilitando as aplicações pretendidas. Figura de autoria própria. As imagens de microscopia foram retiradas do acervo do Laboratório de Biologia Celular e Magnetotaxia.

1.7. Justificativa

A aplicabilidade descrita para as NMOBs e a demanda crescente por NPMs com alta qualidade e baixo custo fazem necessária a transposição de bioprocessos utilizando bactérias magnetotáticas de escalas laboratoriais para escalas industriais. Para tanto, faz-se necessário avaliar a viabilidade tecnológica e financeira do escalonamento deste bioprocesso. Neste sentido, a avaliação técnico-econômica (ATE) é um conjunto de técnicas disponíveis que permitem a estimativa de investimentos, custos capitais e operacionais de processo, dimensionamento de equipamentos e plantas, identificação de gargalos de produção, balanços de massa e energia e avaliação de tecnologias alternativas para um determinado bioprocesso (Petrides et al., 2019).

A ferramenta mais utilizada para a avaliação técnico-econômica é o desenho e a simulação de bioprocessos (Scown et al., 2021). A simulação utiliza dados obtidos em escalas laboratoriais e piloto, tais como consumo, rendimentos e emissões, para modelar e analisar um processo teórico em escalas maiores (Scown et al., 2021). Devido à complexidade dos cálculos necessários à simulação, é comum o uso de softwares voltados para esta finalidade. A utilização destes softwares permite representar graficamente e, simultaneamente, analisar de forma integrada os diversos processos, além de facilitar a avaliação dos efeitos de múltiplas variáveis de processos (Petrides et al., 2019).

A avaliação-técnico econômica também representam importantes produções técnico-científicas, uma vez que fornecem informações sobre a competitividade das tecnologias estudadas em comparação a processos já estabelecidos e os efeitos de variações no processo sobre os indicadores econômicos (Koutinas et al., 2014). Além disso, os dados gerados a partir de avaliações-técnico econômicas podem ser utilizados para a análise de impactos ambientais (Petrides et al., 2019). Devido à relevância, o número de publicações científicas descrevendo avaliações-técnico econômicas tem crescido, principalmente na última década (Figura 7.A). Apesar de a maioria das ATE serem publicadas nas áreas de energia e engenharia química, um número significativo destes trabalhos tem sido conduzido em projetos de microbiologia industrial e biotecnologia (Figura 7.B).

Apesar da descrição disponível de vários bioprocessos já descritos (Tabela 1), ainda existe uma carência de informações sobre o escalonamento da produção de NMOBs. Tais informações são fundamentais para o conhecimento prévio dos desafios

relacionados à transposição desses processos da escala laboratorial para a indústria e podem fornecer uma estimativa dos investimentos iniciais necessários em projetos de escalonamento de produção.

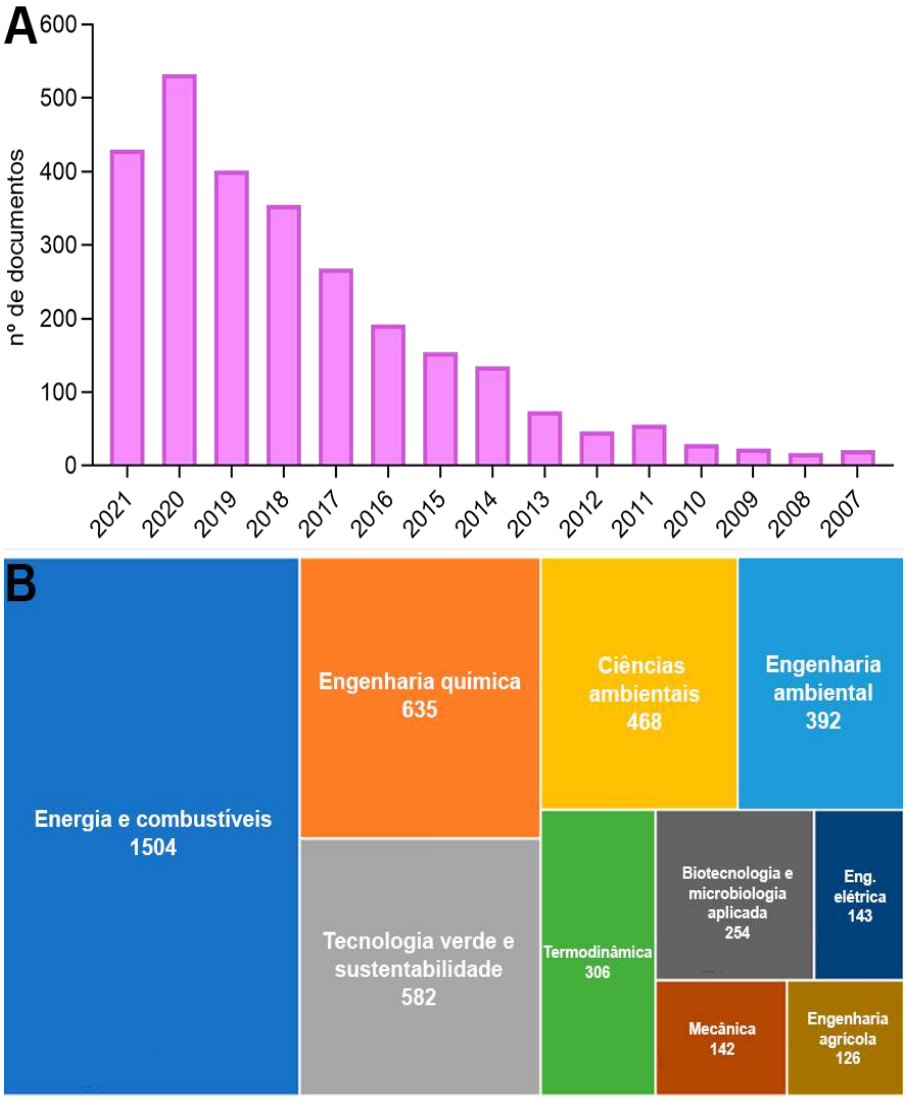

Figura 7. Resultados da busca na base *Web of Science* utilizando a palavra-chave '*techno-economic assessment*' nos campos título, resumo e palavras-chave: número de publicações ao longo dos últimos 15 anos (A) e categorização nas áreas do conhecimento (B). Figura de autoria própria elaborada com dados extraídos de busca.

Um dos processos de maior potencial de consumo de NMOBs produzidas em larga escala é o tratamento de efluentes industriais, sobretudo aqueles com alta concentrações de corantes sintéticos. A poluição causada por corantes presentes em efluentes industriais é um importante problema do ponto de vista ecológico. As indústrias têxteis são os maiores geradores de poluição aquática por esse tipo de substâncias (de Almeida et al., 2014). Este tipo de poluição é de alta importância para o Brasil uma vez que nele está instalado o quarto maior parque produtivo, com uma produção média anual de 1,3 milhão de toneladas de tecidos (ABIT, 2019). Esse setor é, ainda, um forte segmento produtivo

do Estado do Rio de Janeiro, contando com aproximadamente 330 indústrias instaladas (FIRJAN, 2018). O despejo do efluentes dessas em corpos d'água pode afetar a atividade fotossintética de microrganismos e plantas, pois bloqueia a penetração da luz solar (de Almeida et al., 2014). Devido à sua natureza química, a maioria dos corantes é de baixa biodegradabilidade e alta toxicidade aos organismos aquáticos e ao ser humano (de Almeida et al., 2014). Por esse motivo, tecnologias de tratamento de efluentes têm sido aprimoradas para melhorar a remediação desse tipo específico de poluente (Katheresan et al., 2018). Os tratamentos disponíveis para efluentes com altas concentrações de corantes são degradação microbiana, oxidação catalítica e adsorção física (Katheresan et al., 2018). Como discutido anteriormente, nanopartículas magnéticas já são ferramentas conhecidas para a degradação de corantes. Entretanto, no nosso conhecimento, não há trabalhos que explorem a potencialidades das NMOBs na descoloração de resíduos líquidos.

2. Objetivos

2.1. Objetivos gerais

O objetivo geral da primeira parte do presente trabalho de doutorado compreende a execução da simulação do bioprocesso e da avaliação econômica da produção em escala industrial de NMOBs, prevendo oportunidades e desafios relacionados ao escalonamento do processo.

A segunda parte do trabalho teve como objetivo empregar NMOBs *in natura* extraídos de *Mv. blakemorei* cepa MV-1^{T} na descolorização do corante azul de metila na presença e na ausência de peróxido de hidrogênio, avaliando a cinética do processo e reusabilidade da nanopartícula.

2.2. Objetivos específicos

Os objetivos específicos da primeira parte deste trabalho compreendem:

a. Estimar uma escala de produção de NMOBs para suprir a demanda do mercado selecionado;

b. Modelar e simular um processo de produção de NPMs a partir de um bioprocesso;

c. Calcular os custos capitais e operacionais do bioprocesso, incluindo os preços de equipamentos e de fabricação;

d. Determinar preços de venda das NPMs produzidas pelo processo simulado;

e. Compreender os efeitos de variações nos fatores econômicos e operacionais sobre os custos de fabricação e preços de venda;

Os objetivos específicos da segunda parte são:

a. Realizar ensaios de degradação de azul de metila utilizando NMOBs obtidos de *Mv. blakemorei* cepa MV-1^{T} em diferentes condições experimentais;

b. Compreender os efeitos da concentração de NMOBs, pH de reação, presença de peróxido de hidrogênio e remoção de membrana sobre a eficiência de descoloração;

c. Determinar os modelos cinéticos das reações de degradação do corante testado;

d. Investigar a reutilização das NMOBs, avaliando-se a manutenção da atividade de descoloração;

e. Comparar as eficiências de remoção do azul de metila pelas NMOBs obtidas da cepa MV-1^{T} com aquelas de NMOBs obtidas de *Ms. gryphiswaldense* cepa MSR-1 e NPMs sintéticas;

3. Metodologia

3.1. Capacidade de produção

Para a simulação do bioprocesso, calculamos uma produção anual que fosse capaz de atender à demanda de nanopartículas de óxido de ferro da América Latina nas indústrias de meio ambiente e saúde. O cálculo está resumido no Anexo 1 e foi baseado no consumo internacional de nanopartículas de óxido de ferro.

3.2. Base do projeto

A planta foi simulada com uma subdivisão em três seções: inoculação, fermentação e recuperação de NMOBs. O microrganismo selecionado para a produção de NMOBs foi o *Ms. gryphiswaldense* cepa MSR-1.

3.3. *Software* de modelagem e simulação

Foi usado o *software* SuperPro Designer v9.0 (Intelligen, EUA) para modelagem e simulação dos processos nos cenários de batelada alimentada e semicontínuo como

reportado por Zhang e colaboradores (2011). As informações usadas para o projeto e os dados para alimentação do *software* de simulação estão detalhados no Anexo 1.

3.4. Dados e cálculos econômicos

Os dados econômicos foram selecionados para uma planta localizada no estado do Rio de Janeiro, Brasil. Os custos de capital e operacionais, incluindo os custos de equipamento e fabricação, foram calculados a partir de modelos embutidos do SuperPro Designer. Os preços mínimos de venda foram calculados para um tempo de retorno de cinco anos. Os preços e especificações dos materiais, utilidades e dados financeiros coletados para este estudo estão detalhados no Anexo 1.

3.5. Seção de inoculação

A seção de preparação do inóculo foi constituída por três biorreatores de tanque agitados em sequência com um fator de expansão de 10 até o volume do biorreator principal. O meio usado nesta seção foi o mesmo que o meio de fermentação.

3.6. Seção de fermentação

A fermentação assumida para a simulação foi do tipo batelada alimentada. Um tanque de preparação de meio foi alocado para a preparação dos meios de fermentação e alimentação. Foi necessário incluir a compressão de ar para o fornecimento de oxigênio em vazão baixa (0,002-0,003 vvm) durante o crescimento celular. O biorreator principal foi projetado para um volume total de 29 m^3, que deve conter o meio de fermentação inicial (~ 15 m^3) e volumes de alimentação adicionais, sem exceder 80% da capacidade do tanque. O pH inicial do meio de fermentação foi ajustado para a faixa de 6,8-7,0 e a temperatura foi ajustada para 30 °C.

As conduções de fermentação selecionadas, batelada alimentada em estágio único e cultivo semicontínuo, foram baseados no processo descrito por Zhang e colaboradores (2011), por apresentarem os maiores rendimentos de magnetita relatados na literatura.

3.7. Seção de recuperação de NMOBs

O processo simulado de extração de NMOBs foi baseado nos trabalhos de Guo et al. (2011) e Rosenfeldt et al. (2021). Informações detalhadas sobre a modelagem de extração estão disponíveis no Anexo 1. Basicamente, o meio proveniente do fermentador

foi transferido para um homogeneizador de alta pressão para a lise das células. O lisado celular foi, então, eluído por meio de uma CSM, cujo desenho é composto por uma coluna de alumínio com matriz magnetizável. A matriz foi feita de esferas de aço inoxidável de 2 mm de diâmetro magnetizáveis pela colocação de duas placas de neodímio externamente na coluna. O projeto da CSM encontra-se esboçado no Anexo 1, bem como o detalhamento de seus custos. Durante a separação, o concentrado magnético foi lavado com ureia 4 M para a remoção de proteínas residuais do lisado celular. O concentrado magnético foi posteriormente purificado por centrifugação. Em seguida, o concentrado foi eluído em uma segunda CSM para a remoção final das impurezas. O produto final foi um colóide magnético contendo 1 mg/mL de NMOBs em tampão fosfato 0,1 M.

3.8. Análises de sensibilidade

A influência das mudanças nas condições econômicas e operacionais foi estudada para ambos os processos de fermentação, alterando cada parâmetro dentro do software de modelagem e atualizando o balanço de materiais e cálculos econômicos.

3.9. Culturas bacterianas

Para a obtenção de NMOBs de *Mv. blakemorei* cepa MV-1^{T}, foi realizado um cultivo em biorreator (Minifors, Infors^{TM}, Basileia, Suíça) em modo quimiostato nas condições estabelecidas anteriormente pelo nosso grupo (Correa, 2019). A cultura de *Ms. gryphiswaldense* cepa MSR-1 foi realizada no mesmo biorreator com meio de cultivo e condições operacionais descritas por Heyen & Schuler (2003).

3.10. Lise de células bacterianas e extração de NMOBs

Após os cultivos em biorreator, as células de BMTs foram colhidas por centrifugação a 5.700 *x* g por 30 min a 4 °C e lisadas por tratamento ultrassônico seguindo o método de Cypriano et al. (2019).

3.11. Remoção de membrana

As membranas das NMOBs foram removidas de acordo com o método Yoshino e colaboradores (2008), o qual combina a remoção dos fosfolipídios por solvente orgânico e de proteínas por desnaturação alcalina.

3.12. Preparação de NPMs sintéticas

NPMs sintéticas foram preparadas pelo método de coprecipitação descrito por Santos e colaboradores (2018).

3.13. Microscopia eletrônica de transmissão

Todas as nanopartículas magnéticas testadas foram observadas em microscópio eletrônico de transmissão (FEI Morgagni, FEI Company, Hillsboro, OR, EUA) operado a 80 kV.

3.14. Ensaios de remoção de azul de metila

Foi investigada a remoção de azul de metila de solução aquosa, cuja concentração inicial era de 15 mg/L, através de experimentos cinéticos com duração de 10 min, examinando-se o desaparecimento da cor na solução. Os espectros de luz ultravioleta-visível do corante foram obtidos por varredura espectral (UV-1800, Shimadzu, Kyoto, Japão) na faixa de comprimento de onda entre 225 e 700 nm. A descoloração foi medida através de espectrofotometria em comprimento de onda de 600 nm em amostras coletadas em intervalos de 0, 1, 2, 3, 4, 5 e 10 min.

Os experimentos foram realizados variando-se a concentração de NMOBs (20, 40 e 80 mg/L), sem a adição de peróxido de hidrogênio. Em seguida, foram realizados experimentos com diferentes concentrações do peróxido (0, 18 e 36 mM) e diferentes valores de pH (4,8, 7,0 e 8,2). Também foram realizados experimentos utilizando-se as NMOBs cujas membranas foram removidas na presença e ausência do peróxido.

Por fim, dois experimentos comparativos, um utilizado NMOBs de *Ms. gryphiswaldense* cepa MSR-1 e outro utilizando NPMs sintéticas, foram realizados nas condições otimizadas nos experimentos anteriores. Todos os experimentos foram realizados em duplicata.

3.15. Reutilização e extravasamento de ferro

Após cada experimento de degradação, as NMOBs foram concentradas magneticamente, lavadas com água destilada e reutilizadas em novas reações de degradação. Os sobrenadantes separados foram usados na quantificação de ferro solúvel através do método colorimétrico da ferrozina (Viollier et al., 2000).

4. Artigos

O artigo "*Why does not nanotechnology go green? Bioprocess simulation and economics for bacterial-origin magnetite nanoparticles*" de autoria do candidato ao doutorado e coautoria do aluno de graduação Rogério Presciliano de Souza Filho e da orientadora Prof.ª Fernanda de Ávila Abreu foi aceito para publicação na revista *Frontiers in Microbiology* em julho de 2021.

O artigo "*Bacterial-origin magnetic nanoparticles for decolorization of methyl blue dye*" de autoria do candidato ao doutorado e de sua orientadora será submetido para publicação na revista *Journal of Environmental Chemical Engineering* após o depósito de patente referente à metodologia desenvolvida no trabalho.

Outros trabalhos publicados nesta tese estão apresentados como anexos e dizem respeito a revisões de literatura em assunto pertinente a esta tese.

4.1. *Why does not nanotechnology go green? Bioprocess simulation and economics for bacterial-origin magnetite nanoparticles.*

frontiers in Microbiology

ORIGINAL RESEARCH
published: 20 August 2021
doi: 10.3389/fmicb.2021.718232

Why Does Not Nanotechnology Go Green? Bioprocess Simulation and Economics for Bacterial-Origin Magnetite Nanoparticles

*Tarcisio Correa, Rogério Presciliano and Fernanda Abreu**

Laboratório de Biologia Celular e Magnetotaxia, Instituto de Microbiologia Paulo de Góes, Universidade Federal do Rio de Janeiro, Rio de Janeiro, Brazil

Nanotechnological developments, including fabrication and use of magnetic nanomaterials, are growing at a fast pace. Magnetic nanoparticles are exciting tools for use in healthcare, biological sensors, and environmental remediation. Due to better control over final-product characteristics and cleaner production, biogenic nanomagnets are preferable over synthetic ones for technological use. In this sense, the technical requirements and economic factors for setting up industrial production of magnetotactic bacteria (MTB)-derived nanomagnets were studied in the present work. Magnetite fabrication costs in a single-stage fed-batch and a semicontinuous process were US$ 10,372 and US$ 11,169 per kilogram, respectively. Depending on the variations of the production process, the minimum selling price for biogenic nanomagnets ranged between US$ 21 and US$ 120 per gram. Because these prices are consistently below commercial values for synthetic nanoparticles, we suggest that microbial production is competitive and constitutes an attractive alternative for a greener manufacturing of magnetic nanoparticles nanotools with versatile applicability.

Keywords: magnetotactic bacteria, magnetosomes, magnetic nanoparticles, biominerals, techno-economic analysis, process simulation, clean production

OPEN ACCESS

Edited by:
Lucian Constantin Staicu, University of Warsaw, Poland

Reviewed by:
Mihály Pósfai, University of Pannonia, Hungary
Juan C. Cruz, University of Los Andes, Colombia

****Correspondence:***
Fernanda Abreu
fernandaaabreu@micro.ufrj.br

Specialty section:
This article was submitted to Microbiological Chemistry and Geomicrobiology, a section of the journal Frontiers in Microbiology

Received: *31 May 2021*
Accepted: *20 July 2021*
Published: *20 August 2021*

Citation:
Correa T, Presciliano R and Abreu F (2021) Why Does Not Nanotechnology Go Green? Bioprocess Simulation and Economics for Bacterial-Origin Magnetite Nanoparticles. Front. Microbiol. 12:718232. doi: 10.3389/fmicb.2021.718232

INTRODUCTION

The global nanotechnology market is forecast to reach US$ 173 billion in 2025, with a large share of this growth boosted by environmental and biomedical sectors (Gharailou, 2019). One of the significant pillars of nanotechnology relies on magnetic nanoparticles. Revenues generated from iron oxide nanoparticles expand 11% annually, with a projection of US$ 5 billion in 2023 (Nano-Powder Factory, 2020). Clean manufacturing of high-quality nanoparticles must be achieved to sustain such growth and supply the increasing demand for innovative products and processes.

The magnetic-stimuli responsive character of iron-oxide nanoparticles enables their use in environmental remediation, biosensing, and healthcare (Kudr et al., 2017; Jiang et al., 2018). Explored roles of magnetic nanoparticles include but are not limited to oil and heavy metal adsorptive materials, drug delivery vectors, magnetic resonance contrast agents, theranostic agents for cancers and pollution, and pathogen detectors (Kudr et al., 2017; Jiang et al., 2018). However, in real-world applications, these materials require large-scale processes capable of delivering nanomagnets with controlled and reproducible characteristics (Tartaj et al., 2019).

An overwhelming number of published and patented methods were developed for obtaining magnetic nanoparticles through physical, chemical, and biotechnological routes (Krishnan et al., 2016; Tartaj et al., 2019; Abreu et al., 2020a). Within the latter category, magnetotactic bacteria (MTB) constitute the primary microbial magnetic nanoparticle source (Iravani and Varma, 2020). MTB are present in basically all aquatic environments, where they use chains of magnetic organelles as a compass to migrate in a directionally oriented manner (Abreu et al., 2020b). These magnetic structures, or magnetosomes, can be extracted from MTB cells and used as biological-origin magnetic nanoparticles (BMNs).

The intracellular formation of BMNs is a complex and genetically controlled biomineralization process (Correa et al., 2021). Genes responsible for BMNs biomineralization are clustered within the bacterial genome (Abreu et al., 2020b). Steps are iron capture from the environment and precipitation into iron mineral inside intracytoplasmic projections or vesicles formed from the internal bacterial membrane (Correa et al., 2021). The iron mineral composition, either magnetite (Fe_3O_4) or greigite (Fe_3S_4), generally depends on the MTB species (Abreu et al., 2020b; Correa et al., 2021). Due to the gene-level orchestrated biochemistry underlying BMNs formation, the mineral nanocrystals usually have narrow size dispersibility, consistent with a stable single magnetic domain, precise particle shape, and crystalline purity (Vargas et al., 2018; Abreu et al., 2020b). As iron biomineralization occurs within vesicles, each magnetic nanocrystal retains the membrane envelope after physical isolation processes (Vargas et al., 2018).

Applications for various technological purposes have been proposed for purified BMNs (Vargas et al., 2018). Most of these studies make use of magnetite BMNs isolated from MTB affiliated to the *Magnetospirillum* genus, which are cubooctahedral in morphology and whose diameters range between 30 and 40 nm (**Figure 1**; Pósfai et al., 2013). Besides phospholipids, proteins involved in biomineralization are also present in BMNs membranes. These proteins are the basis for surface functionalization of BMNs because they can be either chemically modified for insertion of drugs or antibodies or genetically fused with enzymes, antibodies, receptors, binding proteins, and stimuli-responsive peptides (Vargas et al., 2018). After functionalization, BMNs can integrate vaccine and drug formulations (Tang et al., 2012; Geng et al., 2019), immunomagnetic sensors for food pathogens (Xu et al., 2019; Sannigrahi et al., 2020), and cell sorting nanotools (Yoshino et al., 2008). Owing to heat generation by nanomagnets exposed to oscillating magnetic fields, BMNs have also been used in *in vivo* hyperthermal tumor inhibition (Alphandéry et al., 2019). In the environmental area, BMNs support recoverable and reusable catalysts for pesticide degradation (Ginet et al., 2011) and clean industrial processes (Honda et al., 2015). BMNs could also be used in the generation of clean energy (Smit et al., 2018).

The production of metallic nanoparticles by microbial factories, including MTB, has been extensively reviewed (Ahmad et al., 2019; Grasso et al., 2020; Iravani and Varma, 2020). One consensus is that biological nanomanufacturing of these materials is environmentally friendly because these processes do not usually rely on aggressive chemicals. For this reason, the mass production of nanomagnets through MTB-based bioprocessing is in strong agreement with UN's Sustainable Development Goal 9 to "upgrade infrastructure and retrofit industries to make them sustainable, with [. . .] greater adoption of clean and environmentally sound technologies and industrial processes" (United Nations (UN), 2020).

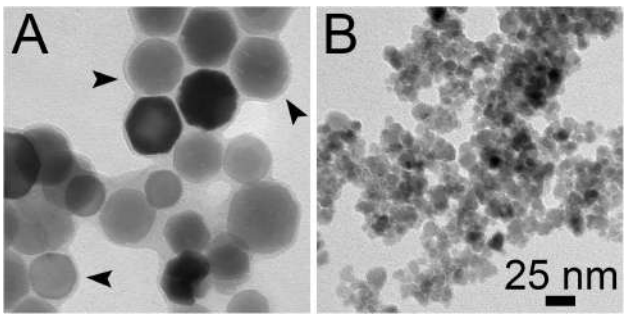

FIGURE 1 | Transmission electron microscopy images of BMNs isolated from a *Magnetospirillum gryphiswaldense* strain MSR-1 **(A)** and synthetic iron oxide nanoparticles **(B)** prepared by co-precipitation (Santos et al., 2018). Arrowheads indicate external BMN membrane, which is retained after isolation process.

Multiple studies have been dedicated to increasing BMNs throughput in bioreactors (3–70 L) MTB cultures (Silva et al., 2013; Basit et al., 2020; Berny et al., 2020). The main challenges concerning the cultivation of MTB in large volumes are the microaerophilic metabolism of this group, relatively slow growth rates, and specific nutritional requirements, in addition to BMNs yields in the order of mg/L (Ali et al., 2017; Basit et al., 2020). Strategies like optimizing oxygen supply and balanced nutrient injection, have been attempted to address such hurdles and led to improved production yields (Liu et al., 2010; Zhang et al., 2011; Fernández-Castané et al., 2018). However, modeling production on a pilot and industrial scale is yet to be done. Thus, given all the applicability and green production of BMNs, we have performed bioprocess simulation and approximate economic assessment of BMNs production at industrial scales. The techno-economic analysis may help identify process opportunities and challenges and is necessary before upgrading BMNs production to industrial levels.

MATERIALS AND METHODS

Production Scale

Our selected process throughput has been calculated to meet the demand of iron oxide nanoparticles of Latin America in environmental and healthcare industries. The calculation is summarized in **Supplementary Table 1** and was based on the International consumption of iron oxide nanoparticles (**Figure 2**; Nano-Powder Factory, 2020) and the number of registered nanoproducts (**Supplementary Figure 1**; StatNano, 2020).

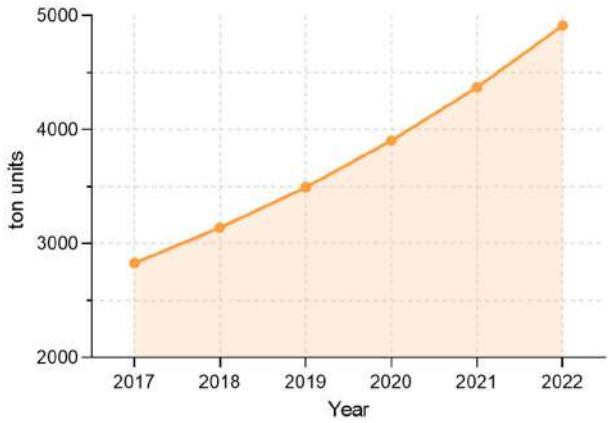

FIGURE 2 | Growth in international consumption of iron-oxide nanoparticles over the years of 2017–2022. Data from Nano-Powder Factory (2020).

Design Basis

The simulated plant comprises three sections: an inoculum train, a fermentation section, and a downstream BMN recovery section. The magnetotactic spirillum *Magnetospirillum gryphiswaldense* strain MSR-1 was chosen as the BMNs-producing microorganism. MSR-1 cells are microaerophilic and produce chains of cubooctahedral magnetite BMNs with a ∼35 nm diameter (Schüler et al., 2020). For transmission electron microscopy images displayed here, cells were deposited on formvar-coated copper grids and observed on a FEI Morgagni transmission electron microscope (Hillsboro, OR, United States) operating at 80 kV.

Modeling and Simulation Software

SuperPro Designer v9.0 (Intelligen, United States) was used for process modeling and simulation in both single-stage fed-batch and semicontinuous scenarios, as well as the proposed variations considered to sensitivity analyses. Information used for process design and data input to simulation software is detailed in the next subsections.

Economic Data and Calculation

The economic data were selected for a plant located in the state of Rio de Janeiro, Brazil. Capital and operational costs, including equipment and fabrication cost, were calculated using built-in models of SuperPro Designer, which are based on the methodology described in **Supplementary Tables 2, 3**. Minimum selling prices (MSP) were determined as stipulated by Seider et al. (2016) for a fixed payback time of 5 years. For that, we performed multiple economic calculations on SuperPro Designer using different hypothetical selling prices (US$ 30–120 thousand/kg Fe_3O_4). Materials, utilities, and financial data collected for this study are detailed in **Supplementary Tables 4–9**.

Upstream Section

The inoculum train was composed of three consecutive seed bioreactors with an expansion factor of 10 up to the volume of the main bioreactor (see section "Fermentation section"). The medium used in this section was the same as the fermentation medium.

Fermentation Section

Fermentation was assumed to be conducted in a fed-batch, as summarized in **Table 1**. A medium preparation tank was allocated for the preparation of both fermentation and feeding media. Air compression was required for low-rate oxygen supplying (0.002–0.003 vvm) during cell growth. The principal bioreactor was designed to a total volume of 29 m^3, which must contain the initial fermentation medium (∼15 m^3) and additional feeding volumes without exceeding 80% of the vessel capacity. The initial pH of the fermentation medium was set to the range 6.8–7.0 and temperature should be kept at 30°C.

The selected fermentation designs, single-stage and semicontinuous, were based on the process described by Zhang et al. (2011) for having the highest reported magnetite yield in literature. The single-stage process was a fed-batch carried in a fermentation medium (Zhang et al., 2011). The feeding medium contained an iron source for magnetite synthesis (iron chloride) and lactic acid as the main carbon source, among other nutrients. The feeding regime was based on the pH change in culture media during cell growth. As cell growth leads to alkalinization in the culture medium, appropriate automatic pH control is necessary. Due to the high concentration of lactic acid, which causes a pH of 2.5–3.0, the feeding medium was supplied to fermentation media in response to increases in pH.

In semicontinuous operation, cultivation is carried out for 40–44 h (first stage) and then, 90% of the fermentation medium is removed to the downstream section (Zhang et al., 2011). Afterward, the original fermentation volume is restored with the addition of sterile fermentation media to the remaining 10% first stage medium. The second stage is started as a fed-batch in the same manner as the first one.

The highest yield of BMNs reported for a large-scale process (356.52 mg/L) was reached in a single-stage fermentation in a 42-L bioreactor for 44 h (Zhang et al., 2011). Nevertheless, this value was associated with a single fermentation and, to our knowledge, such yield has not been reproduced in literature. Other yields reported by the same paper were lower (225–280 mg/L) when cells were cultured in 7.5-L for 40–44 h under an identical fed-batch regime. For this reason, we assumed a yield of 250 mg/L

TABLE 1 | Parameters considered for simulation–fermentation section (base case).

Parameter	Value	References
Fermentation time	42 h	Zhang et al., 2011
Fermentation temperature	30°C	Zhang et al., 2011
pH	6.8–7.0	Zhang et al., 2011
Growth rate (μ)	0.01	Zhang et al., 2011
Aeration rate	0.003 vvm	Zhang et al., 2011
Production of Fe_3O_4	250 mg/L	Zhang et al., 2011
Volume of the main fermenter	29 m^3	Modeled
Maximum working volume	80%	Modeled
Vessel material	Stainless steel 316	Assumed

within 42 h for our base-case simulation. Jajan et al. (2019) reported the production of 186 mg/L of BMNs, which was close to our assumed value and supports a more realistic simulation. The specific cell growth (μ) was calculated from Zhang et al. (2011) and equals 0.10.

The fermentation stoichiometry and molecular formula for *Ms. gryphiswaldense* strain MSR-1 were described in Naresh et al. (2012). The global equation for bacterial growth is:

$$352\ C_3H_6O_3 + 33.6\ NO_3^- + 133\ NH_4^+ + 6.46\ O_2 + 1.25\ Fe^{3+} \rightarrow 718.4\ MTB + 591.3\ H_2O + 314\ CO_2$$

While the molecular formula for the magnetotactic bacterium (MTB) is $CH_{2.06}O_{0.13}N_{0.28}Fe_{0.00174}$.

Downstream Section

Biological-origin magnetic nanoparticles (BMNs) extraction was based on Guo et al. (2011) and Rosenfeldt et al. (2020). The assumed simulation parameters for this section are summarized in **Table 2**. Detailed information on the modeling of the downstream section is available in **Supplementary Material**. Fermented medium was transferred from the bioreactor vessel to a high-pressure homogenizer for cell crushing. The cell lysate was, then, eluted through a magnetic separation column (MSC), whose design is comprised of an aluminum column with a magnetizable matrix. The matrix was made of 2-mm diameter stainless steel beads that can be magnetized by placing two neodymium plates externally onto the column. MSC design was sketched in **Supplementary Figure 2** and its costing details are described in **Supplementary Table 7**. During separation, the magnetic concentrate was washed with 4 M urea for the removal of residual proteins from cell lysate. The magnetic concentrate was further purified by disk-stack centrifugation, which concentrates 90% of BMNs. As in Rosenfeldt et al. (2020), sucrose syrup was mixed to the magnetic concentrate before centrifugation for retention of cell residues. Afterward, the concentrate was eluted in a second MSC, for the final removal of impurities. The final product was a magnetic colloid containing 1 mg/mL BMNs suspended in a phosphate buffer.

TABLE 2 | Parameters considered for simulation–downstream section (base case).

Parameter	Value	References
Number of passes at high pressure homogenizer	4	Rosenfeldt et al., 2020
Magnetic separation column (MSC) matrix	Stainless steel 2-mm beads	Adapted from Guo et al. (2011)
Binding capacity of MSC matrix	85%	Estimated from Guo et al. (2011) and Rosenfeldt et al. (2020)
MSC material	Aluminum + neodymium plates	Assumed
MSC flowrate	3 bed volumes/h	Assumed
Centrifuge sedimentation efficiency	90%	Assumed

Sensitivity Analyses

The influence of changes in economic and operational conditions was studied for both fermentation processes by altering each parameter within modeling software and updating material balance and economic calculations.

RESULTS

The plant capacity assumed from the market study calculations is 640 kg BMNs per year in our base case. From the assumptions described throughout the methodology section, our process flowsheet was designed in SuperPro and is displayed in **Figure 3**. Plant and operating costs are summarized in **Table 3**, as well as batch scheduling information. From the initial project investment, approximately 20% is for equipment purchase in both single-stage and semicontinuous. The remaining project investment is directed to plant engineering and construction, including equipment installation, electrical setup, and piping. The main bioreactor of the fermentation sector represents 30.6% of all equipment cost in a single-stage setting (**Supplementary Table 8**) and 38.2% in semicontinuous (**Supplementary Table 9**).

Operating costs breakdowns for single stage (US$ 6.64 million/year) and semicontinuous (US$ 7.15 million/year) modes are summarized in **Figure 4**. However, for both cases, indirect operating costs (i.e., maintenance, equipment depreciation, local taxes, etc.) are 3–4 times higher (**Figure 4A**) than direct costs (i.e., raw material, labor, quality control, etc.). In single-stage, about half the operating costs are related to the fermentation section, whereas this share increases at 7% in semicontinuous (**Figure 4B**). In both operation modes, material costs represent more than half the direct operating costs (**Figure 4C**). Although total operating costs are higher in semicontinuous mode, direct operating costs are slightly higher in a single stage. This is caused by a 9% growth in labor-dependent cost in a single stage. Lactic acid and urea represent the highest share of material costs in fermentation (64%) and downstream (87%) sections, respectively (**Figures 4D,E**).

Considering the scenarios listed in **Table 1**, MSPs of BMNs are US$ 36.7 and 50.9 thousand/kg Fe_3O_4 for single-stage and semicontinuous processes, respectively (**Figure 5**). Sensitivity analyses indicate economic parameters (material costs, dollar/real exchange rates) seem to have a more slight effect on operating costs and MSP of BMNs than operational and microbial parameters (**Figure 6** and **Supplementary Figure 3**). For example, while a variation from US$ 0.05 to 0.75 in the urea purchasing price caused the operating costs to fall between US$ 9,700 and 12,000/kg (**Figure 6A** and **Supplementary Figure 3A**), a magnetite yield of 80 mg/mL might raise operating costs to US$ 32,000 (**Figure 6B** and **Supplementary Figure 3B**).

DISCUSSION

In recent years, Latin American countries have focused on nanotechnology as a stimulus for economic growth through the production of nanometric materials and incorporation

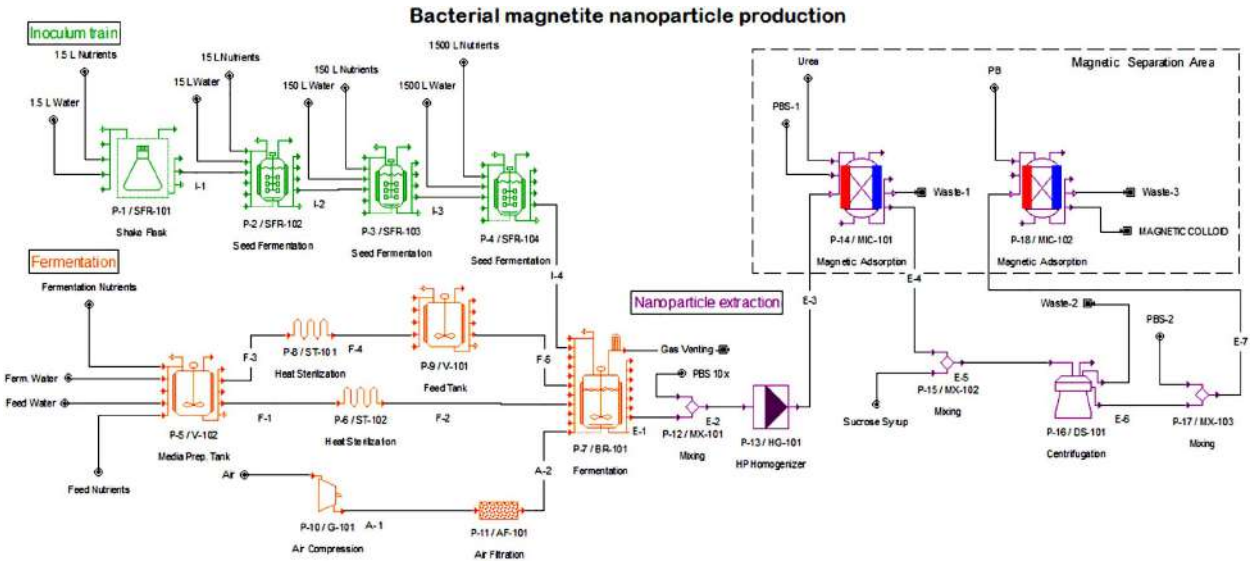

FIGURE 3 | Process flowsheet for the biomanufacturing of BMNs. The flowsheet depicts unit operations and material flows simulated in this work. The overall process is divided into three sections: the inoculum preparation train (in green) with four sequential scale-up steps, 3L (P-1), 30L (P-2), 300L (P-3), and 3000L (P-4), the fermentation (P-7), including media preparation (P-5), sterilization (P-6 and P-8), storage (P-9), air compression (P-10) and filtration (P-11) (in orange) and the downstream BMN extraction, including operations for cell lysis (P-12 and P-13), centrifugation (P-15 and P-16), and magnetic separation (P-14, P-17, and P-18) (in purple).

of nanotechnological tools into industrial processes and products (StatNano, 2016). Despite the share of registered nanotechnological products in the region is still small (2.4%), programs like the Brazilian Initiative for Nanotechnology (Ministério da Ciência, Tecnologia, Inovações e Comunicações (MCTI), 2019) and the Argentine Foundation of Nanotechnology (Fundación Argentina de Nanotecnología (FAN), 2020) are examples of government-led support for an expansion in the nanotechnological industry.

In our assessment, indirect operating costs represented 76–79% of all operating costs due to facility-related expenditures. Usually, facility-related costs represent 10–70% of operating costs while direct costs account for 50% of the total (Harrison et al., 2015). In the Brazilian market, prices of raw material from local suppliers, utilities, and salaries tend to be lowered in comparison to US prices due to the exchange rate in recent years (US$ 1 = R$ 5.20 in June, 2020). In a process simulation for glucosidase production (da Gama-Ferreira et al., 2018), a low direct cost accounting (23–25%) was also attributed to Brazilian market conditions and real-dollar exchange rate. Moreover, as our bioprocess requires large equipment volumes, especially in the fermentation section (**Supplementary Tables 8, 9**), maintenance and depreciation costs are substantially higher than low-cost bacterial growth media components (**Supplementary Table 4**).

TABLE 3 | Overall bioprocess parameters and economic evaluation summary.

	Single stage	Semicontinuous
Annual operating time (h)	7,200	
Recipe batch time (h)	161.7	193.1
Recipe cycle time (h)	46.67	85.75
Number of batches per year	151	82
Annual Fe_3O_4 throughput (kg)	640	
Capital investment	52.11	79.86
Total plant cost (US$ millions)	43.03	66.02
Equipment cost (US$ millions)	8.90	12.89
Operating cost (US$ millions/year)	6.64	7.15
Unit production cost (US$/kg Fe_3O_4)	10,372	11,169

While the fermentation section spends the higher fraction of operating costs, BMN recovery accounted for only 22–29%. The magnetic nature of magnetite crystals along with its high density (5.18 g/cm^3) facilitates their separation from cell lysate during the downstream section. These material properties have facilitated the development of continuous, large-scale strategies for BMN recovery (Guo et al., 2011; Rosenfeldt et al., 2020). The simple design of MSC (**Supplementary Figure 2**) is associated with low purchase and installation costs (**Supplementary Tables 7–9**). Additionally, the durability of the magnetizable separation matrix reduces the necessity of operational intervention and maintenance within the downstream section.

The increase of 7.7% in the cost for the fabrication of one ton of BMNs by semicontinuous operation in relation to single-stage (**Figure 4**) is attributed to an over 50% decrease in magnetite yields during the second stage (Zhang et al., 2011). This reduction is probably because a deacceleration in bacterial growth is observed when cultivation occurs in oxygen levels under 1% and high iron concentrations (Sun et al., 2008; Liu et al., 2010), in which magnetosome synthesis is favored metabolically (Wang et al., 2016). Furthermore, as shown in **Figure 4A** the higher operating costs in semicontinuous are driven by the greater indirect operating costs. The total medium volume per batch in

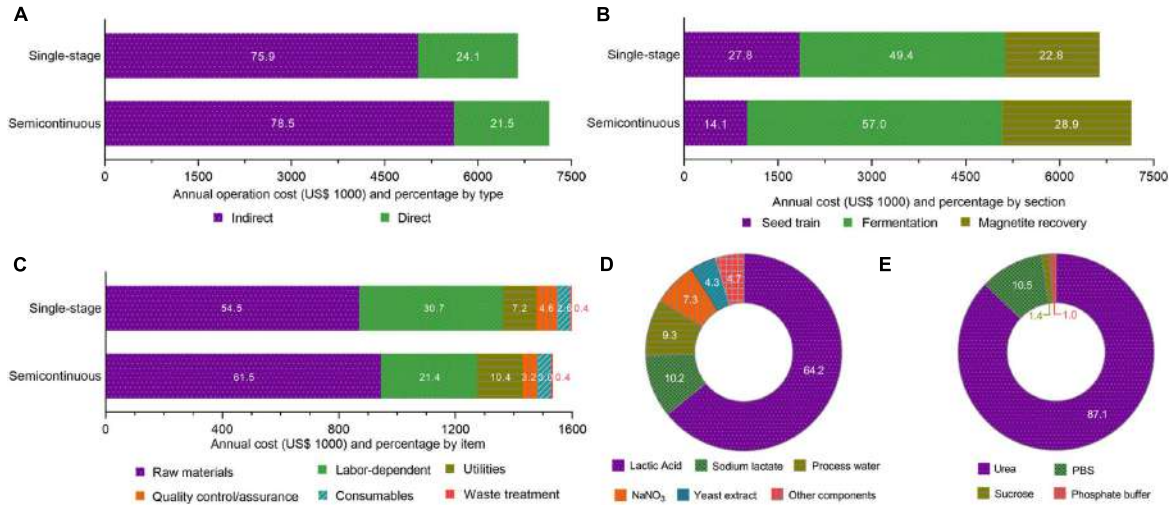

FIGURE 4 | Annual operating costs composition breakdowns. Single-stage and semicontinuous cultivation cost contributions from direct and indirect costs **(A)** and process sections **(B)**. Direct operating costs breakdown showing cost types **(C)**. Material costs compositions from fermentation **(D)** and downstream sections **(E)**.

semicontinuous cultivation is about twice that in a single stage. This increase leads to a necessity of larger and/or multiple pieces of equipment for medium preparation, fermentation, and cell lysis (**Supplementary Table 9**). Consequently, an escalation in equipment-related costs is observed.

On the other hand, the observed increase in direct operating costs in a single stage (**Figure 4C**) is caused by a growth in labor-related demand. This additional demand is explained by a more frequent necessity of operator-supervised inoculation and cleaning-in-place procedures within a year. In semicontinuous cultivation, batch and cycle times are longer because two fermentation stages are conducted from a single inoculation. Therefore, semicontinuous operation demands fewer manual steps per mass of fabricated BMNs than those for a single stage. Our sensitivity analyses (**Figure 6** and **Supplementary Figure 3**) indicate that the proposed bioprocess costs and selling prices are robust to even drastic variations in raw material prices and the dollar-real exchange rate. The minor contribution of materials and utilities to fabrication costs seems to buffer the effect of such variations. Nevertheless, microbial growth and magnetite production have more pronounced pressure on process prices. A 50% reduction in magnetite production doubles production costs and MSP and a 30% reduction in growth rate increases these costs by a factor of 2.5. Such instability might have important implications in process upscaling projects because dramatic differences in the production of magnetite are reported for MTB cultivation processes. For example, while Zhang et al. (2011) reported a 356 mg/L yield, Liu et al. (2010), which used a similar pH-coupled feeding strategy, achieved a magnetite production of only 83.2 mg/L.

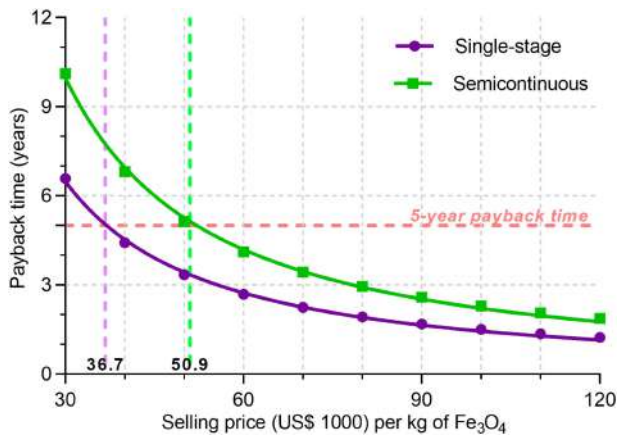

FIGURE 5 | Correlation between selling prices of BMNs and the investment payback time for each bioprocess. The salmon horizontal dashed line indicates the 5-year payback time limit for which MSPs are determined. Vertical dashed lines indicate MSPs for single-stage (purple line, US$ 36.7 thousand) and semicontinuous (green line, US$ 50.9 thousand) processes.

Understanding process cost perturbations due to cultures yields are crucial for process scale-up. Yields obtained in small-scale are not always reproduced in plant scale due to factors, including shear forces, medium homogeneity, and gas diffusion (Mahdinia et al., 2019). As, to our knowledge, MTB cultivation has only been performed in bioreactors of up to 70 L (Berny et al., 2020), there is still a lack of information on process performance in m^3-scales for industrial production. For example, the maintenance of proper microaerophilic or anaerobic conditions for biomineralization, which requires sophisticated control strategies in bench-scale cultivation (Sun et al., 2008; Liu et al., 2010), can be more challenging in larger volumes and might directly affect BMN production. Thus, previous knowledge on the sensitivity to magnetite yields is fundamental for risk assessment associated with processing scale-up. Recently, a molecular engineering tool was used to increase BMN production in *Magnetospirillum magneticum* strain AMB-1 (Arakaki et al., 2020). The technique consisted of inserting

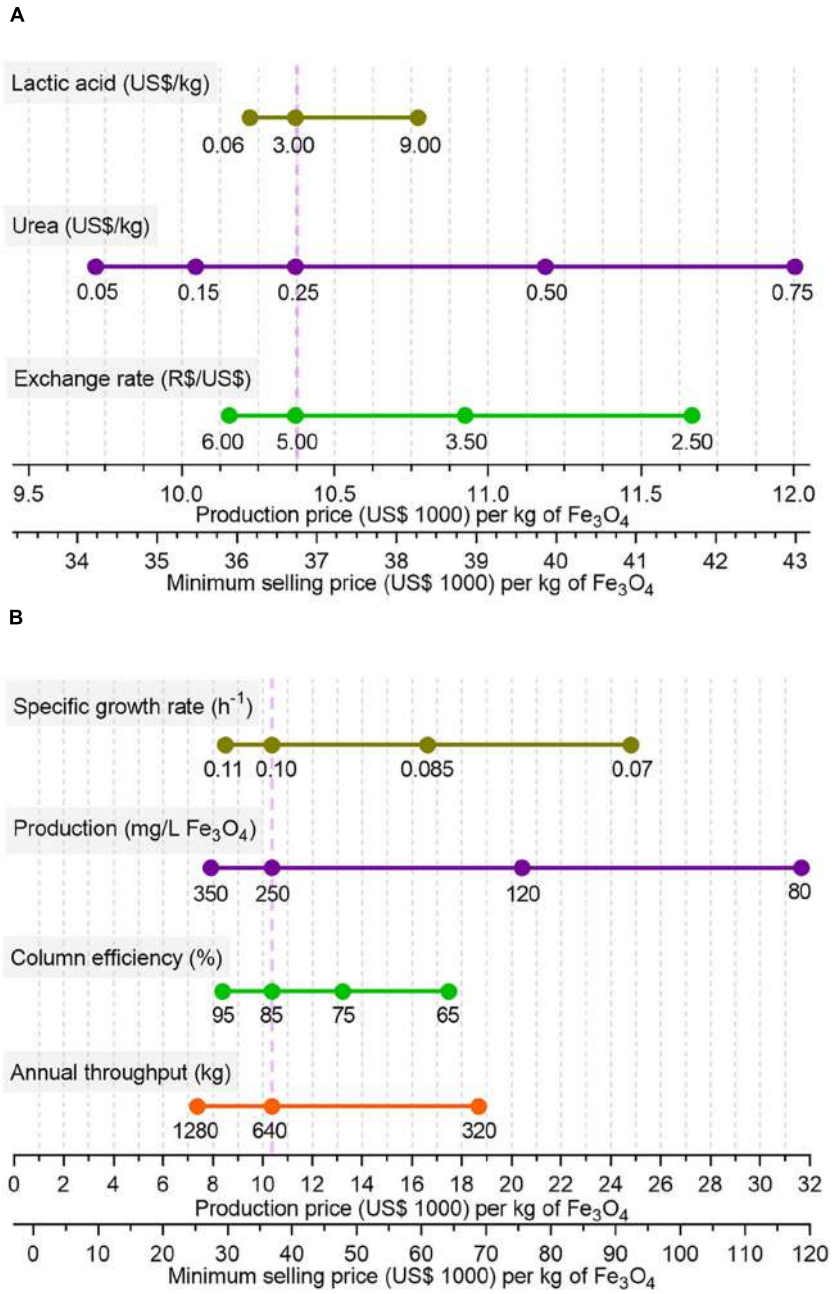

FIGURE 6 | Sensitivity analyses showing effects of variations in market **(A)** and bioprocess-related parameters **(B)** on unitary production costs and minimum selling prices (MSP) for the single-stage process, when one of those individual parameters oscillate from the base-case (purple dashed vertical line). The results of variations in purchase price of two important feedstocks (lactic acid and urea) and fluctuations of the exchange ratio on the final production price are analyzed in panel **(A)**. The effects of specific cell growth rate of *Ms. gryphiswaldense* MSR-1 in fermentation tanks, as well as its magnetite production rate, are analyzed in panel **(B)**. The efficiency in BMN extraction by the MSCs and the plant annual throughput capacity, in terms of total produced magnetite, are also assessed in panel **(B)**. The purple dashed vertical line indicates base-case scenario whose parameters are described in **Tables 1**, **2**.

a plasmid containing a gene region responsible for magnetic BMN synthesis. The transformed AMB-1 cells were able to double their intracellular BMNs number from 21.9 ± 3.5 to 44.4 ± 9.1. In a 10-L fermentation, a 14.6 increase in BMN production was observed for the transformed strain in relation to the wild type. This achievement provides a powerful tool to keep high-producing MTB cells in the industry without affecting process economics.

The efficiency of MSC in recovering BMNs also exert a considerable influence on process economics. An efficiency of 65% might raise the production cost to US$ 18,000/kg (**Figure 6B**). As the performance of the cubic-meter scale, MSC

might be significantly different from the bench-scale apparatus, possible variations in separation must be evaluated. In our simulation, the reduction in the diameter of magnetizable beads from our reference work might prevent reductions in magnetic separation capacity by increasing the matrix surface area.

Alternative annual process throughputs were also investigated in the sensitivity analysis. During project development, the production demand might expand to other regions or industrial sectors or be restricted to a more local market. Interestingly, duplication in the plant processing capacity leads to a 25% drop in production price but when it is half our base case production price and MSP reaches almost US$ 19,000/kg (**Figure 6B**).

Our base-case production cost (US$ 10,372/kg) is still higher than those for magnetite nanoparticles produced by chemical processes (**Figure 7** and **Table 4**). Augusto et al. (2020) reported a technical-economic analysis for the fabrication of bare magnetite nanoparticles produced by co-precipitation and carbon-coated nanoparticles synthesized by hydrothermal precipitation. Fabrication costs for the latter nanomaterials are twenty times higher because of the finer control over final product characteristics, like size and shape uniformity and biocompatible coating (Augusto et al., 2020). The calculated material cost for co-precipitation was eighteen times smaller than in our process (**Table 4**), yet it represented 68% of direct operational costs (**Supplementary Figures 4A,B**). However, hydrothermal synthesis shows both a material cost (**Table 4**) and its relative participation on direct operational costs (**Supplementary Figure 4**) very similar to the bioprocesses. These results indicate that despite expenditures in feedstocks are very close to other processes, non-material costs are the main factors distinguishing bioprocess economics from chemical fabrication. This finding is further supported by the bigger proportion related to direct costs–54.9% for co-precipitation and 68.3% for hydrothermal–among total operational costs (**Supplementary Figure 4A**) in chemical processing. Accordingly, equipment costs in chemical syntheses are about 6–12 times lower than those in our process (**Table 4**). Thus, chemical synthesis presents a significantly lower operational cost. Another aspect to be considered in the techno-economic analysis is the energy consumption by the studied processes. BMN bioprocess shows a power consumption intermediary to co-precipitation and hydrothermal syntheses (**Supplementary Table 10**). As the latter is related to better control of nanoparticle characteristics, energy demand is directly correlated to the quality of the nanoproducts. In this way, BMN production is energy-efficient because even at consumption lower than a chemical process, bioproduction yields high-quality nanomagnets. Despite our product prices are higher than in chemical manufacturing, our MSP (US$ 21–120/g) still ranges significantly lower than commercial prices of most synthetic iron oxide nanoparticles of similar sizes (**Figure 7** and **Supplementary Table 11**). Nanoparticles traded as "iron oxide nanopowders" are significantly cheaper, but often display poor size and shape distribution (refer to websites listed on **Supplementary Table 11**), similarly to those in **Figure 1B**. Bare magnetite nanoparticles prices are US$ 10,000–11,000/kg, values that can be 80–500 times our MSP. BMNs membrane displays a range of functional groups (e.g., ammine, phosphate, and carboxyl) that facilitates surface modification. Average prices for ammine-, PEG- and carboxyl-coated nanomagnets are approximately US$ 40,000, 32,000, and 100,000/kg. Hence, BMNs have a competitive potential for market entry in terms of commercial costing, even if process-related perturbations result in increases in MSP. The discrepancy between MSP and the market price of synthetic nanoparticles also allows an increase in sale prices, which decreases the investment payback time (**Figure 5**) and increases the return on investment in the project as well as the revenues generated.

Production of genetically engineered BMNs designed for specific applications have been successfully performed and might increase BMN competitivity in the nanotechnological market. Recently, the modification of both mineral characteristics (morphology and size) and surface coating can be modulated by genetic engineering (Furubayashi et al., 2020). BMNs expressing protein A on their surface were produced for the detection of pathogens and pollutants molecules (Xu et al., 2019). Applications proofs showed that, when bound to specific antibodies, the nanocomplex could be used for high-sensitivity detection of *Vibrio parahaemolyticus* (detection limit = 5 CFU/mL) and gentamicin (0.01 ng/mL). Costs calculated for their production in a 42-L fed-batch revealed the BMNs-protein A complexes incredibly inexpensive (US$ 0.067/mg) when compared to commercial immunomagnetic beads (US$ 3 or more).

Commercial catalogs of iron-oxide nanoparticles show some properties of their products: size dispersion, zeta potential (Zp), magnetization saturation (Ms), and purity (**Supplementary Table 11**). It is well-documented that BMNs show a narrow size distribution due to genetic-level controlled biomineralization. Because size and shape directly influence magnetic properties, like Ms (Mirabello et al., 2016), uniformity in those characteristics ensures reproducibility in applicability outcomes. Ms of BMNs is reportedly higher (61 emu/g at 290 K–Timko et al., 2009) than commercial nanomagnets (20–50 emu/g). In nanomagnetism, higher Ms values are related to better responsiveness to magnetic fields and higher heating properties in magnetically induced hyperthermia (Abenojar et al., 2016). Indeed, the heating capacity of BMNs has been examined and is compatible with hyperthermal treatments (Timko et al., 2009). Furthermore, BMNs display a very similar Zp (−38 to −25 mV–Geng et al., 2019; Xu et al., 2019) to carboxyl iron-oxide nanoparticles (−35 to −15 mV). This property ensures good colloidal stability of magnetic suspension due to electrostatic repulsion between nanoparticles (Bhattacharjee, 2016). BMNs are single-domain magnetic materials (Abreu et al., 2020b) and those repulsive interactions prevent particle aggregation, which could otherwise hinder applicability.

Although the process requires an entire downstream section dedicated to BMN recovery, the final nanoproduct retains its external membrane. Hence, additional coating procedures, often present in chemical production (Zhang et al., 2012; Augusto et al., 2020; Pinelli et al., 2020), are dispensed. The natural membrane envelope found in BMNs improves biocompatibility characteristics by reducing toxicity against human and animal cells and the environment (Revathy et al., 2017). The low affinity

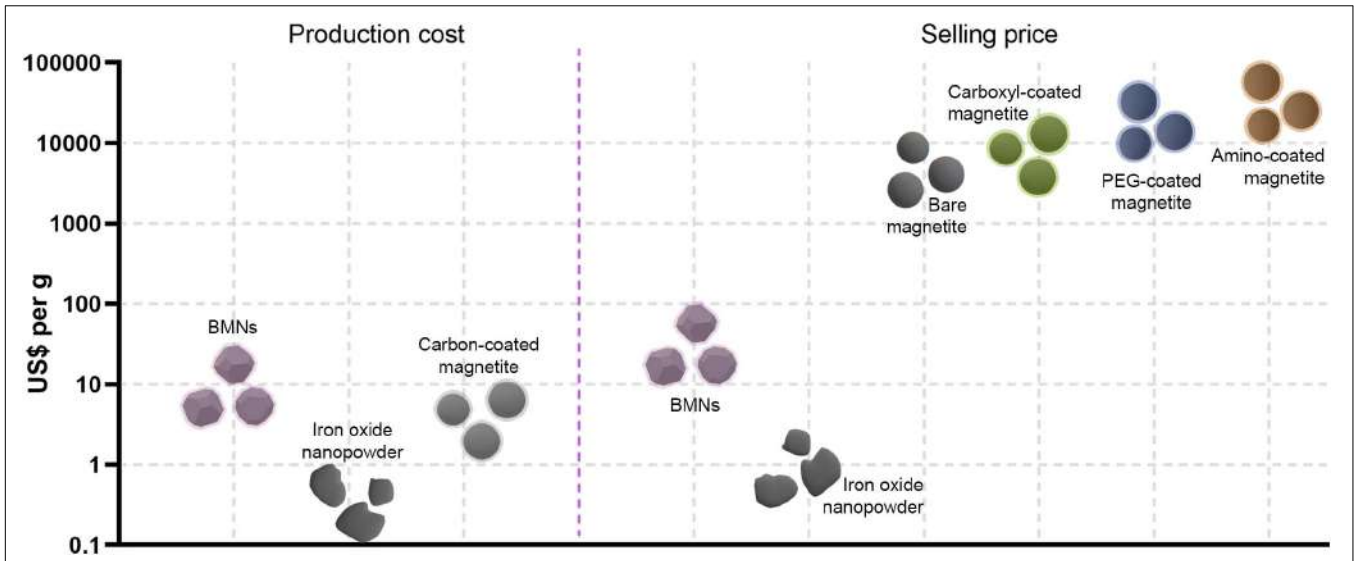

FIGURE 7 | Comparison between production costs (left of dashed vertical line) and market selling prices (right of vertical dashed line) of BMNs and chemically manufactured magnetite nanoparticles, with and without coating. For BMNs, we considered MSPs for market prices. For commercial magnetic nanoparticles, we considered production prices reported by Augusto et al. (2020). For details on the characteristics and suppliers of commercial magnetic nanoparticles, please refer to **Supplementary Table 11**.

TABLE 4 | Comparison between production costs for biogenic and synthetic magnetic nanoparticles.

Nanoparticle	Preparation method	Production costs (US$/kg Fe_3O_4)	Material costs (US$/kg Fe_3O_4)	Equipment costs (US$ millions)	References
Biological-origin magnetic nanoparticles (BMNs)	Single stage	10,372	1,472	8,898	Present work
BMNs	Semicontinuous	11,169	1,477	12,888	Present work
Bare magnetite	Co-precipitation	210	78	1,036	Augusto et al., 2020
Carbon-coated magnetite	Hydrothermal	4,192	1,361	2,027	Augusto et al., 2020

between phospholipids and iron oxide nanometric surfaces poses a technical hurdle for the artificial membrane coating of synthetic nanoparticles (Pinelli et al., 2020).

The effect and the fate of BMNs in the human organism is a primary source of concern regarding biomedical applications such as drug delivery and MRI contrasting. As with other bacterial-derived products, one great concern surrounding BMN biomedical utilization is the contamination with bacterial endotoxins, most notably LPS (World Health Organization (WHO), 2020). Given all known MTB are Gram-negative (Abreu et al., 2020b), residual LPS from cell lysis procedures might persist and invalidate use in healthcare. Nevertheless, laboratory-scale isolation procedures, like ultrasonic crushing and alkaline washing, greatly reduces endotoxin contamination in BMNs to levels compared to chemically synthesized iron oxide nanoparticles (Mandawala et al., 2017). Moreover, the MSC-based BMN extraction has shown efficiencies of up to 99.7% in the removal of cell debris (Rosenfeldt et al., 2020). Recently, a long-term (135 days) *in vivo* study on the biocompatibility of BMNs, showed that even at concentrations 10–50 times higher than previously tested for synthetic nanoparticles, tissue damage was negligible. This biocompatibility trend was maintained even in the liver and spleen where BMN concentration was greater (Nan et al., 2021). The same work also suggested that BMN clearance from the body occurred through biliary excretion, within 1 week from administration, and urinary excretion, up to 120 days (Nan et al., 2021). Given these elimination routes are already well-described for other drugs (Bardal et al., 2011), the pharmacological behavior of BMNs becomes more predictable.

The present work was elaborated in the year 2020 when the COVID-19 pandemic took place. Effects of the pandemic on the global economy may cast some uncertainty on market estimates reported here. However, the production of eco-friendly, bacterial-gestated multipurpose nanoparticles might constitute a valuable opportunity for the urgent sustainable recovery of the Latin American economy (León and Cárdenas, 2020). As an example, a team from Yachay Tech University, in Ecuador, developed a cheap and efficient poly-amino-ester for the extraction of RNA from SARS-Cov-2 preliminarily to PCR testing (Chacón-Torres et al., 2020). As discussed earlier, BMNs are effectively used in highly sensitive pathogen detection technologies through magnetically based cell/antigen concentration (Vargas et al., 2018; Xu et al., 2019). This relatively easy applicability, along with its

low production prices and reproducible physical characteristics, makes BMNs obvious candidates for large-scale use in pandemic control purposes.

The techno-economic assessment of large-scale production of microbial nanomagnets gives a preliminary yet valuable understanding of how feasible the supplying of these promising materials for technological applications is. In the final analysis, the base production cost BMNs (US$ 10–11 thousand/kg Fe_3O_4) is 2.5–53 times higher than the chemical production of bare magnetite nanoparticles depending on the process. This difference is mainly because of indirect operating costs (76–79% of total process costs), which derive from higher equipment purchase costs (6–12 times higher) and labor for maintaining a bioprocess. Production costs and selling prices are significantly influenced by operational parameters (e.g., bacterial magnetite production) but only slightly altered by external economic factors, like material purchase prices. Still, the strong discrepancy between production costs and selling prices of coated artificial magnetite nanoparticles (US$ 11–40 thousand/g) enables BMNs to have economically attractive prices (US$ 21–120/g of MSP). Therefore, it is possible to sell BMNs at values higher than MSP to reduce investment payback time and maximize profits. Due to the superior characteristics of BMNs in relation to synthetic nanoparticles and cleaner production, the bioproduction costs are justifiably higher than chemical manufacturing. Considering the direct functionalization of BMNs due to their natural membrane and the possibility of customizing BMNs through genetic engineering, biogenic nanoparticles are applicable for diverse purposes. Moreover, the industrial production of BMNs might have improved yields either by genetic engineering of known strains of MTB or uncovering new culturable strains with more efficient metabolisms.

DATA AVAILABILITY STATEMENT

The original contributions presented in the study are included in the article/**Supplementary Material**, further inquiries can be directed to the corresponding author/s.

AUTHOR CONTRIBUTIONS

TC executed the process simulation and economic/sensitivity analyses and wrote most of the manuscript. RP contributed to the simulation and economic/sensitivity analysis. FA planned the study design, revised the data presented, wrote and edited the manuscript. All authors contributed to the article and approved the submitted version.

FUNDING

This study was financed in part by the Coordenação de Aperfeiçoamento de Pessoal de Nível Superior–Brasil (CAPES)–Finance Code 001. This work was also supported by the Conselho Nacional de Desenvolvimento Científico e Tecnológico (CNPq) and the Fundação de Amparo à Pesquisa do Estado do Rio de Janeiro (FAPERJ).

ACKNOWLEDGMENTS

We would like to thank financing agencies abovementioned before as well as Unidade de Microscopia Multiusuário Padrón-Lins.

SUPPLEMENTARY MATERIAL

The Supplementary Material for this article can be found online at: https://www.frontiersin.org/articles/10.3389/fmicb.2021.718232/full#supplementary-material

Supplementary Information | Criteria used for modeling the downstream section.

Supplementary Figure 1 | Number of registered nanotechnological products in Latin America categorized by country **(A)** and end-user sector **(B)**. Data from StatNano (2020).

Supplementary Figure 2 | Magnetic separation column design.

Supplementary Figure 3 | Sensitivity analyses showing effects of variations in economic **(A)** and bioprocess-related **(B)** parameters on unitary production costs and minimum selling prices (MSP) for the semicontinuous process when one of those individual parameters oscillates from the base-case (purple dashed vertical line). The results of variations in purchase price of two important feedstocks (lactic acid and urea) and fluctuations of the exchange ratio on the final production price are analyzed in panel **(A)**. The effects of specific cell growth rate of *Ms. gryphiswaldense* MSR-1 in fermentation tanks, as well as its magnetite production rate, are analyzed in panel **(B)**. The efficiency in BMN extraction by the MSCs and the plant annual throughput capacity, in terms of total produced magnetite, are also assessed in panel **(B)**. The purple dashed vertical line indicates base-case scenario whose parameters are described in **Tables 1**, **2**.

Supplementary Figure 4 | Operating costs composition breakdowns for the production of magnetic nanoparticles by synthetic chemical routes based on the data reported by Augusto et al. (2020). Direct and indirect cost contributions for co-precipitation and hydrothermal processes **(A)**. Direct operating costs breakdown showing cost types **(B)**. Material costs compositions from co-precipitation **(C)** and hydrothermal **(D)** processes.

Supplementary Table 1 | Iron oxide nanoparticle demand estimation for the selected market.

Supplementary Table 2 | Method used for plant cost calculations.

Supplementary Table 3 | Method used for operating cost calculations.

Supplementary Table 4 | Cost of raw material.

Supplementary Table 5 | Cost of utilities.

Supplementary Table 6 | Cost of labor, financing conditions and price indices.

Supplementary Table 7 | Material factors and prices for MSC.

Supplementary Table 8 | Purchase costs of equipment for single-stage fed batch.

Supplementary Table 9 | Purchase costs of equipment for a semicontinuous process.

Supplementary Table 10 | Comparison between approximate energy demands for biogenic and synthetic magnetic nanoparticles.

Supplementary Table 11 | Comparison between minimum selling price of biogenic magnetite and commercial prices of synthetic iron oxide nanoparticles.

REFERENCES

Abenojar, E. C., Wickramasinghe, S., Bas-Concepcion, J., and Samia, A. C. S. (2016). Structural effects on the magnetic hyperthermia properties of iron oxide nanoparticles. *Prog. Nat. Sci.* 26, 440–448. doi: 10.1016/j.pnsc.2016.09.004

Abreu, F., Correa, T., Bazylinski, D. A., Godoy, M., and Silveira, F. (2020a). *Processo Para Produção Contínua de Magnetossomos Através do Cultivo de Bactérias Magnetotáticas em Biorreator*. Brazil Patent No 10,20220,015831,7. Rio de Janeiro: Instituto Nacional da Propriedade Industrial.

Abreu, F., Morillo, V., Trubitsyn, D., and Bazylinski, D. A. (2020b). "Magnetotaxis in prokaryotes," in *eLS*. (Chichester: John Wiley & Sons, Ltd), doi: 10.1002/9780470015902.a0000397

Ahmad, F., Ashraf, N., Ashraf, T., Zhou, R. B., and Yin, D. C. (2019). Biological synthesis of metallic nanoparticles (MNPs) by plants and microbes: their cellular uptake, biocompatibility, and biomedical applications. *Appl. Microbiol. Biotechnol.* 103, 2913–2935. doi: 10.1007/s00253-019-09675-5

Ali, I., Peng, C., Khan, Z. M., and Naz, I. (2017). Yield cultivation of magnetotactic bacteria and magnetosomes: a review. *J. Basic Microbiol.* 57, 643–652. doi: 10.1002/jobm.201700052

Alphandéry, E., Idbaih, A., Adam, C., Delattre, J. Y., Schmitt, C., Gazeau, F., et al. (2019). Biodegraded magnetosomes with reduced size and heating power maintain a persistent activity against intracranial U87-Luc mouse GBM tumors. *J. Nanobiotechnol.* 17:126. doi: 10.1186/s12951-019-0555-2

Arakaki, A., Goto, M., Maruyama, M., Yoda, T., Tanaka, M., Yamagishi, A., et al. (2020). Restoration and modification of magnetosome biosynthesis by internal gene acquisition in a magnetotactic macterium. *Biotechnol. J.* 15:2000278. doi: 10.1002/biot.202000278

Augusto, P. A., Castelo-Grande, T., Vargas, D., Pascual, A., Hernández, L., Estevez, A. M., et al. (2020). Upscale design, process development, and economic analysis of industrial plants for nanomagnetic particle production for environmental and biomedical use. *Materials* 13:2477. doi: 10.3390/ma13112477

Bardal, S. K., Waechter, J. E., and Martin, D. S. (2011). *Applied Pharmacology*. Philadelphia, PA: Saunders.

Basit, A., Wang, J., Guo, F., Niu, W., and Jiang, W. (2020). Improved methods for mass production of magnetosomes and applications: a review. *Microb. Cell Fact.* 19:197. doi: 10.1186/s12934-020-01455-5

Berny, C., Le Fèvre, R., Guyot, F., Blondeau, K., Guizonne, C., Rousseau, E., et al. (2020). A method for producing highly pure magnetosomes in large quantity for medical applications using *Magnetospirillum gryphiswaldense* MSR-1 magnetotactic bacteria amplified in minimal growth media. *Front. Bioeng. Biotech.* 8:16. doi: 10.3389/fbioe.2020.00016

Bhattacharjee, S. (2016). DLS and zeta potential–what they are and what they are not? *J. Control. Release* 235, 337–351. doi: 10.1016/j.jconrel.2016.06.017

Chacón-Torres, J. C., Reinoso, C., Navas-León, D. G., Briceño, S., and González, G. (2020). Optimized and scalable synthesis of magnetic nanoparticles for RNA extraction in response to developing countries' needs in the detection and control of SARS-CoV-2. *Sci. Rep.* 10, 1–10. doi: 10.1038/s41598-020-75798-9

Correa, T., Taveira, I., Souza Filho, R., and Abreu, F. (2021). "Biomineralization of magnetosomes: billion-year evolution shaping modern nanotools," in *Biomineralization*, ed. M. Alshaaer (London: InTech Open), doi: 10.5772/intechopen.94465

da Gama-Ferreira, R., Azzoni, A. R., and Freitas, S. (2018). Techno-economic analysis of the industrial production of a low-cost enzyme using *E. coli*: the case of recombinant β-glucosidase. *Biotechnol. Biofuels* 11:81. doi: 10.1186/s13068-018-1077-0

Fernández-Castané, A., Li, H., Thomas, O. R. T., and Overton, T. W. (2018). Development of a simple intensified fermentation strategy for growth of *Magnetospirillum gryphiswaldense* MSR-1: physiological responses to changing environmental conditions. *New Biotechnol.* 46, 22–30. doi: 10.1016/j.nbt.2018.05.1201

Fundación Argentina de Nanotecnología (FAN) (2020). *Nanotecnología*. Available online at: https://www.fan.org.ar/nanotecnologia/ (accessed November 17, 2020).

Furubayashi, M., Wallace, A. K., González, L. M., Jahnke, J. P., Hanrahan, B. M., Payne, A. L., et al. (2020). Genetic tuning of iron oxide nanoparticle size, shape, and surface properties in *Magnetospirillum magneticum*. *Adv. Funct. Mater.* 31:2004813. doi: 10.1002/adfm.202004813

Geng, Y., Wang, J., Wang, X., Liu, J., Zhang, Y., Niu, W., et al. (2019). Growth-inhibitory effects of anthracycline-loaded bacterial magnetosomes against hepatic cancer in vitro and in vivo. *Nanomedecine* 14:296. doi: 10.2217/nnm-2018-0296

Gharailou, D. (2019). *A Review of Market Studies in Different Fields of Nanotechnology*. London: StatNano Publications.

Ginet, N., Pardoux, R., Adryanczyk, G., Garcia, D., Brutesco, C., and Pignol, D. (2011). Single-step production of a recyclable nanobiocatalyst for organophosphate pesticides biodegradation using functionalized bacterial magnetosomes. *PLoS One* 6:e021442. doi: 10.1371/journal.pone.0021442

Grasso, G., Zane, D., and Dragone, R. (2020). Microbial nanotechnology: challenges and prospects for green biocatalytic synthesis of nanoscale materials for sensoristic and biomedical applications. *Nanomaterials* 10:11. doi: 10.3390/nano10010011

Guo, F., Liu, Y., Chen, Y., Tang, T., Jiang, W., Li, Y., et al. (2011). A novel rapid and continuous procedure for large-scale purification of magnetosomes from *Magnetospirillum gryphiswaldense*. *Appl. Microbiol. Biotechnol.* 90, 1277–1283. doi: 10.1007/s00253-011-3189-3

Harrison, R. G., Todd, P., Rudge, S. R., and Petrides, D. P. (2015). *Bioseparations Science and Engineering*. New York, NY: Oxford University Press.

Honda, T., Tanaka, T., and Yoshino, T. (2015). Stoichiometrically controlled immobilization of multiple enzymes on magnetic nanoparticles by the magnetosome display system for efficient cellulose hydrolysis. *Biomacromolecules* 16, 3863–3868. doi: 10.1021/acs.biomac.5b01174

Iravani, S., and Varma, R. S. (2020). Bacteria in heavy metal remediation and nanoparticle biosynthesis. *ACS Sustain. Chem. Eng.* 8, 5395–5409. doi: 10.1021/acssuschemeng.0c00292

Jajan, L. H. G., Hosseini, S. N., Ghorbani, M., Mousavi, S. F., Ghareyazie, B., and Abolhassani, M. (2019). Effects of environmental conditions on high-yield magnetosome production by *Magnetospirillum gryphiswaldense* MSR-1. *Iran. Biomed. J.* 23, 209–219.

Jiang, B., Lian, L., Xing, Y., Zhang, N., Chen, Y., Lu, P., et al. (2018). Advances of magnetic nanoparticles in environmental application: environmental remediation and (bio)sensors as case studies. *Environ. Sci. Pollut. Res.* 25, 1671–1679. doi: 10.1007/s11356-018-3095-7

Krishnan, K. M., Ferguson, R. M., and Khandhar, A. P. (2016). *Tuned Multifunctional Magnetic Nanoparticles for Biomedicine*. U.S. Patent No 9,259,492. Washington, DC: U.S. Patent and Trademark Office.

Kudr, J., Haddad, Y., Richtera, L., Heger, Z., Cernak, M., Adam, V., et al. (2017). Magnetic nanoparticles: from design and synthesis to real world applications. *Nanomaterials* 7:243. doi: 10.3390/nano7090243

León, D. C., and Cárdenas, J. C. (2020). Lessons from COVID-19 for a Sustainability Agenda in Latin America and the Caribbean. UNDP Latin America and the Caribbean Covid-19 Policy Documents Series. 14A. Available online at: https://www.latinamerica.undp.org/content/rblac/en/home/library/crisis_prevention_and_recovery/lecciones-del-covid-19-para-una-agenda-de-sostenibilidad-en-amer.html (accessed January 21, 2021).

Liu, Y., Li, G. R., Guo, F. F., Jiang, W., Li, Y., and Li, L. J. (2010). Large-scale production of magnetosomes by chemostat culture of *Magnetospirillum gryphiswaldense* at high cell density. *Microb. Cell Fact* 9:99. doi: 10.1186/1475-2859-9-99

Mahdinia, E., Cekmecelioglu, D., and Demirci, A. (2019). "Bioreactor scale-up," in *Essentials in Fermentation Technology*, ed. A. Berenjian (Berlin: Springer), doi: 10.1007/978-3-030-16230-6_7

Mandawala, C., Chebbi, I., Durand-Dubief, M., Le Fèvre, R., Hamdous, Y., Guyot, F., et al. (2017). Biocompatible and stable magnetosome minerals coated with poly-L-lysine, citric acid, oleic acid, and carboxy-methyl-dextran for application in the magnetic hyperthermia treatment of tumors. *J. Mater. Chem. B* 5:452. doi: 10.1039/c6tb03248f

Ministério da Ciência, Tecnologia, Inovações e Comunicações (MCTI) (2019). *Portaria No 3,459*. Available online at: https://www.in.gov.br/web/dou/-/portaria-n-3.459-de-26-de-julho-de-2019-209514505 (accessed November 17, 2020).

Mirabello, G., Lenders, J. J., and Sommerdijk, N. A. (2016). Bioinspired synthesis of magnetite nanoparticles. *Chem. Soc. Rev.* 45, 5085–5106. doi: 10.1039/C6CS00432F

Nan, X., Lai, W., Li, D., Tian, J., Hu, Z., and Fang, Q. (2021). Biocompatibility of bacterial magnetosomes as MRI contrast agent: a long-term in vivo follow-up study. *Nanomaterials* 11:1235. doi: 10.3390/nano11051235

Nano-Powder Factory (2020). *Research of the World Market of Nanopowders*. Available online eat: https://eednano.com/ (accessed March 24, 2020).

Naresh, M., Das, S., Mishra, P., and Mittal, A. (2012). The chemical formula of a magnetotactic bacterium. *Biotechnol. Bioeng.* 109, 1205–1216. doi: 10.1002/bit.24403

Pinelli, F., Perale, G., and Rossi, F. (2020). Coating and functionalization strategies for nanogels and nanoparticles for selective drug delivery. *Gels* 6:6. doi: 10.3390/gels6010006

Pósfai, M., Lefèvre, C., Trubitsyn, D., Bazylinski, D. A., and Frankel, R. (2013). Phylogenetic significance of composition and crystal morphology of magnetosome minerals. *Front. Microbiol.* 4:344. doi: 10.3389/fmicb.2013.00344

Revathy, T., Jayasri, M. A., and Suthindhiran, K. (2017). Toxicity assessment of magnetosomes in different models. *3 Biotechnol.* 7:126. doi: 10.1007/s13205-017-0780-z

Rosenfeldt, S., Mickoleit, F., Jörke, C., Clement, J. H., Markert, S., Jérôme, V., et al. (2020). Towards standardized purification of bacterial magnetic nanoparticles for future in vivo applications. *Acta Biomater.* 120, 293–303. doi: 10.1016/j.actbio.2020.07.042

Sannigrahi, S., Arumugasamy, S. K., Mathiyarasu, J., and Suthindhiran, K. (2020). Magnetosome-anti-*Salmonella* antibody complex-based biosensor for the detection of *Salmonella typhimurium*. *Mater. Sci. Eng. C* 61, 396–410. doi: 10.1016/j.msec.2020.111071

Santos, E., Watanabe, A., Vargas, M., Tanaka, M., Garcia, F., and Ronconi, C. (2018). AMF-responsive doxorubicin loaded β-cyclodextrin-decorated superparamagnetic nanoparticles. *New J. Chem.* 42, 671–680. doi: 10.1039/C7NJ02860A

Schüler, D., Monteil, C. L., and Lefevre, C. T. (2020). *Magnetospirillum gryphiswaldense*. *Trends Microbiol.* 28, 1783–1794. doi: 10.1016/j.tim.2020.06.001

Seider, W. D., Lewin, D. R., Seader, J. D., Widagdo, S., Gani, R., and Ng, K. M. (2016). *Product and Process Design Principles: Synthesis, Analysis and Evaluation*. New York, NY: John Wiley & Sons, Inc.

Silva, K. T., Leão, P. E., Abreu, F., López, J. A., Gutarra, M. L., Farina, M., et al. (2013). Optimization of magnetosome production and growth by the magnetotactic vibrio *Magnetovibrio blakemorei* strain MV-1 through a statistics-based experimental design. *Appl. Environ. Microbiol.* 79, 2823–2827. doi: 10.1128/AEM.03740-12

Smit, B. A., Van Zyl, E., Joubert, J. J., Meyer, W., Prévéral, S., Lefevre, C. T., et al. (2018). Magnetotactic bacteria used to generate electricity based on Faraday's law of electromagnetic induction. *Lett. Appl. Microbiol.* 66:12862. doi: 10.1111/lam.12862

StatNano (2016). *Nanotechnology in Latin America*. Available online at: https://product.statnano.com/ (accessed April 25, 2020).

StatNano (2020). *Nanotechnology Products Database*. London: StatNano Publications.

Sun, J.-B., Zhao, F., Tang, T., Jiang, W., Tian, J.-S., Li, Y., et al. (2008). High-yield growth and magnetosome formation by *Magnetospirillum gryphiswaldense* MSR-1 in an oxygen-controlled fermentor supplied solely with air. *Appl. Microbiol. Biotechnol.* 79, 389–397. doi: 10.1007/s00253-008-1453-y

Tang, Y. S., Wang, D., Zhou, C., Ma, W., Zhang, Y. Q., Liu, B., et al. (2012). Bacterial magnetic particles as a novel and efficient gene vaccine delivery system. *Gene Ther.* 19, 1187–1195. doi: 10.1038/gt.2011.197

Tartaj, P., Veintemillas-Verdaguer, S., Gonzalez-Carreño, T., and Serna, C. J. (2019). "Preparation of magnetic nanoparticles for applications in biomedicine," in *Magnetic Nanoparticles in Biosensing and Medicine*, ed. N. J. Darton (Cambridge: Cambridge University Press), 52–67. doi: 10.1017/9781139381222.003

Timko, M., Dzarova, A., Kovac, J., Skumiel, A., Józefczak, A., Hornowski, T., et al. (2009). Magnetic properties and heating effect in bacterial magnetic nanoparticles. *J. Magn. Magn. Mater.* 321:77. doi: 10.1016/j.jmmm.2009.02.077

United Nations (UN) (2020). *Sustainable Development Goals*. Available online at; https://www.un.org/sustainabledevelopment/ (accessed November 16, 2020).

Vargas, G., Cypriano, J., Correa, T., Leão, P., Bazylinski, D. A., and Abreu, F. (2018). Applications of magnetotactic bacteria, magnetosomes and magnetosome crystals in biotechnology and nanotechnology: mini-review. *Molecules* 23:2438. doi: 10.3390/molecules23102438

Wang, X., Wang, Q., Zhang, Y., Wang, Y., Zhou, Y., Zhang, W., et al. (2016). Transcriptome analysis reveals physiological characteristics required for magnetosome formation in *Magnetospirillum gryphiswaldense* MSR-1. *Environ. Microbiol. Rep.* 8, 371–381. doi: 10.1111/1758-2229.12395

World Health Organization (WHO) (2020). *The International Pharmacopoeia*, 9th Edn, Available online at: https://digicollections.net/phint//2020/index.html#d/b.1 (accessed July 2021).

Xu, J., Liu, L., He, J., Ma, S., Li, S., Wang, Z., et al. (2019). Engineered magnetosomes fused to functional molecule (protein A) provide a highly effective alternative to commercial immunomagnetic beads. *J. Nanobiotechnol.* 17:37. doi: 10.1186/s12951-019-0469-z

Yoshino, T., Hirabe, H., Takahashi, M., Kuhara, M., Takeyama, H., and Matsunaga, T. (2008). Magnetic cell separation using nano-sized bacterial magnetic particles with reconstructed magnetosome membrane. *Biotechnol. Bioeng.* 101, 470–477. doi: 10.1002/bit.21912

Zhang, S., Niu, H., Zhang, Y., Liu, J., Shi, Y., Zhang, X., et al. (2012). Biocompatible phosphatidylcholine bilayer coated on magnetic nanoparticles and their application in the extraction of several polycyclic aromatic hydrocarbons from environmental water and milk samples. *J. Chromatogr. A* 2012:1238. doi: 10.1016/j.chroma.2012.03.056

Zhang, Y., Zhang, X., Jiang, W., Li, Y., and Li, J. (2011). Semicontinuous culture of *Magnetospirillum gryphiswaldense* MSR-1 cells in an autofermentor by nutrient-balanced and isosmotic feeding strategies. *Appl. Environ. Microbiol.* 77, 5851–5856. doi: 10.1128/AEM.05962-11

Conflict of Interest: The authors declare that the research was conducted in the absence of any commercial or financial relationships that could be construed as a potential conflict of interest.

Publisher's Note: All claims expressed in this article are solely those of the authors and do not necessarily represent those of their affiliated organizations, or those of the publisher, the editors and the reviewers. Any product that may be evaluated in this article, or claim that may be made by its manufacturer, is not guaranteed or endorsed by the publisher.

4.2. *Bacterial-origin magnetic nanoparticles for decolorization of methyl blue dye*

Tarcísio Correa[a] and Fernanda Abreu[a]*

[a] Instituto de Microbiologia Professor Paulo de Góes, Universidade Federal do Rio de Janeiro, Brasil

* Corresponding author at: Departamento de Microbiologia Geral, Instituto de Microbiologia Professor Paulo de Góes, Universidade Federal do Rio de Janeiro, Rio de Janeiro, RJ, Brazil. E-mail address: fernandaaabreu@micro.ufrj.br.

Abstract: Magnetotactic bacteria are the main microbial source of biogenic magnetic nanoparticles (BMs). The structure of BMs comprises an iron mineral core and an external biological membrane, which is made up of phospholipids and proteins dedicated to the biosynthesis of these nanostructures. Because BM proteins are diverse in biochemical function, BM might display intrinsic activities yet to be explored in nanobiotechnology. Thus, the present work aims at the application of non-modified BMs extracted from the marine magnetotactic vibrio *Magnetovibrio blakemorei* strain MV-1^T for the decolorization of methyl blue (MB) dye. The experiments were carried out in the presence and absence of hydrogen peroxide (H_2O_2) and the degradation kinetics was evaluated, as well as BM reusability. At a concentration of 80 mg/L, BMs at were able to degrade 90% of MB within 5 min in the absence of H_2O_2. In the presence of H_2O_2, the removal achieved in the first 1 min was over 80%. Kinetic studies revealed a first-order degradation kinetics without H_2O_2 and a second-order kinetics with H_2O_2. BM performance is optimal at neutral pH and removal of BM membrane caused dye degrading activity to cease. BMs can be recovered and reused for, at least, 4 cycles while retaining an activity over 75% in the presence of H_2O_2. Despite a slightly lower activity, their reusability is also possible at the absence of H_2O_2. Taken together, these findings uncover the use of BMs as naturally-derived and recoverable nanocatalyst for dye wastewater treatment. Moreover, their possible use without highly oxidizing H_2O_2 further support BM potential in environmental remediation.

Keywords: magnetic nanoparticles, dye degradation, magnetosomes, magnetotactic bacteria

1.Introduction

Since the patenting of production and large-scale commercialization of mauveine by William Perkin in 1857, synthetic dyes have been in use in different industries, making it a billion-dollar market worldwide (Hagan & Poulin, 2021; Zanoni & Yanamaka, 2016). Despite its market value, estimates are that 20-50% of dyes used in textile industries are discharged in wastewater while approximately 70% of those in hair coloring are flushed into sewage (Zanoni & Yanamaka, 2016).

Because traditional treatment processes remove only a fraction of dyes in wastewaters, receptive waterbodies remain vulnerable to impacts related to these substances (Cardoso et al., 2016). An evident impact of dyes in the environment is the absorption of sun light and inhibition of photosynthesis by plants and microorganisms (Cai et al., 2020; Pereira & Alves, 2012). Further impacts are linked to their chemical nature, which makes dyes poorly biodegradable and with a complex toxicity profiles to aquatic organisms (Cai et al., 2020; Lellis et al., 2019).

To reduce ecotoxicity, new technologies have been developed for the treatment of high-dye content wastewaters (Katheresan et al., 2018). Some of the advanced dye removal methods include biocatalysis, photooxidation, and electrochemical processes (Choi, 2021; Katheresan et al., 2018). More recently, the use of nanobased technologies, especially magnetic nanoparticles (MNPs), have been intensely explored for decolorization and detoxication of dyes (Mondal et al., 2020).

Magnetic nanoparticles have been used in dye removal as supports for immobilized enzymes (Darwesh et al., 2019) as heterogeneous catalysts in Fenton or Fenton-like reactions (Zhiqiang Wang et al., 2014; Weng et al., 2013) and as sorption agents (Zhenxing Wang et al., 2015). The use of magnetic nanotools is advantageous because they can be easily recovery by magnetic collection. The recoverability might cheapen dye treatment processes as removal agent can reused multiple times.

Biosynthesized magnetic nanoparticles (BMs) are promising for application in dye removal with additional environmental benefits as their manufacture dispenses the use of potentially toxic chemicals (Vargas et al., 2018). The main microbial route for BMs synthesis is biomineralization by magnetotactic bacteria (Vargas et al., 2018). BMs are composed of a mineral iron core (magnetite - Fe_3O_4 or greigite - Fe_3S_4), which is surrounded by a biological membrane. The biological control of the synthesis gives these nanoparticles properties superior to those of artificial nanoparticles, such as controlled size and shape, chemical purity and unique magnetic domain per particle (Correa et al., 2020). Nevertheless, although frequently applied for biomedical purposes, BMs are still underexplored in environmental applications.

In the present work, we have applied non-modified BMs extracted from the marine magnetotactic vibrio *Magnetovibrio blakemorei* strain MV-1^T for the decolorization of methyl blue (MB) dye. The experiments were carried out in the presence and absence of hydrogen peroxide (H_2O_2) and the degradation kinetics was evaluated, as well as BM reusability.

2. Methodology

2.1. Bacterial culture

A large-scale cultivation of *M. blakemorei* strain MV-1^T was carried out in a 5-L bioreactor (3 L working volume) using culture media and conditions (28°C, 192 h) as in Silva et al, 2013 for obtaining prismatic BMs. An additional culture of *Magnetospirillum gryphiswaldense* strain MSR-1 (DMS 6361) was performed in the same bioreactor (30 °C, 80 h) with medium and operational settings described as in Heyen & Schüler, 2003.

2.2. Bacterial cell lysis and BM extraction

After bioreactor cultivations, MTB cells were harvested by centrifugation at 5,700 x g for 30 min at 4 °C and lysed by ultrasonic disruption following the method of Cypriano et al., 2019. BMs were concentrated from magnetic cell lysate with a boron-neodymium permanent magnet (1.5 cm h x 2.5 cm ⌀) and washed repeatedly with 20 mM HEPES buffer until total removal of debris as observed under electron microscope.

2.3. BM membrane removal

Membranes from *M. blakemorei* strain MV-1^T BMs were removed using a protocol adapted from Yoshino et al., 2008. Membrane proteins were removed by treating 1 mg BMs with a boiling alkaline detergent solution (1% w/v sodium dodecylsulfate, pH 9) for 30 min. Afterwards, BMs were repeatedly washed with MilliQ with in-between magnetic collections until no foam formation were observed. Phospholipids were then removed with a chloroform-methanol (1:1 v/v) solution with occasional stirring for 2 h. The BM-solvent suspension was stored overnight at 4 °C. Finally, BMs were magnetically collected and washed with MilliQ water.

2.4. Preparation of sMNPs

Synthetic iron-oxide nanoparticles were prepared by a co-precipitation method as described by Santos et al., 2018.

2.5. Transmission electron microscopy

All tested magnetic nanoparticles were examined under transmission electron microscopy (TEM) using a FEI Morgagni apparatus (FEI Company, Hillsboro, OR, USA) operated at 80 kV. The integrity of BMs mineral core and membrane were evaluated. Changes in membrane thickness were measured using ImageJ (NIH, USA) image analysis software.

2.6. Dye removal assays

The removal of MB from aqueous solution by BMs extracted from *M. blakemorei* strain MV-1^T (unless otherwise stated) was investigated in kinetic experiments (10 min) by examining the disappearance of color in solution during 10 min. Ultra-violet-visible (UV-Vis) spectra of MB in solution were obtained by scanning spectrophotometry (UV-1800, Shimadzu, Kyoto, Japan) in 225-700 nm wavelength range. Discoloration kinetics were measured spectrophotometrically at 600 nm wavelength at samples collected at 0-, 1-, 2-, 3-, 4-, 5- and 10-min intervals.

Experiments were performed using a 15 mg/L MB solution, which was prepared using MilliQ water. The first batch of experiment, removal was carried out with different BM concentrations (20, 40 and 80 mg/L), and no H_2O_2 was added. The second raw of experiments was carried with the BM concentration with the best removal profile with the addition of 0, 18 and 36 mM H_2O_2 from a 10% stock solution. Control experiments were also run in absence of BMs to record the MB removal by H_2O_2. A third batch of experiments were performed with varying pHs from 7.0 to 4.8 and 8.2 using both BM and H_2O_2-optimized concentrations. pHs were adjusted by adding 0.1 M NaOH or 0.1 M HCl. Membrane-removed BMs were then used in additional experiments in the presence and absence of H_2O_2 in optimized BM concentration and medium pH.

Two comparative experiments, one using BMs from *M. gryphiswaldense* MSR-1 and another with synthetic MNPs (sMNPs), were run using optimized conditions. All experiments were carried out in duplicates.

2.7. Reusability and iron leaching

After each degradation experiment, BMs were magnetically concentrated, washed with distilled water and reused in new degradation reactions. The separated supernatants were used in quantification of iron to investigate possible iron ions leaching from tested nanoparticles. Soluble iron determination was done by colorimetric ferrozine method (Viollier et al., 2000).

3. Results and discussion

3.1. Dye chemical profile

MB is a synthetic dye widely used for histological and botanical staining and in colorization of stationery, detergents and personal care products (Clariant, 2013; Sabnis, 2010). Its structure possesses both aniline and triarylmethane moieties (**Figure 1A**), which are linked to considerable aquatic ecotoxicity (Bhunia et al., 2003; Chen et al., 2019). Two prominent peaks are visible in MB UV-Vis spectrum (**Figure 1B**): a sharper one – assigned peak *a* – ranging from 290-310 nm, relative to aniline (NIST, 2018), and a broader one – peak *b* – in 580-620 nm, which is due to its highly conjugated organic structure (**Figure 1A**).

3.2. Influence of BM concentration on MB removal

In the first group of experiments, we tested different BM concentrations for the degradation of 15 mg/L MB in the absence of H_2O_2 (**Figure 2A**). Among the tested concentrations (20, 40 and 80 mg/L), the greatest concentration led to the fastest degradation, with over 90% of MB being degraded within 5 min. Thus, reaction kinetics is directly proportional to the nanoparticle concentration. Both 40 and 80 mg/L were capable of virtually total removal of MB within 10 min (**Figure 2A**).

3.3. Influence of hydrogen peroxide

In the second set of experiment, the influence of H_2O_2 of MB degradation rate was investigated (**Figure 2B**). Using BMs with and without 36 mM H_2O_2 led approximately to the same removal rate within 5 min. Nevertheless, in the presence of H_2O_2, the removal achieved in the first 1 min was over 80%, while this value was ~20% lower for the reaction using solely BM. This finding indicates BMs may act as a catalyst by accelerating MB degradation by H_2O_2. However, the use of BM in the absence of H_2O_2 may have a greener character because it avoids a toxic, oxidizing reagent that can be potentially hazardous itself.

3.4. Influence of reaction pH

All the results described to this point were obtained using a medium pH of 7.0. The third set of experiments was performed to evaluate the influence of different pHs on the MB removal kinetics using 80 mg/L BM and 36 mM H_2O_2 (**Figure 2C**). When pH was set at 4.8, there was a reduction in the initial removal rate: only 38% of MB was removed at 1 min and 64% at 2 min. This is an important reduction in removal ability from pH 7.0, which led to approximately 90% degradation at 2 min. The decrease in removal activity was more dramatic when the pH was 8.2. In that case, only a 30% removal was achieved in 10 min. The highest activity in neutral pH is an indication that the degradation mechanism is a biological catalysis rather than Fenton's oxidation. This hypothesis is in tandem with the work of Darwesh et al., 2019, which that demonstrated that an MNP-immobilized peroxidase has its peak textile-dye-degrading activity at a pH 6 and approximately 90% active in a pH 7. In that work, a substantial reduction of the activity is also observed pHs over 7.5 and under 5.5, which further corroborates our hypothesis. On the other hand, Fenton reactions rely on the iron-catalyzed formation of reactive oxygen species like hydroxyls radicals (OH·) (Pignatello et al., 2006). Fenton's reactions, which commonly applies magnetic nanoparticles, are favored and accelerated in acidic media (Jung et al., 2009) while BM-mediated degradation is optimal at neutrality.

3.5. Effect of membrane removal

To the fourth set of experiments, BMs were subject to membrane removal to investigate the effect of the external coating on their activity in the presence and absence of H_2O_2. In the absence of H_2O_2, little MB degradation was observed and 82% of MB remained in medium after 10 min (**Figure 2D**). The dramatic decline in MB removal performance is a strong evidence that most catalytic activity is performed by membrane components, probably anchored proteins. This finding also reinforces a non-Fenton mechanism underlying MB degradation. Due to crystallographic precision of BM magnetite core, iron atoms are orderly confined within the mineral structure and might not be available to perform Fenton's oxidations. Intriguingly, even in the presence of H_2O_2 at the same concentration of the previous experiments (36 mM), the degradation of MB was significantly hindered when bare BMs were used. This is probably because of H_2O_2 decomposition into H_2O and O_2, but not OH· radicals, as observed for other heterogeneous catalysts with ordered crystalline surfaces.

These findings further support the importance of BM membrane to biotechnological applications. The phospholipid portion of the biological membrane causes a negative external charge and, thus provides BMs aqueous suspensions with colloidal stability (Vargas et al., 2018). Proteins, whose functions in biomineralization process include iron uptake, crystal nucleation and growth and pH and redox control, are also components of BM membrane (Correa et al., 2020). These intrinsic BM protein functions could be explored for real-world applications. As described in earlier studies, some of these proteins could be acting as natural catalysts for MB degradation by oxidation. BMs extracted from *M. gryphiswaldense* strain MSR-1 (Guo et al., 2012) and *Magnetospirillum magneticum* strain AMB-1 (Li et al., 2015) have already been assigned

peroxidase-like activity linked to BMs. MSR-1 BMs also displayed a more intense activity when applied with its original membrane than after membrane removal (Guo et al., 2012).

3.6. Kinetic profile

From the experiments using 80 mg/L BM, 36 mM H_2O_2 and a combination of both, we used the variation of MB concentrations along reaction time to calculate the kinetic law of the reactions, as well as the rate constants (k). Linear regressions were performed with ln[MB] (for first order kinetics) and 1/[MB] (for second order kinetics) versus time (**Figure 3**). The angular coefficients correspond to k (k_1 for 1st order and k_2 for 2nd order) and R^2 values were used to evaluate the fitness of removal data to each kinetic model (either 1st or 2nd order). Results for rate constants and kinetic modelling are on table 1. While removal with BM only resulted in a first order kinetics, the other two treatments are second order. When both BM and H_2O_2 were employed, k_2 equaled to 0.242 $L.mg^{-1}.min^{-1}$, which is about 4 times that of H_2O_2 only. These results suggest that, when used alongside, BMs accelerates the degradation of MB by H_2O_2. However, the degradation of MB by BM only probably occurs through an intrinsic mechanism, with is complemental to the catalysis.

Linear regression analysis of kinetic data also allowed us to compare the removal efficiencies of prismatic BMs from *M. blakemorei* strain MV-1^T, with integer and removed membrane, with those of cubooctahedral BMs from *M. gryphiswaldense* strain MSR-1 and sMNPs (**Table 2**). All nanoparticles displayed a second-order kinetics, with MV-1^T BMs displaying the highest activity among them. Nevertheless, cubooctahedral BMs from MSR-1 also showed a superior activity compared to sMNPs. This result coincides with previous work (Guo et al., 2012) in which degrading activity of MSR-1 BMs was more similar to that of peroxidase than to synthetic nanoparticles. Dye-degrading activities found for BMs are among the highest among nanoparticles claiming a green synthetic route (**Table 3**). In a MB adsorption process using mussel-inspired MNPs, Wang and coauthors reached up to 95% removal rate. Nevertheless, the highest performance was reached at a pH = 4, which requires acidification during decolorization. Considering a second-order kinetics, dye-removing activity of BMs still seems significantly higher than that of mussel-inspired MNPs (**Table 3**). Hence, the efficient decolorizing character along with a sustainable bioproduction provide BMs with a high competitiveness due to the increased environmental performance.

Furthermore, iron leaching from nanoparticles to the reaction media was measured. Significant iron leaching (4% of Fe mass) was only detected using sMNPs (**Table 2**). This result indicates that membranes surrounding MV-1^T and MSR-1 BMs also act as a protective layer against iron mobilization from Fe_3O_4 core.

3.7. Reusability

Following MB degradation experiments with and without H_2O_2, BMs were recovered through magnetic collection and their reusability was tested. The results (**Figure 4**) indicate BMs can be recovered and reused for, at least, 4 cycles while maintaining an activity over 75% that of the first use in the presence of H_2O_2. In the absence of H_2O_2, the reduction in activity after the first use was more pronounced. Nevertheless, over 40% activity was retained for three reuse cycles. In environmental applications, such reusability is a major advantage of biogenic nanomagnets. Costs and resource utilization for production of novel BMs, as well as disposal volumes of used nanoparticles, are significantly reduced. In comparison with an MNP-immobilized peroxidase, which could be reused in up to 100 cycles (Darwesh et al. 2019), BMs seemed less resilient to sequential reutilizations. However, the reported tests were performed against azo-dyes, whose chemical degradability is different from triarylmethanes like MB. Despite a better reuse

characteristic, MNP-immobilized peroxidase takes about 6 h to achieve a complete decolorization.

Membrane integrity, which is important to maintain BM activity between reuse cycles, was investigated by BM observation and membrane measurement under transmission electron microscopy (**Figure 5**). In the experiments with H_2O_2, membrane thickness was virtually preserved from first to third utilization (**Figure 5A-C**, **Table 4**) while a significantly (**Table S1**) shrinking (**Figure 5C**, **Table S1**) was observed after the fourth reuse cycle. The 23-% reduction in the mean membrane thickness is related to a 57-% decrease in dye degradation activity (**Figure 4** and **Table 4**), evidencing that membrane disruption hinder BM catalytic activity. Moreover, **Figure 4D** evidences the accumulation of a nebulous substance between BMs after 4th reuse. This observation might suggest the accumulation of MB degradation products and detachment of BM membrane components. A significantly reduction (77%) in BM activity is also observed when reuse is performed in the absence of H_2O_2. However, as measured by microscopy (**Figure S1**), the observed decrease in membrane thickness was only 6.7%. On the other hand, material accumulation, presumably degradation products, onto the surface of BMs (**Figure S1**) might prevent the contact between BM surface proteins and soluble dye, thus hindering BM degradation. It might be suggested that, in the presence of H_2O_2, MB degradation products are further decomposed by peroxidation while they accumulate in the absence of the oxidative agent.

3.8. Possible reaction mechanism

UV-Vis spectrometry analyses of treated dye samples were also performed to investigate spectral changes arising from dye degradation after treatments. The characteristic blue chromophore peak *b* decreases in magnitude in all treatments, but the sharpest reduction (98%) occurs with BMs and H_2O_2 treatment, which is in good agreement with spectrophotometric experiment results (**Figure 1B**). The peak b also shows 27% reduction with H2O2 and 68% with BMs. Conversely, the sharp peak *a*, relative to aniline, increased after all treatments but that using solely H_2O_2. The observed increase in the peak *a* could be associated to an accumulation of degradation MB products, like aniline, and, thus, further supports a predominantly degradative mechanism of MB removal by BMs. This suggestion is further supported by the fact the highest peak, 13% higher than raw dye, is formed in the presence of BMs only. The slightly lower peaks in the treatments with H2O2 (with and without BMs) an indication of unspecific oxidation of both MB and its BM-formed degradation products by peroxidation.

4. Conclusion

In this paper, we have explored intrinsic protein-mediated activities of BMs for decolorization of MB, an industrially important dye. BMs were capable of removing MB in the presence and absence of H_2O_2 and, despite commonplace for other MNPs, removal mechanism is different from a Fenton's catalysis. The sustainable characteristic of BM production by magnetotactic bacteria-based bioprocesses, added to a highly efficient removal and reusability prompt BMs for use as a green nanocatalyst in wastewater decolorization. Further research is needed to assess BMs in the degradation of other pollutants, including other dyes, and examine the toxicity of degradation products. Finally, due to the complexity of BMs proteome, there could be other natural activities of BM without surface functionalization still to be explored in environmental remediation.

5. References

Bhunia, F., Saha, N. C., & Kaviraj, A. (2003). Effects of Aniline - An Aromatic Amine to Some Freshwater Organisms. *Ecotoxicology*, *12*(5), 397–404. https://doi.org/10.1023/A:1026104205847

Cai, H., Liang, J., Ning, X. an, Lai, X., & Li, Y. (2020). Algal toxicity induced by effluents from textile-dyeing wastewater treatment plants. *Journal of Environmental Sciences (China)*, *91*(2015), 199–208. https://doi.org/10.1016/j.jes.2020.01.004

Cardoso, J. C., Bessegato, G. G., & Zanoni, M. V. B. (2016). Análie crítica dos processos emgregados no tratamento de efluentes têxteis. In M. V. B. Zanoni & H. Yanamaka (Eds.), *Corantes: Caracterização química, toxicológica, métodos de detecção e tratamento* (pp. 215–239). Cultura Acadêmica Ed.

Chen, S. H., Cheow, Y. L., Ng, S. L., & Ting, A. S. Y. (2019). Biodegradation of Triphenylmethane Dyes by Non-white Rot Fungus Penicillium simplicissimum: Enzymatic and Toxicity Studies. *International Journal of Environmental Research*, *13*(2), 273–282. https://doi.org/10.1007/s41742-019-00171-2

Choi, K. Y. (2021). Discoloration of indigo dyes by eco-friendly biocatalysts. *Dyes and Pigments*, *184*(July 2020), 108749. https://doi.org/10.1016/j.dyepig.2020.108749

Clariant. (2013). Duasyn Ink Blue SLK. In *Pigments special applications*.

Correa, T., Taveira, I., Souza-Filho, R., & Abreu, F. (2020). Biomineralization of Magnetosomes: Billion-Year Evolution Shaping Modern Nanotools. In *Biomineralization*. https://doi.org/10.5772/intechopen.94465

Cypriano, J., Werckmann, J., Vargas, G., Dos Santos, A. L., Silva, K. T., Le#x000E3;o, P., Almeida, F. P., Bazylinski, D. A., Farina, M., Lins, U., & Abreu, F. (2019). Uptake and persistence of bacterial magnetite magnetosomes in a mammalian cell line: Implications for medical and biotechnological applications. *PLoS ONE*, *14*(4), 1–11. https://doi.org/10.1371/journal.pone.0215657

Darwesh, O. M., Matter, I. A., & Eida, M. F. (2019). Development of peroxidase enzyme immobilized magnetic nanoparticles for bioremediation of textile wastewater dye. *Journal of Environmental Chemical Engineering*, *7*(1), 102805. https://doi.org/10.1016/j.jece.2018.11.049

Guo, F. F., Yang, W., Jiang, W., Geng, S., Peng, T., & Li, J. L. (2012). Magnetosomes eliminate intracellular reactive oxygen species in Magnetospirillum gryphiswaldense MSR-1. *Environmental Microbiology*, *14*(7), 1722–1729. https://doi.org/10.1111/j.1462-2920.2012.02707.x

Hagan, E., & Poulin, J. (2021). Statistics of the early synthetic dye industry. *Heritage Science*, *9*(1), 1–14. https://doi.org/10.1186/s40494-021-00493-5

Heyen, U., & Schüler, D. (2003). Growth and magnetosome formation by microaerophilic Magnetospirillum strains in an oxygen-controlled fermentor. *Applied Microbiology and Biotechnology*, *61*, 536–544. https://doi.org/10.1007/s00253-002-1219-x

Jung, Y. S., Lim, W. T., Park, J. Y., & Kim, Y. H. (2009). Effect of pH on Fenton and Fenton-like oxidation. *Environmental Technology*, *30*(2), 183–190. https://doi.org/10.1080/09593330802468848

Katheresan, V., Kansedo, J., & Lau, S. Y. (2018). Efficiency of various recent wastewater dye removal methods: A review. *Journal of Environmental Chemical Engineering*, *6*(4), 4676–4697. https://doi.org/10.1016/j.jece.2018.06.060

Lellis, B., Fávaro-Polonio, C. Z., Pamphile, J. A., & Polonio, J. C. (2019). Effects of textile dyes on health and the environment and bioremediation potential of living organisms. *Biotechnology Research and Innovation*, *3*(2), 275–290. https://doi.org/10.1016/j.biori.2019.09.001

Li, K., Chen, C., Chen, C., Wang, Y., Wei, Z., Pan, W., & Song, T. (2015). Magnetosomes extracted from Magnetospirillum magneticum strain AMB-1 showed enhanced peroxidase-like activity under visible-light irradiation. *Enzyme and Microbial Technology*, *72*, 72–78. https://doi.org/10.1016/j.enzmictec.2015.02.009

Mondal, P., Anweshan, A., & Purkait, M. K. (2020). Green synthesis and environmental application of iron-based nanomaterials and nanocomposite: A review. *Chemosphere*, *259*, 127509. https://doi.org/10.1016/j.chemosphere.2020.127509

NIST. (2018). *Aniline*. NIST Chemistry WebBook. https://webbook.nist.gov/cgi/cbook.cgi?ID=C62533&Type=IR-SPEC&Index=1

Pereira, L., & Alves, M. (2012). Dyes—Environmental Impact and Remediation. In *Environmental Protection Strategies for Sustainable Development* (Vol. 55, Issue 12, pp. 111–162). Springer Netherlands. https://doi.org/10.1007/978-94-007-1591-2_4

Pignatello, J. J., Oliveros, E., & Mackay, A. (2006). Advanced oxidation processes for organic contaminant destruction based on the Fenton reaction and related chemistry. *Critical Reviews in Environmental Science and Technology*, *36*(1), 1–84.

Sabnis, R. W. (2010). Handbook of Biological Dyes and Stains: Synthesisand Industrial Applications. In *Handbook of Biological Dyes and Stains: Synthesisand Industrial Applications*. https://doi.org/10.1002/9780470586242

Santos, E. C. D. S., Watanabe, A., Vargas, M. D., Tanaka, M. N., Garcia, F., & Ronconi, C. M. (2018). AMF-responsive doxorubicin loaded β-cyclodextrin-decorated superparamagnetic nanoparticles. *New Journal of Chemistry*, *42*(1), 671–680. https://doi.org/10.1039/c7nj02860a

Silva, K. T., Leão, P. E., Abreu, F., López, J. A., Gutarra, M. L., Farina, M., Bazylinski, D. A., Freire, D. M. G., & Lins, U. (2013). Optimization of magnetosome production and growth by the magnetotactic vibrio Magnetovibrio blakemorei strain MV-1 through a statistics-based experimental design. *Applied and Environmental Microbiology*, *79*(8), 2823–2827. https://doi.org/10.1128/AEM.03740-12

Vargas, G., Cypriano, J., Correa, T., Leão, P., Bazylinski, D., & Abreu, F. (2018). Applications of magnetotactic bacteria, magnetosomes and magnetosome crystals in biotechnology and nanotechnology: mini-review. *Molecules*, *23*(10), 1–25. https://doi.org/10.3390/molecules23102438

Viollier, E., Inglett, P. ., Hunter, K., Roychoudhury, A. ., & Van Cappellen, P. (2000). The ferrozine method revisited: Fe(II)/Fe(III) determination in natural waters. *Applied Geochemistry*, *15*(6), 785–790. https://doi.org/10.1016/S0883-2927(99)00097-9

Wang, Zhenxing, Guo, J., Ma, J., & Shao, L. (2015). Highly regenerable alkali-resistant magnetic nanoparticles inspired by mussels for rapid selective dye removal offer high-efficiency environmental remediation. *Journal of Materials Chemistry A*, *3*(39), 19960–19968. https://doi.org/10.1039/c5ta04840k

Wang, Zhiqiang, Fang, C., & Megharaj, M. (2014). Characterization of iron-polyphenol nanoparticles synthesized by three plant extracts and their fenton oxidation of azo dye. *ACS Sustainable Chemistry and Engineering*, *2*(4), 1022–1025. https://doi.org/10.1021/sc500021n

Weng, X., Huang, L., Chen, Z., Megharaj, M., & Naidu, R. (2013). Synthesis of iron-based

nanoparticles by green tea extract and their degradation of malachite. *Industrial Crops and Products*, *51*, 342–347. https://doi.org/10.1016/j.indcrop.2013.09.024

Yoshino, T., Hirabe, H., Takahashi, M., Kuhara, M., Takeyama, H., & Matsunaga, T. (2008). Magnetic cell separation using nano-sized bacterial magnetic particles with reconstructed magnetosome membrane. *Biotechnology and Bioengineering*, *101*(3), 470–477. https://doi.org/10.1002/bit.21912

Zanoni, M. V. B., & Yanamaka, H. (2016). *Corantes: Caracterização química, toxicológica, métodos de detecção e tratamento*. Cultura Acadêmica Ed.

Table 1. Rate constants obtained from linear regression analysis of the dye removal data by *M. blakemorei* strain MV-1^T BMs in different conditions. Results in bold indicate best fit to the corresponding kinetic law.

Treatment	First order		Second order	
	k_1 (min^{-1})	R^2	k_2 ($L.mg^{-1}.min^{-1}$)	R^2
BM	0.3583	**0.9686**	0.0726	0.9042
H_2O_2	0.2955	0.7620	0.0565	**0.9203**
BM + H_2O_2	0.5185	0.7836	0.242	**0.9869**

Table 2. Comparison between rate constants obtained from linear regression analysis of the dye removal data from experiments using *M. blakemorei* strain MV-1^T BMs, *M. gryphiswaldense* strain MSR-1 BMs and synthetic MNPs. Results in bold indicate best fit to the corresponding kinetic law.

	First order		Second order		Iron leaching
	k_1 (min^{-1})	R^2	k_2 ($L.mg^{-1}.min^{-1}$)	R^2	% (m/m)
MV-1	0.5185	0.7836	**0.242**	**0.9869**	0,2083
MSR-1	0.7800	0.9652	**0.081**	**0.9852**	0,182263
MNP	0.1950	0.9634	**0.021**	**0.9903**	4,27015

Table 3. Comparison between kinetic data from the present work and results available in the literature. For this comparison, only MNPs claiming a green synthetic route were considered.

Nanoparticle	**dye**	**Removal mechanism**	**Reaction order**	***k***	**additional results**	**reference**
Green tea-stabilized iron oxide NPs	methylene blue	Fenton-like catalysis	Second	0.0039 $L.mg^{-1}.min^{-1}$	> 99% removal within 6 h	Shahwan et al., 2011
	methyl orange		First	0,019 min^{-1}		
Green tea γ-Fe_2O_3/Fe_3O_4 NPs	malachite green	Direct degradation	First	0.057 min^{-1}	96% removal within 60 min	Weng et al., 2013
Eucalyptus tereticornis iron-polyphenol NPs *Melaleuca nesophila* iron-polyphenol NPs *Rosemarinus officinalis* iron-polyphenol NPs	acid black 194	Fenton-like catalysis	First	~0.017 min^{-1}	100% removal within 200 min	Wang et al., 2014
Mussel-inspired Fe_3O_4-PDA/PEI NPs	methyl blue	Adsorption	Pseudo-second	0.0034 $L.mg^{-1}.min^{-1}$	>95% removal in 5 min	Wang et al., 2015
	bengal rose			0.052 $L.mg^{-1}.min^{-1}$	> 90% activity after 10 cycles	
Humic acid-stabilized Fe_3O_4 NPs	malachite green	Adsorption	Pseudo-first	0.02811 min^{-1}		Abate et al., 2020

NP = nanoparticles; PDA = poly-dopamine; PEI = polyethylenimine; k = rate constant

Table 4. Average activity (% in relation to first use) and mean values (nm) of membrane thickness of BM after each reuse cycle in the presence of H_2O_2.

		Reuse cycle			
	Raw	1st	2nd	3rd	4th
Activity	100	87.76	78.97	81.31	43.46
sd	-	1.43	1.98	3.97	11.24
Thickness	7,215	7,428	7,414	7,307	5,54
sd	1,225	2,709	1,917	1,749	1,281
n	225	399	446	333	292

Figure 1. Chemical structure of MB dye (A), showing aniline (encircled in purple dashed line) and triarylmethane (central, encircled in green dotted line). UV-Vis spectrum of raw and treated MB (B) indicating typical absorption peaks a, at 300 nm, and b at 600 nm. Treatment agents are BM solely, H_2O_2 solely and a mixture of both.

Figure 2. Kinetics of dye concentration along 10-min treatments. Effects of BM concentration (A) in absence of H_2O_2, H_2O_2 concentration (B) in the presence and absence of BM, pH (C) and BM membrane removal (D) are plotted.

Figure 3. Linear regression plots for first (A-C) and second (D-F) order kinetics. These plots were used to determine kinetics parameters of MB removal by 80 mg/L BMs (A and D), 36 mM H_2O_2 (B and E) and both (C and F). Note that time considered here was only 5 min because, in most cases, MB concentration at later times were zero.

Figure 4. Relative activity retention of BMs after four reuse cycles in removal of MB in concentrations of 0 and 36 mM H_2O_2.

Figure 5. Transmission electron microscopy of BMs after first to fourth (A-D, respectively) reuse cycles. Arrows indicate BM membranes. * indicates a nebulous substance, presumably degradation products, accumulated between BMs after four cycles.

Figure 1.

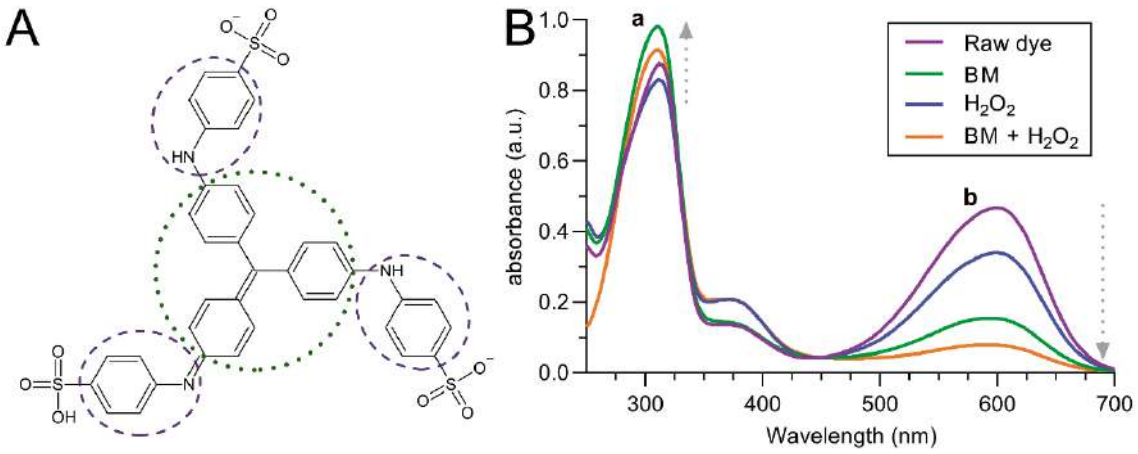

Figure 2.

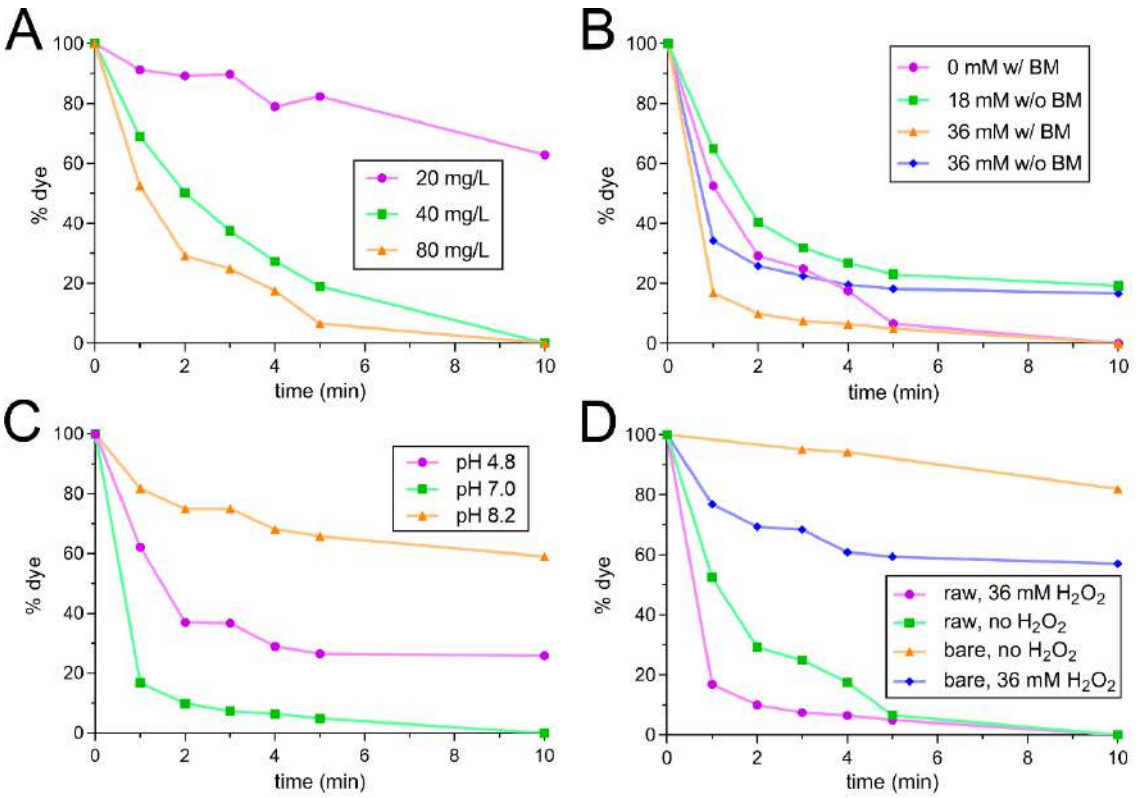

Figure 3.

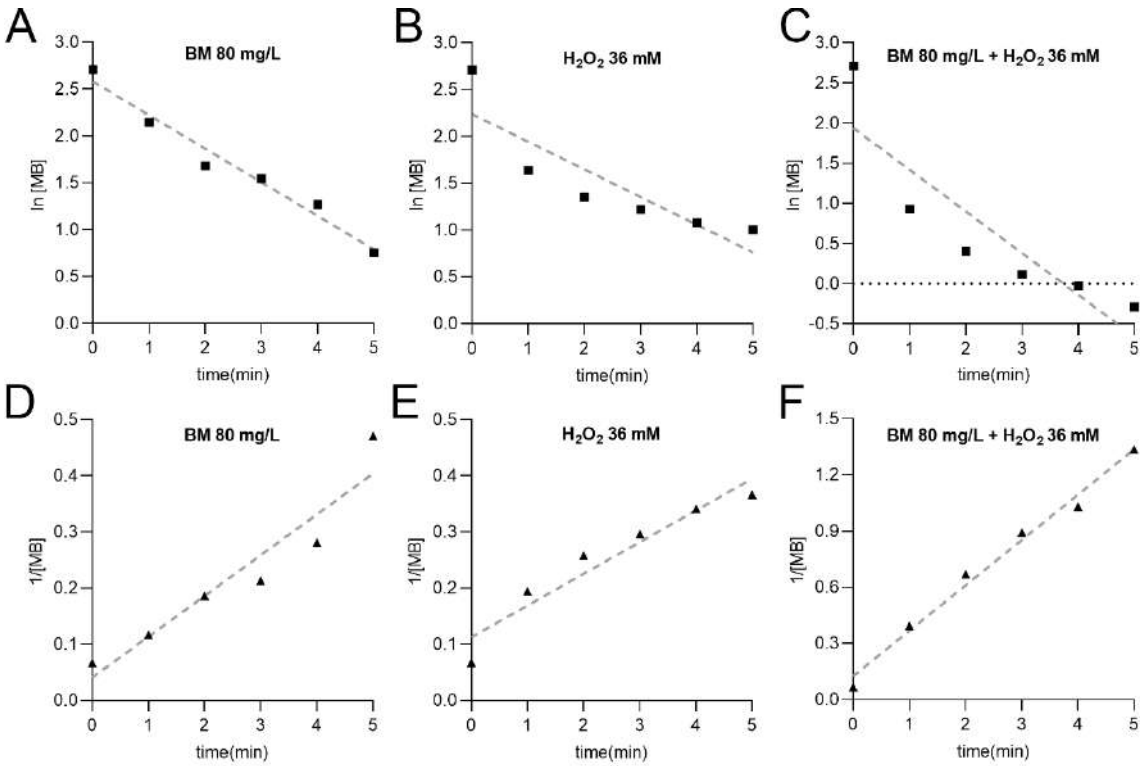

Figure 4.

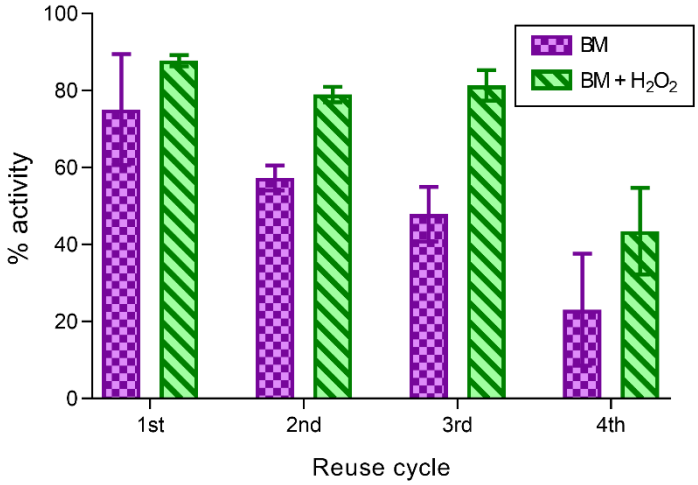

Figure 5.

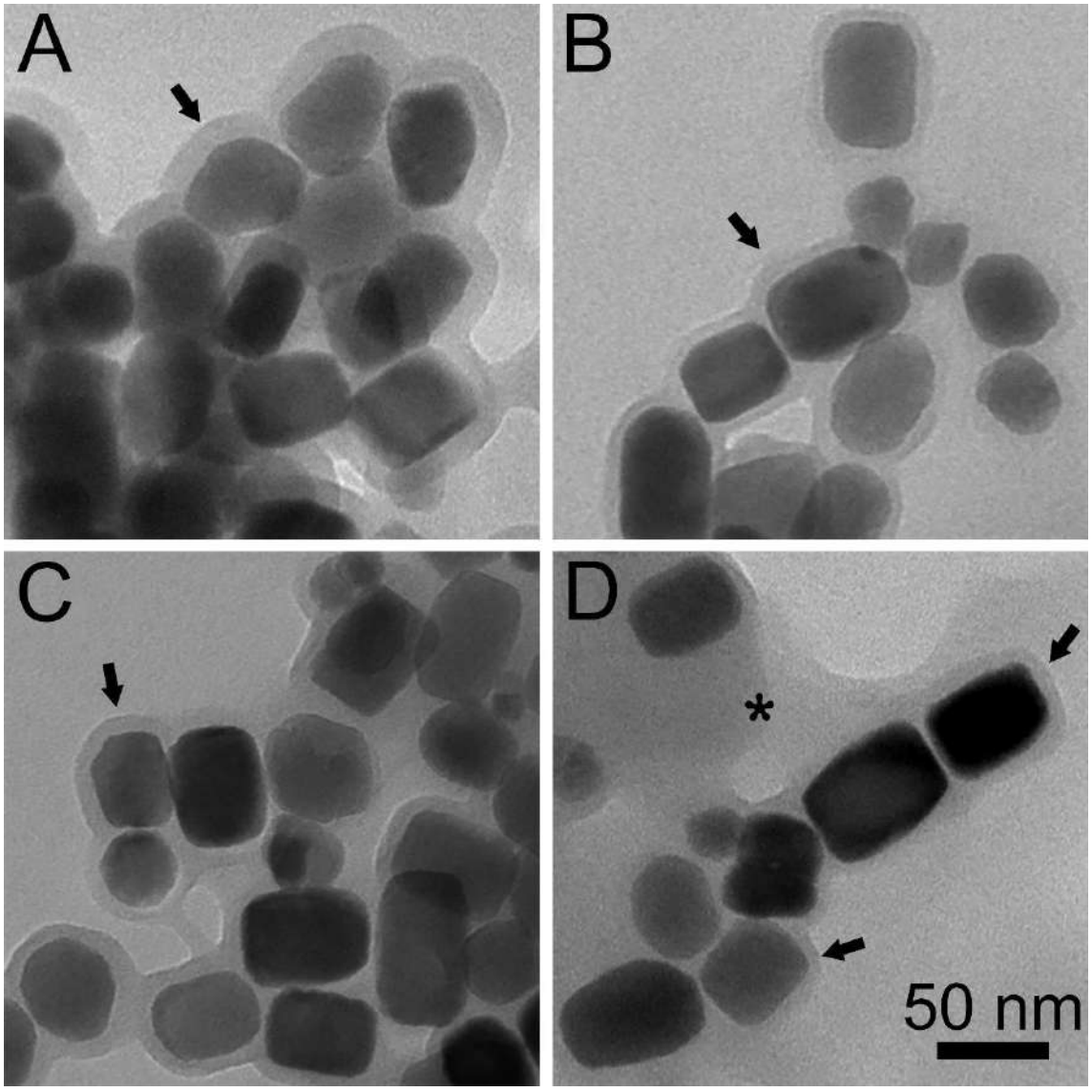

5. Considerações finais

No presente trabalho de tese, foram simulados os processos de fabricação de NMOBs em escala industrial para os processos de batelada alimentada e cultivo semicontínuo do espirilo magnetotático *Ms. gryphiswaldense* cepa MSR-1. Apesar de as BMTs terem sido descritas há cinco décadas e os cultivos em biorreatores terem sido iniciados há vinte anos, até o momento não é do nosso conhecimento a comercialização de NMOBs. Portanto, faz-se necessário prever os possíveis desafios relacionados ao escalonamento do bioprocesso.

Apesar de os custos para a fabricação de NMOBs, os quais derivam essencialmente de custos indiretos de processos, ainda serem superiores àqueles relacionados a processos químicos, as características superiores das NMOBs em relação às sintéticas justificam o maior valor de produção.

Os fatores operacionais, tais como os rendimentos em magnetita e a eficiência de separação magnética, influenciam mais o custo de produção que fatores econômicos, como preço de matérias-primas, taxa de câmbio e capacidade de produção. Independentemente das eventuais variações causadas por tais fatores, os custos mínimos de venda estipulados para as NMOBs são substancialmente inferiores aos valores de mercado de NPMs concorrentes. Essa discrepância pode permitir a comercialização de NMOBs a preços mais elevados e favorecer um rápido retorno aos investimentos de projeto.

Deste modo, a simulação do bioprocesso corrobora a viabilidade da fabricação de NMOBs com vistas a aplicações para fins tecnológicos. Nos curto e médio prazos, os dados gerados neste trabalho irão subsidiar a busca por financiamento de pesquisas para escalonamento dos processos em projetos-piloto. Além disso, o trabalho contribuiu para um levantamento detalhado sobre consumo de matérias-primas, água e energia, além de ter gerado informações sobre emissões ambientais. Esses dados estão atualmente sendo utilizados pelo nosso grupo na elaboração de uma avaliação de ciclo de vida, a qual busca identificar e mensurar os impactos ambientais relacionados à cadeia produtiva do processo estudado.

Ainda como parte do presente trabalho, foi desenvolvida uma solução inovadora para a remoção de um corante têxtil utilizando-se de propriedades intrínsecas de NMOBs.

Nas condições experimentais, obteve-se 100% de degradação do corante azul de metila, inclusive na ausência de peróxido de hidrogênio. A atividade descolorante das NMOBs na ausência de peróxido, que possui uma alta toxicidade devido ao seu caráter oxidante, torna os processos de remediação de corantes mais "verdes".

Os nossos resultados sugerem que a descoloração ocorre através de uma catálise oxidativa, provavelmente desempenhada por proteínas com atividades de peroxidase inseridas na membrana das NMOBs. O reuso das NMOBs em múltiplas reações de degradação com retenção, ainda que parcial, de sua atividade aumenta o caráter econômico da utilização de NPMs microbianas, assim como seus baixos valores de venda.

Como perspectiva, pretende-se expandir a aplicabilidade de NMOBs para a remoção de outros poluentes orgânicos, incluindo outros corantes, presentes em efluentes industriais, principalmente do estado do Rio de Janeiro. Pretende-se, também, realizar avaliações de toxicidade entre as amostras brutas e tratadas, a fim de se confirmar a redução dos potenciais impactos causados pelos efluentes após seu tratamento com NMOBs.

6. Referências

ABIT. (2019). Perfil do setor. Acesso em 10 de março de 2020, disponível em: https://www.abit.org.br/cont/perfil-do-setor.

Abreu, F., Morillo, V., Trubitsyn, D., & Bazylinski, D. A. (2020) Magnetotaxis in Prokaryotes. *eLS*, 1-14.

Ali, A., Shah, T., Ullah, R., Zhou, P., Guo, M., Ovais, M., ... & Rui, Y. (2021). Review on recent progress in magnetic nanoparticles: synthesis, characterization, and diverse applications. *Frontiers in chemistry*, 548.

de Almeida, É. J. R., Dilarri, G., & Corso, C. R. (2014). A indústria têxtil no Brasil: Uma revisão dos seus impactos ambientais e possíveis tratamentos para os seus efluentes. *Conexão Água*.

Alphandéry, E. (2014). Applications of magnetosomes synthesized by magnetotactic bacteria in medicine. *Frontiers in bioengineering and biotechnology*, *2*, 5.

Amor, M., Mathon, F. P., Monteil, C. L., Busigny, V., & Lefevre, C. T. (2020). Iron-biomineralizing organelle in magnetotactic bacteria: function, synthesis and preservation in ancient rock samples. *Environmental microbiology*, *22*(9), 3611-3632.

Askeland, D., & Wright, W. (2016). The science and engineering of materials. 7ª ed. *Boston: Cengage Learning*.

Augusto, P. A., Castelo-Grande, T., Vargas, D., Pascual, A., Hernández, L., Estevez, A. M., & Barbosa, D. (2020). Upscale design, process development, and economic analysis of industrial plants for nanomagnetic particle production for environmental and biomedical use. *Materials*, *13*(11), 2477.

Basit, A., Wang, J., Guo, F., Niu, W., & Jiang, W. (2020). Improved methods for mass production of magnetosomes and applications: a review. *Microbial Cell Factories*, *19*(1), 1-11.

Bayda, S., Adeel, M., Tuccinardi, T., Cordani, M., & Rizzolio, F. (2020). The history of nanoscience and nanotechnology: from chemical–physical applications to nanomedicine. *Molecules*, *25*(1), 112.

Bazylinski, D. A., & Frankel, R. B. (2004). Magnetosome formation in prokaryotes. *Nature reviews microbiology*, *2*(3), 217-230.

Bazylinski, D. A., Williams, T. J., Lefevre, C. T., Trubitsyn, D., Fang, J., Beveridge, T. J., ... & Simpson, B. (2013). *Magnetovibrio blakemorei* gen. nov., sp. nov., a magnetotactic bacterium (Alphaproteobacteria: Rhodospirillaceae) isolated from a salt marsh. *International journal of systematic and evolutionary microbiology*, *63*(5), 1824-1833.

Berny, C., Le Fèvre, R., Guyot, F., Blondeau, K., Guizonne, C., Rousseau, E., ... & Alphandéry, E. (2020). A method for producing highly pure magnetosomes in large quantity for medical applications using *Magnetospirillum gryphiswaldense* MSR-1 magnetotactic bacteria amplified in minimal growth media. *Frontiers in bioengineering and biotechnology*, *8*, 16.

de Carvalho, J. C., Medeiros, A. B. P., Letti, L. A. J., Kirnev, P. C. S., & Soccol, C. R. (2017). Cell Disruption and Isolation of Intracellular Products. In *Current Developments in Biotechnology and Bioengineering* (pp. 807-822). Elsevier.

Coelho, M. A. Z., & Ribeiro, B. D. (Eds.). (2016). *White biotechnology for sustainable chemistry*. Royal Society of Chemistry.

Correa, T. N. (2019). Otimização do processo de produção de nanopartículas magnéticas de origem bacteriana funcionalizadas com anfotericina B. (Dissertação de mestrado, Universidade Federal do Rio de Janeiro).

Correa, T. N., Taveira, I. N., de Souza Filho, R. P., & de Avila Abreu, F. (2020). Biomineralization of magnetosomes: Billion-year evolution shaping modern nanotools. In *Biomineralization*. IntechOpen.

Correa, T., Bazylinski, D. A., Garcia, F. & Abreu, F. (2021). A rapid and simple preparation of amphotericin B-loaded bacterial magnetite nanoparticles. *RSC advances*, *11*(45), 28000-28007.

Cypriano, J., Werckmann, J., Vargas, G., dos Santos, A. L., Silva, K. T., Leao, P., ... & Abreu, F. (2019). Uptake and persistence of bacterial magnetite magnetosomes in a mammalian cell line: Implications for medical and biotechnological applications. *PloS one*, *14*(4).

Emergen Research (2021). *Nanotechnology Market Size: Nanotechnology Industry Overview by 2028*. https://www.emergenresearch.com/industry-report/nanotechnology-market. Acesso em 10 de agosto de 2021.

Faivre, D., Menguy, N., Pósfai, M., & Schüler, D. (2008). Environmental parameters affect the physical properties of fast-growing magnetosomes. *American mineralogist*, *93*(2-3), 463-469.

Fernández-Castané, A., Li, H., Thomas, O. R., & Overton, T. W. (2018). Development of a simple intensified fermentation strategy for growth of *Magnetospirillum gryphiswaldense* MSR-1: Physiological responses to changing environmental conditions. *New biotechnology*, *46*, 22-30.

FIRJAN. (2018). Os setores têxtil e de confecção e a Firjan. Acesso em 10 de março de 2020, disponível em: https://www.firjan.com.br/o-sistema-firjan/setores-de-atuacao/textil-e-confeccao.htm.

Ginet, N., Pardoux, R., Adryanczyk, G., Garcia, D., Brutesco, C., & Pignol, D. (2011). Single-step production of a recyclable nanobiocatalyst for organophosphate pesticides biodegradation using functionalized bacterial magnetosomes. *PLoS One*, *6*(6), e21442.

Grasso, G., Zane, D., & Dragone, R. (2020). Microbial nanotechnology: challenges and prospects for green biocatalytic synthesis of nanoscale materials for sensoristic and biomedical applications. *Nanomaterials*, *10*(1), 11.

Guo, F., Liu, Y., Chen, Y., Tang, T., Jiang, W., Li, Y., & Li, J. (2011). A novel rapid and continuous procedure for large-scale purification of magnetosomes from Magnetospirillum gryphiswaldense. *Applied microbiology and biotechnology*, *90*(4), 1277-1283.

Heyen, U., & Schüler, D. (2003). Growth and magnetosome formation by microaerophilic *Magnetospirillum* strains in an oxygen-controlled fermentor. *Applied microbiology and biotechnology*, *61*(5-6), 536-544.

Jain, K., Patel, A. S., Pardhi, V. P., & Flora, S. J. S. (2021). Nanotechnology in wastewater management: a new paradigm towards wastewater treatment. *Molecules*, *26*(6), 1797.

Katheresan, V., Kansedo, J., & Lau, S. Y. (2018). Efficiency of various recent wastewater dye removal methods: A review. *Journal of environmental chemical engineering*, *6*(4), 4676-4697.

Ke, L., Chen, Y., Liu, P., Liu, S., Wu, D., Yuan, Y., ... & Gao, M. (2018). Characteristics and optimised fermentation of a novel magnetotactic bacterium, Magnetospirillum sp. ME-1. *FEMS microbiology letters*, *365*(14), fny052.

Kim, D., Lee, N., Park, M., Kim, B. H., An, K., & Hyeon, T. (2009). Synthesis of uniform ferrimagnetic magnetite nanocubes. *Journal of the American Chemical Society*, *131*(2), 454-455.

Koutinas, A. A., Chatzifragkou, A., Kopsahelis, N., Papanikolaou, S., & Kookos, I. K. (2014). Design and techno-economic evaluation of microbial oil production as a renewable resource for biodiesel and oleochemical production. *Fuel*, *116*, 566-577.

Kudr, J., Haddad, Y., Richtera, L., Heger, Z., Cernak, M., Adam, V., & Zitka, O. (2017). Magnetic nanoparticles: From design and synthesis to real world applications. *Nanomaterials*, *7*(9), 243.

Lefèvre, C. T., & Bazylinski, D. A. (2013). Ecology, diversity, and evolution of magnetotactic bacteria. *Microbiology and molecular biology reviews*, *77*(3), 497-526.

Li, J., & Pan, Y. (2012). Environmental factors affect magnetite magnetosome synthesis in *Magnetospirillum magneticum* AMB-1: implications for biologically controlled mineralization. *Geomicrobiology Journal*, *29*(4), 362-373.

Lin, W., Bazylinski, D. A., Xiao, T., Wu, L. F., & Pan, Y. (2014). Life with compass: diversity and biogeography of magnetotactic bacteria. *Environmental microbiology*, *16*(9), 2646-2658.

Lin, W., Zhang, W., Zhao, X., Roberts, A. P., Paterson, G. A., Bazylinski, D. A., & Pan, Y. (2018). Genomic expansion of magnetotactic bacteria reveals an early common origin of magnetotaxis with lineage-specific evolution. *The ISME journal*, *12*(6), 1508-1519.

Liu, J., Ding, Y., Jiang, W., Tian, J., Li, Y., & Li, J. (2008). A mutation upstream of an ATPase gene significantly increases magnetosome production in *Magnetospirillum gryphiswaldense*. *Applied microbiology and biotechnology*, *81*(3), 551-558.

Liu, Y., Li, G. R., Guo, F. F., Jiang, W., Li, Y., & Li, L. J. (2010). Large-scale production of magnetosomes by chemostat culture of *Magnetospirillum gryphiswaldense* at high cell density. *Microbial cell factories*, *9*(1), 1-8.

Lower, B. H., & Bazylinski, D. A. (2013). The bacterial magnetosome: a unique prokaryotic organelle. *Journal of molecular microbiology and biotechnology*, *23*(1-2), 63-80.

Mamat, U., Wilke, K., Bramhill, D., Schromm, A. B., Lindner, B., Kohl, T. A., ... & Woodard, R. W. (2015). Detoxifying *Escherichia coli* for endotoxin-free production of recombinant proteins. *Microbial cell factories*, *14*(1), 1-15.

Mandawala, C., Chebbi, I., Durand-Dubief, M., Le Fèvre, R., Hamdous, Y., Guyot, F., & Alphandéry, E. (2017). Biocompatible and stable magnetosome minerals coated with poly-l-lysine, citric acid, oleic acid, and carboxy-methyl-dextran for application in the magnetic hyperthermia treatment of tumors. *Journal of Materials Chemistry B*, *5*(36), 7644-7660.

McNeil, B., & Harvey, L. (Eds.). (2008). *Practical fermentation technology*. John Wiley & Sons.

Mondal, P., Anweshan, A., & Purkait, M. K. (2020). Green synthesis and environmental application of iron-based nanomaterials and nanocomposite: A review. *Chemosphere*, 127509.

Nan, X., Lai, W., Li, D., Tian, J., Hu, Z., & Fang, Q. (2021). Biocompatibility of Bacterial Magnetosomes as MRI Contrast Agent: A Long-Term In Vivo Follow-Up Study. *Nanomaterials*, *11*(5), 1235.

Organização Mundial da Saúde. (2019). *The international pharmacopoeia*. 4ª ed. World Health Organization.

Park, J., An, K., Hwang, Y., Park, J. G., Noh, H. J., Kim, J. Y., ... & Hyeon, T. (2004). Ultra-large-scale syntheses of monodisperse nanocrystals. *Nature materials*, *3*(12), 891-895.

Petrides, D., Carmichael, D., Siletti, C., & Koulouris, A. (2019). Bioprocess Simulation and Economics. In *Essentials in Fermentation Technology* (pp. 273-305). Springer, Cham.

Pi, F., Sun, J., Liu, W., Sun, X., & Zhang, Y. (2017). Elimination of aflatoxin B1 in vegetable oil based on immuno-magnetosomes probes from a novel magnetotactic bacterium. *Food Control*, *80*, 319-326.

Pignatello, J. J., Oliveros, E., & MacKay, A. (2006). Advanced oxidation processes for organic contaminant destruction based on the Fenton reaction and related chemistry. *Critical reviews in environmental science and technology*, *36*(1), 1-84.

Pósfai, M., Lefèvre, C., Trubitsyn, D., Bazylinski, D. A., & Frankel, R. (2013). Phylogenetic significance of composition and crystal morphology of magnetosome minerals. *Frontiers in microbiology*, *4*, 344.

Rosenfeldt, S., Mickoleit, F., Jörke, C., Clement, J. H., Markert, S., Jérôme, V., ... & Schenk, A. S. (2021). Towards standardized purification of bacterial magnetic nanoparticles for future in vivo applications. *Acta Biomaterialia*, *120*, 293-303.

Sannigrahi, S., Arumugasamy, S. K., Mathiyarasu, J., & Suthindhiran, K. (2020). Development of magnetosomes-based biosensor for the detection of *Listeria monocytogenes* from food sample. *IET nanobiotechnology*, *14*(9), 839-850.

Santos, E. C. D. S., Watanabe, A., Vargas, M. D., Tanaka, M. N., Garcia, F., & Ronconi, C. M. (2018). AMF-responsive doxorubicin loaded β-cyclodextrin-decorated superparamagnetic nanoparticles. *New Journal of Chemistry*, *42*(1), 671-680.

Schübbe, S., Kube, M., Scheffel, A., Wawer, C., Heyen, U., Meyerdierks, A., ... & Schüler, D. (2003). Characterization of a spontaneous nonmagnetic mutant of *Magnetospirillum gryphiswaldense* reveals a large deletion comprising a putative magnetosome island. *Journal of Bacteriology*, *185*(19), 5779-5790.

Scown, C. D., Baral, N. R., Yang, M., Vora, N., & Huntington, T. (2021). Technoeconomic analysis for biofuels and bioproducts. *Current Opinion in Biotechnology*, *67*, 58-64.

Shahwan, T., Sirriah, S. A., Nairat, M., Boyacı, E., Eroğlu, A. E., Scott, T. B., & Hallam, K. R. (2011). Green synthesis of iron nanoparticles and their application as a Fenton-like catalyst for the degradation of aqueous cationic and anionic dyes. *Chemical Engineering Journal*, *172*(1), 258-266.

Silva, K. T., Leão, P. E., Abreu, F., López, J. A., Gutarra, M. L., Farina, M., ... & Lins, U. (2013). Optimization of magnetosome production and growth by the magnetotactic vibrio *Magnetovibrio blakemorei* strain MV-1 through a statistics-based experimental design. *Applied and environmental microbiology*, *79*(8), 2823-2827.

Simeonidis, K., Liébana-Viñas, S., Wiedwald, U., Ma, Z., Li, Z. A., Spasova, M., ... & Angelakeris, M. (2016). A versatile large-scale and green process for synthesizing magnetic nanoparticles with tunable magnetic hyperthermia features. *RSC advances*, *6*(58), 53107-53117.

Sparks, N. H. C., Mann, S., Bazylinski, D. A., Lovley, D. R., Jannasch, H. W., & Frankel, R. B. (1990). Structure and morphology of magnetite anaerobically-produced by a marine magnetotactic bacterium and a dissimilatory iron-reducing bacterium. *Earth and planetary science letters*, *98*(1), 14.

Sun, J. B., Zhao, F., Tang, T., Jiang, W., Tian, J. S., Li, Y., & Li, J. L. (2008). High-yield growth and magnetosome formation by *Magnetospirillum gryphiswaldense* MSR-1 in an oxygen-controlled fermentor supplied solely with air. *Applied microbiology and biotechnology*, *79*(3), 389-397.

Ullrich, S., Kube, M., Schübbe, S., Reinhardt, R., & Schüler, D. (2005). A hypervariable 130-kilobase genomic region of *Magnetospirillum gryphiswaldense* comprises a magnetosome island which undergoes frequent rearrangements during stationary growth. *Journal of bacteriology*, *187*(21), 7176-7184.

Vargas, G., Cypriano, J., Correa, T., Leão, P., Bazylinski, D. A., & Abreu, F. (2018). Applications of magnetotactic bacteria, magnetosomes and magnetosome crystals in biotechnology and nanotechnology: mini-review. *Molecules*, *23*(10), 2438.

Viollier, E., Inglett, P. W., Hunter, K., Roychoudhury, A. N., & Van Cappellen, P. (2000). The ferrozine method revisited: Fe (II)/Fe (III) determination in natural waters. *Applied geochemistry*, *15*(6), 785-790.

Wallyn, J., Anton, N., & Vandamme, T. F. (2019). Synthesis, principles, and properties of magnetite nanoparticles for in vivo imaging applications — A review. *Pharmaceutics*, *11*(11), 601.

Wang, Z., Fang, C., & Megharaj, M. (2014). Characterization of iron–polyphenol nanoparticles synthesized by three plant extracts and their fenton oxidation of azo dye. *ACS Sustainable Chemistry & Engineering*, *2*(4), 1022-1025.

Wu, L., Mendoza-Garcia, A., Li, Q., & Sun, S. (2016). Organic phase syntheses of magnetic nanoparticles and their applications. *Chemical reviews*, *116*(18), 10473-10512.

Yang, C., Takeyama, H., & Matsunaga, T. (2001). Iron feeding optimization and plasmid stability in production of recombinant bacterial magnetic particles by *Magnetospirillum magneticum* AMB-1 in fed-batch culture. *Journal of bioscience and bioengineering*, *91*(2), 213-216.

Yang, Z., Qiao, S., Sun, S., & Hou, Y. (2017). Overview of magnetic nanomaterials. *Magnetic Nanomaterials: Fundamentals, Synthesis and Applications*.

Yang, W., Tang, Q., Bai, Y., Wang, K., Dong, X., Li, Y., & Fang, M. (2020). Bacterial magnetic particles-polyethylenimine vectors deliver target genes into multiple cell types with a high efficiency and low toxicity. *Applied microbiology and biotechnology*, *104*(15), 6799-6812.

Yoshino, T., Hirabe, H., Takahashi, M., Kuhara, M., Takeyama, H., & Matsunaga, T. (2008). Magnetic cell separation using nano-sized bacterial magnetic particles with reconstructed magnetosome membrane. *Biotechnology and bioengineering*, *101*(3), 470-477.

Zhang, Y., Zhang, X., Jiang, W., Li, Y., & Li, J. (2011). Semicontinuous culture of *Magnetospirillum gryphiswaldense* MSR-1 cells in an autofermentor by nutrient-balanced and isosmotic feeding strategies. *Applied and environmental microbiology*, *77*(17), 5851-5856.

7. Anexos

Anexo 1. Materiais suplementares para o artigo "*Why does not nanotechnology go green? Bioprocess simulation and economics for bacterial-origin magnetite nanoparticles* (Correa et al., 2021)"

Anexo 2. Materiais suplementares para o artigo "*Bacterial-origin magnetic nanoparticles for decolorization of methyl blue dye"*

Anexo 3. Artigo sobre nanoformulação magnética de anfotericina B (Correa et al., 2021)

Anexo 4. Patente depositada sobre os bioprocessos contínuos de *Magnetovibrio blakemorei* cepa MV-1^{T}

Anexo 5. Patente depositada sobre a nanoformulação magnética de anfotericina B

Anexo 6. Capítulo de livro sobre produtos biotecnológicos de microrganismos da Antártida (Correa et al., 2020)

Anexo 7. Capítulo de livro sobre biomineralização em BMTs (Correa et al., 2020)

Supplementary Material

1 Supplementary Information - Downstream section design

Guo et al., (2011) designed a magnetic isolation system comprised of a high-pressure homogenizer, a magnetic separation column (MSC), an ultrasonic bath tank, and an electro-elution tank. Because of extreme energy consumption and heat release – and the consequent need for refrigeration – ultrasonic lysis is not adapted for industrial scales (de Carvalho, 2017). Thus, we have not considered this operation in our simulation. Another magnetic separation system has been developed by Rosenfeldt et al., (2020), where, like the previous one, high-pressure cell lysate goes through an MSC for BMNs enrichment. Nevertheless, the designs of MSCs in those two works show a crucial difference. While 5-mm carbon stells beads are used as the magnetizable matrix in the first work, the matrix in the latter is a ferromagnetic fiber. The matrix material seems to substantially influence BMNs separation. In the first case, 300 mg BMNs are recovered from 6 L culture – approximately 50 mg/L of final yield. Using a fibrous matrix, it was related that only 66.5% of adsorbed iron (in form of BMNs) is recovered after column percolation. Therefore, our simulated MSC matrix is composed of 2-mm stainless beads (Figure S2), assuming a presumably better BMNs recovery. Here, the bead diameter is reduced for a larger adsorbing surface. Additionally, the column wall material, aluminum, was chosen because it is a non-ferromagnetic metal. In Rosenfeldt et al., (2020), MSC elution is followed by an ultracentrifugation step in which BMNs are sedimented onto a sucrose cushion. In industry, ultracentrifugation is not usually used for large-scale separation (Harrison et al., 2015). Alternatively, we opted for a disk-stack centrifuge due to its versatility in separating small-dimension solids, high rotation speeds, and large-volume processing capacity (Talerton & Wakeman, 2006).

2 Supplementary Figures

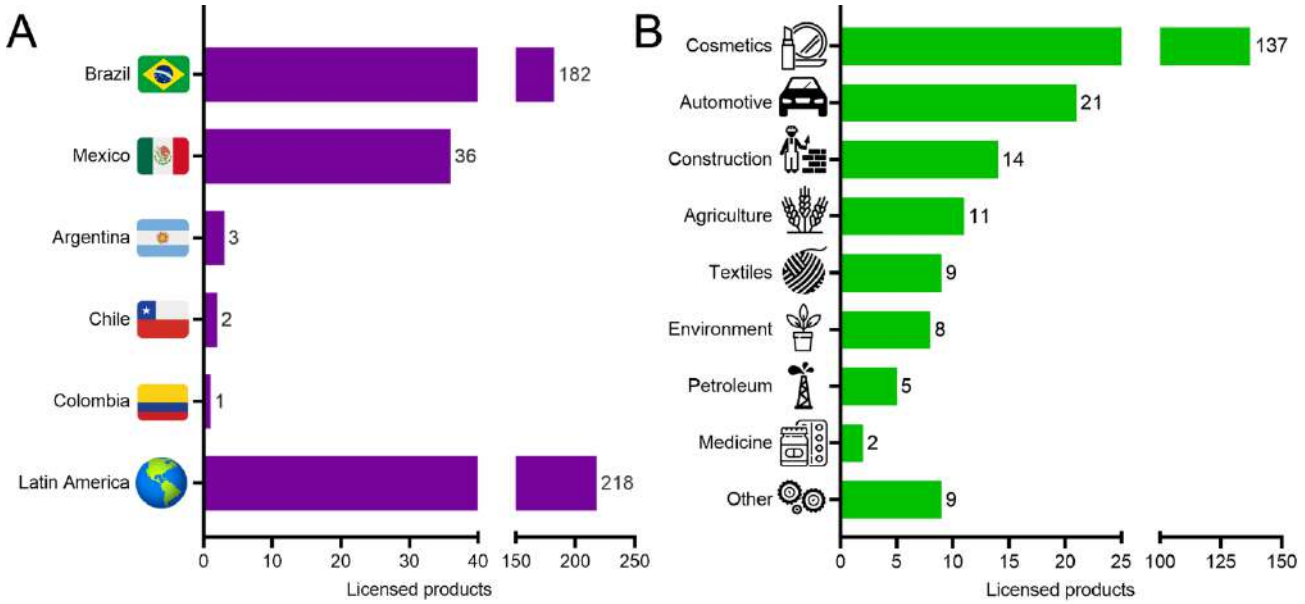

Supplementary Figure 1. Number of registered nanotechnological products in Latin America categorized by country (A) and end-user sector (B). Data from StatNano (2020).

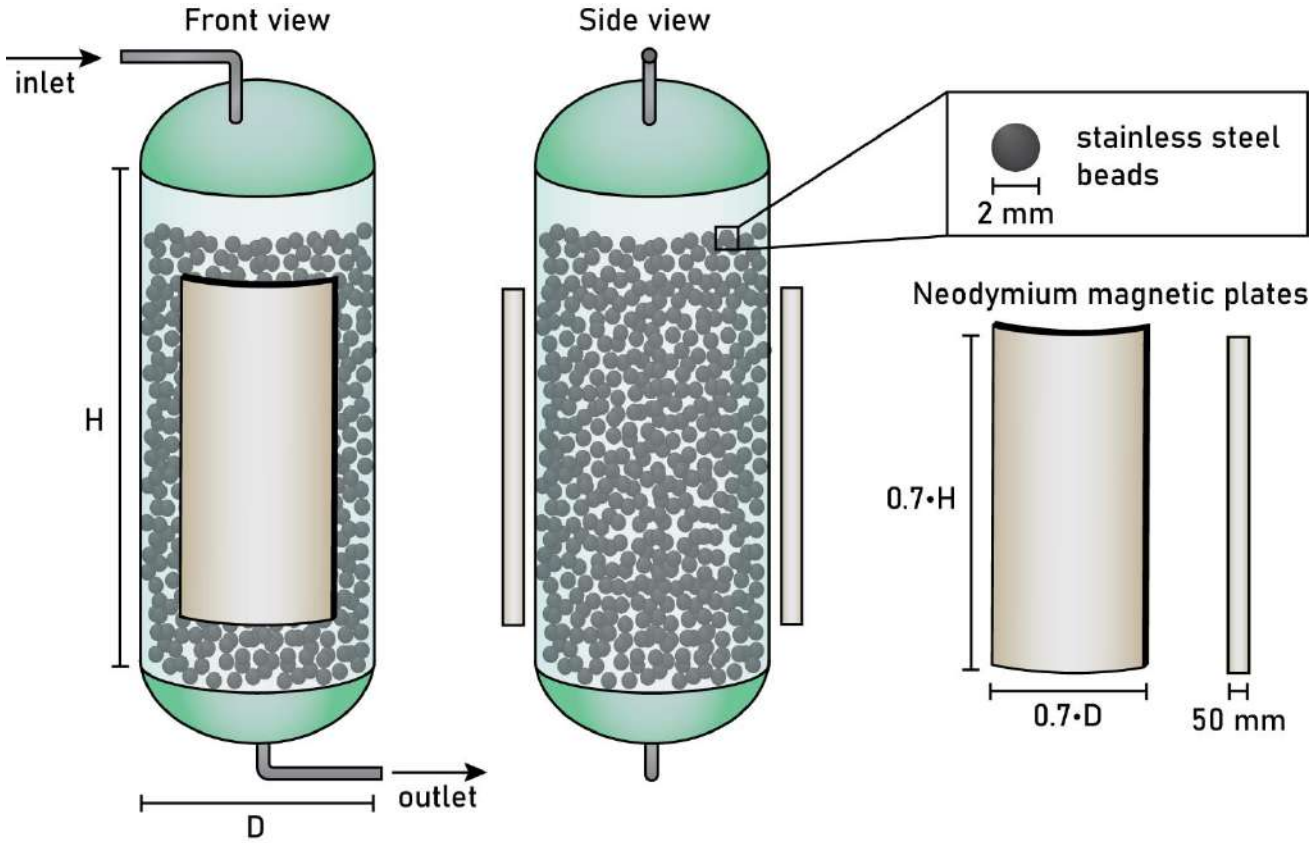

Supplementary Figure 2. Magnetic separation column design.

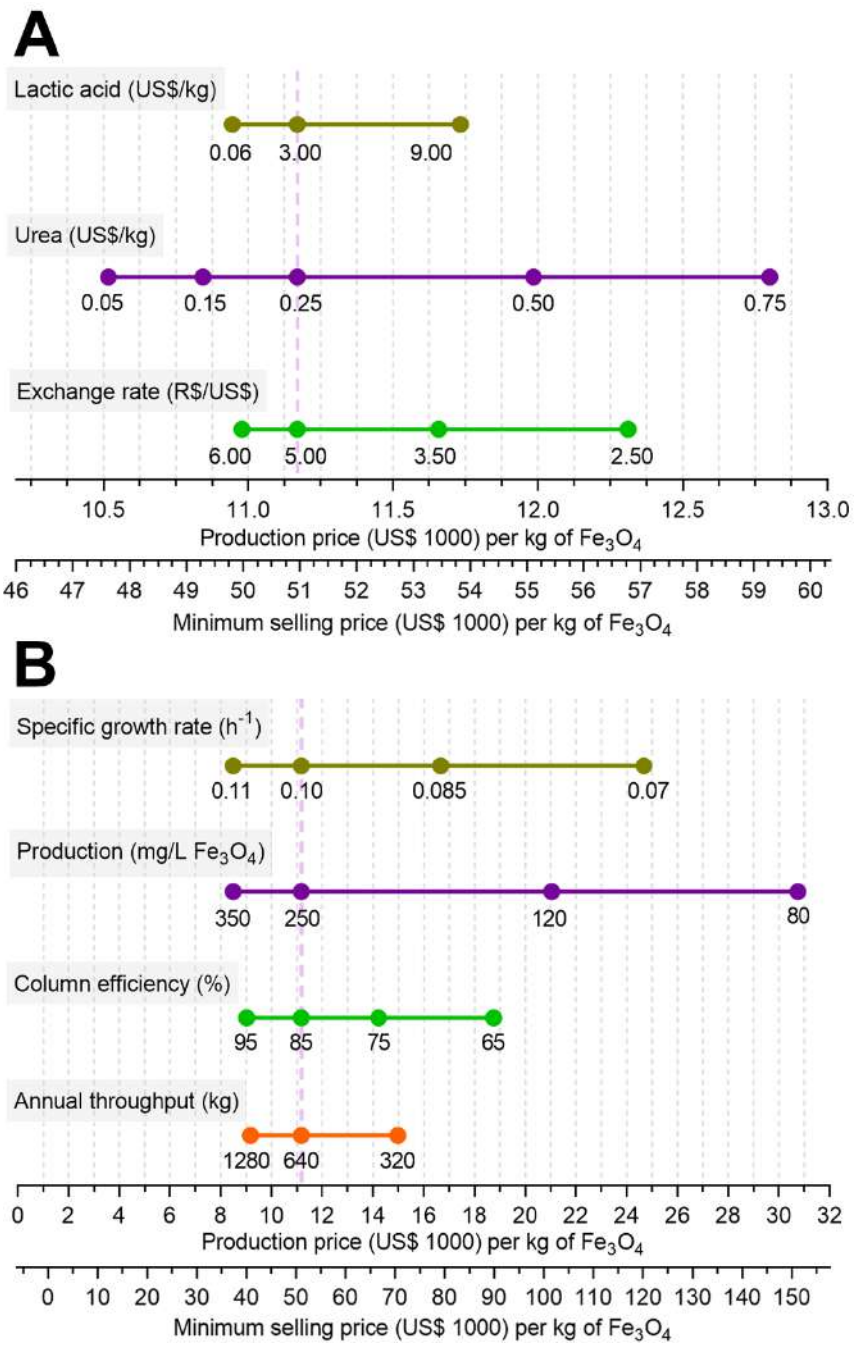

Supplementary Figure 3. Sensitivity analyses showing effects of variations in economic (A) and bioprocess-related (B) parameters on unitary production costs and minimum selling prices (MSP) for the semicontinuous process. The purple dashed vertical line indicates base-case scenario.

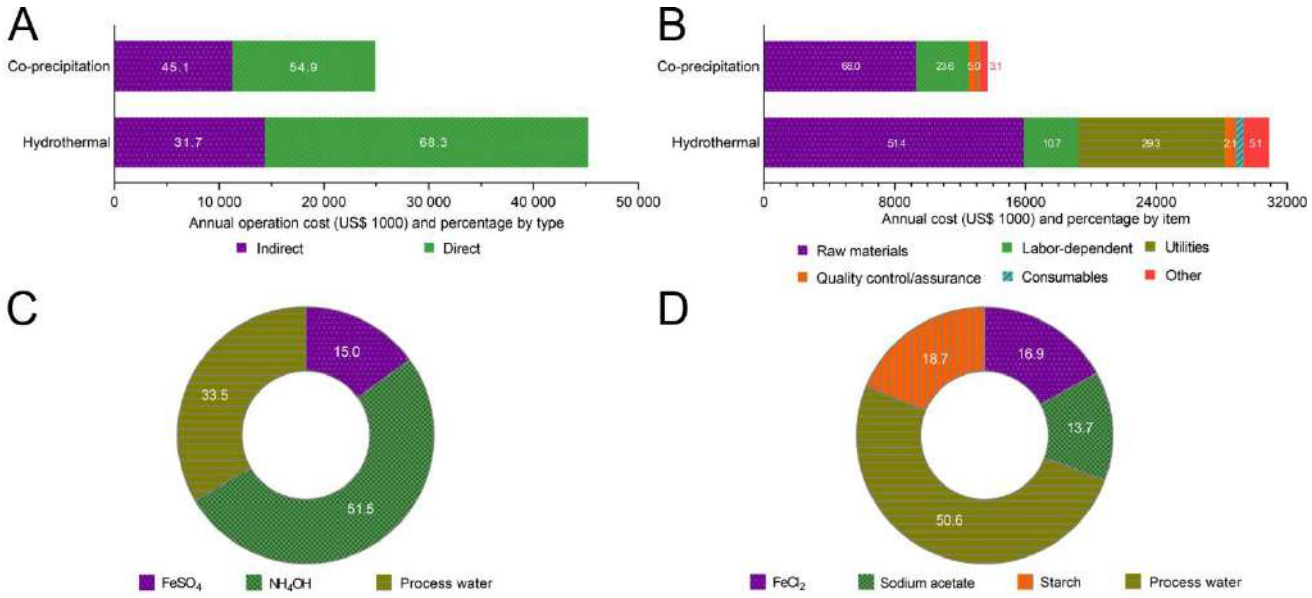

Supplementary Figure 4. Operating costs composition breakdowns for the production of magnetic nanoparticles by synthetic chemical routes based on the data reported by Augusto et al (2020). Direct and indirect cost contributions for co-precipitation and hydrothermal processes (A). Direct operating costs breakdown showing cost types (B). Material costs compositions from co-precipitation (C) and hydrothermal (D) processes.

3 Supplementary Tables

Supplementary Table 1. Iron oxide nanoparticle demand estimation for the selected market

Parameter	Value	Reference
International consumption (2019)	3500 ton	Nano-Powder Factory (2020)
Demand increase for the period 2020-2022	12%	Nano-Powder Factory (2020)
Registered nanotechnological products - World	8963	Nano-Powder Factory (2020)
Share of nanotechnological products in Latin America	2.4%	Nano-Powder Factory (2020)
Share of products in the biomedical and environmental sectors	4.6%	Nano-Powder Factory (2020)
Estimated annual demand in Latin America for the selected sectors	640 kg	estimated

Supplementary Table 2. Method used for plant cost calculations.

Parameter	Method of calculation
Total plant direct cost (TPDC)	$TPDC = PC + C_{installation} + C_{piping} + C_{instrumentation} + C_{insulation} + C_{electrical} + C_{buildings} + C_{yard} + C_{auxiliary}$
Equipment purchase cost (PC)	Simulated based on process sizing and cost indexes
Instalation ($C_{installation}$)	= PC × 0.30 (for fermentation section and seed train) = PC × 0.50 (for nanoparticle extraction section)
Process piping (C_{piping})	= PC × 0.35

Instrumentation ($C_{instrumentation}$)	= PC × 0.40
Insulation ($C_{insulation}$)	= PC × 0.03
Electrical facilities ($C_{electrical}$)	= PC × 0.10
Buildings ($C_{buildings}$)	= PC × 0.45
Yard improvement (C_{yard})	= PC × 0.15
Auxiliary facilities ($C_{auxiliary}$)	= PC × 0.40
Total plant indirect cost (TPIC)	PIC = $C_{engineering}$ + $C_{construction}$
Engineering ($C_{engineering}$)	= TPDC × 0.25
Construction ($C_{construction}$)	= TPDC × 0.35
Total plant cost (TPC)	TPC = TPDC + TPIC
Contractor's fee	= TPC × 0.05
Contingency	= TPC × 0.10
Direct fixed capital (DFC)	DFC = TPC + Contractor's fee + Contingency
Working capital	= DFC × 0.003
Start-up validation	= DFC × 0.05
Capital Investment	**= DFC + Working capital + Start-up validation**

Supplementary Table 3. Method used for operating cost calculations.

Cost item	Type	Method of calculation

Raw materials	Direct	Simulated based on prices listed on Table S2
Labor	Direct	= Basic rate (Table S4) × 1.3
Consumables	Direct	Simulated based on prices listed on Table S5
Laboratory / Quality control	Direct	= Labor × 0.15
Waste treatment and disposal	Direct	Simulated based on prices listed on Table S3
Utilities	Direct	Simulated based on prices listed on Table S3
Facility-related	Indirect	Equipment-dependent
Miscellaneous	Indirect	= 0.08 × TPC

Supplementary Table 4. Cost of raw material

Material	US$/kg	Source
Lactic acid	3.00	Adicel.com.br
Sodium lactate	1.50	Molbase.com
NH_4OH	0.45	Echemi.com
NH_4Cl	0.093	Echemi.com
Yeast extract	2.5	Molbase.com
$FeCl_3$	0.49	Echemi.com
$MgSO_4$	0.086	Echemi.com

$NaNO_3$	1.25	Echemi.com
Mineral elixir[a]	0.32	Echemi.com
Na_2HPO_4	5.06	Molbase.com
KH_2PO_4	1.13	Echemi.com
NaCl	0.335	Echemi.com
KCl	0.269	Echemi.com
Urea	0.25	Echemi.com
Sucrose	0.26	Mfrural.com.br
NaOH	0.01	Molbase.com
H_3PO_4	0.03	Echemi.com
Process water	5.91[b]	de Andrade (2014)
[a] calculated from individual components as in Wolin, Wolin and Wolfe (1963)		
[b] price in US$/m³, based on the process of BioManguinhos, Rio de Janeiro, Brazil		

Supplementary Table 5. Cost of utilities

Material	Price (US$)	Source
Potable water	3.27/m³	de Andrade (2014)
Steam[a]	16.82/MT	Ruediger (2014)
Electricity	86.11/MWh	ANEEL (2020)

Effluent treatment[b]	0.63/m³	Dalri-Cecato et al. (2019)
[a] for steam generated on natural gas		
[b] for a membrane bioreactor treatment		

Supplementary Table 6. Cost of labor, financing conditions and price indices

Labour		
Average salary for pharma-chemical sector	R$ 52 746.57/year	IBGE (2019)
Financing		
Debt	up to 80% of project	Finep (2020)
Loan period	up to 10 years	Finep (2020)
Loan interest rate	8.42%	Calculated Finep rate for innovative medium-sized industrial projects
Price indices		
CE Plant Cost Index	607.5 (for 2019)	Chemical Engineering (2020)
Producer Price Index (Brazil)	116.29 (for 2020)	IBGE (2020)
Dollar/Real exchange rate	5.20 (as of June, 2020)	Banco Central do Brasil (2020)

Supplementary Table 7. Material factors and prices for magnetic separation columns

Item	Material factor or price	Reference

Carbon steel	1.0	Towler & Sinnott (2013)
Aluminium and bronze	1.07	Towler & Sinnott (2013)
Aluminium plus neodymium plates	1.27	Calculated from Towler & Sinnott (2013) and neodymium magnet prices
Stainless steel beads (2 mm)	US$ 24/kg	mercadolivre.com.br
Neodymium plates	US$ 0.44/cm³	mercadolivre.com.br

Supplementary Table 8. Purchase costs of equipment for single-stage fed batch

Section / Equipment ID	Description	Purchase cost (US$)
Inoculum train		
SFR-102	Seed Fermentor (24.7 L)	588 000
SFR-103	Seed Fermentor (247 L)	630 000
SFR-104	Seed Fermentor (2470 L)	872 000
Fermentation		
BR-101	Bioreactor (29 m³)	2 724 000
V-10	Blending Tank (2.8 m³)	263 000
V-102	Blending Tank (20 m³)	348 000
ST-101	Heat Sterilizer (Feed medium)	489 000

ST-102	Heat Sterilizer (Fermentation medium)	574 000
G-101	Centrifugal Air Compressor	87 000
AF-101	Air Filter	9 000
HG-101	High-pressure homogenizer	125 000
Nanoparticle Extraction		
MIC-102	MS Column (725 L)	100 000
MIC-101	MS Column (2250 L)	177 000
DS-101	Disk-Stack Centrifuge	133 000
Whole process		
Not tagged	Pumping, inoculum media sterilizers, etc.	1 780 000
	TOTAL	8 898 000

Supplementary Table 9. Purchase costs of equipment for a semicontinuous process

Section / Equipment ID	Description	Purchase cost (US$)
Inoculum train		
SFR-102	Seed Fermentor (36.1 L)	588 000
SFR-103	Seed Fermentor (361 L)	665 000

SFR-104	Seed Fermentor (3610 L)	920 000
Fermentation		
BR-101	Bioreactor (22.6 m^3 x 2)	4 924 000
V-10	Blending Tank (3.9 m^3 x 2)	552 000
V-102	Blending Tank (32 m^3)	390 000
ST-101	Heat Sterilizer (Feed medium)	673 000
ST-102	Heat Sterilizer (Fermentation medium) (x 2)	1 175 000
G-101	Centrifugal Air Compressor	87 000
AF-101	Air Filter	9 000
HG-101	High-pressure homogenizer (x 3)	354 000
Nanoparticle Extraction		
MIC-102	MS Column (1334 L)	136 000
MIC-101	MS Column (4140 L)	240 000
DS-101	Disk-Stack Centrifuge	133 000
Whole process		
Not tagged	Pumping, inoculum media sterilizers, etc.	1 990 000
	TOTAL	12 888 000

Supplementary Table 10. Comparison between approximate energy demands for biogenic and synthetic magnetic nanoparticles.

Nanoparticle	Preparation method	Power consumption (kWh/kg Fe_3O_4)	Energy costs (US$/kg Fe_3O_4)	% Fabrication costs	Reference
BMNs	Single stage	1334.14	112.47	4.5	Present work
BMNs	Semicontinuous	1795.48	151.36	6.3	Present work
Bare magnetite	Co-precipitation	N/A	42.00	20	Augusto et al., 2020
Carbon-coated magnetite	Hydrothermal	N/A	838.40	20	Augusto et al., 2020

Supplementary Table 11. Comparison between minimum selling price of biogenic magnetite and commercial prices of synthetic iron oxide nanoparticles

Nanoparticle	Size (nm)	Price (US$/g)	Available description
Magnetosomes	33	21 – 120 (MSP)	see text
Ocean Nanotech (https://www.oceannanotech.com/products/)			
Amine iron oxide nanopaticles	30	31 960	ZP = +5 to +15 mV
Carboxyl iron oxide nanoparticles	30	15 980	ZP = -35 to -15 mV
PEG iron oxide nanoparticles	30	31 960	ZP = -10 to 0 mV

Cytodiagnostics (https://www.cytodiagnostics.com/)			
Iron oxide magnetic nanoparticles	20 ± 3	11 000	Ms > 20 emu/g
Millipore-Sigma (https://www.sigmaaldrich.com/)			
Iron (II,III) oxide nanopowder	50-100	1.30	97% purity
Iron oxide (II,III), nanoparticles	30	10 480	-
Iron oxide (II,III), nanoparticles, amine functionalized	30	48 600	Ms > 45 emu/g
Iron oxide (II,III), nanoparticles, carboxilic functionalized	30	255 000	Ms > 45 emu/g
Iron oxide (II,III), nanoparticles, PEG	30	34 800	Ms > 48 emu/g
SkySpring Nanomaterials Inc. (https://ssnano.com/)			
Iron Oxide Nanopowder	20-30	0.34	98% purity

4 References

Guo, F., Liu, Y., Chen, Y., Tang, T., Jiang, W., Li, Y., and Li, J. (2011). A novel rapid and continuous procedure for large-scale purification of magnetosomes from *Magnetospirillum gryphiswaldens*e. Appl. Microbiol. Biotechnol. 90:4. doi: 10.1007/s00253-011-3189-3

Rosenfeldt, S., Mickoleit, F., Jörke, C., Clement, J.H., Markert, S., Jérôme, V., Schwarzinger, S., Freitag, R., Schüler, D., Uebe, R., and Schenk, A.S. (2020). Towards standardized purification of bacterial magnetic nanoparticles for future in vivo applications. Acta Biomater [Preprint]. Available at: https://doi.org/10.1016/j.actbio.2020.07.042

Abreu, F., Morillo, V., Trubitsyn, D., and Bazylinski, D.A. (2020b). "Magnetotaxis in Prokaryotes." in eLS. (Chichester: John Wiley & Sons, Ltd). doi: 10.1002/9780470015902.a0000397.pub3

Harrison, R.G., Todd, P., Rudge, S.R., and Petrides, D.P. (2015). Bioseparations science and engineering. New York: Oxford University Press.

StatNano. (2020). Nanotechnology Products Database. StatNano Publications.

Nano-Powder Factory. (2020). Research of the world market of nanopowders. https://eednano.com/ [Accessed March 24, 2020]

De Carvalho, J.C., Medeiros, A.B.P., Letti, L.A.J., Kirnev, P.C.S., and Soccol, C.R. (2017). "Cell Disruption and Isolation of Intracellular Products." in Current Developments in Biotechnology and Bioengineering: Production, Isolation and Purification of Industrial Products, ed. A. Pandey (Amsterdam: Elsevier B. V.)

Tarleton, T., and Wakeman, R. (2006). Solid/Liquid Separation: Equipment Selection and Process Design. Oxford: Elsevier Science.

De Andrade, B. (2014) Reuso de efluentes industriais gerados durante a produção de água purificada na Central de Tratamento de Água do Centro Tecnológico de Vacinas de BioManguinhos/FIOCRUZ. [dissertation/master's thesis]. [Rio de Janeiro, Brazil]: Fundação Oswaldo Cruz.

Dalri-Cecato, L., Battistelli, A.A., Schneider, E.E., Hassemer, M.E.N., and Lapolli, F.R. (2019). Operating cost assessment of a membrane bioreactor. REVISTA DAE. 217:1778. doi: 10.4322/dae.2019.025

Towler, G., and Sinnott, R. (2013). Chemical Engineering Design. Boston: Butterworth-Heinemann

Ruediger, R. (2014). Uso Racional do Vapor na Indústria. https://fiesc.com.br/sites/default/files/inline-files/PALESTRA%20BERMO.pdf [Access March 24, 2020]

ANEEL – Agência Nacional de Energia Elétrica. (2020). Tarifas médias por classe de consumo. https://www.aneel.gov.br/dados/tarifas [Access March 24, 2020]

IBGE – Instituto Brasileiro de Geografia e Estatística. (2019). Emprego, salário e encargos das empresas industriais com 30 ou mais pessoas ocupadas, segundo as divisões, os grupos e as classes de atividades – Brasil. https://sidra.ibge.gov.br/tabela/7241 [Access March 24 2020]

IBGE – Instituto Brasileiro de Geografia e Estatística. (2020). Índice de Preços ao Produtor - Indústrias Extrativas e de Transformação – IPP. https://www.ibge.gov.br/estatisticas/economicas/precos-e-custos/9282-indice-de-precos-ao-produtor-industrias-extrativas-e-de-transformacao.html [Access September, 1, 2020]

FINEP – Financiadora de Estudos e Projetos. (2020). Condições Operacionais. http://www.finep.gov.br/images/a-finep/Condi%C3%A7oes_Operacionais/CondicoesOperacionais.pdf [Access September 1, 2020]

Chemical Engineering. (2020). 2019 Chemical Engineering Plant Cost Index Annual Average. https://www.chemengonline.com/2019-chemical-engineering-plant-cost-index-annual-average/ [Access September 1, 2020]

Banco Central do Brasil. (2020). Cotações e boletins. https://www.bcb.gov.br/estabilidadefinanceira/historicocotacoes [Access September 1, 2020]


frontiers

Bacterial-origin magnetic nanoparticles for decolorization of methyl blue dye

Tarcísio Correa[a] and Fernanda Abreu[a]*

[a] Instituto de Microbiologia Professor Paulo de Góes, Universidade Federal do Rio de Janeiro, Brasil

* Corresponding author at: Departamento de Microbiologia Geral, Instituto de Microbiologia Professor Paulo de Góes, Universidade Federal do Rio de Janeiro, Rio de Janeiro, RJ, Brazil. E-mail address: fernandaaabreu@micro.ufrj.br.

Supplementary material

Figure S1. Transmission electron microscopy of BMs after four reuse cycles in the absence of H_2O_2. Arrows indicate BM membranes. * indicates a nebulous substance, presumably degradation products, accumulated between BMs after four cycles.

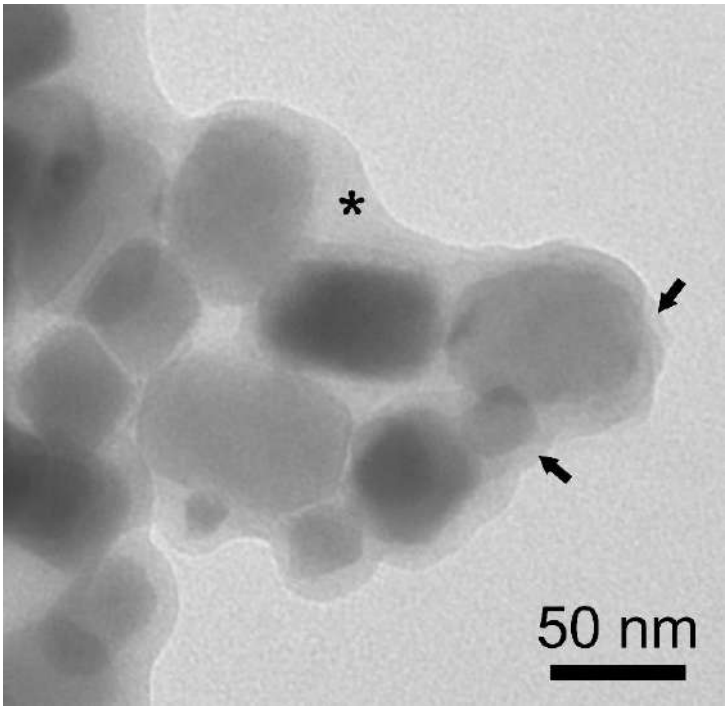

Table S1. Adjusted P values in nonparametric, *posthoc* multiple-comparison tests (MCTs) between membrane thicknesses of BMNs after each reuse cycle in the presence of H_2O_2.

Dunns's MCT				
1st cycle	0,6586			
2nd cycle	>0,9999	0,1047		
3rd cycle	>0,9999	0,9735	>0,9999	
4th cycle	**<0,0001**	**<0,0001**	**<0,0001**	**<0,0001**
	Raw	1st cycle	2nd cycle	3rd cycle
Dunnett's MCT (considering raw BMNs as control group)				
	1st cycle	2nd cycle	3rd cycle	4th cycle
Raw	0,445	0,4886	0,938	**<0,0001**

RSC Advances

PAPER

View Article Online
View Journal | View Issue

Cite this: *RSC Adv.*, 2021, **11**, 28000

A rapid and simple preparation of amphotericin B-loaded bacterial magnetite nanoparticles†

Tarcisio Correa,[a] Dennis A. Bazylinski,[b] Flávio Garcia [c] and Fernanda Abreu *[a]

Magnetotactic bacteria, which synthesize biological magnetite nanoparticles (BMs), are the main microbial source of magnetic nanomaterials. Although the use of BMs has been explored *in vitro* and *in vivo* for new anticancer formulations, targeted treatments of fungal and parasitic diseases would also benefit from biogenic magnetic nanoformulations. Due to the necessity of new formulations of amphotericin B, we developed a magnetic-nanoparticle based conjugate of this drug using bacterial magnetosomes. Different amphotericin B preparations were obtained using BMs extracted from *Magnetovibrio blakemorei* strain MV-1^T as well as glutaraldehyde and poly-L-lysine as linking reagents. The highest capture efficiencies and drug loadings were achieved using 0.1‰ poly-L-lysine as the only linking agent (52.7 ± 2.1%, and 25.3 ± 1.9 μg per 100 μg, respectively) and 0.1‰ poly-L-lysine and glutaraldehyde 12.5% (45.0 ± 5.4%, and 21.6 ± 4.9 μg per 100 μg, respectively). Transmission electron microscopy and infrared spectroscopy analyses confirmed the association of amphotericin B to the BM surface. Moreover, controlled drug release from these nanoparticles was achieved by applying an alternating magnetic field. In this condition the release of amphotericin B in PBS increased approximately four-fold as compared to the release under standard conditions with no applied magnetic fields. Hence, the functionalization of BMs with amphotericin B produces stable nanoformulations with a controllable drug release profile, thus, enabling its potential in the treatment of fungal and parasitic diseases.

Received 20th May 2021
Accepted 10th August 2021

DOI: 10.1039/d1ra03950d

rsc.li/rsc-advances

Introduction

Magnetic nanoparticles have extensive usage in nanomedicine, mainly because of their employability in drug delivery, biomolecule immobilization, and cell separation.[1] In drug immobilization, nanoparticles lead to the increased biocompatibility of these compounds as they reduce toxic effects by preventing systemic distribution.[1,2] Besides, they drive therapeutic molecules to the site of interest (*i.e.*, site of infection or tumors) leading to a higher local concentration than when using non-immobilized drugs.[2] Several magnetic nanoparticle systems have been developed in the last decades.[1] Most of them comprise synthesis of nanoparticles by precipitation of iron minerals such as magnetite.[1,3] Surface modifications of these nanoparticles are usually performed to make them able to bind to functional moieties.[3] However, processes of chemical synthesis may not yield particles with uniform sizes, and shapes and their magnetic properties are difficult to predict.[4]

Bacterial magnetite nanoparticles (BMs), known as magnetosomes, overcome these limitations.[5] These nanoparticles, which are synthesized in a finely-controlled biomineralization process by magnetotactic bacteria,[6] comprise a core mineral crystal of magnetite or greigite enveloped by a lipid bilayer membrane.[7] Biomineralization process yields single domain magnetic nanoparticles within a narrow size range (30–100 nm) and uniform shape.[8] Further surface modification steps are straightforward because of the natural membrane bilayer of these nanoparticles. Proteins responsible for the magnetosome synthesis are embedded in this outer lipid bilayer,[6] being useful for functionalization processes.[5,10] They can work as anchors for expression genetically-engineered fusion proteins such as enzymes or antibodies.[11,12] Alternatively, their amino groups ($-NH_2$) may serve as sites for crosslinking with other molecules, such as drugs.[13,14]

All those characteristics are advantageous for biomedical applications.[5,8] Additionally, bacterial synthesis of magnetite nanoparticles is considered environmentally friendly.[3,9] Several applications for BMs have been described. In small-molecule immobilization, gangliosides and the antitumor drugs doxorubicin and cytarabine have been surface-bound to BMs and, in all cases, their activities were shown to be enhanced in the magnetic conjugate.[13,15,16] However, all of these tests were performed with highly hydrophilic molecules and both drugs tested were anticancer.[13,15,16]

[a]*Instituto de Microbiologia Paulo de Góes, Universidade Federal do Rio de Janeiro, Avenida Carlos Chagas Filho, 373, CCS, UFRJ, Rio de Janeiro, RJ 21941-902, Brazil. E-mail: fernandaabreu@micro.ufrj.br*

[b]*School of Life Sciences, University of Nevada at Las Vegas, Las Vegas, Nevada, USA*

[c]*Centro Brasileiro de Pesquisas Físicas, Rio de Janeiro, Rio de Janeiro, Brazil*

† Electronic supplementary information (ESI) available: Supplementary Fig. S1–S4. See DOI: 10.1039/d1ra03950d

Unlike the examples above, amphotericin B (AmB) is a poorly water-soluble, antifungal and leishmanicidal drug belonging to polyene class.[17] Because of poor dispersibility in aqueous media and serious toxic side-effects, nanoparticle formulations for this drug could come as beneficial for its therapeutic use.[18–20] Different formulations have been developed for AmB such as Fungizone® and AmBisome®, which are less toxic and disperse well in bodily fluids.[20] Zaioncz *et al.*[21] reviewed several works on AmB formulations using nanoparticles as carriers, including polymeric-based, protein-based, and solid lipid-based nanoparticles, some of the which with more efficacy, bioavailability, and less toxicity than other formulations on market. More recently, a formulation of AmB-loaded polycaprolactone (PCL) was designed for topical treatment with significant lower IC_{50} compared with free AmB and AmBisome®.[22] To benefit from the stimuli-responsiveness of magnetic materials, Niemirowicz and colleagues developed a magnetic nanoformulation that was efficient at inhibiting biofilm formation of *Candida* sp. and increase the antifungal activity of polyene antibiotics, even in resistant *Candida* strains.[23] Nevertheless, the nanoparticle tested was chemically synthesised. The use of BMs for immobilizing AmB could bring additional advantages to magnetic formulations, such as low side-effects, and, additionally, the surrounding biological membrane could facilitate functionalization because of the availability of functional groups on their surface for chemical modification. In addition, AmB biocompatibility and dispersibility would be enhanced.

In the present work, we describe a rapid and simple preparation of BMs–AmB conjugates. The drug was attached to the surface of elongated prismatic BMs from the magnetotactic vibrio *Magnetovibrio blakemorei* strain MV-1^T through crosslinking with glutaraldehyde (GA), coating with poly-L-lysine (PLL) and a combination of both in different concentrations. Finally, we investigate AmB release under standard condition and under application of an alternating magnetic field (AMF).

Experimental

Materials

All reagents used in experiments were purchased from Sigma-Aldrich (St. Louis, MO, USA) with the exception of AmB, that was purchased from Inlab (São Paulo, Brazil). PLL was of a molecular weight range of 70 000–150 000 in a solution at 0.01%.

Bacterial culture

Cells of *Mv. blakemorei* strain MV-1^T were anaerobically cultured in an optimized medium[24] in vials for 48 hours at 28 °C before being used in fermentation experiments.

Bioreactor culture

Volumes corresponding to a final cell concentration of 10^8 cells per mL were inoculated into a 5 L benchtop bioreactor (2 L working volume) (Minifors, Infors HT-Basel, Switzerland) containing fresh optimized medium. The culture parameters were set as it follows: pH 7.0 (adjusted with 1.0 N NaOH or HCl), stir rate of 100 rpm, temperature 28 °C and undetectable oxygen. The anaerobic condition was achieved by purging sterile nitrogen and in fresh medium until the oxygen sensor reading reached zero. The medium was then purged with N_2O for 15 minutes.

Isolation of BMs

At the end of the growth period in bioreactor, cells were collected by centrifugation at 6100 × *g* at 4 °C for 15 min. The cell pellets were washed and resuspended in 15 mL of HEPES buffer (10 mM). Afterwards, the cells were lysed in ultrasonic cell crusher (VCX 500, Sonics, Newtown, CT, USA) at 40% amplitude, 20 kHz frequency, in 60 cycles of 30 s between intervals of 30 s. The BMs were magnetically concentrated by a neodymium–boron magnet attached to the outside of the tube for 12 h at 4 °C. The crystals were transferred into 1.5 mL polypropylene tubes and resuspended in HEPES buffer (10 mM) with NaCl (200 mM). The crystals were then washed in an ultrasonic bath (Branson 2200, Emerson, Rochester, NY, USA) for 4 cycles of 30 min, with magnetic concentration and exchange of the buffer at each cycle. The washing efficiency and conservation of the BM membrane were verified by transmission electron microscopy.

Transmission electronic microscopy

Suspensions of pure and functionalized BMs were added on Formvar-coated copper grids and vacuum-dried. Samples were observed in a transmission electron microscope (FEI Morgagni, Hillsboro, OR, USA) operating at 80 kV in magnifications of 16 000 and 42 000 times.

Size measurements of BMs

Measurements of length and width of the BMs used in this study as well as evaluation of the membrane thickness surrounding the BMs before and after functionalization were performed using the iTEM (Olympus, Tokyo, Japan) program. The length and width of the crystals were obtained from the measurements of maximum diameter and minimum diameter, respectively. Graphs and statistical analyzes of the data were carried out with the aid of the Prism 5.0 program (GraphPad Software, San Diego, CA, USA).

Preparation of functionalized nanoparticles

The functionalization of the isolated BMs with AmB were performed by an adapted method.[2] Briefly, 100 μg of BMs were added to 100 μL of 0.1 M phosphate buffer (pH 7.4). GA was added for crosslinking at different final concentrations (0.2, 3.5 and 12.5% v/v). AmB dispersed in DMSO was then added to a final concentration of 125 μg mL^{-1}. The system was subjected to 5 cycles of 10 minutes sonication at 60 W in a sonicator bath, at 10 min intervals under ice bath cooling. The same procedure was performed with BMs pre-treated with PLL at different concentrations (0.1, 0.01 and 0.001‰). At the end, the functionalized BMs were magnetically concentrated and the supernatant was removed and used to estimate the capture efficiency

of AmB by absorbance at 410 nm. The loading of drug was also calculated from the amount of drug captured and the mass of magnetite added to the functionalization reaction. Aliquots of them were also submitted to transmission electron microscopy observation, as previously described. The experiments were performed in triplicate and the capture efficiency displayed by each system was compared statistically by the ANOVA test using the Prism 5.0 program. The functionalized nanoparticles were vacuum dried and stored frozen at −20 °C until used for experiments.

Fourier transform infrared spectroscopy

Lyophilized samples of approximately 1 mg were placed in direct contact with the infrared attenuated total reflection (ATR) diamond crystal of an IRPrestige-21 Spectrometer (Shimadzu, Kyoto, Japan). All preparations were analysed in the wavenumber range of 3000 to 500 cm^{-1} by co-adding 80 scans with a resolution of 1 cm^{-1}.

Ultraviolet-visible spectrometry

The preparations showing the highest drug loadings were analysed according to the Identity Test described in The International Pharmacopoeia.[25] The protocol has been slightly adapted to allow the analysis of magnetic nanoparticles. Briefly, lyophilized samples of 100 μg were treated with methanol for the extraction of membrane-bound material. The extracts were, then, analysed in a UV-1800 (Shimadzu, Kyoto, Japan) spectrophotometer operating in scanning mode in the wavelength range of 300–450 nm. A negative control was performed using raw BMs. A positive control with free AmB was performed according to the Pharmacopoeia without adaptations.

Zeta potential

The zeta potential of resuspended nanoparticles in ultrapure water (30 μg mL^{-1}) was measured on a Zeta Analyzer (ZetaPlus, Brookhaven Instruments Corp., Holtsville, USA). Ten measurements were performed on each sample and the individual values were used to calculate the mean and standard deviation.

Magnetic hyperthermia

The heating capacity of the BMs in response to the application of AMF was investigated. The analysis was performed on a magnetic induction heating system (DM2-s53, Nanoscale Biomagnetics, Zaragoza, Spain) equipped with an optic fiber temperature probe and vacuum thermal insulation. Suspensions of BMs in PBS (pH 7.4) were transferred to a glass vial (1 mL) at concentrations of 1.2 and 4.8 mg mL^{-1}. The system temperature was stabilized at 22 °C for 8 min and the AMF was applied at a frequency of 307 kHz and magnetic field strength of 200 Oe.

Drug release profile

Three types of conjugates were tested for the released profile of AmB. Basically, BM–PLL–AmB and BM–PLL–GA–AmB complexes were dispersed in PBS and incubated at 37 °C under agitation at 60 rpm.[26] At 5, 10, 20 and 60 minutes, magnetic nanoparticles were magnetically concentrated and a supernatant sample was collected for the determination of AmB in a spectrophotometer (UV 330G, Gehaka, São Paulo, Brazil) at 410 nm. Thereafter, the BMs were redistributed and the PBS volume was restored. To assess the release of AmB from the nanoparticles in response to AMF, the same procedure was performed for supernatant collection and released drug quantification.

Magnetic measurements

The magnetization properties of BMs was investigated at room temperature using a SQUID vibration sample magnetometer (MPMS3, Quantum Design, San Diego, CA, USA). An amount of 13.9 mg of lyophilized BMs were placed inside a gelatin capsule prior to insertion into SQUID sample holder. Measurements were performed at 300 K.

Results & discussion

BM production

BMs were obtained from a culture of *Mv. blakemorei* strain MV-1^T grown in a 5 L bioreactor using medium and operational optimized conditions.[24] Cells were then lysed by sonication and extracted BMs were washed four times using HEPES buffer (10 mM; pH 6.8) before their utilization in the experiments. Size of isolated BMs ($n = 540$) averaged 64.3 ± 0.5 nm in length and 41.6 ± 0.3 nm in width (Fig. S1†) as measured from transmission electron microscopy (TEM) images.

Preparation of functionalized nanoparticles

Although the abundance of phosphatidyl components of BM membrane[11] gives these nanostructures an overall negative charge, other functional groups are present.[5] The functional groups available on the BM surface are those from side chains of amino acid residues making up membrane proteins.[5] The most important for chemical modifications are amino groups, as these groups have been extensively reported in literature[5,10,14] as anchors for covalent binding of functional molecules. The immobilization of drug molecules onto BMs is usually achieved with iminium-forming crosslinkers, like GA.[13] From that knowledge, different concentrations of GA, ranging from 0.2% to 12.5%, were used for the treatment of BM with AmB (BM–GA–AmB) in this work. In addition, polyaminoacids are also promising agents for adsorption of drugs onto these nanoparticles based on charge interactions.[5,10] Thus, BMs were coated with PLL (concentrations ranging from 0.001 to 0.1‰) before treatment with AmB. PLL-coated BMs were also treated with AmB in the presence and absence of GA (BM–PLL–GA–AmB and BM–PLL–AmB, respectively) in the concentration that yielded the best drug capture efficiency (0.1‰ PLL). When applied as the only linking agent, maximum tested concentrations of either GA and PLL returned the most substantial encapsulation efficiency (35.2 ± 3.5% for BM–GA–AmB and 52.7 ± 2.1% for BM–PLL–AmB) and drug loading (15.5 ± 3.1 μg per 100 μg for BM–GA–AmB and 25.3 ± 1.9 μg per 100 μg for BM–PLL–AmB)

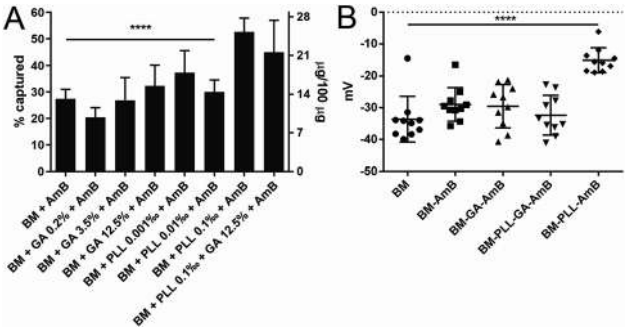

Fig. 1 Encapsulation efficiencies (%) and drug loadings (μg per 100 μg) (A) for different concentrations of GA and PLL in functionalization of BMs. Average zeta potential (B) ($n = 10$) for each preparation. In both analysis PLL and GA were used in the maximum tested concentrations (0.1‰ and 12.5%, respectively). ANOVA tests showed statistically significant difference in efficiencies ($p < 0.0001$, ****).

(Fig. 1A). Overall, all BMs treated with tested PLL concentrations returned better drug entrapment than those using GA. This is probably due to the fact GA links only to amino groups located in proteins of BM membrane whereas PLL covers BM surface as a whole because of net negative charge provided by phospholipids. No statistically significant difference in encapsulation efficiency and drug loading was found between BM–PLL–AmB (0.1‰ PLL; 45.0 ± 5.4% and 21.6 ± 4.9 μg per 100 μg, respectively) and when both reagents (BM–PLL–GA–AmB) were used (0.1‰ PLL + 12.5% GA; 52.7 ± 2.1% and 25.3 ± 1.9 μg per 100 μg, respectively).

Spectroscopy analyses and chemical structure

The attachment and adsorption of AmB onto BMs were then confirmed using ATR-FTIR spectroscopy analyses (Fig. S2†) and a schematic representation of each preparation is displayed on Fig. 2. Fe–O stretching vibration peaks from magnetite were found in all nanoparticle preparations, ranging from 534 to 564 cm^{-1}. Additionally, the multiplicity of functional groups, including primary amines, has been confirmed in our spectroscopic analysis of raw BMs by the characteristic fingerprint region (1400 to 500 cm^{-1}). The peaks 1643 and 1654 cm^{-1} in BM–GA–AmB and BM–PLL–GA–AmB are assigned to (–CN) vibrations, suggesting the covalent attachment of AmB,[13,23] as illustrated in structures (Fig. 2B and C). The bands ranging from 2943 and 2827 cm^{-1} correspond to $–CH_2$ and $–CH_3$ stretching vibrations of the polyene structure of AmB.[27] In BM–PLL–AmB and BM–PLL–GA–AmB the peak 1622 cm^{-1} is assigned to bending vibration of N–H of amide groups from polyaminoacid backbone of PLL[28] (Fig. 2D and E). Peaks 1528 cm^{-1} in BM–PLL–AmB and BM–PLL–GA–AmB and 1562 cm^{-1} in BM–GA–AmB and AmB correspond to superposed $–NH_2$ bending and $–COO^-$ stretching vibrations from AmB[27] (Fig. 2D and E). Peaks 1383–1401 cm^{-1} in functionalized nanoparticles and AmB correspond to $–COO^-$ stretching and –C=O bending vibrations from AmB.[27] Finally, peaks 1072–1037 cm^{-1} and 1000–1014 cm^{-1} from the same spectra are assigned to pyranose C–O–C stretching and –CH *trans* bending from polyene structure[27]

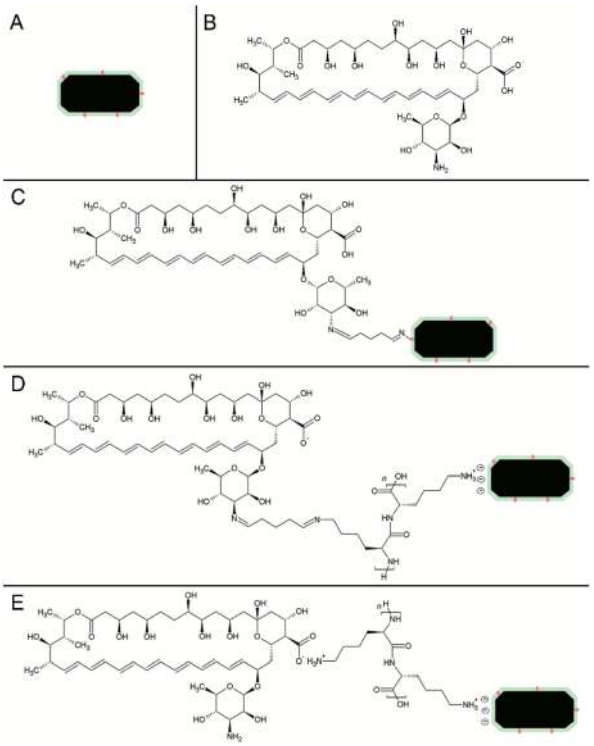

Fig. 2 Representation of free magnetosome (A) and structures of free amphotericin B, with the mycosamine ring at the bottom right, (B) and their conjugates: BM–GA–AmB (C), BM–PLL–GA–AmB (D) and BM–PLL–AmB (E).

(Fig. 2B–E). These findings support the effective binding of AmB in these preparations and indicate the possible mechanisms in which GA, PLL and AmB interacts with BMs during the preparation of nanoconjugates. When used as the sole linking agent (BM–GA–AmB), GA activates BM surfaces for the covalent binding to molecules containing primary or secondary amino groups through iminium formation.[10,29] When AmB is added to a GA-activated BM suspension, the amino group presents within the mycosamine ring (Fig. 2B) reacts with GA-derived aldehyde group to form a second covalent iminium bond (Fig. 2C). In preparations containing PLL (BM–PLL–AmB and BM–PLL–GA–AmB), the polyaminoacid side chain, which is comprised of a four-carbon chain with a terminal primary amine, is positively charged at neutral pH. Thus, positively charged PLL side chains electrostatically binds to negatively charged phospholipids on the surface of BMs (Fig. 2D and E). The interaction of AmB with PLL in BM–PLL–AmB probably occurs by a hydrogen bond between amine side chain of PLL and carboxyl group present in AmB (Fig. 2E). For BM–PLL–GA–AmB, the BMs are first coated with PLL prior to activation by GA (refer to Preparation of functionalized nanoparticles in Experimental section). In this sense, one of aldehyde groups of GA forms an iminium bond with the aliphatic amino group of the PLL coating (Fig. 2D). Then, the GA-activated complex binds covalently to AmB molecules in a manner analogous to that of BM–GA–AmB.

The adsorption and the stability of AmB attached to the BM–PLL–AmB and BM–PLL–GA–AmB – chosen due to the highest

drug loadings – were investigated through UV-vis spectroscopy. For both preparations, absorption peaks were observed, in crescent intensity order, at 364, 382 and 406 nm (Fig. S3†). The relative intensities between peaks were maintained for the tested nanoformulations, as enforced by the International Pharmacopoeia.[25] This finding corroborates that our synthesized nanoformulations are in accordance to regulatory requirements and meet quality standards for pharmaceutical use.

Membrane thickening measurements

Measurements of membrane thickness of different BMs preparations from TEM images revealed the surface interactions observed after functionalization experiments. All preparations had progressively larger membrane thickness measurements than non-functionalized BMs (Fig. 3 and S4†), with the largest membrane thickness observed for BM–PLL–GA–AmB, when most reagents were attached to the surface of BMs. These results suggest the BM membrane became thicker as more functional moieties were added to its surface. The increase in BM membrane thickness as result of insertion of organic molecules has also been observed in other works.[10,30] It is suggested that such phenomenon could prevent aggregation of BMs caused by interaction between nuclei of single magnetic domain.[31] TEM images also suggested some level of aggregation of nanoparticles, especially in those prepared with GA. This is probably due to unspecific BM–BM crosslinking, which could also explain a lower encapsulation efficiency when using this GA as crosslinking agent.

Zeta potential

The zeta potential was measured to evaluate the dispersive properties of the functionalized nanoparticles. For non-functionalized BMs, a zeta potential of -33.6 ± 2.3 mV was found and agrees with values found for cuboctahedral BM from *Magnetospirillum* strains[14,31] (Fig. 1B). As in other *Magnetospirillum*, BMs in *Mv. blakemorei* strain MV-1^{T} are formed from vesicles internalized from the inner cell membrane,[32] which is composed of negatively charged phospholipids and causes a negative zeta potential. Values between -33 and -28 mV were observed for preparations tested, except BM–PLL–AmB, whose potential was -15.1 ± 3.8 mV (Fig. 1B). Despite the increase of zeta potential value towards zero, all dispersions of tested preparations may be considered at least relatively stable.[33] The change in zeta potential of particles derived from different functionalization methods showed the response of membrane charge to the interaction with the foreign molecules, as corroborated by the encapsulation, membrane thickening and spectroscopic results. This trend has been recently discussed by another work,[29] in which immobilization of anthracycline molecules also leads to significant changes in BM surface charges, as evaluated by zeta potential.

Magnetic characterization

To our knowledge, this is the first time BMs of prismatic shape have its functionalization potential explored. Because of that, magnetic properties for this type of nanoparticle were not

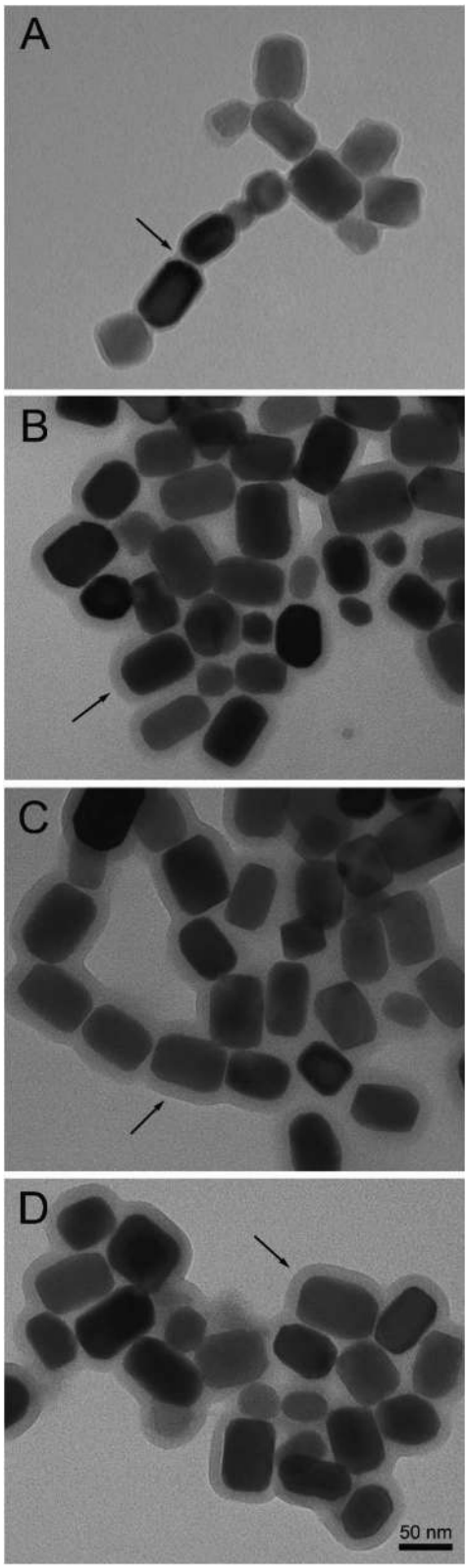

Fig. 3 TEM images of free BMs (A) and its conjugates: BM–GA–AmB (B), BM–PLL–GA–AmB (C) and BM–PLL–AmB (D). Note the membrane thickness increase for different preparations.

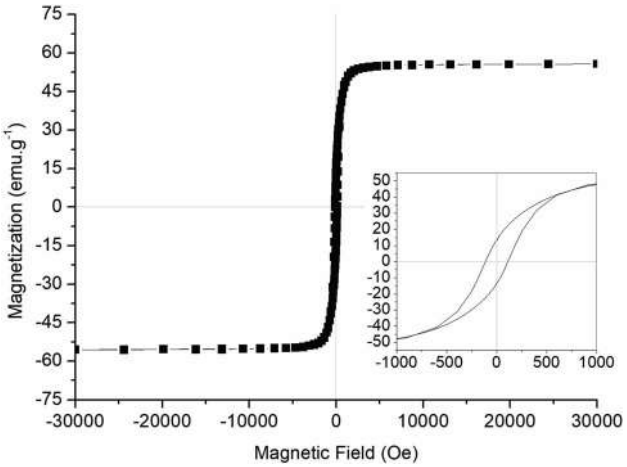

Fig. 4 Magnetization curve of lyophilized magnetosomes from *Mv. blakemorei* strain MV-1^T showing hysteresis loops (inset).

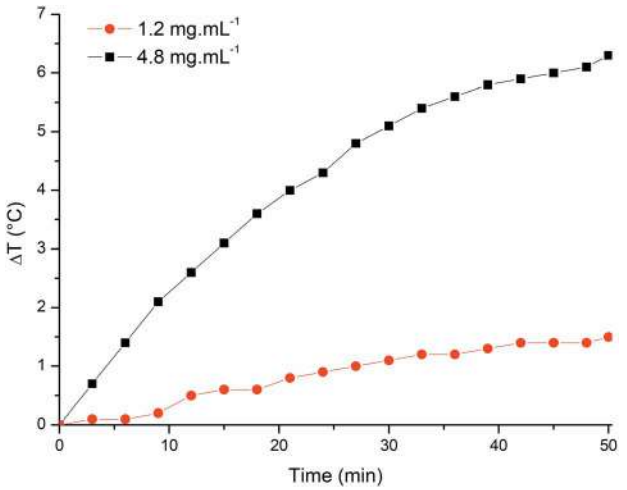

Fig. 5 Heating profile of BM samples (1.2 mg mL^{-1} and 4.8 mg mL^{-1}) subjected to an AMF of 200 Oe and frequency of 307 kHz.

available and had to be evaluated. Magnetization measurements were performed on non-functionalized BMs and presented a behaviour of single magnetic domain particle, as expected (Fig. 4). The values for saturation magnetization and coercivity were 52 emu g^{-1} and 115 Oe. These characteristics and measured values were compatible with the values reported for the cuboctahedral BM of *Magnetospirillum magneticum* strain AMB-1 (ref. 34) and bioinspired greigite nanoparticles.[35] These findings reflect similar applicability potential for the elongated prismatic BMs from *Mv. blakemorei* strain MV-1^T and those nanoparticles already studied.

Heating capacities of suspensions containing 1.2 and 4.8 mg mL^{-1} of magnetite in water were examined under an AMF (field amplitude = 200 Gs; frequency = 307 kHz). The increase in temperature in response to the application of an AMF was the highest (6.3 °C) in the suspension containing the largest amount of magnetite (Fig. 5). When the concentration of magnetite was 1.2 mg mL^{-1}, the temperature increase was also

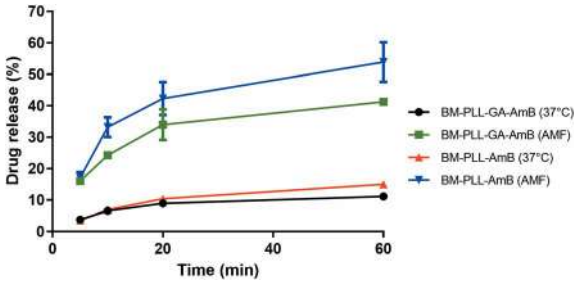

Fig. 6 Cumulative release profile of AmB from different preparations under standard (37 °C) and AMF. PLL and GA were used in the maximum tested concentrations (0.1‰ and 12.5%, respectively).

lower (1.4 °C). The specific absorption rate (SAR) is defined as the rate in which magnetic energy is converted into thermal energy by unit of mass.[36] This property is dependent on mass, shape, size of nanoparticle and on the frequency and the intensity of the applied magnetic field.[36] The SAR values calculated from our experiments are 2.9 and 7.0 W $g_{Fe_3O_4}^{-1}$ for suspensions of BMs with 1.2 and 4.8 mg mL^{-1}, respectively. Both the temperature variation and SAR value achieved here are lower than previously reported values for hyperthermia using BMs.[34,37] However, a similar temperature increase was obtained using similar parameters for AMF-induced heating of BMs from *Magnetospirillum gryphiswaldense* strain MSR-1.[38]

AmB-releasing profile

The amount of AmB released into the medium relative to the amount of drug associated within the nanoparticle was measured in the standard drug release condition (37 °C)[26] and under the application of an AMF. For these experiments, only the preparations with the highest loading of AmB were used (Fig. 6). The release in the standard condition within 1 h was 11.1 ± 0.4% for BM–PLL–GA–AmB and 15.0 ± 1.2% for BM–PLL–AmB. When the suspension was subjected to the AMF, the drug release in the same time interval increased by approximately four times, reaching 41.3 ± 0.5% for BM–PLL–GA–AmB and 53.8 ± 6.2% for BM–PLL–AmB. This increase in the release is attributed to Brown relaxation, which responds for rotation of nanoparticles under AMF, rather than hyperthermia.[36,39] This was also observed in a study in which an increase of about four times of doxorubicin release from cyclodextrin-decorated magnetite nanoparticles was observed without the rise in temperature.[39] In another study, a sharp release of rhodamine B from rhodamine B-fluorescent BMs in response to an AMF occurred in a temperature variation smaller than 2.5 °C.[40]

Conclusions

Here we first demonstrated the functionalization of magnetosomes from *Mv. blakemorei* strain MV-1^T and the decoration of magnetosomes with an antifungal/antiparasitic drug.‡ In our

‡ The results obtained in this study have been registered under the patent number BR1020210056835 held in Brazil.

experiments, it is evidenced that PLL increase binding of AmB onto magnetosomes in the presence and absence of GA. We also demonstrated the controlled drug release from these conjugates with the application of an AMF, which can be useful in localized chemotherapy. These results expand the potential applicability of these magnetic nanoparticles in the treatment of neglected diseases.

Author contributions

All authors contributed to activities necessary to this manuscript. T. C. performed material preparation, data collection and analysis. F. G. analysed the magnetization and heating properties of BMs. T. C., F. G., D. A. B. and F. A. contributed to the study conception and design. All authors read and approved the final manuscript.

Conflicts of interest

There are no conflicts to declare.

Acknowledgements

We acknowledge financial support from the Brazilian agencies Conselho Nacional de Desenvolvimento Científico e Tecnológico (CNPq), Fundação de Amparo à Pesquisa do Estado do Rio de Janeiro (FAPERJ) and Coordenação de Aperfeiçoamento de Pessoal de Nível Superior (CAPES). D. A. B. is supported by U.S. National Science Foundation grant EAR-1423939. Microscopy Facility: Unidade de Microscopia Multiusuário Souto-Padrón & Lins (UniMicro, UFRJ). Optical Spectroscopy Laboratory (Institute of Natural Products Research, UFRJ). We thank Professor Susana Carvajal (Laboratório de Ultraestrutura Celular Hertha Meyer, Institute of Biophysics, UFRJ) for the help in zeta potential analysis.

Notes and references

1 L. H. Reddy, J. L. Arias, J. Nicolas and P. Couvreur, *Chem. Rev.*, 2012, **112**, 5818–5878.
2 M. Estanqueiro, M. H. Amaral, J. Conceição and J. M. Sousa Lobo, *Colloids Surf., B*, 2015, **126**, 631–648.
3 B. I. Kharisov, H. V. R. Dias, O. V. Kharissova, A. Vázquez, Y. Peña and I. Gómez, *RSC Adv.*, 2014, **4**, 45354–45381.
4 E. Alphandery, *Front. Bioeng. Biotechnol.*, 2014, **2**, 5.
5 G. Vargas, J. Cypriano, T. Correa, P. Leão, D. A. Bazylinski and F. Abreu, *Molecules*, 2018, **23**, 2438.
6 R. Uebe and D. Schüler, *Nat. Rev. Microbiol.*, 2016, **14**, 621–637.
7 B. H. Lower and D. A. Bazylinski, *J. Mol. Microbiol. Biotechnol.*, 2013, **23**, 63–80.
8 A. Arakaki, H. Nakazawa, M. Nemoto, T. Mori and T. Matsunaga, *J. R. Soc., Interface*, 2008, **5**, 977–999.
9 J. R. Lloyd, J. M. Byrne and V. S. Coker, *Curr. Opin. Biotechnol.*, 2011, **22**, 509–515.
10 J. Sun, Y. Li, X. J. Liang and P. C. Wang, *J. Nanomater.*, 2011, **469031**, 1–13.
11 T. Yoshino, H. Hirabe, M. Takahashi, M. Kuhara, H. Takeyama and T. Matsunaga, *Biotechnol. Bioeng.*, 2008, **101**, 470–477.
12 T. Honda, T. Tanaka and T. Yoshino, *Biomacromolecules*, 2015, **16**, 3863–3868.
13 J. B. Sun, J. H. Duan, S. L. Dai, J. Ren, L. Guo, W. Jiang and Y. Li, *Biotechnol. Bioeng.*, 2008, **101**, 1313–1320.
14 Q. Deng, Y. Liu, S. Wang, M. Xie, S. Wu, A. Chen and W. Wu, *Materials*, 2013, **6**, 3755–3763.
15 F. Guan, X. Li, J. Guo, G. Yang and X. Li, *Int. J. Nanomed.*, 2015, **10**, 6919–6930.
16 Q. Dai and W. Wu, *Int. J. Nanomed.*, 2015, 1387–1397.
17 J. J. Torrado, R. Espada and M. P. Ballesteros, *J. Pharm. Sci.*, 2008, **97**, 2405–2425.
18 H. Van De Ven, C. Paulussen, P. B. Feijens, A. Matheeussen, P. Rombaut, P. Kayaert, G. Van Den Mooter, W. Weyenberg, P. Cos, L. Maes and A. Ludwig, *J. Controlled Release*, 2012, **161**, 795–803.
19 C. A. Saldanha, M. P. Garcia, D. C. Iocca, L. G. Rebelo, A. C. O. Souza, A. L. Bocca, M. d. F. M. Almeida Santos, P. C. Morais and R. B. Azevedo, *PLoS Neglected Trop. Dis.*, 2016, **10**, 1–18.
20 R. Fernández-García, E. de Pablo, M. P. Ballesteros and D. R. Serrano, *Int. J. Pharm.*, 2017, **525**, 139–148.
21 S. Zaioncz, N. M. Khalil and R. M. Mainardes, *Curr. Pharm. Des.*, 2017, **23**, 509–521.
22 M. Saqib, A. S. A. Bhatti, N. M. Ahmad, N. Ahmed, G. Shahnaz, N. Lebaz and A. Elaissari, *Nanomaterials*, 2020, **10**, 1152.
23 K. Niemirowicz, B. Durnaś, G. Tokajuk, K. Głuszek, A. Z. Wilczewska, I. Misztalewska, J. Mystkowska, G. Michalak, A. Sodo, M. Wątek, B. Kiziewicz, S. Góźdź, S. Głuszek and R. Bucki, *Nanomedicine*, 2016, **12**, 2395–2404.
24 K. T. Silva, P. E. Leão, F. Abreu, J. A. López, M. L. Gutarra, M. Farina, D. A. Bazylinski, D. M. G. Freire and U. Lins, *Appl. Environ. Microbiol.*, 2013, **79**, 2823–2827.
25 *The International Pharmacopoeia*, 8th edn, https://digicollections.net/phint/2018/index.html, accessed May 2019.
26 P. Legrand, M. Chéron, L. Leroy and J. Bolard, *J. Drug Targeting*, 1997, **4**, 311–319.
27 M. Gagoś and M. Arczewska, *Biochim. Biophys. Acta, Biomembr.*, 2010, **1798**, 2124–2130.
28 E. Alphandéry, A. Idbaih, C. Adam, J. Y. Delattre, C. Schmitt, F. Guyot and I. Chebbi, *Biomaterials*, 2017, **141**, 210–222.
29 Y. Geng, J. Wang, X. Wang, J. Liu, Y. Zhang, W. Niu, A. Basit, W. Liu and W. Jiang, *Nanomedicine*, 2019, **14**, 1663–1680.
30 F. Mickoleit, C. B. Borkner, M. Toro-Nahuelpan, H. M. Herold, D. S. Maier, J. M. Plitzko, T. Scheibel and D. Schüler, *Biomacromolecules*, 2018, **19**, 962–972.
31 J. Xu, J. Hu, L. Liu, L. Li, X. Wang, H. Zhang, W. Jiang, J. Tian, Y. Li and J. Li, *Front. Microbiol.*, 2014, **5**, 4–11.
32 F. Abreu, A. A. Sousa, M. A. Aronova, Y. Kim, D. Cox, R. D. Leapman, L. R. Andrade, B. Kachar, D. A. Bazylinski and U. Lins, *J. Struct. Biol.*, 2013, **181**, 162–168.
33 S. Bhattacharjee, *J. Controlled Release*, 2016, **235**, 337–351.

34 M. Timko, A. Dzarova, J. Kovac, A. Skumiel, A. Józefczak, T. Hornowski, H. Gojzewski, V. Zavisova, M. Koneracka, A. Sprincova, O. Strbak, P. Kopcansky and N. Tomasovicova, *J. Magn. Magn. Mater.*, 2009, **321**, 1521–1524.
35 M. Feng, Y. Lu, Y. Yang, M. Zhang, Y. J. Xu, H. L. Gao, L. Dong, W. P. Xu and S. H. Yu, *Sci. Rep.*, 2013, **3**, 1–6.
36 V. N. Nikiforov and E. Y. Filinova, in *Magnetic Nanoparticles*, ed. S. P. Gubin, Wiley-VCH, 2009, pp. 393–455.
37 E. Alphandéry, S. Faure, L. Raison, E. Duguet, P. A. Howse and D. A. Bazylinski, *J. Phys. Chem. C*, 2011, **115**, 18–22.
38 S. Mannucci, L. Ghin, G. Conti, S. Tambalo, A. Lascialfari, T. Orlando, D. Benati, P. Bernardi, N. Betterle, R. Bassi, P. Marzola and A. Sbarbati, *PLoS One*, 2014, **9**, 108959.
39 E. C. D. S. Santos, A. Watanabe, M. D. Vargas, M. N. Tanaka, F. Garcia and C. M. Ronconi, *New J. Chem.*, 2018, **42**, 671–680.
40 E. Alphandéry, D. Abi Haidar, O. Seksek, F. Guyot and I. Chebbi, *Nanoscale*, 2018, **10**, 10918–10933.

INSTITUTO NACIONAL DA PROPRIEDADE INDUSTRIAL

03/08/2020 870200097179 18:12

29409161920418333

Pedido nacional de Invenção, Modelo de Utilidade, Certificado de Adição de Invenção e entrada na fase nacional do PCT

Número do Processo: BR 10 2020 015831 7

Dados do Depositante (71)

Depositante 1 de 2

Nome ou Razão Social: UNIVERSIDADE FEDERAL DO RIO DE JANEIRO

Tipo de Pessoa: Pessoa Jurídica

CPF/CNPJ: 33663683000116

Nacionalidade: Brasileira

Qualificação Jurídica: Instituição de Ensino e Pesquisa

Endereço: Av. Pedro Calmon, 550 - Cidada Universitária

Cidade: Rio de Janeiro

Estado: RJ

CEP: 21941901

País: Brasil

Telefone: (21)37331793

Fax:

Email: agenciadeinovacao@inovacao.ufrj.br

Depositante 2 de 2

Nome ou Razão Social:	THE BOARD OF REGENTS OF THE NEVADA SYSTEM OF HIGHER EDUCATION, ON BEHALF OF THE UNIVERSITY OF NEVADA, LAS VEGAS
Tipo de Pessoa:	Pessoa Jurídica
CPF/CNPJ:	
Nacionalidade:	Norte Americana
Qualificação Jurídica:	Instituição de Ensino e Pesquisa
Endereço:	4505 S. Maryland Parkway
Cidade:	Las Vegas, Nevada
Estado:	
CEP:	
País:	ESTADOS UNIDOS DA AMÉRICA
Telefone:	(70) 289 55832
Fax:	(70) 289 53956
Email:	

Dados do Pedido

Natureza Patente:	10 - Patente de Invenção (PI)
Título da Invenção ou Modelo de Utilidade (54):	PROCESSO PARA PRODUÇÃO CONTÍNUA DE MAGNETOSSOMOS ATRAVÉS DO CULTIVO DE BACTÉRIAS MAGNETOTÁTICAS EM BIORREATOR
Resumo:	A presente invenção descreve um processo de produção contínua e em larga escala de magnetossomos através do cultivo de bactérias magnetotáticas Magnetovibrio blakemorei cepa MV-1T em biorreator. Este processo em larga escala possui maior produtividade de magnetossomos, com baixo custo e características físico-químicas controladas, tornando viável a sua aplicação. A otimização do cultivo de Mv. blakemorei cepa MV-1T em biorreator é vantajosa pois seus magnetossomos prismáticos apresentam uma superfície disponível maior que a dos magnetossomos cuboctaédricos do gênero Magnetospirillum. Adicionalmente, a presente invenção promove uma produção estável de magnetossomos por períodos mais extensos de cultivo, sendo uma das vantagens da invenção frente ao estado da técnica atual. As aplicações dos magnetossomos incluem o carreamento e liberação de fármacos, hipertermia induzida magneticamente, separação de células e biomoléculas e imobilização de enzimas
Figura a publicar:	7

PROCESSO PARA PRODUÇÃO CONTÍNUA DE MAGNETOSSOMOS ATRAVÉS DO CULTIVO DE BACTÉRIAS MAGNETOTÁTICAS EM BIORREATOR

CAMPO DE APLICAÇÃO

[0001] A presente invenção se aplica no campo medicinal e/ou laboratorial e descreve a produção contínua e em larga escala de magnetossomos através do cultivo da bactéria magnetotática *Magnetovibrio blakemorei* cepa MV-1^T em biorreator. As aplicações dos magnetossomos incluem o carreamento e liberação de fármacos, hipertermia induzida magneticamente, separação de células e biomoléculas, a imobilização de enzimas, o seu uso como agente de contraste para imageamento por ressonância magnética nuclear. Também podem ser aplicadas à catálise heterogênea para degradação de poluentes orgânicos, à adsorção e precipitação de metais pesados e óleo bruto e ao melhoramento de difusão de gases em bioprocessos aeróbicos e anaeróbicos.

FUNDAMENTOS DA INVENÇÃO

[0002] A nanotecnologia e a biotecnologia se desenvolveram expressivamente nas últimas décadas, a interface entre essas duas áreas de conhecimento tem aumentado, gerando conhecimentos básicos e aplicados sobre a síntese biológica de nanomateriais e a utilização de ferramentas nanotecnológicas para fins biomédicos. As nanopartículas magnéticas, ou magnetossomos, evidenciam grandemente esta interface.

[0003] A principal fonte de magnetossomos são as bactérias magnetotáticas e eles se encontram organizados em uma ou mais cadeias no citoplasma bacteriano. Eles são compostos por um cristal magnético constituído por mineral ferro envolto em membrana fosfolipídica.

[0004] A morfologia dos cristais dos magnetossomos tende a ser única para uma espécie particular, sendo que as três principais morfologias de cristais de magnetita encontradas são a cuboctaédrica, a prismática alongada e a anisotrópica em forma de "ponta de lança".

[0005] Porém, a obtenção de grandes quantidades dessas nanopartículas é um desafio devido ao crescimento fastidioso das bactérias magnetotáticas e do baixo rendimento de magnetossomos durante o cultivo, dificultando a sua aplicação em biotecnologia. Uma vez atingida à produção em larga escala com alta produtividade, baixo custo e características físico-químicas controladas, torna-se viável a aplicação de magnetossomos em ciências farmacêuticas e biomédicas.

[0006] Portanto, com o intuito de solucionar os problemas enfrentados, a presente invenção se refere a um processo de produção contínua e em larga escala de magnetossomos através do cultivo da bactéria magnetotática *Magnetovibrio blakemorei* cepa MV-1^T em biorreator. Este processo em larga escala possui maior produtividade de magnetossomos, com baixo custo e características físico-químicas controladas, tornando viável a aplicação dos mesmos. A otimização do cultivo de *Mv. blakemorei* cepa MV-1^T em biorreator é vantajosa pois seus magnetossomos prismáticos apresentam uma superfície disponível maior que a dos magnetossomos cuboctaédricos do gênero *Magnetospirillum*, além de beneficiar a funcionalização e a aplicação destes magnetossomos.

[0007] Outra vantagem trazida pelo cultivo de *Mv. blakemorei* cepa MV-1^T em biorreator é por permitir o controle

mais simples na gasificação do meio. No gênero *Magnetospirillum* ocorre a condição na qual o crescimento celular é maior na presença de oxigênio, enquanto que a produção de magnetossomos é maior em anaerobiose. Portanto, neste gênero, há a necessidade de um controle fino de aeração e agitação para manter um nível de oxigênio condizente com uma condição microaeróbica (0,5 a 2%) ou um sistema de retroalimentação no qual ocorra a alternação entre condições anaeróbicas e aeróbicas a fim de se balancear o crescimento com a formação de magnetossomos.

[0008] Adicionalmente, a presente invenção promove uma produção estável de magnetossomos por períodos mais extensos de cultivo, sendo uma das vantagens da invenção frente ao estado da técnica atual.

ESTADO DA TÉCNICA

[0009] O artigo "Optimization of magnetosome production and growth by the magnetotactic vibrio magnetovibrio blakemorei strain MV-1 through a statistics based experimental design", de Silva *et. al* (2013), descreve um estudo com a finalidade de encontrar meios de otimizar a produção de magnetossomos a partir da bactéria *Magnetovibrio blakemorei* cepa MV-1^T através de um processo de produção do tipo batelada alimentada. A bactéria é cultivada em meio contendo N_2O, depois são dispostas em biorreator, onde oxigênio é retirado por purga para obter um meio anaeróbio. Adiciona-se ao reator cisteína e solução de sulfato de ferro. Há a adição de $FeSO_4$, como substrato, a medida que o ferro é consumido no meio e tal fonte de $FeSO_4$ é controlada manualmente.

[00010] Na presente invenção o ferro é adicionado em conjunto com o meio de cultivo e tal diferença acarreta na homogeneidade da disponibilidade do nutriente ferro ao longo do cultivo. Isso garante que, durante a continuidade do cultivo, a concentração deste nutriente não sofra alterações bruscas, como no caso descrito no artigo. Além disso, este artigo não contempla a adição do aceptor final de elétrons (N_2O), assim como não há disponibilidade imediata do produto bacteriano. Ademais, o aumento de produção de magnetita pela presente invenção é de 4,2% em relação ao trabalho de Silva e colaboradores (2003) e a manutenção da produtividade em 22,7 $mg.L^{-1}.d^{-1}$ em 120 h representa um aumento de 3 vezes em relação a produtividade reportada nesse trabalho. Além disso, o tempo morto de processo, que é relacionado ao esvaziamento, lavagem, esterilização e inoculação do biorreator, é estimado em 18 h para o processo em batelada. Através do cultivo contínuo, o volume de cultura equivalente a 2 ou mais bateladas pode ser obtido sem a necessidade desse intervalo ocioso.

[00011] O documento US20020012698, que aqui é incorporado por referência, compreende um processo para obter magnetossomos a partir da bactéria *Magnetospirillum gryphiswaldense* utilizando um meio de cultura simples com concentração de oxigênio abaixo de 2%, com adição de acetato de sódio e $FeSO_4$. As células magnéticas são coletadas por centrifugação e são rompidas para se obter os magnetossomos após serem separados dos fragmentos de células.

[00012] Apesar de o referido documento apresentar o mesmo objetivo da presente invenção, eles se distanciam, pois se trata de um processo em batelada em fermentador, com processo

produtivo e meio de cultura empregados que são distintos dos revelados pela presente invenção. Além disso, a otimização do cultivo de *Mv. blakemorei* cepa MV-1^T em biorreator é vantajosa pois seus magnetossomos prismáticos apresentam uma superfície disponível maior que a dos magnetossomos cuboctaédricos do gênero *Magnetospirillum*.

[00013] Já o artigo entitulado "Large-scale production of magnetosomes by chemostat culture of *Magnetospirillum gryphiswaldense* at high cell density", de Liu *et. al.* (2010), descreve um processo para produzir magnetossomos a partir de *Magnetospirillum gryphiswaldense* em larga escala. É revelada uma cultura quimiostática que se baseia no refinamento da alimentação, levando a um rápido crescimento celular e a uma formação de magnetossomos maximizada. Nessa técnica, é adicionado mais substrato à medida que o pH se altera, sendo um processo do tipo batelada alimentada, por se tratar de um sistema fechado e que permite apenas a adição de substrato conforme necessário.

[00014] No entanto, o referido documento se distancia da presente invenção, pois na presente invenção a produção de magnetossomos ocorre de maneira contínua. Adicionalmente, a escolha do momento de início de entrada de meio de cultura fresco na presente invenção diferencia-se da apresentada por este documento, por ser baseada no tempo em que ocorre a maior concentração de magnetossomos no meio. Deste modo, a presente invenção baseia-se na manutenção de um estado fisiológico das células, o de maior número de magnetossomos, por um período prolongado. Em Liu *et. al.* (2010), o meio de alimentação é cerca de 100 vezes mais concentrado em termos de fonte de carbono e lactato do que o meio de alimentação

empregado pela presente invenção, o que implica na alimentação de pequenos volumes deste meio. Desta forma, o isolamento dos magnetossomos só se torna prático após o término da batelada. Deste modo, a presente invenção diferencia-se deste documento, visto que não há a necessidade de aguardo pelo fim do cultivo, uma vez que ocorre a saída do meio contendo magnetossomos durante o processo, que é contínuo.

[00015] O artigo intitulado "Continuous cultivation and recovery of magnetotactic bacteria", de Bahaj*et al.* (1997), descreve um processo de produção contínua de magnetossomos a partir de bactérias do gênero *Magnetospirillum*.

[00016] Porém o referido documento se distancia da presente invenção, pois o processo é fechado, sendo permitida apenas a adição de nutrientes e injeção de gás nitrogênio. Outro ponto de diferença é a forma de manejar o meio, onde, na invenção, o meio fresco é introduzido e o meio gasto é retirado do biorreator, com as bactérias crescidas e, no documento, o meio é recirculado dentro do sistema, retornando ao reservatório onde ocorre o cultivo. Por conta do exposto, entendemos que essa diferença acarreta na diminuição da presença de metabólitos tóxicos, sendo uma das vantagens da invenção proposta. Adicionalmente, a presente invenção se distancia deste documento, pois prevê a otimização do cultivo de magnetossomos de *Mv. blakemorei* cepa MV-1^{T} em biorreator, que possuem magnetossomos prismáticos com uma superfície disponível maior que a dos magnetossomos cuboctaédricos do gênero *Magnetospirillum*.

SÚMARIO DA INVENÇÃO

[00017] A presente invenção descreve um processo para produção contínua e em larga escala de magnetossomos através do cultivo de bactérias magnetotáticas *Magnetovibrio blakemorei* cepa MV-1^T em biorreator. Este processo em larga escala possui maior produtivade de magnetossomos, com baixo custo e características físico-químicas controladas, tornando viável a sua aplicação. Adicionalmente, a presente invenção promove uma produção estável de magnetossomos por períodos mais extensos de cultivo, sendo uma das vantagens da invenção frente ao estado da técnica atual.

BREVE DESCRIÇÃO DAS FIGURAS

[00018] A Figura 1 demonstra vista externa do vaso do biorreator contendo tubo amostrador.

[00019] A Figura 2 descreve as indicações da conexão entre o tubo coletor e a tubulação de saída e do recipiente coletor.

[00020] A Figura 3 demonstra as indicações dos sensores de oxigênio e pH, da válvula controladora de fluxo de massa e da tubulação de N_2O.

[00021] A Figura 4 descreve a vista interna da tampa da garrafa do meio de alimentação mostrando a saída de meio e a saída de ar.

[00022] A Figura 5 mostra as bombas peristálticas de alimentação e de efluxo.

[00023] A Figura 6 descreve a garrafa contendo meio de alimentação, evidenciando a tubulação de saída de meio e o filtro de saída de ar.

[00024] A Figura 7 mostra Imagens em microscopia eletrônica de transmissão e percentual de PLL-FITC ligada à superfície de magnetossomos das cepas MV-1^T e AMB-1.

DESCRIÇÃO DETALHADA DA INVENÇÃO

[00025] A presente invenção descreve um processo de produção contínua e em larga escala de magnetossomos através do cultivo de bactérias magnetotáticas *Magnetovibrio blakemorei* cepa MV-1^T em biorreator, de acordo com as seguintes etapas:

(a) inocular o meio otimizado com as células da bactéria *Magnetovibrio blakemorei* cepa MV-1^T, utilizando inóculo com densidade óptica de 0,01 no biorreator;

(b) etapa em batelada simples do referido processo, com duração na faixa entre 60 a 84 horas, na qual as células de *Magnetovibrio blakemorei* cepa MV-1^T são cultivadas até atingirem a fase exponencial de crescimento;

(c) etapa contínua através da entrada de meio otimizado fresco no biorreator e da saída de meio (11) otimizado contendo magnetossomos do mesmo, em vazão calculada a partir da taxa de crescimento na fase exponencial;

(d) recuperar os magnetossomos.

[00026] Antes do início da etapa (a) do referido processo, precisa-se preparar o inóculo de células da bactéria *Magnetovibrio blakemorei* cepa MV-1^{T}e o meio de cultivo que será empregado no processo de cultivo. Estas células são criopreservadas em nitrogênio líquido na forma de alíquotas de 2mL contendo meio de cultivo padrão definido por Bazylinski et al. (2013) e glicerol a 20%. Tais células encontram-se depositadas na Deutsche Sammlung von Mikroorganismen und Zellkulturen (DSMZ) sob o registro 23250.

[00027] Em seguida, prepara-se o inóculo, por meio do cultivo destas células em meio otimizado e anaeróbio, cuja composição é conforme descrita em Silva et al. (2013), em frascos de 50 mL por 36 a 60 h a 28 °C. O volume de inóculo é calculado a partir de sua densidade óptica (DO) e do volume de meio otimizado no biorreator, neste caso, entre 2 L a 10 L. Este volume deve ser aquele necessário para se obter uma DO de 0,01 no biorreator após a inoculação. A densidade de células bacterianas é determinada através da medida densidade óptica (DO) em uma alíquota do meio em espectrofotômetro a um comprimento de onda de 600 nm.

[00028] O processo de produção das referidas células em biorreator ocorre utilizando o mesmo meio de cultivo otimizado que é empregado para preparar o inóculo, que deve ser esterilizado antes de ser empregado no cultivo. A esterilização ocorre em autoclave numa faixa de 110 a 130°C e 1atm entre 10 a 30 min. A adição das soluções de cisteína (0,2 g / 5 mL de água) e sulfato ferroso ($FeSO_4$) a 10 mM é feita após a esterilização do meio. Após a adição desses componentes pela tubulação de N_2O (9), a purga com N_2O é feita e, em seguida, a inoculação é realizada. A coleta para medição da DO deve ser feita em intervalos regulares para se determinar o crescimento bacteriano, sendo que o intervalo mínimo de tempo para se medir a DO é entre a faixa de 6 até 24 h desde o início do processo.

[00029] Finalmente, a etapa (a) do referido processo inicia-se com a inoculação do meio otimizado com as células da bactéria *Magnetovibrio blakemorei* cepa MV-1^T, utilizando inóculo com densidade óptica de 0,01 no biorreator quando a condição anaeróbica é alcançada. Tal condição anaeróbica é

alcançada pela purga de nitrogênio (N_2) estéril a uma vazão na faixa de 0,2 a 1,5 $L.min^{-1}$ por 15 min no meio otimizado fresco até a leitura do sensor de O_2 chegar a zero. O biorreator empregado neste processo é do tipo tanque agitado com capacidade de 5 L. Preferencialmente, o equipamento é o modelo Minifors do fabricante Infors.

[00030] Consecutivamente, a etapa (b) do referido processo é iniciada com o cultivo em batelada simples, com duração na faixa de 60 a 84 h, na qual as células de *Magnetovibrio blakemorei* cepa $MV\text{-}1^T$ são cultivadas até atingirem a fase exponencial de crescimento. Os parâmetros de cultura são configurados da seguinte forma: pH na faixa entre 6,8 a 7,2, velocidade de agitação na faixa entre 90 a 110 RPM, temperatura na faixa entre 26 a 30°C e O_2 não detectável. O pH é medido em linha através de um sensor de pH (7) tipo *gel-filled* acoplado no biorreator e ajustado para 7,0 com solução de NaOH 1-5% ou solução de HCl 1-2 mol/L, estéril à medida em que for necessário. O sensor de oxigênio (6) é do tipo polarográfico. Há a suplementação da fonte de ferro, cujo volume adequado é calculado com base na concentração atual, medida através do método colorimétrico da ferrozina. Uma solução estéril e livre de oxigênio de sulfato ferroso 10mM é aliquotada utilizando uma seringa com agulha. A seringa/agulha injeta o stopper de borracha presente na parte superior do vaso do biorreator e o pistão é pressionado até a completa transferência do volume. O N_2O é injetado em pulsos a uma vazão na faixa entre 0,2 a 1,5 $L.min^{-1}$ por 15 min, a cada 24 h.

[00031] A etapa (c) do referido processo, que é uma etapa de cultivo contínua do tipo quimiostato, é iniciada através

da entrada de meio otimizado fresco no biorreator e da saída de meio (11) otimizado contendo magnetossomos do mesmo, em vazão calculada a partir da taxa de crescimento na fase exponencial. A taxa de crescimento (μ) em h^{-1} entre dois tempos (1 e 2), por sua vez, é calculada como mostra a equação 1 abaixo:

[00032] $$\mu = \frac{[ln(DO_{tempo}\ )) - (ln\ (DO_{tempo1})]}{tempo\ 2 - tempo\ 1}$$ (Equação 1)

[00033] A vazão de entrada e saída de meio é calculada conforme a equação 2 a seguir:

[00034] Vazão= μ*0,7*Volume de meio no biorreator (Equação 2)

[00035] onde a vazão é dada em $L.h^{-1}$.

[00036] O referido de cultivo otimizado já está previamente pronto e parte dele é transferido para uma garrafa de 2 L, denominada de recipiente alimentador (5), que é vedada com uma tampa em rosca com duas saídas: um filtro de ar (10) com porosidade na faixa de 0,20 a 0,22 μm e uma saída de meio (11), conectada a tubulação de saída de meio (2). Uma tubulação interna de saída de meio (11) otimizado deve ser ligada, em uma de suas extremidades, na parte inferior da tampa e deve ter comprimento suficiente para que a outra extremidade atinja o fundo da garrafa.

[00037] A parte externa da tubulação de saída de meio (2) é ligada na entrada de uma bomba peristáltica de alimentação, a qual bombeia o meio otimizado do recipiente alimentador (5) para o vaso do biorreator. O meio otimizado contendo crescimento é removido do interior do biorreator através da ligação de uma tubulação conectada em uma de suas extremidades na saída do tubo amostrador (16) e a outra em outra bomba peristáltica de efluxo. A partir da bomba de

efluxo, o meio contendo crescimento é bombeado para um recipiente coletor (4).

[00038] Durante a fase de produção contínua, a injeção de N_2O é feita em pulsos a cada 8 horas, a uma vazão de 0,2 a 1,5 $L.min^{-1}$ por 5 min, a cada 24 h. Nesta etapa o pH encontra-se na faixa entre 6,9 a 7,1, a temperatura está na faixa entre 26 a 30°C, a concentração dos componentes é a mesma que a do cultivo em batelada e o tempo de residência é de 28,5 h. O regime de injeção deste gás foi determinado experimentalmente e inicia-se juntamente com o cultivo contínuo, no período de tempo entre 60 a 84 h. Em cada pulso, o gás é injetado durante 5 minutos em uma vazão de 0,5 $L.min^{-1}$ e a velocidade de agitação das pás é aumentada de 100 para 200 RPM durante o tempo de injeção.

[00039] A vazão de injeção do N_2O é controlada por uma válvula controladora de fluxo de massa (8). O controle remoto das funções do biorreator e da válvula controladora de fluxo de massa (8) é feito de forma integrada através do software IRIS versão 6 (INFORSTM, Suíça), arquitetado em um sistema do tipo SCADA (Supervisory Control And Data Acquisition). O regime de injeção intermitente de N_2O desenvolvido para esta invenção é controlado através da inserção da linha de comando abaixo no software de controle de processo:

[00040] #0

stirrer.sp=100

MVC.sp=0

IF(SEQ_TIME>28800) {SEQ=1}

[00041] #1

stirrer.sp=200

MVC.sp=40

IF(SEQ_TIME>300) {SEQ=0}

[00042] As condições basais de cultivo, que são agitação a 100 RPM e sem injeção de N_2O, estão configuradas na sequência #0: stirrer.sp=100 (100 RPM), MVC.sp=0 (MVC desligado), IF(SEQ_TIME>28800){SEQ=1} (se o tempo decorrido desde o início da sequência #0 for maior que 8 h ou 28800 s, a sequência #1 é iniciada). A sequência #1 é configurada como: stirrer.sp=200 (agitação aumentada para 200 RPM), MVC.sp=40 (equivalente a 0,5 L.min-1 de N2O), IF(SEQ_TIME>300){SEQ=1} (se o tempo decorrido desde o início da sequência #1 for maior que 5 min ou 300 s, a sequência #0 é reestabelecida).

[00043] Em seguida, os magnetossomos são recuperados, consistindo na etapa (d) do referido processo. Os magnetossomos produzidos são recuperados através das seguintes etapas:

d.1) coletar as células são coletadas por sifonamento;

d.2) centrifugá-las a 6100 × g a 4 °C por 15 min;

d.3) lavar e ressuspender os *pellets* de células em 15 mL de tampão Hepes (20 mM, pH 6,8);

d.4) realizar a lise por desrupção ultrassônica em sonicador de ponteiras na amplitude de 40%, frequência 20 kHz, em 60 ciclos com duração de 30 s com intervalos de 30 s entre si;

d.5) concentrar os magnetossomos de modo magnético por um ímã de neodímio-boro fixado na parte externa do tubo por 12 h a 4 °C;

d.6) transferir os cristais para tubos de polipropileno de 1,5 mL e ressuspensos em tampão Hepes com 10 mM e pH 6,8 e com NaCl 200 mM;

d.7) lavar os cristais são lavados com tampão Hepes com 10 mM e pH 6,8 e com NaCl 200 mM em banho de ultrassom por 4 ciclos de 30 min, com concentração magnética e troca do tampão a cada ciclo;

d.8) armazenar os magnetossomos extraídos em tampão Hepes 20 mM e pH 6,8.

[00044] Para a recuperação dos magnetossomos, as células são coletadas por sifonamento e centrifugadas a 6100 × g a 4 °C por 15 min. Os *pellets* de células são lavados e ressuspendidos em 15 mL de tampão Hepes (20 mM, pH 6,8). Em seguida, as células são submetidas à lise por desrupção ultrassônica em sonicador de ponteiras (VCX 500, Sonics, Newtown, EUA) na amplitude de 40%, frequência 20 kHz, em 60 ciclos com duração de 30 s com intervalos de 30 s entre si. Os magnetossomos são concentrados magneticamente por um ímã de neodímio-boro fixado na parte externa do tubo por 12 h a 4 °C. Os cristais são transferidos para tubos de polipropileno de 1,5 mL e ressuspensos em tampão Hepes (10 mM, pH 6,8) com NaCl (200 mM). Em seguida, os cristais são lavados com o mesmo tampão em banho de ultrassom (Branson 2200, Emerson, Rochester, EUA) por 4 ciclos de 30 min, com concentração magnética e troca do tampão a cada ciclo. Os magnetossomos extraídos são armazenados em tampão Hepes (20 mM, pH 6,8).

[00045] As configurações das estruturas empregadas para este processo são conforme ilustradas pelas figuras 1, 2, 3, 4, 5 e 6. As figuras 1, 2 e 3 mostram vistas externas do biorreator adaptado para cultivo contínuo do tipo quimiostato.

[00046] A Figura 1 mostra a vista externa do vaso do biorreator contendo tubo amostrador (1), o qual será conectado a tubulação de saída de meio (2) com crescimento.

[00047] Especificamente, a Figura 2 mostra as indicações da conexão (3) entre o tubo coletor (1) e a tubulação de saída (2) e do recipiente coletor (4).

[00048] A figura 3 mostra as indicações dos sensores de oxigênio (6) e pH (7), da válvula controladora de fluxo de massa (8) e da tubulação de N_2O (9).

[00049] Os componentes do biorreator relacionados à invenção são mostrados nas figuras 1, 4, 5, e 6.

[00050] A Figura 4 mostra a vista interna da tampa da garrafa do meio de alimentação mostrando a saída de ar (12) e a saída de meio (11) onde serão conectadas, respectivamente, o filtro de ar (10) e as tubulações de saída de meio de alimentação para o vaso (15).

[00051] A figura 5 mostra as bombas peristálticas de alimentação e de efluxo. A Figura 6 mostra a garrafa contendo meio de alimentação, evidenciando a tubulação de saída de meio (2) e o filtro de ar (10).

EXEMPLOS ILUSTRATIVOS

Exemplo 1

[00052] Como um experimento preliminar, foi realizado o cultivo em batelada alimentada com suplementação de $FeSO_4$ e injeção de N_2O em pulsos de 24 h a 0,5 $L.min^{-1}$ sem alteração da agitação, com pH na faixa de 6,9 a 7,1, temperatura na faixa de 26 a 30°C e agitação na faixa de 90 a 110 rpm. Após 120 h de cultivo, a produção de magnetita atingiu 24,5 $mg.L^{-1}$. A produtividade máxima (16,8 $mg.L^{-1}.d^{-1}$) foi atingida entre 48 e 72 h. Entretanto, a produtividade e o número médio de

magnetossomos por célula diminuiu 25% entre 72 h a 96 h, enquanto que a produtividade caiu para 4,5 $mg.L^{-1}.d^{-1}$. Diante disso, o cultivo contínuo na modalidade quimiostato com injeção intermitente de óxido nitroso foi estabelecido. O cultivo contínuo foi capaz de manter a cultura com produção e produtividade de magnetita de 27,1 $mg.L^{-1}$ e 22,7 $mg.L^{-1}.d^{-1}$, respectivamente, em 120 h, mantendo valores próximos até 168 h. Esta condição foi atingida pois foram evitadas a perda de síntese de magnetita e redução no número de magnetossomos por célula, como havia ocorrido no cultivo em batelada alimentada.

Exemplo 2

[00053] A maior capacidade de ligação a moléculas funcionais por magnetossomos prismáticos de *Mv. blakemorei* cepa MV-1T em comparação aos magnetossomos cuboctaédricos de *Magnetospirillum magneticum* cepa AMB-1 foi comprovada através do experimento descrito a seguir.

[00054] O experimento consistiu na incubação de 100 µg de magnetossomos de ambas as cepas com uma 1 mL de uma solução de poli-L-lisina ligada ao marcador fluorescente isotiocianato de fluoresceína (PLL-FITC). A solução de PLL-FITC possuía uma concentração de 200 µg/L em tampão fosfato 0,1 M (pH 7,4). A incubação foi feira em um banho de ultrassom (Branson 2200) a 60 W durante 3 ciclos de 5 min. Em seguida, os magnetossomos foram concentrados por meio de um imã de neodímio colocado externamente ao tubo. Em seguida, o sobrenadante foi removido e armazenado para leitura fluorimétrica. Foram feitas duas lavagens consecutivas com água ultrapura e os sobrenadantes foram guardados para leitura fluorimétrica.

[00055] A quantificação de PLL-FITC ligado aos magnetossomos foi feita através da leitura da intensidade de fluorescência dos sobrenadantes em um fluorímetro. Foram utilizados os comprimentos de onda de 488 nm para excitação e 525 nm para emissão. Foi realizada a leitura de um controle de PLL-FITC na concentração 200 µg/L. A proporção de PLL-FITC ligada aos magnetossomos foi calculada pela diferença entre a leitura do controle e a leitura dos sobrenadantes dividida pela leitura do controle.

[00056] Os magnetossomos de *Mv. blakemorei* cepa MV-1^{T} apresentaram maior eficiência de ligação à PLL-FITC, com uma média de 65,05 ± 2,77% (n=7) (Figura 7). Os magnetossomos de *Ms. magneticum* cepa AMB-1 apresentaram uma média de 39,55 ± 7,6% (n=7) de eficiência.

[00057] A presente invenção foi revelada neste relatório descritivo em termos de sua modalidade preferida. Entretanto, outras modificações e variações são possíveis a partir da presente descrição, estando ainda inseridas no escopo da invenção aqui revelada.

SINAIS DE REFERÊNCIA

1- tubo coletor;

2- tubulação de saída de meio;

3- conexão;

4- recipiente coletor;

5- recipiente alimentador;

6- sensor de oxigênio;

7- sensor de pH;

8- válvula controladora de fluxo de massa;

9- tubulação de N_2O;

10- filtro de ar;

11- saída de meio;

12- saída de ar;

13- entrada de meio proveniente do vaso;

14- efluxo de meio para recipiente coletor;

15- saída de meio de alimentação para o vaso;

16- entrada de meio de alimentação;

REIVINDICAÇÕES

1. Processo para produção contínua de magnetossomos através do cultivo de bactérias magnetotáticas *Magnetovibrio blakemorei* cepa MV-1^T em biorreator **CARACTERIZADO** pelo fato de cumprir as seguintes etapas:

(a) inocular o meio otimizado com as células da bactéria *Magnetovibrio blakemorei* cepa MV-1^T, utilizando inóculo com densidade óptica de 0,01 a um comprimento de onda de 600 nm no biorreator;

(b) etapa em batelada simples do referido processo, com duração na faixa entre 60 a 84 horas, na qual as células de *Magnetovibrio blakemorei* cepa MV-1^T são cultivadas até atingirem a fase exponencial de crescimento com suplementação da fonte de ferro;

(c) etapa contínua do tipo quimiostato através da entrada de meio otimizado fresco no biorreator e da saída de meio otimizado contendo magnetossomos do mesmo, em vazão calculada a partir da taxa de crescimento na fase exponencial;

(d) recuperar os magnetossomos.

2. Processo, de acordo com a reivindicação 1, **CARACTERIZADO** pelo fato de que os parâmetros do processo em batelada simples são pH na faixa entre 6,8 a 7,2, velocidade de agitação na faixa entre 90 a 110 RPM, temperatura na faixa entre 26 a 30°C, O_2 não detectável e com a injeção de N_2O em pulsos a uma vazão na faixa entre 0,2 a 1,5 L.min-1 por 15 min, a cada 24 h.

3. Processo, de acordo com a reivindicação 1, **CARACTERIZADO** pelo fato de que os parâmetros do processo em batelada contínua são pH na faixa entre 6,9 a 7,1,

temperatura na faixa entre 26 a 30°C, a concentração dos componentes é a mesma que a do cultivo em batelada, o tempo de residência de 28,5 h, injeção de N_2O em feita em pulsos a cada 8 horas, a uma vazão de 0,2 a 1,5 $L.min^{-1}$ por 5 min, com velocidade de agitação das pás na faixa de 100 a 200 RPM.

4. Processo, de acordo com qualquer uma das reivindicações de 1 a 3, **CARACTERIZADO** pelo fato de que a condição anaeróbica no biorreator é alcançada pela purga de nitrogênio (N_2) estéril a uma vazão na faixa de 0,2 a 1,5 $L.min^{-1}$ por 15 min no meio otimizado fresco até a leitura do sensor de O_2 chegar a zero.

5. Processo, de acordo com qualquer uma das reivindicações de 1 a 4, **CARACTERIZADO** pelo fato de que o biorreator é do tipo tanque agitado com capacidade de 5 L.

6. Processo, de acordo com qualquer uma das reivindicações de 1 a 5, **CARACTERIZADO** pelo fato de que o sensor de pH é do tipo gel-filled acoplado no biorreator e ajustado para 7,0 com solução de NaOH 1-5% ou solução de HCl 1-2 mol/L, estéril à medida em que for necessário.

7. Processo, de acordo com qualquer uma das reivindicações de 1 a 6, **CARACTERIZADO** pelo fato de que o sensor de oxigênio é do tipo polarográfico.

8. Processo, de acordo com qualquer uma das reivindicações de 1 a 7, **CARACTERIZADO** pelo fato de que o volume adequado para suplementar a fonte de ferro é calculado com base na concentração atual a partir da injeção de uma alíquota de uma solução estéril e livre de oxigênio de sulfato ferroso 10mM no biorreator.

9. Processo, de acordo com qualquer uma das reivindicações de 1 a 8, **CARACTERIZADO** pelo fato de que a taxa de crescimento (μ) em h^{-1} entre dois tempos é calculada da seguinte forma:

$$\mu = \frac{[ln(DO_{tempo2})) - (ln\,(DO_{tempo1})]}{tempo\ 2 - tempo\ 1}$$

10. Processo, de acordo com qualquer uma das reivindicações de 1 a 9, **CARACTERIZADO** pelo fato de que a vazão de entrada e saída de meio é calculada pela relação Vazão= μ*0,7*Volume de meio no biorreator.

11. Processo, de acordo com qualquer uma das reivindicações de 1 a 10, **CARACTERIZADO** pelo fato de que a etapa (d) de recuperação dos magnetossomos ocorre através das seguintes etapas:

d.1) coletar as células são coletadas por sifonamento;

d.2) centrifugá-las a 6100 × g a 4 °C por 15 min;

d.3) lavar e ressuspender os *pellets* de células em 15 mL de tampão Hepes (20 mM, pH 6,8);

d.4) realizar a lise celular por desrupção ultrassônica em sonicador de ponteiras na amplitude de 40%, frequência 20 kHz, em 60 ciclos com duração de 30 s com intervalos de 30 s entre si;

d.5) concentrar os magnetossomos de modo magnético por um ímã de neodímio-boro fixado na parte externa do tubo por 12 h a 4 °C;

d.6) transferir os cristais para tubos de polipropileno de 1,5 mL e ressuspensos em tampão Hepes com 10 mM e pH 6,8 e com NaCl 200 mM;

d.7) lavar os cristais são lavados com tampão Hepes com 10 mM e pH 6,8 e com NaCl 200 mM em banho de ultrassom por

4 ciclos de 30 min, com concentração magnética e troca do tampão a cada ciclo;

d.8) armazenar os magnetossomos extraídos em tampão Hepes 20 mM e pH 6,8.

Figura 1

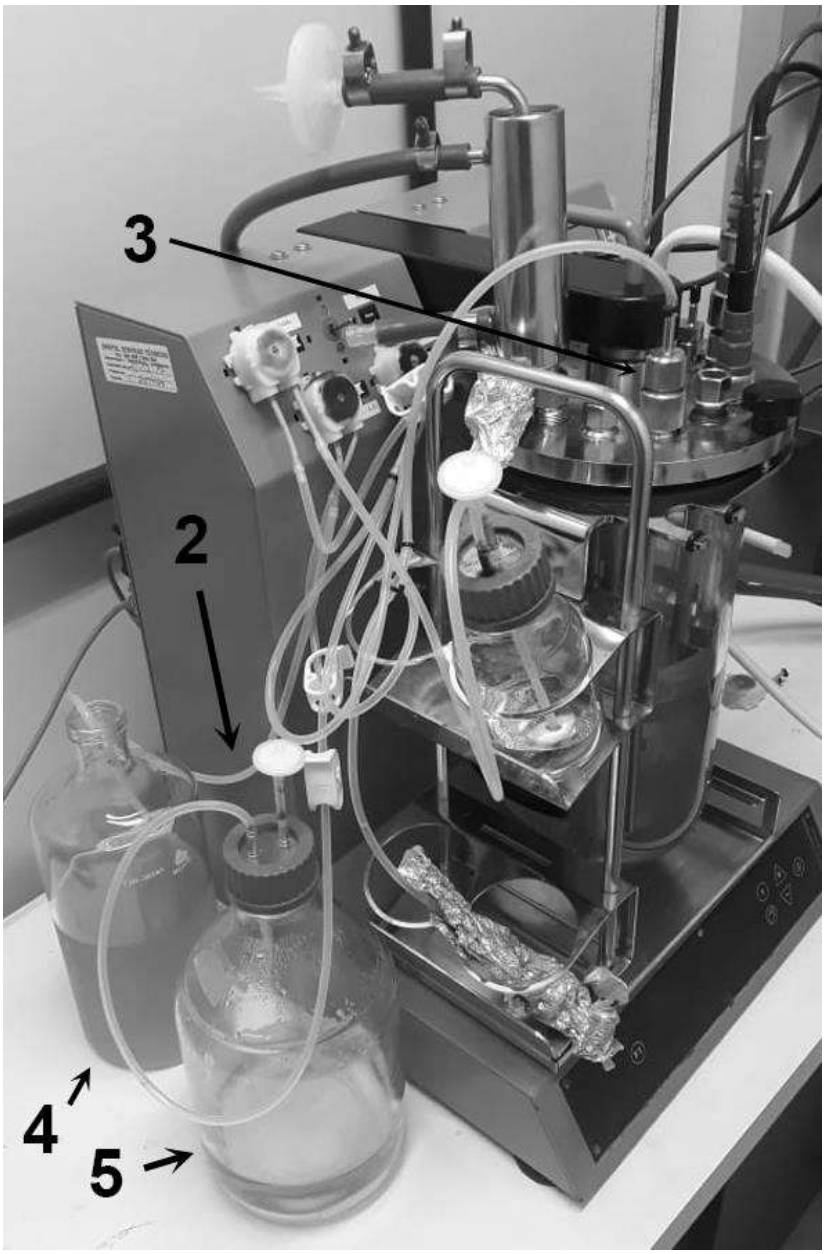

Figura 2

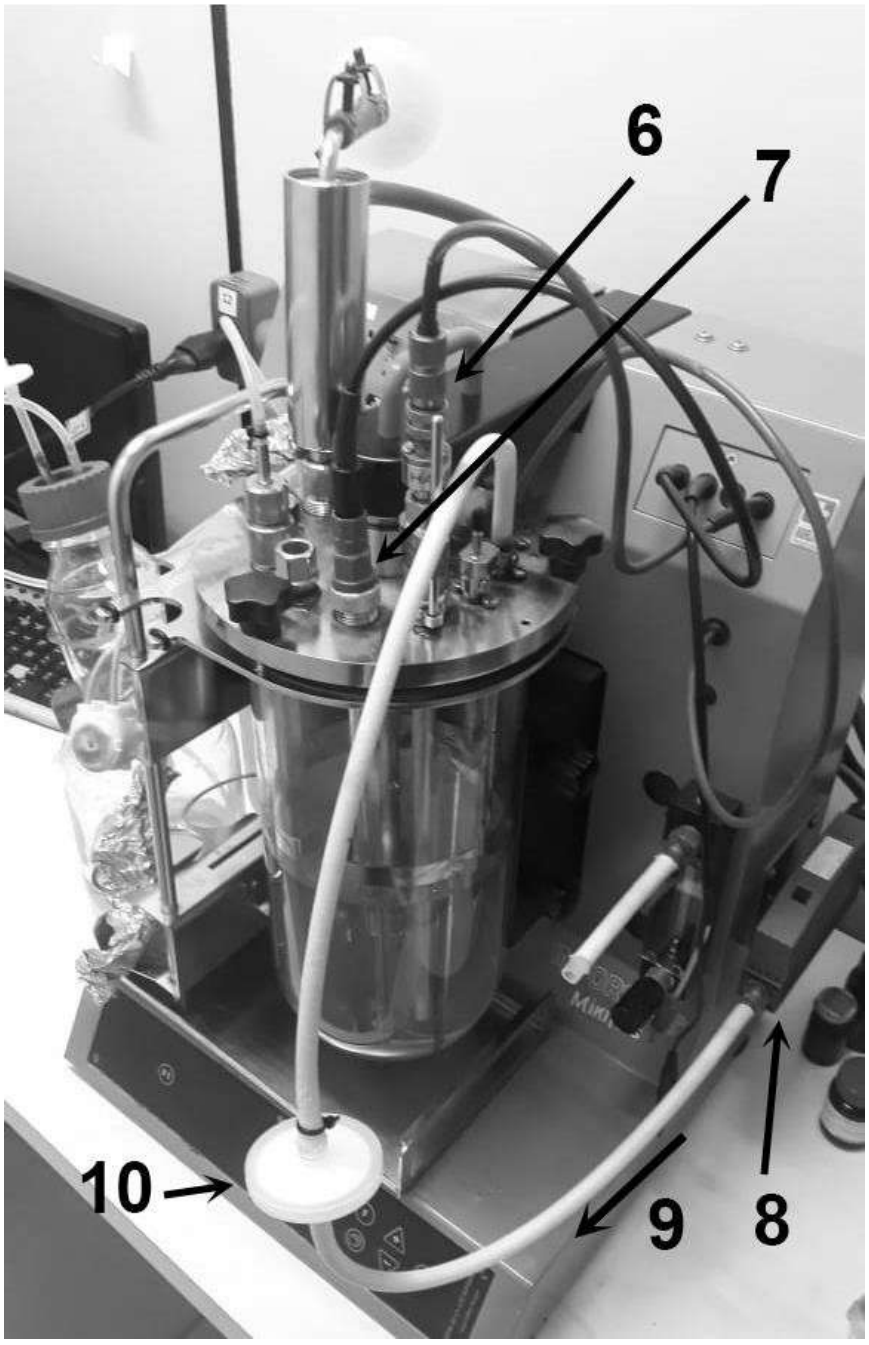

Figura 3

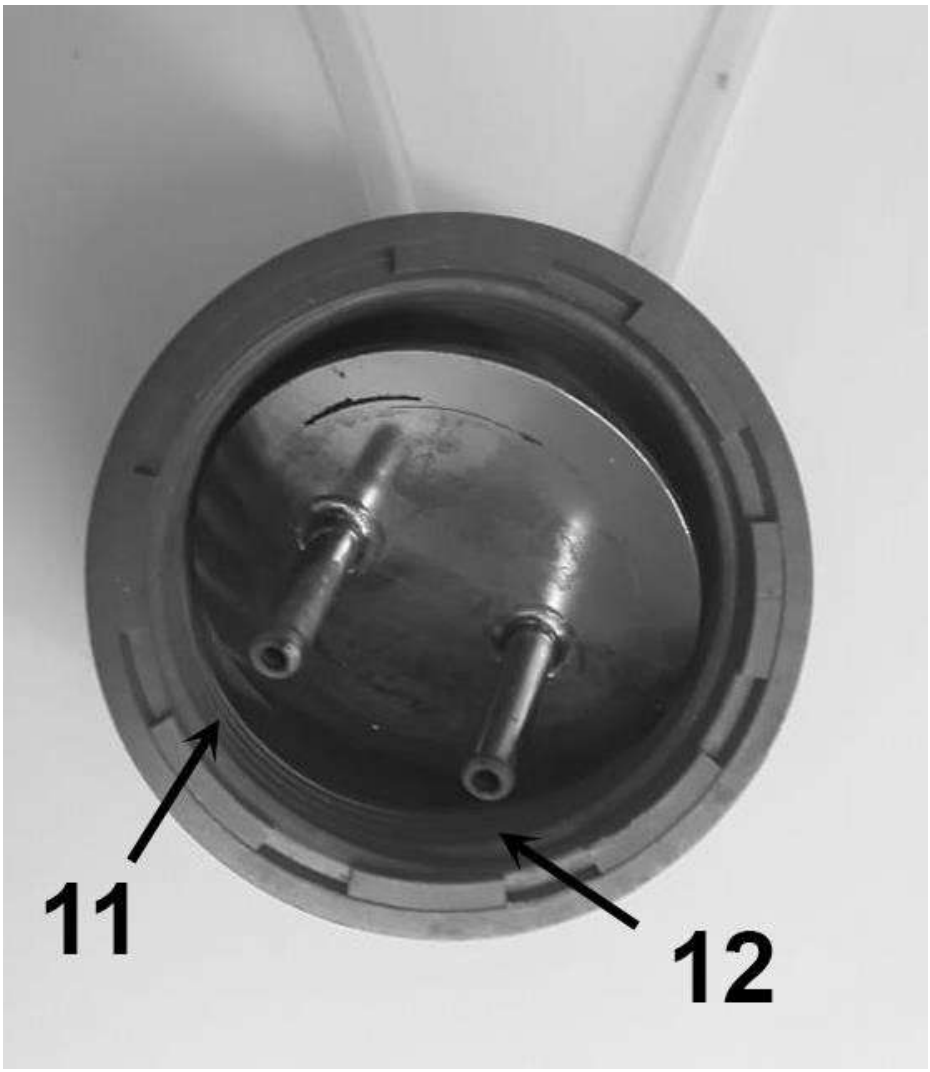

Figura 4

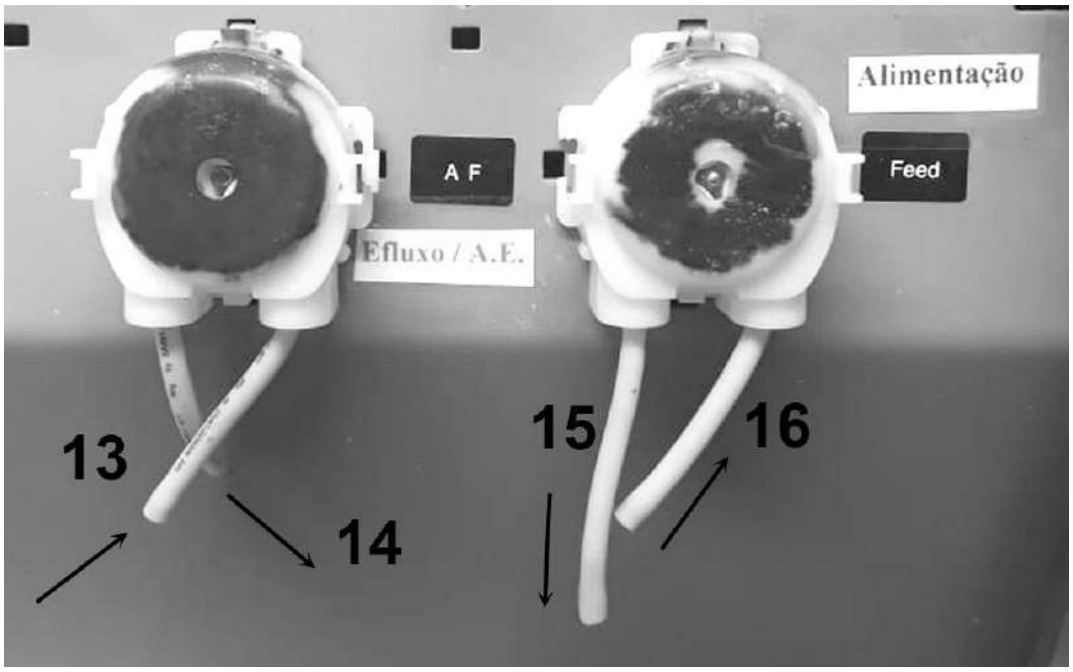

Figura 5

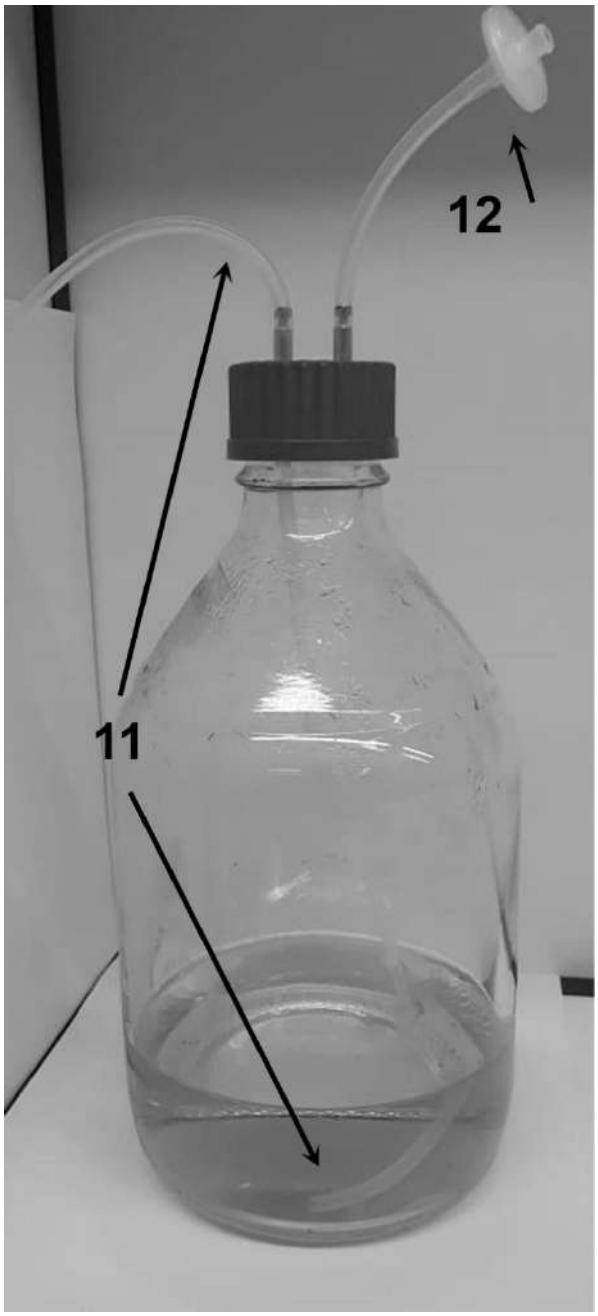

Figura 6

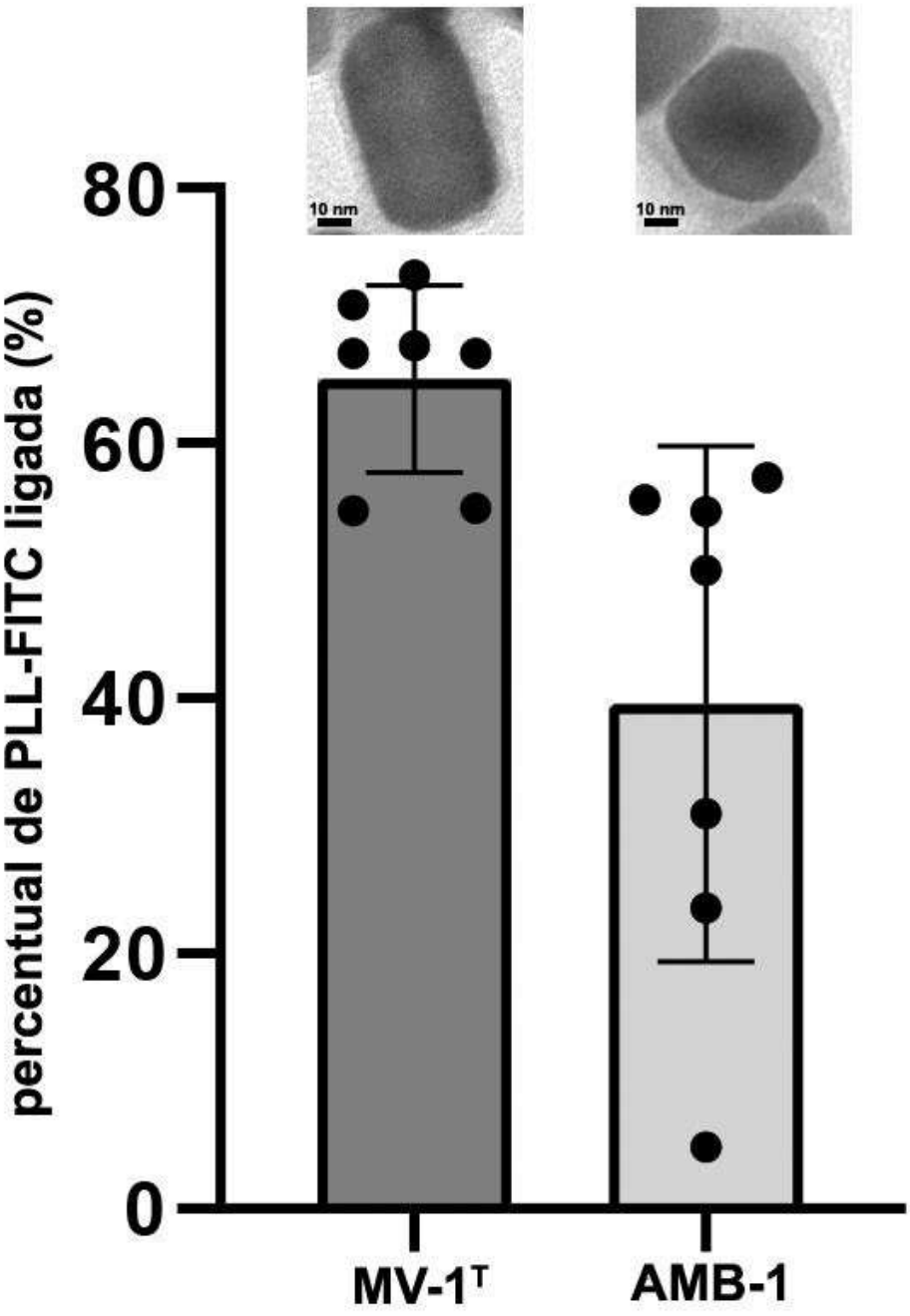
10 nm
10 nm
80
60
40
20
0
percentual de PLL-FITC ligada (%)
MV-1T
AMB-1

Figura 7

RESUMO

PROCESSO PARA PRODUÇÃO CONTÍNUA DE MAGNETOSSOMOS ATRAVÉS DO CULTIVO DE BACTÉRIAS MAGNETOTÁTICAS EM BIORREATOR

A presente invenção descreve um processo de produção contínua e em larga escala de magnetossomos através do cultivo de bactérias magnetotáticas *Magnetovibrio blakemorei* cepa MV-1^T em biorreator. Este processo em larga escala possui maior produtividade de magnetossomos, com baixo custo e características físico-químicas controladas, tornando viável a sua aplicação. A otimização do cultivo de *Mv. blakemorei* cepa MV-1^T em biorreator é vantajosa pois seus magnetossomos prismáticos apresentam uma superfície disponível maior que a dos magnetossomos cuboctaédricos do gênero *Magnetospirillum*. Adicionalmente, a presente invenção promove uma produção estável de magnetossomos por períodos mais extensos de cultivo, sendo uma das vantagens da invenção frente ao estado da técnica atual. As aplicações dos magnetossomos incluem o carreamento e liberação de fármacos, hipertermia induzida magneticamente, separação de células e biomoléculas e imobilização de enzimas.

INSTITUTO NACIONAL DA PROPRIEDADE INDUSTRIAL

24/03/2021 870210027856 17:36

29409161928466698

Pedido nacional de Invenção, Modelo de Utilidade, Certificado de Adição de Invenção e entrada na fase nacional do PCT

Número do Processo: BR 10 2021 005683 5

Dados do Depositante (71)

Depositante 1 de 2

Nome ou Razão Social: UNIVERSIDADE FEDERAL DO RIO DE JANEIRO
Tipo de Pessoa: Pessoa Jurídica
CPF/CNPJ: 33663683000116
Nacionalidade: Brasileira
Qualificação Jurídica: Instituição de Ensino e Pesquisa
Endereço: Av. Pedro Calmon, 550 - Cidada Universitária
Cidade: Rio de Janeiro
Estado: RJ
CEP: 21941901
País: Brasil
Telefone: (21)37331793
Fax:
Email: agenciadeinovacao@inovacao.ufrj.br

Depositante 2 de 2

Nome ou Razão Social:	CENTRO BRASILEIRO DE PESQUISAS FÍSICAS - CBPF
Tipo de Pessoa:	Pessoa Jurídica
CPF/CNPJ:	04044443000135
Nacionalidade:	Brasileira
Qualificação Jurídica:	Instituição de Ensino e Pesquisa
Endereço:	Rua Doutor Xavier Sigaud, nº 150, Urca
Cidade:	Rio de Janeiro
Estado:	RJ
CEP:	22290-180
País:	BRASIL
Telefone:	
Fax:	
Email:	

Dados do Pedido

Natureza Patente:	10 - Patente de Invenção (PI)
Título da Invenção ou Modelo de Utilidade (54):	PROCESSO DE SÍNTESE DE MAGNETOSSOMO FUNCIONALIZADO COM FÁRMACO E MAGNETOSSOMO FUNCIONALIZADO OBTIDO A PARTIR DESTE
Resumo:	A presente invenção descreve um processo de síntese de magnetossomo funcionalizado com fármaco, assim como o magnetossomo funcionalizado obtido a partir deste. O magnetossomo utilizado é oriundo do cultivo de bactérias magnetotáticas. A produção desse composto tem por objetivo fornecer um composto passível de liberação controlada de fármacos, especificamente fármaco aplicado no tratamento de doenças infecciosas de etiologia fúngica ou parasitária. Assim como trazer o advento de uma produção a baixo custo e por meio de tecnologia verde
Figura a publicar:	1

PROCESSO DE SÍNTESE DE MAGNETOSSOMO FUNCIONALIZADO COM FÁRMACO E MAGNETOSSOMO FUNCIONALIZADO OBTIDO A PARTIR DESTE

CAMPO DE APLICAÇÃO

[0001] A presente invenção se aplica no campo químico e da nanotecnologia e revela um processo de síntese de nanopartículas magnéticas de origem bacteriana funcionalizadas com fármacos.

FUNDAMENTOS DA INVENÇÃO

[0002] A nanotecnologia e a biotecnologia se desenvolveram expressivamente nas últimas décadas. A interface entre essas duas áreas de conhecimento tem aumentado, gerando conhecimentos básicos e aplicados sobre a síntese biológica de nanomateriais e a utilização de ferramentas nanotecnológicas para fins biomédicos.

[0003] Dentre a diversidade de nanopartículas que são utilizadas como ferramenta em aplicações médicas, existem as nanopartículas magnéticas. Uma propriedade importante das nanopartículas magnéticas é a possibilidade de manipulação das mesmas por meio de um campo magnético externo, o que é vantajoso em inúmeras abordagens, como o transporte de fármacos para uma região específica do corpo humano.

[0004] Propriedades das nanopartículas magnéticas, como o tamanho nanométrico (1 a 100 nm), a capacidade de manipulação por campo magnético externo e a possibilidade de revestimento com compostos que as tornam biocompatíveis e viabilizam sua funcionalização, permitem sua aplicação em diversas abordagens biotecnológicas.

[0005] As nanopartículas magnéticas são sintetizadas por métodos variados. Convencionalmente, são utilizados os métodos de co-precipitação, síntese hidrotérmica,

microemulsão, processo poliol e pirólise em aerossol. Além de tais metodologias sintéticas convencionais, as nanopartículas magnéticas podem ser produzidas biologicamente por bactérias magnetotáticas, nas quais os nanocristais magnéticos são produzidos sob controle genético em uma vesícula formada pela invaginação da membrana citoplasmática, contendo proteínas exclusivas do processo de biomineralização. As nanopartículas magnéticas derivadas por meio deste método são denominadas magnetossomos (BMs, do inglês *bacterial magnetosomes*). O cultivo em batelada de bactérias para a produção de magnetossomos foi revelado no documento BR 10 2020 015831 7.

[0006] A utilização de BMs apresenta as seguintes vantagens quando comparada com o uso de nanopartículas magnéticas sintéticas:

- Citotoxicidade mais baixa;
- Melhor internalização por células de mamíferos;
- Menor custo de produção;
- Menor impacto ambiental na produção por apenas utilizar produtos biocompatíveis; e
- Maior estabilidade em relação a degradação.

[0007] Até o momento, as aplicações dos magnetossomos incluem carreamento e liberação de fármacos, hipertermia induzida magneticamente, separação de células e biomoléculas e imobilização de enzimas.

[0008] O tratamento disponível para diversas doenças infecciosas faz uso de fármacos que geram elevada toxicidade, devido a distribuição inespecífica desses para vários tecidos do organismo vivo, o que, por vezes, torna a biodisponibilidade destes fármacos reduzida no tecido alvo,

diminuindo sua eficiência.

[0009] Portanto, com o intuito de solucionar tais problemas, a presente invenção se refere a um processo de síntese magnetossomos funcionalizados com fármacos de ação antimicrobiana, para a liberação controlada de fármaco e direcionamento para o local de ação, através da utilização de campo magnético externo. Acrescenta-se ainda, a possibilidade de associação do invento com a técnica de hipertermia magnética, a fim de realizar o tratamento de doenças causadas por microrganismos.

ESTADO DA TÉCNICA

[0001] O documento BR 11 2012 011767 0, que aqui é incorporado por referência, revela cadeias extraídas de magnetossomos obtidas pela síntese bacteriana, as quais podem ser encapsuladas dentro de uma vesícula lipídica na presença ou não de um princípio ativo e utilizadas desta forma em termoterapia. O documento ainda ensina que a rotação das cadeias de magnetossomos *in vivo* pode ser melhorada pelo seu encapsulamento dentro de uma vesícula lipídica ou de um tipo semelhante de estrutura.

[0002] O revelado por este documento se diferencia da presente invenção por não revelar magnetossomos funcionalizados com um fármaco, e especificamente anfotericina b. O magnetossomo, encapsulado em uma vesícula lipídica, está estritamente relacionado com o direcionamento do fármaco, não estando necessariamente ligado ao fármaco, conforme a presente invenção revela.

[0003] O documento CN105193733A descreve um medicamento de nanopartículas de liberação lenta que envolve magnetossomos de origem biológica e um método de preparação

desse medicamento. O método compreende as etapas: (1) coleta das bactérias magnetotáticas e quebra da parede por ultrassom para liberação dos magnetossomos, após é aplicado um campo magnético externo para adsorver e separar os magnetossomos; (2) O corpo magnético é lavado várias vezes com soro fisiológico, e o quitosano, o material auxiliar (um dentre: metilcelulose, hidroxietilcelulose, hidroxietilcelulose, hidroxipropilcelulose, hidroxipropilmetilcelulose, hidroximetilcelulose, carboximetilcelulose de sódio, lactose, mananol, pectina, alginato de sódio, alginato de potássio, ágar, gelatina e dentre outros) e o ingrediente farmacêutico (um ou mais dos medicamentos antitumorais camptotecina, doxorubicina, vincristina, paclitaxel, colchicina e puromicina) são misturados uniformemente; (3) As nanosferas obtidas, por fim, são preparadas secando a mistura da etapa (2).

[0004] A diferença entre este documento e a presente invenção é que os constituintes do medicamento revelado por este documento estão aderidos em um excipiente farmacêutico, ou seja, tanto o fármaco como o magnetossomo não estão diretamente ligados. O método revelado por este documento baseia-se em um procedimento físico, basicamente de misturar os componentes até chegar em um aspecto uniforme, conforme descrito no documento. Além disso os fármacos relacionados são antitumorais como camptotecina, doxorubicina, vincristina, paclitaxel, colchicina e puromicina, não sendo ensinado e nem sugerido fármacos de ação antimicrobiana.

[0005] O artigo “Preparation and *in vitro* antitumor effects of cytosine arabinoside-loaded genipin-poly-L-glutamic acid-modified bacterial magnetosomes”, de Liu YG

et. al (2015), descreve uma preparação e estudo *in vitro* de magnetossomos de origem biológica (BM) modificados com fármacos antitumorais, especificamente citosina-arabinosídeo (ara-C). A imobilização do fármaco é realizada pelos agentes de ligação ácido poli-L-glutâmico (PLGA), genipina (GP) e EDC. A genipina promove a ligação covalente entre o grupamento amino (-NH2) do PLGA e do magnetossomo. O EDC, por sua vez, realiza a ligação covalente, entre o grupamento carboxila (-COOH) do PLGA com o grupamento -NH2 da molécula de AraC.

[0006] Sendo assim, uma das diferenças entre este documento e a presente invenção é a fixação da AraC aos magnetossomos, que ocorre, mesmo que indiretamente, por meio de ligações covalentes. Por outro lado, a presente invenção faz uso de agentes de ligação que propiciam interações eletrostáticas com os magnetossomos e o fármaco. Com isso, a interação da AmB com os magnetossomos ocorre de forma mais fraca, o que possibilita uma liberação controlada da AmB quando se faz uso de um campo magnético alternado, como descrito no exemplo 3 do presente relatório descritivo. Deste modo, a controlabilidade da liberação da AmB, conforme a presente invenção, é maior. Importante ressaltar que este documento acima referenciado apenas testou a liberação do fármaco utilizando a condição de agitação de 60 rpm e temperatura de 37 °C, sem aplicação de um campo magnético alternado.

[0007] A dissertação de mestrado "Síntese, caracterização, estabilidade e efeitos biológicos in vitro de nanopartícula magnética associada a anfotericina B", de Diêgo Cesar Iocca (2013), fornece uma síntese de

nanopartículas de maguemita estabilizadas com ácido láurico (BCL) sendo estas conjugadas com anfotericina B (BCL-AmB), a funcionalização de uma nanopartícula magnética com AmB. A origem das nanopartículas de maguemita decorre a partir de uma síntese inorgânica.

[0008] A diferença entre este documento e a presente invenção é que a presente invenção revela a funcionalização e aplicação de magnetossomos prismáticos produzidos pela espécie *Magnetovibrio blakemorei* cepa MV-1^{T}. Devido à natureza química do ácido láurico e de acordo com o documento acima mencionado, a molécula de anfotericina B se ancora à BCL por meio de interações hidrofóbicas. Com isso, a presente invenção difere pelo fato de a AmB se acoplar ao magnetossomo recoberto com poli-L-lisina (PLL) por meio de interações eletrostáticas. Essa diferença implica diretamente na liberação do fármaco da nanopartícula funcionalizada.

[0009] O artigo "Preparation and anti-tumor efficiency evaluation of doxorubicin-loaded bacterial magnetosomes: Magnetic nanoparticles as drug carriers isolated from *Magnetospirillum gryphiswaldense*", de Sun JB *et. al* (2008), fornece uma análise comportamental, bem como uma síntese de magnetossomos bacterianos (BM), originário de *Magnetospirillum gryphiswaldense* cepa MRS-1, acoplados ao fármaco doxorrubicina (DBM) com o auxílio do agente ligante glutaraldeído (GA). Obtiveram como resultado um alto índice de complexação do fármaco no magnetossomo, bem como observaram a não perda de atividade antitumoral com a complexação dos constituintes. Outro resultado apontado foi a alta estabilidade do complexo formado.

[00010] A diferença entre este artigo e a presente invenção

é que neste artigo foi utilizado o glutaraldeído como agente de ligação, que promove a ligação covalente entre o magnetossomo e o fármaco em questão. Com isso e como descrito no artigo supracitado, 95% do fármaco DOX permanece ligado à nanopartícula funcionalizada após 2 h de teste de liberação em PBS. Como já dito anteriormente, a presente invenção utiliza a poli-L-lisina, que promove a interação eletrostática, que proporcionou à invenção um controle e uma maior liberação da AmB frente à aplicação de um campo magnético alternado.

SÚMARIO DA INVENÇÃO

[00011] A presente invenção descreve um processo de síntese de uma nanopartícula magnética de origem biológica, magnetossomos, funcionalizada com fármaco, assim como a nanopartícula obtida a partir deste.

[00012] O objetivo da produção destes magnetossomos funcionalizados é a sua aplicação médica, incluindo medicina veterinária, no tratamento de doenças infecciosas de etiologia fúngica ou parasitária.

[00013] O processo, ora revelado, reduz custos de produção se comparado com metodologias convencionais sintéticas, além de produzir nanopartículas funcionalizadas com uma melhor ação e estabilidade.

BREVE DESCRIÇÃO DAS FIGURAS

[00014] A Figura 1 revela a representação estrutural dos magnetossomos (A), da anfotericina B (B) e dos magnetossomos funcionalizados, BMs-GA-AmB (C), BMs-PLL-GA-AmB (D) e BMs-PLL-AmB (E).

[00015] A Figura 2 mostra os resultados dos testes de percentual de Anfotericina B ligada e carregamento do

fármaco.

[00016] A Figura 3 mostra os resultados obtidos através de Microscopia eletrônica de transmissão (MET) para os magnetossomos livres (A) e seus conjugados: BM-AmB (B), BM-GA-AmB (C), BM-PLL-GA-AmB (D) e BM-PLL-AmB (E) e os resultados de testes de análise de variância por ANOVA (F).

[00017] A Figura 4 mostra os resultados obtidos para os testes de potencial zeta para os magnetossomos livres e com conjugados. Os símbolos representam cada medida individual do potencial em milivolts (mV).

[00018] A Figura 5 mostra os resultados obtidos para os espectros de Espectrometria no infravermelho com transformada de Fourier (FTIR) dos magnetossomos, Amb e conjugados.

[00019] A Figura 6 mostra o espectro de UV-Vis de preparações selecionadas (BM-PLL-AmB, BM-PLL-GA-AmB) indicando os três picos de absorção característicos da AmB.

[00020] A Figura 7 mostra a curva de magnetização de magnetossomos de *Mv. blakemorei* liofilizados.

[00021] A Figura 8 mostra a variação de temperatura em suspensões de BMs de *Mv. blakemorei* cepa MV-1^{T} em duas diferentes concentrações (1,2 e 4,8 mg.mL^{-1}) ao longo de 50 min.

[00022] A Figura 9 mostra o perfil de liberação cumulativa de AmB a partir de BM-PLL-GA-AmB e BM-PLL-AmB sob condições-padrão (37°C) e sob aplicação de um campo magnético alternado (AFM).

[00023] A Figura 10 mostra a estabilidade de nanopartículas funcionalizadas em termos de quantidade de AmB que permanece ligada a nanopartículas após 3 ciclos

consecutivos de congelamento-descongelamento.

[00024] A Figura 11 mostra a análise da atividade antimicrobiana de magnetossomos e magnetossomos funcionalizados em *L. amazonensis*. Promastigotas de *L. amazonensis* foram tratadas por 72 horas com diferentes concentrações de BMs, BMs-PLL, BMs-PLL-AmB e AmB, teste de ANOVA, **** $p \leq 0,0001$.

[00025] A Figura 12 mostra a avaliação da citotoxicidade em células (A) queratinócitos HaCaT, (B) fibroblastos hFB e (C) macrófagos J774.16 através do ensaio MTS, com células incubadas com BMs-PLL-AmB, em diversas concentrações por 24 horas, 48 horas e 72 horas. Teste de ANOVA. *$p < 0,05$; **$p < 0,01$; *** $p < 0,001$.

[00026] A Figura 13 mostra imagens em microscopia eletrônica de transmissão e percentual de PLL-FITC ligada à superfície de magnetossomos das cepas MV-1T e AMB-1.

DESCRIÇÃO DETALHADA DA INVENÇÃO

[00027] A presente invenção revela um processo síntese de um magnetossomo funcionalizado com fármaco por meio de um agente de ligação e o magnetossomo funcionalizado obtido a partir deste processo.

[00028] O processo síntese de um magnetossomo funcionalizado com fármaco compreende as seguintes etapas de:

a) preparação dos magnetossomos e fármaco;

b) funcionalizar os precursores das etapas a) com o agente de ligação; e

c) separação dos magnetossomos funcionalizados.

[00029] Os magnetossomos são extraídos de bactéria magnetotática. Preferencialmente, os magnetossomos são

extraídos de bactéria magnetotática selecionada do grupo compreendendo: a espécie *Magnetovibrio blakemorei* cepa MV-1^{T}, *Desulfovibrio magneticus* cepa RS-1, *Magnetospirillum magneticum* cepa AMB-1, *Magnetospirillum magneticum* strain MGT-1, *Magnetospirillum magneticum* cepa RSS-1, M*agnetospirillum gryphiswaldense* cepa MSR-1, *Magnetospirillum magnetotacticum* cepa MS-1, *Magnetospirillum* sp. cepa ME-1, *Magnetovibrio blakemorei* cepa MV-2, *Magnetospira thiophila* cepa MMS-1, *Magnetococcus marinus* cepa MC-1 e *Magnetofaba australis* cepa IT-1 e combinações entre as mesmas. Preferencialmente, os magnetossomos são prismáticos da espécie *Magnetovibrio blakemorei* cepa MV-1^{T}, pois esses magnetossomos são capazes de adsorver uma quantidade 1,6 vezes maior conforme evidenciado pelo exemplo comparativo 6 e figura 13.

[00030] Os fármacos alvos da presente invenção, são fármacos da classe dos polienos, sendo selecionado do grupo consistindo em nistatina, anfotericina B e filipina. Em uma modalidade preferida o fármaco utilizado é a anfotericina B (AmB).

[00031] O agente de ligação é um constituinte intermediário entre o magnetossomo e o fármaco, que está relacionado diretamente à velocidade de liberação do fármaco. O agente de ligação alvo para a presente invenção necessariamente deve ser um biopolímero catiônico, uma vez que ocasiona interações eletrostáticas fracas com a superfície negativas dos magnetossomos e com o grupamento –COOH da molécula do fármaco. Os agentes de ligação são selecionados do grupo consistindo em poli-L-lisina, poliarginina, polietilenimina, glutaraldeído, ou combinação

destes. Em uma modalidade preferida o agente de ligação é a poli-L-lisina (PLL), ou o glutaraldeído (GA), ou combinação destes.

[00032] A preparação dos magnetossomos, etapa a), se dá pela adição de 50 a 150 µl de tampão fosfato entre 0,05 a 0,2 M com pH 7,2 a 7,6 a 50 a 150 µg de magnetossomos. Sendo preferencialmente, 100 µl de tampão fosfato (0,1 M, pH 7,4) a 100 µg de magnetossomos.

[00033] Na etapa a), também, o fármaco é solubilizado em um solvente dimetilsulfóxido (DMSO) até concentração final de 80 a 200 $\mu g.mL^{-1}$, sendo preferencialmente 125 $\mu g.mL^{-1}$.

[00034] A ordem de preparação dos magnetossomos e do fármaco na etapa a) é independente, ou seja, a ordem de execução das preparações não altera os precursores obtidos da etapa a).

[00035] Sequencialmente, na etapa b), o agente de ligação é adicionado aos magnetossomos da etapa a) na proporção de 1:1, sendo que o agente de ligação está na concentração entre 0,02% a 25% v/v. O fármaco solubilizado da etapa a) é então adicionado à mistura do agente de ligação e magnetossomo. A mistura resultante é submetida a 4 a 6 ciclos de 5 a 15 minutos de sonicação a 50 a 120 W em banho de ultrassom, com intervalos de 5 a 30 minutos sob resfriamento com banho de gelo estando entre – 4 a 4°C. Em uma modalidade preferida a mistura resultante é submetida à 5 ciclos de 10 minutos de sonicação a 60 W em banho de ultrassom, com intervalos de 10 min sob resfriamento com banho de gelo entre – 4 a 4°C.

[00036] Alternativamente, na etapa b) quando utilizado o agente de ligação poli-L-lisina, este é adicionado aos magnetossomos da etapa a) na proporção de 1:1, sendo que o

agente de ligação está na concentração entre 0,0001 a 0,05% v/v; a mistura é submetida a 5 a 15 minutos de ultrassom de 50 a 120 W em banho de ultrassom, sendo o sobrenadante separado por ímã, fixado na parte externa do recipiente, e o produto resultante é lavado com 75 a 150 μL de água e suspensos com 100 μL de tampão fosfato 0,1 M e pH 7,4; sequencialmente, o fármaco precursor da etapa a) ou o fármaco precursor da etapa a) e outro agente de ligação na concentração entre 0,02% a 25% v/v, serem adicionados à mistura e submetidos a 4 a 6 ciclos de 5 a 15 minutos de sonicação a 50 a 120 W em banho de ultrassom, com intervalos de 5 a 30 minutos sob resfriamento com banho de gelo entre -4 a 4°C. Em uma modalidade preferida a mistura resultante é submetida à 5 ciclos de 10 minutos de sonicação a 60 W em banho de ultrassom, com intervalos de 10 min sob resfriamento com banho de gelo entre – 4 a 4°C.

[00037] A concentração de PLL, na etapa b), é de 0,0001 a 0,05%, preferencialmente 0,005% a 0,02% e GA nas concentrações finais de 0,2 a 25% v/v, preferencialmente 10 a 25% v/v.

[00038] As estruturas relacionadas com as modalidades preferidas da presente invenção se encontram na Figura 1. Sequencialmente na etapa c), a separação dos magnetossomos funcionalizados ocorre pela ação de um campo magnético externo onde é removido o sobrenadante. O campo magnético externo utilizado foi um imã, podendo ser de forma cilíndrica, de aresta, cúbica ou paralelepídica de quaisquer dimensões, sendo preferencialmente um ímã cilíndrico entre 0,5 a 5 cm de diâmetro, mais preferencialmente um ímã cilíndrico de 1 cm de espessura e 1,5 cm de diâmetro. O ímã

é fixado, de forma removível, na parte externa do recipiente onde se encontra a suspensão de magnetossomos, e em seguida o recipiente é reservado entre 15 minutos a 24 horas, preferencialmente 15 minutos, em temperatura de 2 a 8°C. Sequencialmente, o sobrenadante é retirado, e somente após isso, o ímã é removido da superfície do recipiente em questão.

[00039] Como resultado é obtido um magnetossomo funcionalizado com fármaco devido ao auxílio de um agente de ligação, em uma modalidade preferida é obtido um magnetossomo funcionalizado com anfotericina B e agente de ligação, podendo ser poli-L-lisina (PLL), ou glutaraldeído (GA), ou combinação destes (PLL-GA).

[00040] O tamanho dos magnetossomos funcionalizados isolados medidos em microscopia eletrônica de transmissão foram, em média, de 63,3 ± 3,9 nm (n = 120) em comprimento e 39,7 ± 3,5 nm em largura (Figura 3). A esses valores devem ser somadas as espessuras de membrana: 5,2 ± 0,9 nm para os magnetossomos puros, 8,9 ± 1,1 nm para a preparação obtida apenas com glurataldeído, 12,0 ± 1,2 nm para a preparação obtida apenas com poli-L-lisina e 13,5 ± 1,3 para a preparação obtida com ambos os agentes (Figura 3).

[00041] A preparação feita apenas com poli-L-lisina teve estabilidade média de 65,6 ± 2,9% em pH 7,4 após 5 dias em agitação de 60 rpm a 37° C. Nas mesmas condições, a preparação feita apenas com glutaraldeído teve estabilidade média de 75,8 ± 6,7%, enquanto aquela feita com os dois agentes apresentou estabilidade de 80,9 ± 0,5%.

[00042] Quando a suspensão contendo os nanoconjugados foi submetida ao campo magnético alternado, a liberação do

fármaco durante 60 minutos aumentou aproximadamente quatro vezes, atingindo 41,3 ± 0,5% para a preparação feita com poli-L-lisina e glutaraldeído e 53,8 ± 6,2% para a preparação feita apenas com a poli-L-lisina (Figura 9).

[00043] Valores de potencial zeta entre -35 e -25 mV foram observados para todos os métodos de funcionalização testados, com exceção daquele em que apenas a PLL foi empregada como único reagente de ligação, cujo potencial foi de 15,1 ± 3,8 mV (Figura 4).

[00044] O magnetossomo funcionalizado conforme a presente invenção pode ser aplicado na preparação de medicamentos para o tratamento de doenças causadas por microrganismos, que abrange tratamentos com fármacos antimicrobianos, como os da classe dos polienos. O magnetossomo funcionalizado obtido conforme a presente invenção pode ser uma alternativa em tratamentos que utilizam a formulação lipossomal da anfotericina de forma a atenuar os seus efeitos colaterais e a melhorar a biocompatibilidade e a dispersibilidade do fármaco em condições fisiológicas devido à presença da membrana. A anfotericina B lipossomal pode, por exemplo, ser substituída pelo nanoconjugado magnético ora revelado em uma segunda linha de tratamento farmacológico contra leishmanioses viscerais e cutâneas e em combinações antifúngicas contra meningite criptocócica em pacientes HIV-positivos. Nestes exemplos, o nanoconjugado pode ser aplicado no desenvolvimento de terapias combinadas, por exemplo, com hipertermia por aplicação de campo magnético alternado para liberação controlada do fármaco.

Exemplos

[00045] Para fins de comparação, foram utilizados

magnetossomos funcionalizados com AmB e PLL, magnetossomos funcionalizados com AmB e GA, magnetossomos funcionalizados com AmB, PLL e GA e magnetossomos funcionalizados diretamente com AmB.

[00046] Os nanoconjugados foram congelados durante a noite a -20 °C e então submetidos ao processo de liofilização durante 2 horas. O processo de liofilização inicia-se no processamento dos nanoconjugados, ou seja, na etapa de congelamento. Os microtubos contendo os nanoconjugados congelados são inseridos com a tampa aberta no liofilizador, para a secagem das amostras através da remoção da água por sublimação. Após a liofilização, a esterilização dos nanoconjugados é realizada através da irradiação por cobalto-60 (60Co) (15 kGy) e então são armazenados a -20 °C.

[00047] Após a liofilização e esterilização, os nanoconjugados seguiram para as avaliações que serão descritas a seguir.

Exemplo comparativo 1 - Avaliação da eficácia de funcionalização

[00048] Amostras liofilizadas de aproximadamente 100 µg foram tratadas com metanol e analisadas por absorbância a 410 nm em espectrofotômetro equipado com ultravioleta.

[00049] A maior eficiência de ligação pelo processo descrito se apresentou pelo emprego da PLL, sendo a eficiência de 52,7 ± 5,1%, conforme mostra a Figura 2A. O carregamento de fármaco também foi calculado a partir da razão quantidade de fármaco capturado e a massa de magnetita adicionada à reação de funcionalização. Nesse mesmo nanoconjugado, o carregamento de AmB foi de 25,3 ± 1,9 µg por 100 µg de magnetossomos, conforme Figura 2B.

Exemplo comparativo 2 - Caracterização dos magnetossomos

Métodos utilizados

1. Microscopia eletrônica de transmissão (MET) e medidas dos magnetossomos

[00050] Magnetossomos virgens e funcionalizados foram adicionados sobre grades de cobre revestidas com filme-suporte de polivinilformal e carbono, sendo secas ao ar para observação em microscópio eletrônico de transmissão (FEI Morgagni, Hilsboro, EUA) operando a 80 kV em um aumento direto de 36.000 e 89.000 vezes para cada caso, respectivamente. Avaliações da espessura da membrana que envolve os magnetossomos antes e após funcionalização foram realizadas utilizando o programa iTEM. Os gráficos e as análises estatísticas dos dados foram realizados com o auxílio do programa Prism 5.0 (GraphPad Software, San Diego, EUA).

2. Espectrometria no infravermelho com transformada de Fourier (FTIR)

[00051] Amostras liofilizadas de aproximadamente 1 mg foram colocadas em contato direto com o cristal de diamante de reflexão total atenuada de um Espectrômetro IRPrestige-21 (Shimadzu, Kyoto, Japão). As preparações foram analisadas na faixa de número de onda de 3000 a 500 cm^{-1} e foram realizadas 80 varreduras com uma resolução de 1 cm^{-1}.

3. Espectrometria no ultravioleta-visível (UV-Vis)

[00052] As preparações que apresentaram os maiores carregamentos de fármacos foram analisadas de acordo com o Teste de Identidade constante na Farmacopeia Internacional (OMS, 2018) adaptado para as nanopartículas magnéticas funcionalizadas. De forma resumida, amostras liofilizadas de

aproximadamente 100 µg foram tratadas com metanol para a extração da membrana e moléculas ligadas. As preparações foram analisadas em espectrofotômetro UV-1800 (Shimadzu, Kyoto, Japão) na faixa de comprimento de onda de 300 a 450 nm. Um controle com AmB livre foi realizado de acordo com o método farmacopeico sem adaptações (OMS, 2018).

4. Potencial zeta

[00053] O potencial zeta das nanopartículas ressuspensas em água ultrapura (30 µg.mL^{-1}) foi medido em um analisador Zeta (ZetaPlus, Brookhaven Instruments Corp., Holtsville, EUA). Foram realizadas 10 medições em cada amostra e os valores individuais foram utilizados para calcular a média e o desvio padrão.

5. Medida de magnetização

[00054] A propriedade de magnetização dos magnetossomos foi investigada em temperatura ambiente utilizando um magnetômetro de vibração SQUID (MPMS3, Quantum Design, San Diego, EUA). Uma amostra de 13,9 mg de magnetossomos liofilizados foram transferidas para uma cápsula de gelatina para a inserção no porta-amostras do magnetômetro. As medidas foram executadas a 300 K.

6. Hipertermia magnética

[00055] Foi investigada a capacidade de aquecimento dos magnetossomos em resposta à aplicação de um campo magnético alternado. A análise foi realizada em um sistema de aquecimento por indução magnética (DM2-s53, Nanoscale Biomagnetics, Zaragoza, Espanha) equipado com uma sonda de temperatura de fibra óptica e isolamento térmico a vácuo. As suspensões de magnetossomos em tampão fosfato salino (PBS) com pH 7,4 foram transferidas para um vial de vidro (1 mL)

em concentrações de 0,5, 1 e 5 $mg.mL^{-1}$. Primeiramente, deixou-se o sistema atingir o equilíbrio térmico (aproximadamente 25 °C) e, em seguida, o campo magnético alternado foi aplicado a uma frequência de 307 kHz e intensidade de campo magnético de 200 Oe por 60 min.

Resultados

[00056] A observação das nanopartículas funcionalizadas por MET evidenciou o aumento na espessura da membrana quando as nanopartículas eram submetidas aos diferentes processos de funcionalização (Figura 3). A maior espessura média de membrana (13,5 ± 1,3 nm) foi observada quando as nanopartículas foram funcionalizadas com ambos os agentes de ligação (BM-PLL-GA-AmB; Figura 3D e 3E). As medidas foram submetidas ao teste ANOVA apresentando diferença estatística relevante ($p < 0,0001$; Figura 3E).

[00057] A medida do potencial zeta foi realizada para avaliar as propriedades dispersivas das nanopartículas funcionalizadas. Valores entre -35 e -25 mV foram observados para todos os métodos de funcionalização testados, com exceção daquele em que apenas a PLL foi empregada como único reagente de ligação, cujo potencial foi de 15,1 ± 3,8 mV (Figura 4).

[00058] A ligação covalente da AmB aos magnetossomos nas preparações que utilizaram GA foi verificada através da análise por FTIR. Os picos que foram analisados para se inferir a estrutura dos conjugados encontram-se sinalizados nos espectros, nota-se a ausência desses picos na amostra contendo apenas BMs (Figura 5). A adsorção e a estabilidade da AmB incorporada às nanopartículas foram investigadas através da análise por UV-Vis. Nas três preparações podem

ser observados os picos de absorção, em ordem crescente de intensidade, em 364, 382 e 406 nm, no inserto, nota-se a histerese exibida pelas nanopartículas (Figura 6). As intensidades relativas entre os picos de absorção são mantidas entre as nanopartículas funcionalizadas.

[00059] Medidas de magnetização foram realizadas em magnetossomos não-funcionalizados e revelaram valores de magnetização de saturação e coercividade de 52 emu.g-1 e 115 Oe, respectivamente (Figura 7).

[00060] A capacidade de aquecimento de suspensões contendo magnetossomos nas concentrações de 1,2 e 4,8 mg.mL-1 foi examinada sob um campo magnético alternado nas condições descritas anteriormente. O aumento da temperatura em resposta à aplicação de um campo magnético alternado foi o mais alto (6,3 °C) na suspensão contendo a maior quantidade de magnetita (Figura 8). Quando a concentração de magnetita foi de 1,2 $mg.mL^{-1}$, o aumento da temperatura também foi menor (1,4 °C).

Exemplo comparativo 3 - Estabilidade e liberação

Métodos utilizados

1. Perfil de liberação do fármaco

[00061] Três tipos de conjugados foram testados quanto ao perfil liberado da AmB segundo o método de Legrand e colaboradores (1997). Basicamente, os complexos BMs-AmB obtidos com tratamento com GA, PLL, GA com PLL e os obtidos sem quaisquer reagentes de ligação foram dispersos em PBS e incubados a 37 °C sob agitação a 60 RPM. Em intervalos de 12 h, os magnetossomos foram concentrados magneticamente e uma amostra de sobrenadante foi coletada para determinação da AmB em espectrofotômetro a 410 nm. Depois disso os

magnetossomos foram redistribuídos e foi restaurado o volume de PBS. Para avaliar a liberação de AmB das nanopartículas submetidas ao campo magnético, o mesmo procedimento foi realizado por 1 h com as duas preparações de maior carregamento nas condições de hipertermia descritas no item anterior, excetuando-se a incubação e a agitação.

2. Estabilidade durante congelamento-descongelamento

[00062] Uma alíquota de 100 µg das duas preparações de maior carregamento foram dispersas em PBS e armazenadas a -20 °C por 16 h. Ao final deste tempo, as suspensões foram descongeladas em temperatura ambiente e, sob concentração magnética dos magnetossomos, uma amostra de sobrenadante foi coletada para determinação da AmB em espectrofotômetro a 410 nm. Depois disso, o volume de PBS foi restaurado e as alíquotas foram submetidas a outros 3 ciclos de congelamento-descongelamento.

Resultados

[00063] A liberação de AmB na condição padrão (37 °C) dentro de 1 h foi de 11,1 ± 0,4% para o BM-PLL-GA-AmB e de 15,0 ± 1,2% para o BM-PLL-AmB (Figura 9). Quando a suspensão contendo os nanoconjugados foi submetida ao campo magnético alternado (AMF), a liberação do fármaco no mesmo intervalo de tempo aumentou aproximadamente quatro vezes, atingindo 41,3 ± 0,5% para o BM-PLL-GA-AmB e 53,8 ± 6,2% para o BM-PLL-AmB (Figura 9).

[00064] O estudo de liberação frente ao congelamento-descongelamento revelou que após 4 ciclos desse tratamento a nanopartícula funcionalizada retém 43,8 ± 10,6% do carregamento inicial de AmB para BM-PLL-AmB e 45,7 ± 3,2% para o BM-PLL-GA-AmB (Figura 10).

Exemplo comparativo 4 - atividade antimicrobiana

[00065] A atividade antimicrobiana do nanoconjugado de magnetossomos funcionalizados com anfotericina B (AmB) utilizando poli-L-lisina (PLL) como agente de ligação foi testada contra o protozoário *Leishmania amazonensis* MHOM/BR/PH8.

[00066] O experimento realizado consistiu em incubar promastigotas de *L. amazonensis* com diferentes concentrações do nanoconjugado por 72h na presença das nanopartículas. As formas promastigotas de *L. amazonensis* foram obtidas após repiques semanais em meio Schneider suplementado com 10% de soro fetal bovino inativado por calor, em estufa a 28 °C. Após 3 dias de cultivo, as células foram coletadas e contadas em câmara de Neubauer. Uma suspensão de células foi preparada e foram depositados 10^5 células em cada poço de uma placa de 96 poços. Em seguida, foram adicionados os tratamentos dos nanoconjugados de magnetossomos com PLL e AmB nas concentrações de 0,40 µg/mL a 25 µg/mL, totalizando um volume de 100 µL em cada poço da placa.

[00067] Ao todo, foram feitos 4 experimentos para estudo da atividade antimicrobiana do nanoconjugado e em cada um dos experimentos, cada concentração do tratamento foi repetida 6 vezes. Em cada um dos experimentos, células sem adição de nenhum tipo de tratamento de *L. amazonensis* foram utilizadas como controle para efeitos de comparação.

[00068] As placas contendo células tratadas com o nanoconjugado foram incubadas durante 72 horas em estufa a 28 °C. Após o período de incubação com o tratamento, o reagente MTT (brometo de 3-(4,5-dimetil-2-tiazolil)-2, 5-difenil-2H-tetrazólio) foi utilizado para analisar a

suscetibilidade do protozoário ao nanoconjugado. Foi adicionado em cada poço da placa 10 µL de MTT e a placa foi incubada por 4 horas, a 28 °C e sem contato com luz. Depois da incubação, 100 µL de DMSO foi adicionado em cada poço. Por fim, a placa foi lida no comprimento de onda de 570 nm em leitor de placas.

[00069] Foi observado atividade antimicrobiana a partir da concentração de 12,5 µg/mL de BMs funcionalizados, onde é observado uma queda de mais de 50% na viabilidade celular do protozoário *L. amazonensis*, demonstrando assim que o nanoconjugado é efetivo contra o protozoário *in vitro* (Figura 11A).

[00070] Quando comparadas a AmB, a eficiência da AmB funcionalizada diretamente nos magnetossomos foi reduzida. Em 25 µg de BMs-PLL-AmB há 6,25 µg de AmB encapsulada, enquanto concentrações muito menores de AmB (0,20, 0,40, 0,80 e 1,56 µg/ml) apresentaram atividade contra o protozoário (Figura 11B). Dessa forma, o composto não apresentou redução da concentração da AmB que possui atividade contra a *L. amazonensis*.

Exemplo comparativo 5 - citotoxicidade do nanoconjugado

[00071] O estudo da citotoxicidade do nanoconjugado a base de BMs funcionalizados com anfotericina B (AmB) utilizando poli-L-lisina (PLL) como agente de ligação (BMs-PLL-AmB) foi feito em três linhagens celulares de mamíferos. As linhagens utilizadas foram macrófagos (J774.16), fibroblastos (hFB) e queratinócitos (HaCaT).

[00072] Para realização dos testes, as três linhagens celulares foram cultivadas em meio DMEM (*Dulbecco's modified Eagle's medium*) *High Glucose* (pH 7,2) enriquecido com 10% de

soro fetal bovino (SFB) inativado por calor e 1% do antimicrobiano PenStrep (Penicilina-Estreptomicina 10.000 U/mL) e incubadas em estufa a 37 °C com atmosfera de 5% de CO_2.

[00073] As células foram cultivadas em frascos de cultura de 7,5 cm^2 e para a remoção das células aderidas ao frasco foi utilizado uma solução de tripsina-EDTA (0,05% de 1:250 de tripsina e 0,02% de EDTA; pH 7,2). Um volume de 5 mL de solução de tripsina-EDTA foi adicionado no frasco da cultura, as células foram incubadas por 5 minutos a 37 °C e observadas ao microscópio até a monocamada soltar do frasco. Então, 5 mL de meio acrescido de 10% de SFB foram adicionados, as células foram coletadas e centrifugadas a 200 g por 3-5 minutos. As células foram ressuspendidas em meio DMEM High glucose, contadas em câmara de Neubauer e depositadas em placas de 96 poços nas concentrações como se segue:

- Queratinócitos (HaCaT): 1,25 x 10^5 células/mL
- Fibroblastos (hFB): 3,75 x 10^5 células/mL
- Macrófagos (J774.16): 10^6 células/mL

[00074] Foi utilizado um volume total de 100 µL por poço. Após plaqueadas, as células foram incubadas por 24 horas a 37 °C em atmosfera com 5% de CO_2. Então, o meio das células foi removido, as células foram lavadas com PBS 1x (pH 7,2). O nanoconjugado BMs-PLL-AmB ressuspendido em meio de cultura foi adicionado, nas concentrações de 0,40 µg/mL a 25 µg/mL. As células foram incubadas nas mesmas condições descritas anteriormente, por períodos de 24, 48 e 72 horas. Todos os experimentos foram feitos em triplicata e repetidos 3 vezes. Como controle de células viáveis, foram utilizadas células sem nenhum tipo de tratamento em seu meio de cultura.

[00075] Após o período de incubação, foi adicionado 10 µL do reagente MTS (3-(4,5-dimetiltiazol-2-il)-5-(3-carboximetóxifenil)-2-(4-sulfofenil)-H tetrazólio) em cada poço da placa. A placa foi incubada ao abrigo da luz por 3 horas, nas mesmas condições. A leitura de absorbância foi realizada a 490 nm em leitor de placas.

[00076] Os resultados obtidos, conforme Figura 12, demonstraram que em todas as concentrações de BMs-PLL-AmB e tempos testados, a viabilidade celular se manteve acima de 80% para os três tipos celulares. Com exceção das células J774.16 tratadas por 72 horas, onde a viabilidade celular foi reduzida, se mantendo acima de 60%. Os resultados obtidos demonstram que o nanoconjugado BMs-PLL-AmB não apresenta alta citotoxicidade para células mamíferas, em específico as aqui testadas, como macrófagos (J774.16), queratinócitos (HaCaT) e fibroblastos (hFB).

Exemplo comparativo 6 – capacidade de carreamento do fármaco

[00077] A maior capacidade de ligação a moléculas funcionais por magnetossomos prismáticos de *Mv. blakemorei* cepa MV-1T em comparação aos magnetossomos cuboctaédricos de *Magnetospirillum magneticum* cepa AMB-1 foi comprovada através do experimento descrito a seguir.

[00078] O experimento consistiu na incubação de 100 µg de magnetossomos de ambas as cepas com uma 1 mL de uma solução de poli-L-lisina ligada ao marcador fluorescente isotiocianato de fluoresceína (PLL-FITC). A solução de PLL-FITC possuía uma concentração de 200 µg/L em tampão fosfato 0,1 M (pH 7,4). A incubação foi feira em um banho de ultrassom (Branson 2200) a 60 W durante 3 ciclos de 5 min. Em seguida, os magnetossomos foram concentrados por meio de um imã de

neodímio colocado externamente ao tubo. Em seguida, o sobrenadante foi removido e armazenado para leitura fluorimétrica. Foram feitas duas lavagens consecutivas com água ultrapura e os sobrenadantes foram guardados para leitura fluorimétrica.

[00079] A quantificação de PLL-FITC ligado aos magnetossomos foi feita através da leitura da intensidade de fluorescência dos sobrenadantes em um fluorímetro. Foram utilizados os comprimentos de onda de 488 nm para excitação e 525 nm para emissão. Foi realizada a leitura de um controle de PLL-FITC na concentração 200 µg/L. A proporção de PLL-FITC ligada aos magnetossomos foi calculada pela diferença entre a leitura do controle e a leitura dos sobrenadantes dividida pela leitura do controle.

[00080] Os magnetossomos de *Mv. blakemorei* cepa MV-1^{T} apresentaram maior eficiência de ligação à PLL-FITC, com uma média de 65,05 ± 2,77% (n=7) (Figura 13). Os magnetossomos de *Ms. magneticum* cepa AMB-1 apresentaram uma média de 39,55 ± 7,6% (n=7) de eficiência.

[00081] A presente invenção foi revelada neste relatório descritivo em termos de sua modalidade preferida. Entretanto, outras modificações e variações são possíveis a partir da presente descrição, estando ainda inseridas no escopo da invenção aqui revelada.

REIVINDICAÇÕES

1. Processo de síntese de magnetossomo funcionalizado com fármaco **CARACTERIZADO** por compreender as etapas de:

a) preparar os magnetossomos e o fármaco;

b) funcionalizar os precursores da etapa a) com o agente de ligação; e

c) separar os magnetossomos funcionalizados.

2. Processo, de acordo com a reivindicação 1, **CARACTERIZADO** pelo fato de os magnetossomos serem extraídos de *Magnetovibrio blakemorei* cepa MV-1^{T}, *Desulfovibrio magneticus* cepa RS-1, *Magnetospirillum magneticum* cepa AMB-1, *Magnetospirillum magneticum* strain MGT-1, *Magnetospirillum magneticum* cepa RSS-1, M*agnetospirillum gryphiswaldense* cepa MSR-1, *Magnetospirillum magnetotacticum* cepa MS-1, *Magnetospirillum* sp. cepa ME-1, *Magnetovibrio blakemorei* cepa MV-2, *Magnetospira thiophila* cepa MMS-1, *Magnetococcus marinus* cepa MC-1 e *Magnetofaba australis* cepa IT-1.

3. Processo, de acordo com a reivindicação 1, **CARACTERIZADO** pelo fato de magnetossomos serem preferencialmente prismáticos da espécie *Magnetovibrio blakemorei* cepa MV-1^{T}.

4. Processo, de acordo com a reivindicação 1, **CARACTERIZADO** pelo fato de o fármaco ser da classe dos polienos, sendo selecionado do grupo consistindo em anfotericina B, nistatina e filipina.

5. Processo, de acordo com a reivindicação 1, **CARACTERIZADO** pelo fato de o fármaco ser preferencialmente anfotericina B.

6. Processo, de acordo com a reivindicação 1,

CARACTERIZADO pelo fato de o agente de ligação ser um biopolímero catiônico selecionado do grupo consistindo em poli-L-lisina, poliarginina, polietilnimina e glutaraldeído, ou combinação destes.

7. Processo, de acordo com a reivindicação 1, **CARACTERIZADO** pelo fato de o agente de ligação ser preferencialmente poli-L-lisina, ou o glutaraldeído, ou combinação destes.

8. Processo, de acordo com qualquer uma das reivindicações de 1 a 7, **CARACTERIZADO** pelo fato de, na etapa a), a preparação dos magnetossomos ocorrer pela adição de 50 a 150 µl de tampão fosfato entre 0,05 a 0,2 M com pH 7,2 a 7,6 a 50 a 150 µg de magnetossomos;

em que a preparação do fármaco ocorrer pela solubilização em solvente DMSO até concentração final de 80 a 200 $\mu g.mL^{-1}$.

9. Processo, de acordo com qualquer uma das reivindicações de 1 a 8, **CARACTERIZADO** pelo fato de, na etapa a), a ordem de preparação dos magnetossomos e fármaco ser independente.

10. Processo, de acordo com qualquer uma das reivindicações de 1 a 9, **CARACTERIZADO** pelo fato de, na etapa a), a preparação dos magnetossomos, preferencialmente, ocorrer com a adição de 100 µl de tampão fosfato 0,1 M e pH 7,4 a 100 µg de magnetossomos.

11. Processo, de acordo com a reivindicação 1, **CARACTERIZADO** pelo fato de, a preparação do fármaco, preferencialmente, na etapa a), ocorrer pela solubilização em solvente DMSO até concentração final de 125 $\mu g.mL^{-1}$.

12. Processo, de acordo com qualquer uma das reivindicações de 1 a 11, **CARACTERIZADO** pelo fato de, na etapa b), o agente de ligação ser adicionado aos

magnetossomos da etapa a) na proporção de 1:1, sendo que o agente de ligação está na concentração entre 0,02% a 25% v/v, e sequencialmente, o fármaco precursor da etapa a) ser adicionado à mistura; e

a mistura resultante ser submetida a 4 a 6 ciclos de 5 a 15 minutos de sonicação de 50 a 120 W em banho de ultrassom, com intervalos de 5 a 30 minutos sob resfriamento com banho de gelo entre -4 a 4°C.

13. Processo, de acordo com qualquer uma das reivindicações de 1 a 11, **CARACTERIZADO** pelo fato de, na etapa b), o agente de ligação poli-L-lisina ser adicionado aos magnetossomos da etapa a) na proporção de 1:1, sendo que o agente de ligação está na concentração entre 0,0001 a 0,05 % v/v;

a mistura ser submetida a 5 a 15 minutos de ultrassom de 50 a 120 W em banho de ultrassom, sendo o sobrenadante separado por ímã, fixado na parte externa do recipiente, e o produto resultante é lavado com 75 a 150 μL de água e suspensos com 100 μL de tampão fosfato 0,1 M e pH 7,4;

o fármaco precursor da etapa a) ou o fármaco precursor da etapa a) e outro agente de ligação na concentração entre 0,02 % a 25% v/v, serem adicionados à mistura, sendo a mistura resultante submetida a 4 a 6 ciclos de 5 a 15 minutos de sonicação de 50 a 120 W em banho de ultrassom, com intervalos de 5 a 30 minutos sob resfriamento com banho de gelo entre -4 a 4°C.

14. Processo, de acordo com a reivindicação 12 ou 13, **CARACTERIZADO** pelo fato de preferencialmente a mistura resultante ser submetida à 5 ciclos de 10 minutos de sonicação a 60 W em banho de ultrassom, com intervalos de 10

minutos sob resfriamento com banho de gelo entre – 4 a 4°C.

15. Processo, de acordo com a reivindicação 13, **CARACTERIZADO** pelo fato de poli-L-lisina estar preferencialmente na concentração de 0,01%.

16. Processo, de acordo com a reivindicação 12 ou 13, **CARACTERIZADO** pelo fato de glutaraldeído estar na concentração final de 0,2 a 12,5% v/v.

17. Processo, de acordo com a reivindicação 12 ou 13, **CARACTERIZADO** pelo fato de glutaraldeído estar preferencialmente na concentração final de 12,5% v/v.

18. Processo, de acordo com qualquer uma das reivindicações de 1 a 17, **CARACTERIZADO** pelo fato de que na etapa c) um ímã é fixado, de forma removível, na parte externa do recipiente da suspensão de magnetossomos, e em seguida o recipiente é reservado entre 15 minutos a 24 horas, preferencialmente por 15 minutos, em temperatura de 2 a 8°C, sequencialmente, ocorre a retirada do sobrenadante e o ímã é removido da superfície do recipiente.

19. Magnetossomo funcionalizado com fármaco obtido pelo processo, conforme definido em qualquer uma das reivindicações de 1 a 18, **CARACTERIZADO** por ser um magnetossomo funcionalizado com anfotericina B e poli-L-lisina, ou glutaraldeído, ou combinação destes.

20. Magnetossomo funcionalizado com fármaco, de acordo com a reivindicação 19, **CARACTERIZADO** por possuir o tamanho médio de 63,3 ± 3,9 nm em comprimento e 39,7 ± 3,5 nm em largura, e adicionalmente as espessuras de membrana: 8,9 ± 1,1 nm para a preparação com GA; 12,0 ± 1,2 nm para a preparação obtida com PLL; e 13,5 ± 1,3 para a preparação obtida com PLL-GA.

21. Magnetossomo funcionalizado com fármaco, de acordo com a reivindicação 19, **CARACTERIZADO** por a preparação com PLL possuir estabilidade média de 65,6 ± 2,9% em pH 7,4 após 5 dias em agitação de 60 rpm a 37°C.

22. Magnetossomo funcionalizado com fármaco, de acordo com a reivindicação 19, **CARACTERIZADO** por a preparação com GA possuir estabilidade média de 75,8 ± 6,7% em pH 7,4 após 5 dias em agitação de 60 rpm a 37°C.

23. Magnetossomo funcionalizado com fármaco, de acordo com a reivindicação 19, **CARACTERIZADO** por a preparação com GA-PLL possuir estabilidade média de 80,9 ± 0,5% em pH 7,4 após 5 dias em agitação de 60 rpm a 37°C.

24. Magnetossomo funcionalizado com fármaco, de acordo com a reivindicação 19, **CARACTERIZADO** por a liberação do fármaco durante 60 minutos ser de 41,3 ± 0,5% para a preparação feita com PLL-GA e 53,8 ± 6,2% para a preparação feita com PLL na presença de um campo magnético alternado.

25. Magnetossomo funcionalizado com fármaco, de acordo com a reivindicação 19, **CARACTERIZADO** por o potencial zeta ser entre -35 e -15 mV.

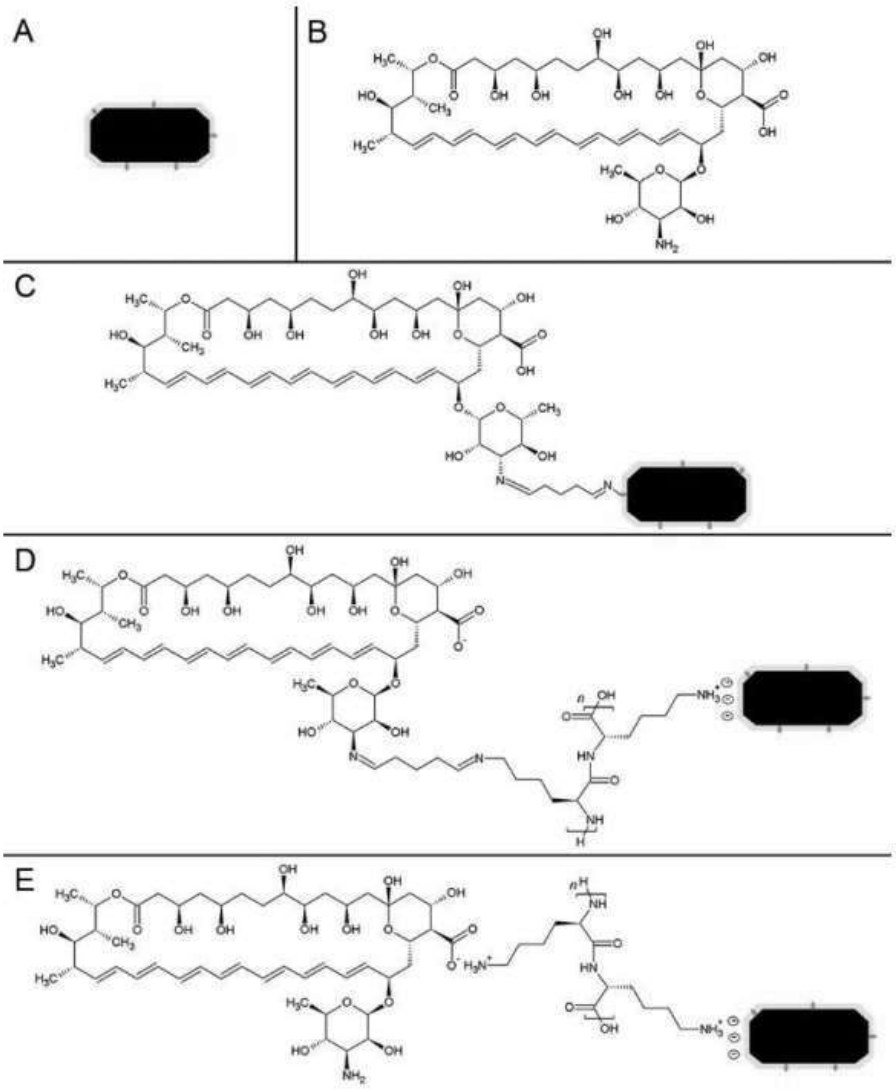

FIGURA 1

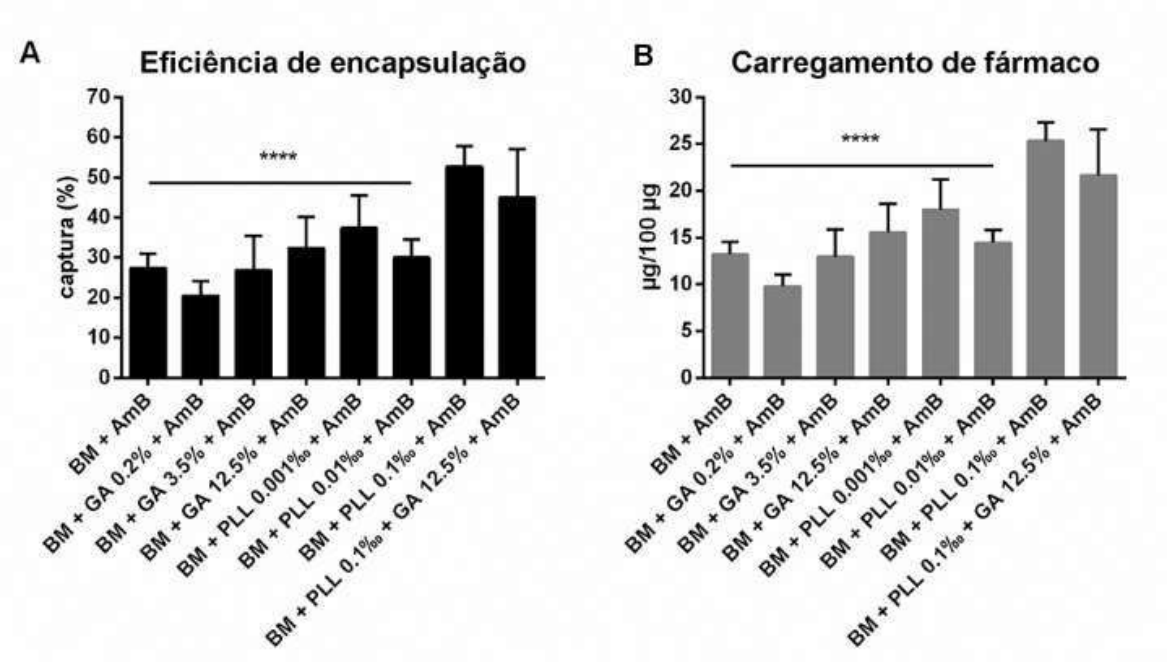
A
Eficiência de encapsulação
captura (%)
****
BM + AmB
BM + GA 0.2% + AmB
BM + GA 3.5% + AmB
BM + GA 12.5% + AmB
BM + PLL 0.001‰ + AmB
BM + PLL 0.01‰ + AmB
BM + PLL 0.1‰ + AmB
BM + PLL 0.1‰ + GA 12.5% + AmB
B
Carregamento de fármaco
µg/100 µg
****
BM + AmB
BM + GA 0.2% + AmB
BM + GA 3.5% + AmB
BM + GA 12.5% + AmB
BM + PLL 0.001‰ + AmB
BM + PLL 0.01‰ + AmB
BM + PLL 0.1‰ + AmB
BM + PLL 0.1‰ + GA 12.5% + AmB

FIGURA 2

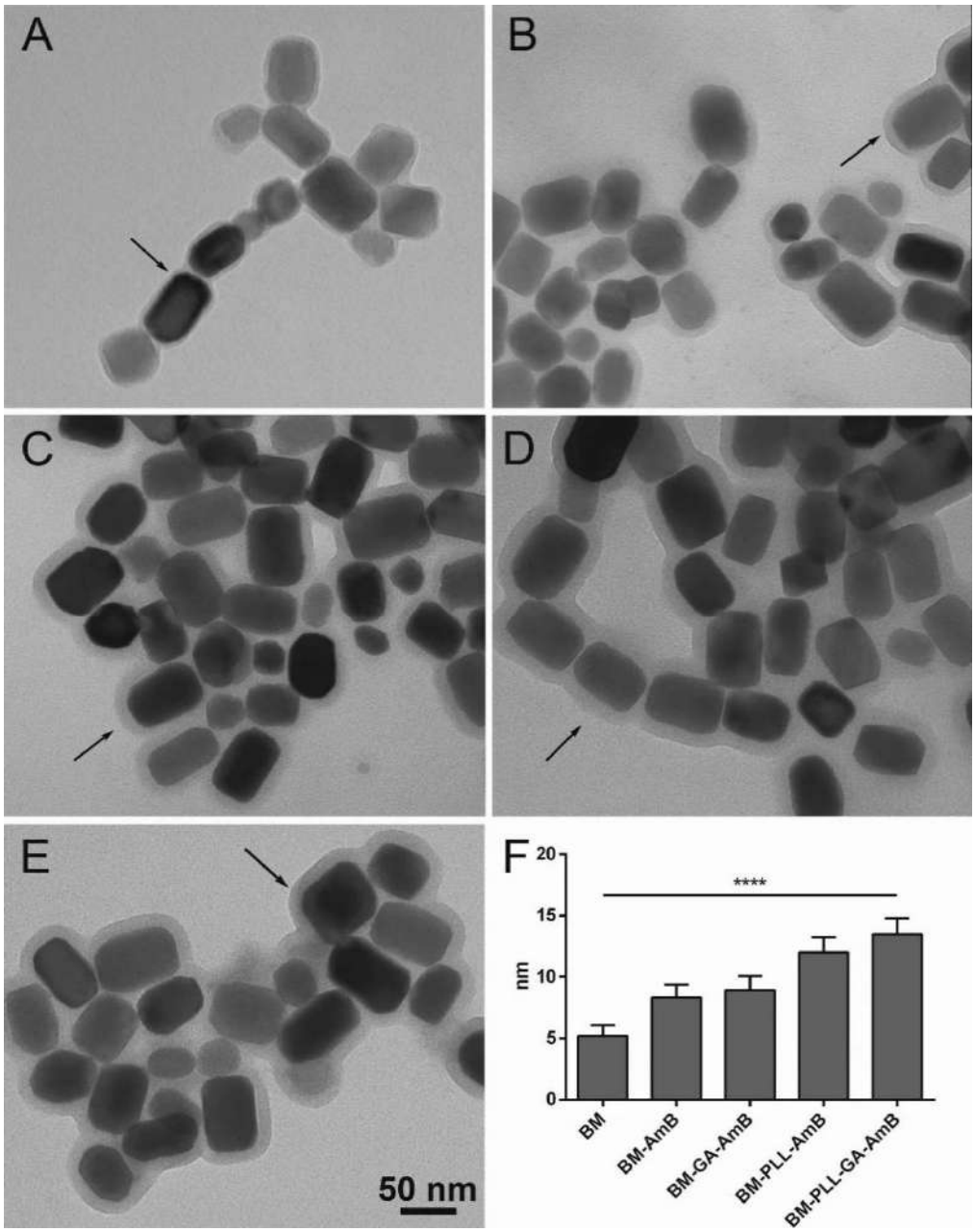
A
B
C
D
E
50 nm
F
****
nm
20
15
10
5
0
BM
BM-AmB
BM-GA-AmB
BM-PLL-AmB
BM-PLL-GA-AmB

FIGURA 3

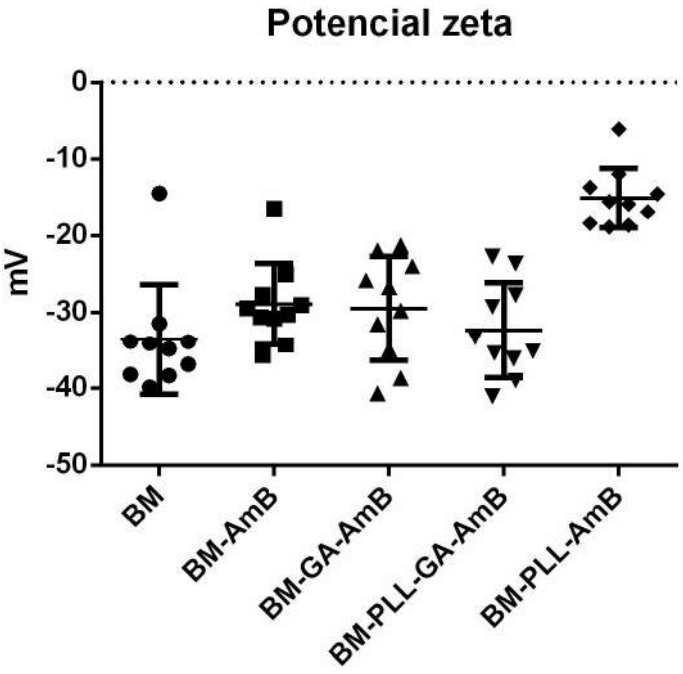

Legenda:

BM (●), BM-AmB (■), BM-GA-AmB (▲), BM-PLL-GA-AmB (▼) e BM-PLL-AmB (♦).

FIGURA 4

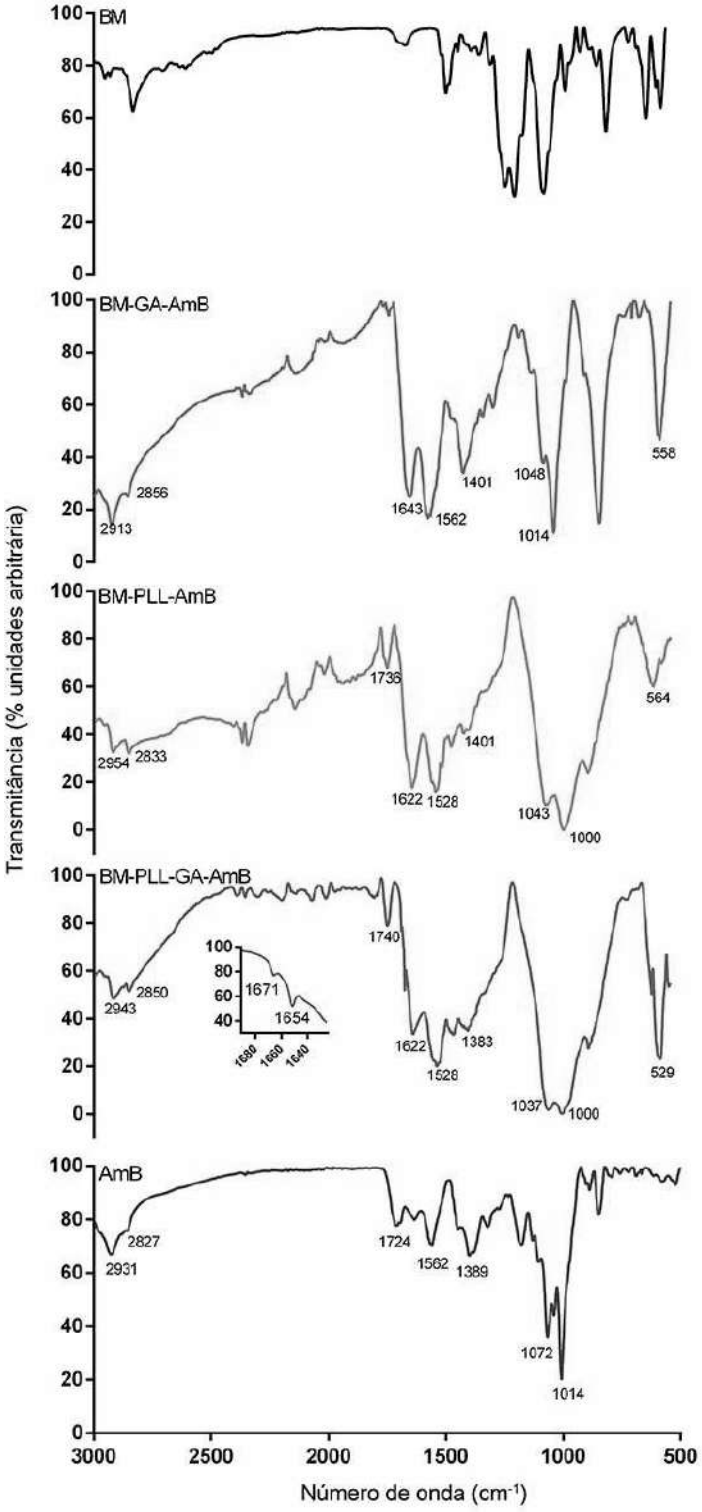
BM
BM-GA-AmB
2913
2856
1643
1562
1401
1048
1014
558
BM-PLL-AmB
2954
2833
1736
1622
1528
1401
1043
1000
564
BM-PLL-GA-AmB
2943
2850
1740
1671
1654
1622
1528
1383
1037
1000
529
AmB
2931
2827
1724
1562
1389
1072
1014
Transmitância (% unidades arbitrária)
Número de onda (cm-1)

FIGURA 5

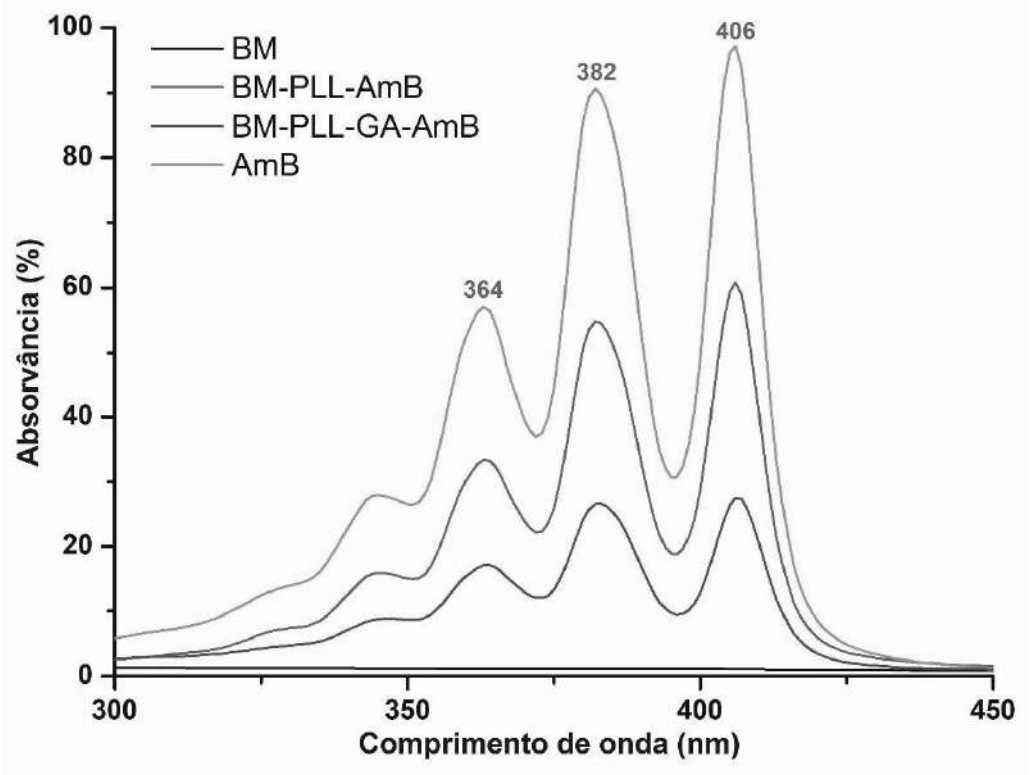

FIGURA 6

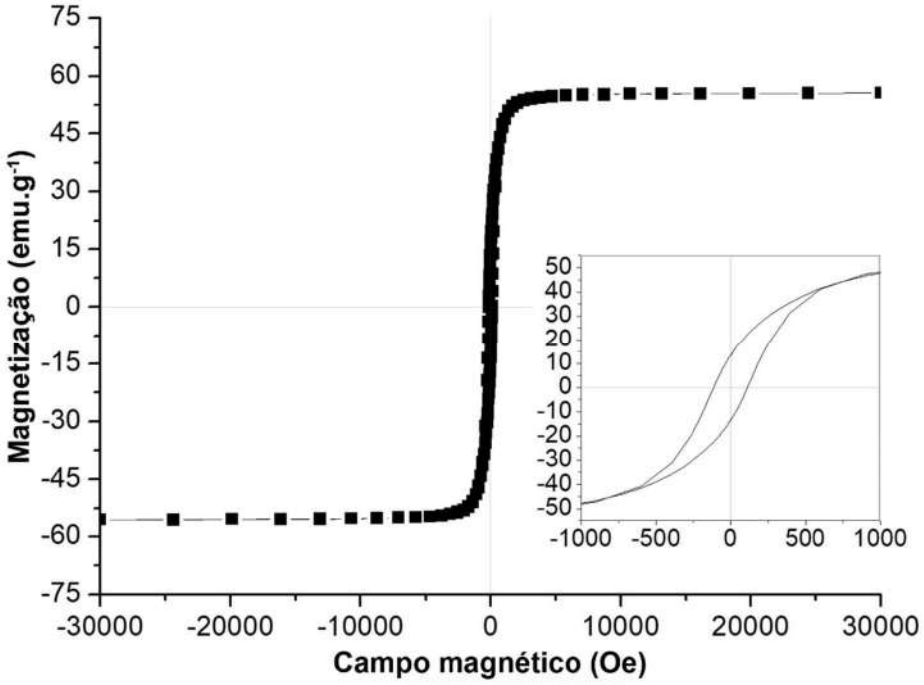

FIGURA 7

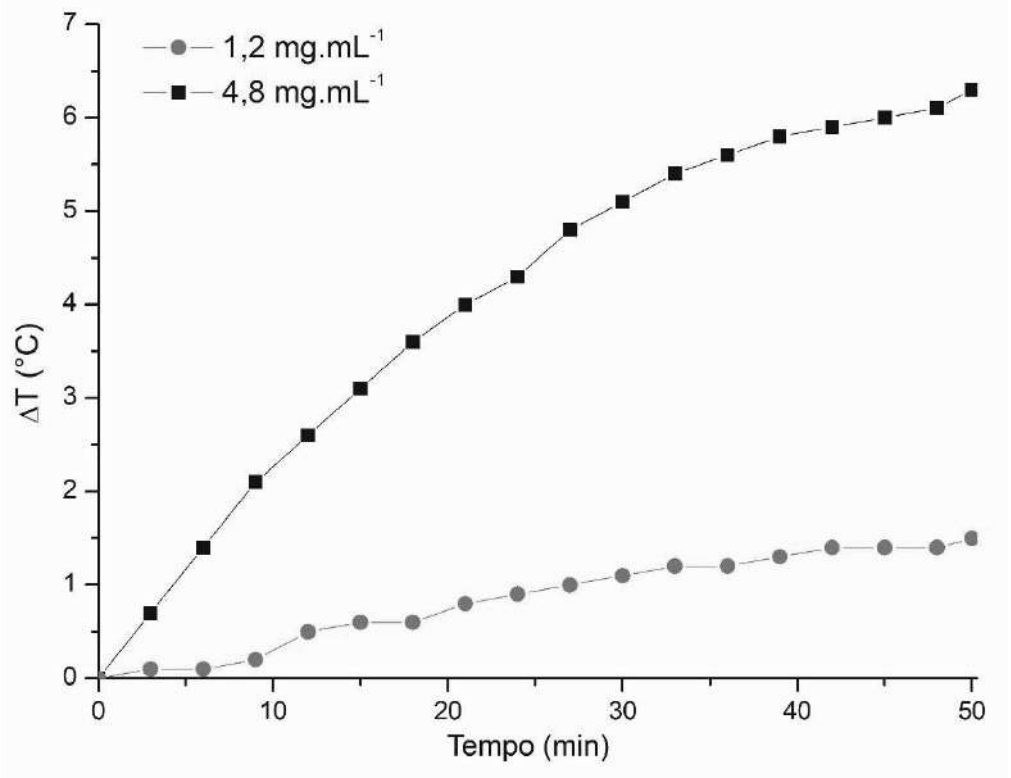

FIGURA 8

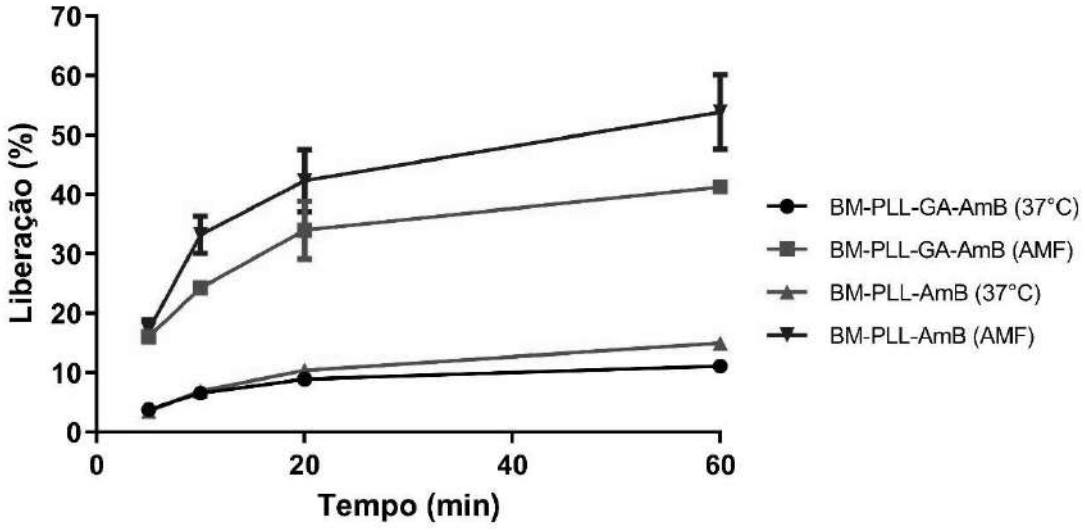

FIGURA 9

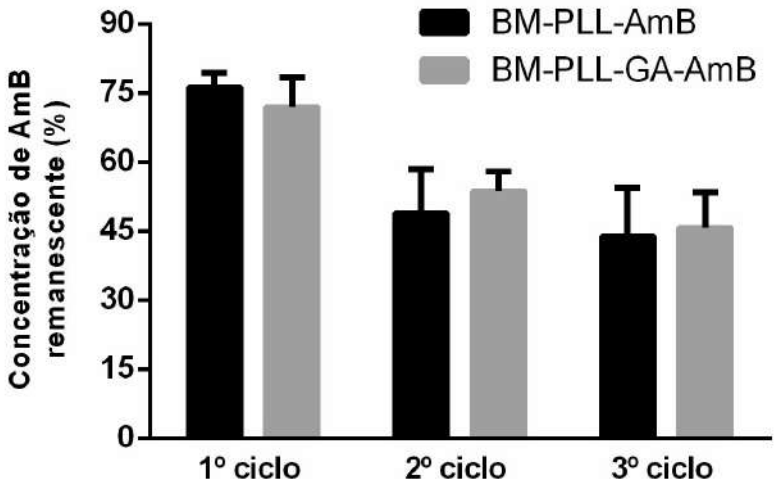
BM-PLL-AmB
BM-PLL-GA-AmB
Concentração de AmB remanescente (%)
90
75
60
45
30
15
0
1º ciclo
2º ciclo
3º ciclo

FIGURA 10

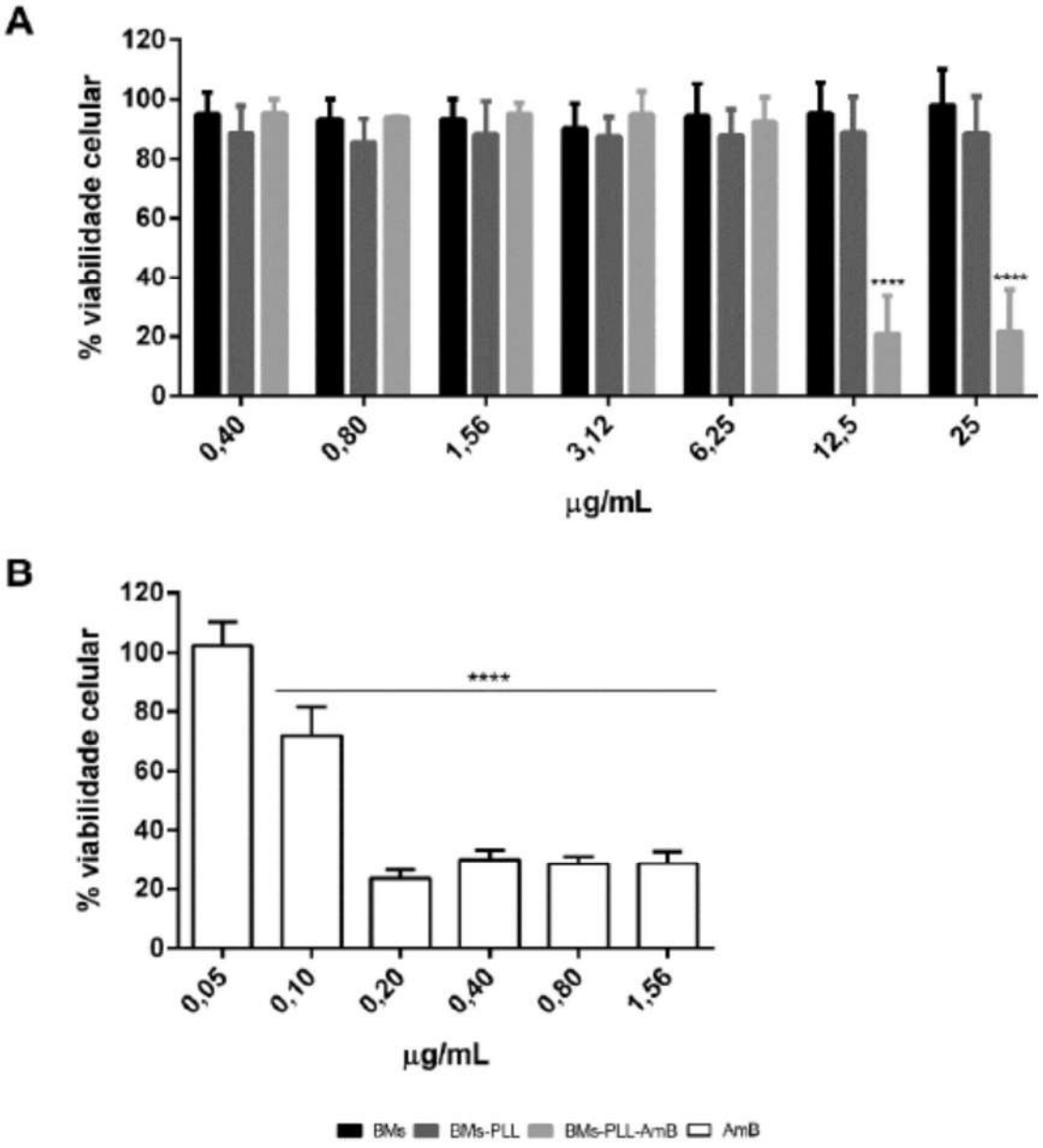
A
% viabilidade celular
120
100
80
60
40
20
0
0,40
0,80
1,56
3,12
6,25
12,5
25
μg/mL
****
****
B
% viabilidade celular
120
100
80
60
40
20
0
****
0,05
0,10
0,20
0,40
0,80
1,56
μg/mL
BMs
BMs-PLL
BMs-PLL-AmB
AmB

FIGURA 11

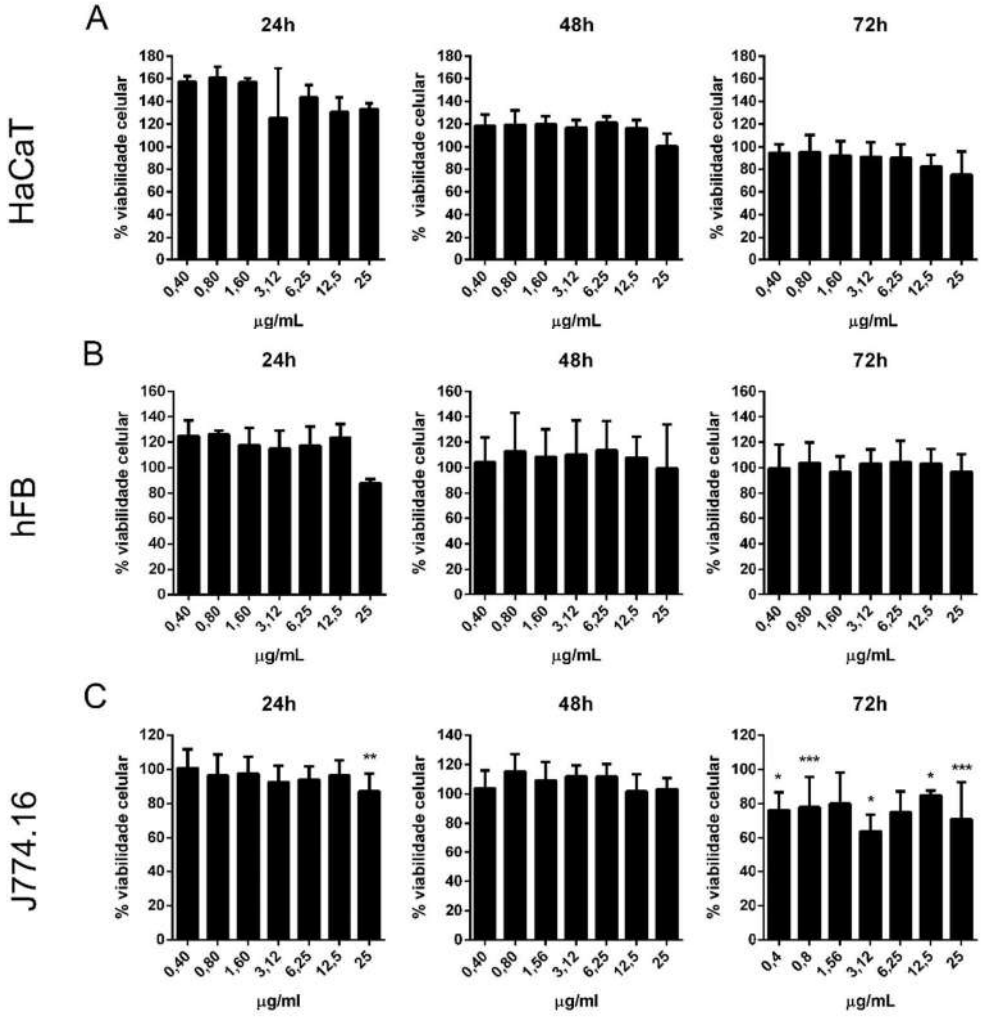
A
B
C
HaCaT
hFB
J774.16
24h
48h
72h
% viabilidade celular
µg/mL
µg/ml
0,40
0,80
1,60
1,56
3,12
6,25
12,5
25
0,4
0,8
*
**
***

FIGURA 12

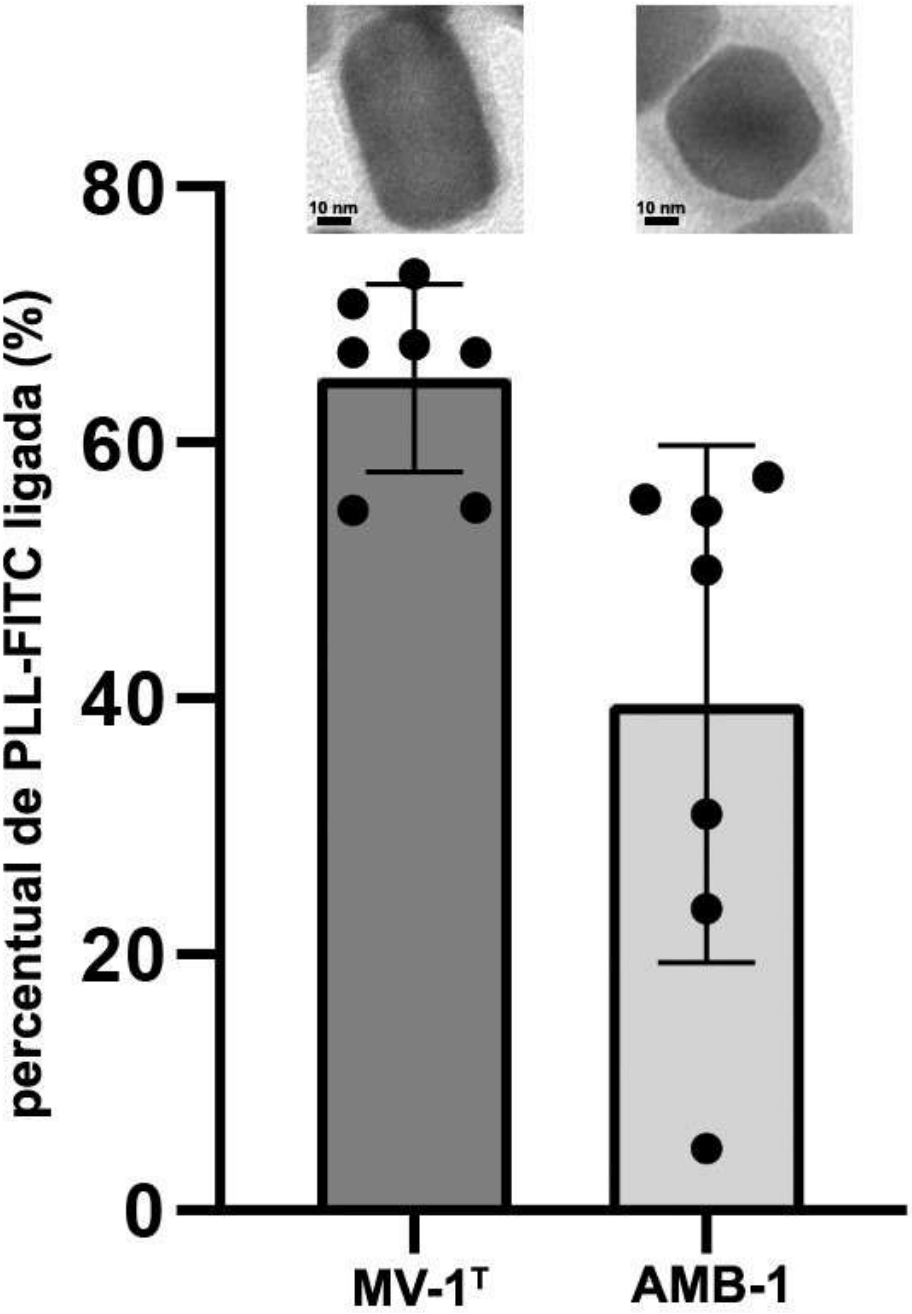
10 nm
10 nm
80
60
40
20
0
percentual de PLL-FITC ligada (%)
MV-1T
AMB-1

FIGURA 13

RESUMO

PROCESSO DE SÍNTESE DE MAGNETOSSOMO FUNCIONALIZADO COM FÁRMACO E MAGNETOSSOMO FUNCIONALIZADO OBTIDO A PARTIR DESTE

A presente invenção descreve um processo de síntese de magnetossomo funcionalizado com fármaco, assim como o magnetossomo funcionalizado obtido a partir deste. O magnetossomo utilizado é oriundo do cultivo de bactérias magnetotáticas. A produção desse composto tem por objetivo fornecer um composto passível de liberação controlada de fármacos, especificamente fármaco aplicado no tratamento de doenças infecciosas de etiologia fúngica ou parasitária. Assim como trazer o advento de uma produção a baixo custo e por meio de tecnologia verde.

Chapter 20

Antarctic microorganisms as sources of biotechnological products

Tarcísio Correa and Fernanda Abreu
Paulo de Góes Microbiology Institute, Federal University of Rio de Janeiro, Rio de Janeiro, Brazil

20.1 Introduction

For many years, Antarctica remained an unexplored continent. In 1961, the Antarctic Treaty System (ATS) was implemented and established this continent as a scientific preserve. Currently, ATS regulates international relations within this complex and fragile environment. Despite the challenging access to this extreme environment, the number of publications about the diversity/bioprospection of microorganisms in this continent has increased significantly over the years (Fig. 20.1). Antarctic continent is home to a substantial diversity of marine and continental environments. Extreme abiotic conditions of Antarctic environments like cold, high salinity, and ultraviolet light incidence play selective pressures over bacterial and fungal aquatic and terrestrial communities [2,3]. Antarctic microorganisms had evolved survival strategies to resist such harsh conditions, and these include but are not limited to cold-tolerant enzymes, antimicrobials, and antifreezing components [4]. As depicted in Fig. 20.2, bioactive compounds are known to be produced in a diversity of microbial habitats, such as sediments of lakes and bays, seawater, soils, and permafrost [4,5].

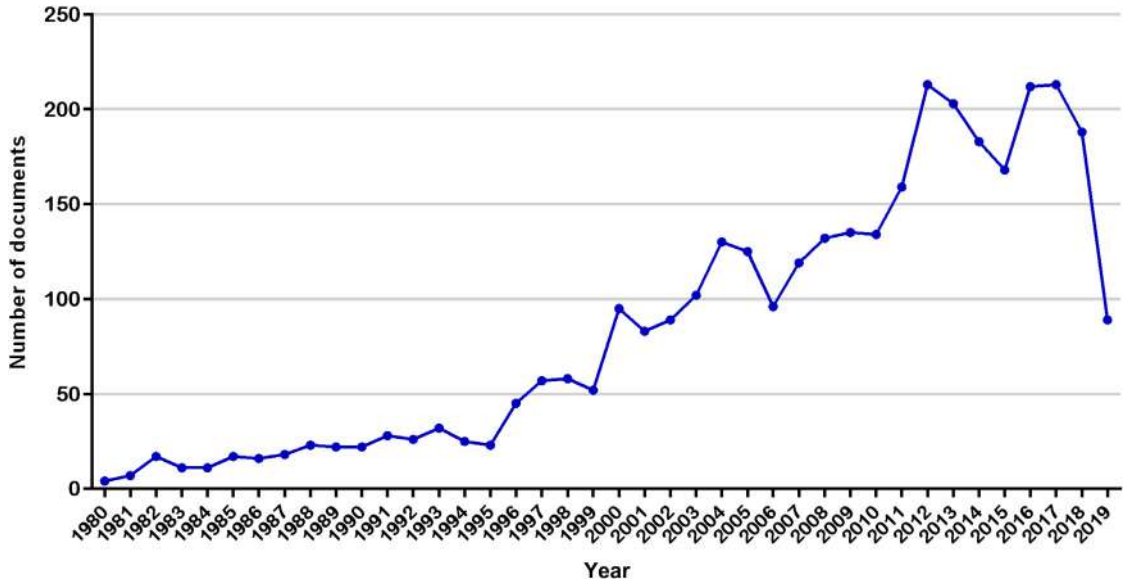

FIGURE 20.1 Global publication records (January 1, 1980–May 29, 2019) for Antarctic microbial diversity. The search using keywords "Antarctic" and "Antarctica" combined with "microorganism(s)," "bacterium(a)," "fungus(i)," and "yeast(s)" was performed on Scopus database. Selection of data was done as described in Ref. [1].

Physiological and Biotechnological Aspects of Extremophiles. DOI: https://doi.org/10.1016/B978-0-12-818322-9.00020-4

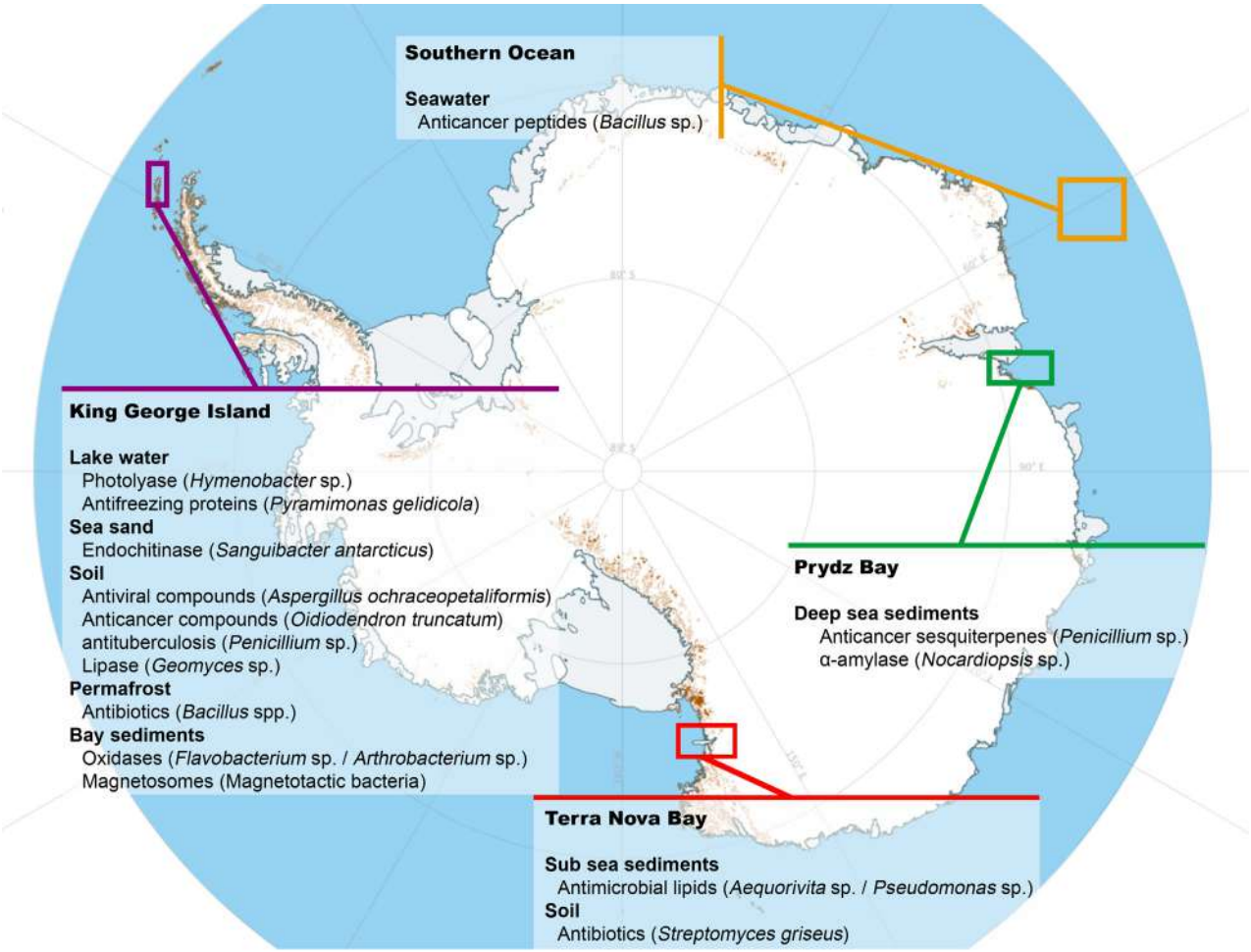

FIGURE 20.2 Diversity of Antarctic environments and bioactive compounds obtained from Antarctic microbiota.

20.2 Bioprospection of microbial derived bioactive compounds in Antarctica

In this chapter, we focus on Antarctic-derived-enzymes, which are by far the most explored microbial products from Antarctica, but we also give some insights in drug discovery, antifreezing biomolecules, and nanotechnology.

20.2.1 Enzymes

Extremophilic enzymes are preferred for use in diverse industrial processes because of their stability under harsh conditions [6]. While thermophilic enzymes are advantageous because they preserve activity under high temperatures, psychrophilic enzymes can dispense the use of heat in productive processes, since their activity is relatively high at low temperatures [6]. This property would be economically beneficial because energy consumption costs for heat generation are saved. Moreover, when heating is avoided, degradation of thermolabile products in bioreactors is prevented [6]. Here, we focus on describing purified, partially purified, or extracellular enzymes with potential to industrial application from microorganisms isolated from different Antarctic environments. Most enzymes display maximum activities in the range 30°C−37°C, but they are able to significantly retain their activities in temperatures as low as 5°C−15°C. Table 20.1 summarizes isolated Antarctic enzymes and their potential applications.

20.2.1.1 Discovery and purification

The first step of discovery of cold-adapted enzymes is the isolation and identification of producing microorganisms from environmental samples. One classic approach for the enzyme discovery is the detection of substrate degradation in diagnostic growth media by microorganisms. In a search for proteolytic enzymes [25], water samples were collected

TABLE 20.1 Enzyme classes isolated from Antarctic microorganisms, their activity and potential uses.

Enzyme class	Source microorganisms	Higher classification	Activity	Application	Reference
Photoliase	*Hymenobacter* sp. UV-11	Flavobacteria	UV-induced DNA damage repair	Formulation of dermatological cosmetics	Marizcurrena et al. [7]
Leucine dehydrogenase	*Pseudoalteromonas* sp. ANT178	Gammaproteobacteria	Conversion of branched chain amino acids into alpha-ketoacids	Pharmaceutical synthesis	Wang et al. [8]
Homoserine-lactonase	*Planococcus versutus* L10.15	Firmicutes	Degradation of homoserine-latones (quorum-sensing mediators)	Inhibition of phytopathogens	See-Too et al. [9]
β-Galactosidase	*Halorubrum lacusprofundi*	Archaea	Hydrolysis of β-galactosides into monosaccharides	Production of lactose-free dairy products	Laye et al. [10]
	Pseudoalteromonas sp. 22b	Gammaproteobacteria			Turkiewicz et al. [11]
	Alicyclobacillus acidocaldarius	Firmicutes			Gul-Guven et al. [12]
Alcohol dehydrogenase	*Flavobacterium* sp.	Flavobacteria	Enantioselective oxidation of alcohols	Pharmaceutical and agrochemical synthesis	Araujo et al. [13]
	Arthrobacter sp.	Actinobacteria			
Alkaline phosphatase	TAB5		Dephosphorylation of 5′ and 3′ ends of DNA and RNA phosphomonoesters	Molecular biology (cloning, probes preparation)	Guthrie et al. [14]
Keratinase	*Lysobacter* sp. A03	Gammaproteobacteria	Proteolysis of keratin	Recycling of poultry wastes into livestock feed	Pereira et al. [15]
Chitinase	*Lecanicillium muscarium*	Ascomycota	Hydrolysis of chitin into *N*-acetyl-glucosamine dimers	Control of fungal infections and treatment of chitin-rich waste	Barghini et al. [16]
	Sanguibacter antarcticus	Actinobacteria			Park et al. [17]
Xylanases	*Cladosporium* sp.	Ascomycota	Hydrolysis of β1→4 linkages of xylan	Biobleaching of paper and pulps	Gil-Durán et al. [18]
Lipases	*Janibacter* sp. R02	Actinobacteria	Hydrolysis of acyl-glicerols, release of fatty acids	Biodiesel production; bioremediation; and detergents	Castilla et al. [19]
	Pseudomonas sp. AMS8	Gammaproteobacteria			Ganasen et al. [20]
	Geomyces sp. P7	Ascomycota			Florczak et al. [21]

(*Continued*)

TABLE 20.1 (Continued)

Enzyme class	Source microorganisms	Higher classification	Activity	Application	Reference
Amylases	*Nocardiopsis* sp. 7326	Actinobacteria	Breakdown of starch polysaccharides	Baking and brewing and food industries	Zhang and Zeng [22]
	Tetracladium sp.	Ascomycota			Carrasco et al. [23]
	Geomyces pannorum	Ascomycota			He et al. [24]

from an Antarctic lake and aliquots were plated onto Luria–Bertani solid agar. Petri dishes were incubated at 4°C to obtain isolated colonies. Then, isolated colonies were streaked onto minimal milk medium for the detection of protease-producing colonies through formation of milk-degradation halo during incubation. It is worth highlighting the importance of incubation at low temperatures for mimicking natural psychrophile conditions at searching cold-active enzymes. A qualitative screening of multiple hydrolytic activities of different yeast strains cultivated from soil, bay, and lake samples collected on King George Island revealed 12 strains produced extracellular proteases when incubated at 8°C but not at 20°C [26]. Among isolated bacteria, *Guehomyces pullulans* showed the most diverse enzyme production profile at psychrophilic conditions, with the presence of proteases, esterases, amylases, pectinases, and inulinases being detected. This finding corroborates the idea that the bioprocesses for enzyme production themselves benefit from psychrophile characters of Antarctic microorganisms.

Enrichment techniques are also used for the screening of certain types of microbial biocatalysts. In these techniques, media compositions are changed so that the survival and growth of microorganisms that are capable of producing a particular type of enzymes are stimulated over other microorganisms. As an example, microorganisms from sediments and soils from King George Island were isolated in media containing (*RS*)-1-(phenyl)ethanol as the carbon source [23]. This approach led to the isolation of organisms producing enantioselective alcohol-degrading oxidases or dehydrogenases either by selecting constitutively producing microorganisms or by inducting formation of these oxidative enzymes.

Classical screening techniques have led to the discovery of most enzymes isolated from Antarctic microbiota, including the notable enzymatic product Antarctic phosphatase derived from psychrophilic strain TAB5 and marketed by New England Biolabs Inc [14,27]. On the other hand, a significant portion of enzymes may not be detected by classic screening due to lack of cultivability of some producing microorganisms [27]. In this sense, genome-based discovery can be useful for enzyme discovery as it dispenses cultivation steps during screening [27].

A typical workflow for identification and laboratory-scale production of cold-tolerant enzymes is described in Fig. 20.3 and comprises the following: (i) screening of degrading enzyme–producing bacteria or fungi, usually by the detection of substrate-degradation halo formed during growth of inoculated organism from an environmental sample on agar plate; (ii) isolation of substrate-degrading colony and cultivation in enrichment liquid media under low temperature (4°C–15°C); (iii) cell concentration and lysis in the case of intracellular enzymes or supernatant concentration in the case of extracellular enzymes; and (iv) multistep purification of lysate or concentrated supernatant (e.g., precipitation and affinity and ionic chromatography). More recently, molecular tools are often used for phylogenetic analyses and enzyme-coding gene identification, cloning, and construction of expression vectors for recombinant production.

20.2.1.2 Activity retention

Enzymes obtained from Antarctic microorganisms have been reported as thermostable [12,21,19,25], halotolerant [19,28], acidophilic [12], alkaliphilic [20], organic-solvent-tolerant [20], in addition to cold-adapted activity. Despite that, little is known about biochemical adaptation of biocatalysts in Antarctic environment.

One study analyzed β-galactosidase from *Halorubrum lacusprofundi* (archaeon) from deep-lake sediment and found a small number of differences in enzyme amino acid sequence underlies stability and activity retention [10]. *H. lacusprofundi* β-galactosidase have been described as polyextremophile, maintaining activity under low temperatures and high salinity and even elevated concentrations of highly oxidative perchlorate salts [29], making this enzyme a good

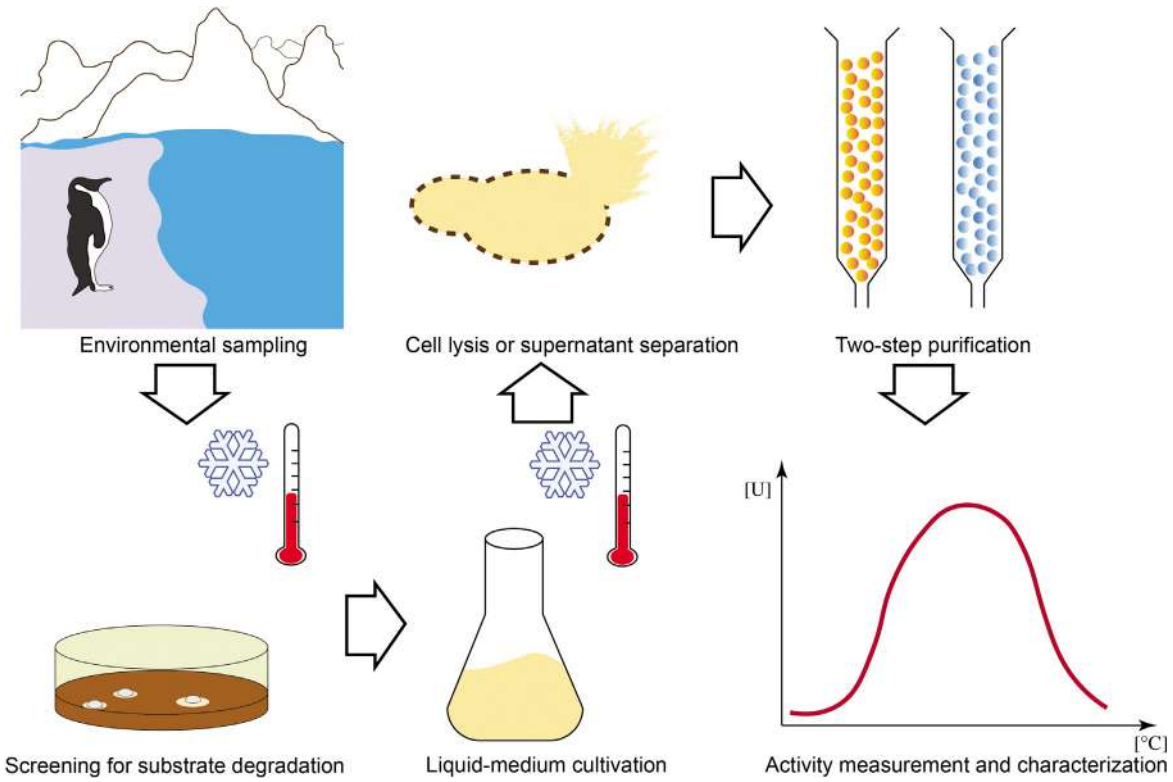

FIGURE 20.3 A typical workflow describing steps of Antarctic enzymes discovery process.

model for understanding superstability mechanisms. The alignment of β-galactosidases sequences of closely related mesophilic archaea allowed the identification of conserved amino acid residues that differed from those of *H. lacusprofundi*. Only a small number (<1%) of residues differed from mesophilic enzyme and these were attributed to the retention of enzymatic activity in cold and highly saline environment. Nonconserved residues were substituted by conserved ones in β-galactosidase sequences by site-directed mutagenesis to generate mutated enzymes. Kinetics studies of mutated and wild-type β-galactosidases indicated that those minor differences in amino acid residues are responsible for the reduced surface charge, which loosens binding of water molecules, permitting greater flexibility in low temperatures; the increased negative internal charge, which prevents aggregation in cold and high salinity and the decreased internal amino acid packing, possibly enhancing substrate binding to active site [10].

20.2.1.3 Enzymes for biorefinery and biodiesel production

The ability of some microorganisms to grow feeding on complex biopolymeric substrates relies on the secretion of digestive enzymes that degrades these polymers into smaller fragments that can be taken up by the cells [30]. For this reason, many of enzymes used for industrial degradation of such matrixes have been obtained from microorganisms isolated from sources rich in that substrate. In this context, a keratinolytic bacterium *Lysobacter* sp. A03 has been isolated from decomposing feathers from penguins inhabiting Elephant Island, Antarctica [15]. This bacterium was then cultivated in feather-meal broth, from where a cold-active keratinase was partially isolated [15].

As in the case of keratin, polymeric substrates are usually available from renewable and low-cost sources and may be employed as substrate for biotechnological production of hydrolytic enzymes. Crustacean shells are rich in chitin, an *N*-acetyl-glucosamine polymer, which can be used as substrate for chitinolytic microorganisms [31]. An optimized large-scale (3 L) cultivation of shrimp-shell degrading Antarctic fungus *Lecanicillium muscarium* was developed for cold-tolerant chitinase production [16]. The developed bioprocess led to a chitinase production of 243 U/L, with an enzymatic activity described as an endochitinase (i.e., cleaving nonreducing ends of chitin chain). Complimentarily, an endochitinase, which cleaves internal sites of chitin generating shorter fragments, was isolated from *Sanguibacter antarcticus* [17]. This bacterium was isolated from Antarctic seawater and the purified enzyme retained 40% and 60% of its activity at 0°C and 10°C, respectively. Another example of hydrolytic enzymes are xylanases, which degrades

β1→4 linkages of xylan, a major component of plant cell walls [32]. Degradation products of xylan varies depending on the hydrolysing enzyme [32]. A thermolabile endoxylanase (a type of xylanase that releases xylooligosaccharides) from sponge-associated fungus *Cladosporium* sp. has been heterologously expressed and purified [18]. The purified enzyme showed higher activity on arabinose-rich xylans (rye arabinoylan and wheat arabinoxylan). The advantage of applying cold-active degrading enzymes in industrial processes is the reduction of production costs deriving from heat generation. Processes of conversion of poultry waste into reusable materials (for keratinase), treatment of chitin-rich wastes (for chitinases), and pulp and paper bleaching (for xylanases) would benefit from the hydrolytic activities at low or moderate temperatures.

Lipases catalyse the hydrolysis of long-chain triacylglycerols yielding free fatty acids, glycerol, and mono- and diglycerols [30]. These enzymes have been applied in food, detergents, and pharmaceutical industries, probably making lipase the most important enzyme class for industrial catalyzes. In biodiesel production, lipases catalyse two-step transesterifications of vegetable, animal, and algal oils [33]. Lipases from Antarctic microorganisms present unusual stability profiles. A lipase from soil bacterium *Janibacter* sp. R02 presents a thermophilic, halophilic, and alkaliphilic profile [19]. Its optimum activity occurs in pH 8−9, at 80°C, at a 10 mM concentration of NaCl/KCl mixture with a higher affinity for short-chain butyrate (C_4) than for heptanoate (C_7) and oleate (C_{18}). A cold-tolerant lipase purified from *Pseudomonas* sp. AMS8 showed good stability in the presence of organic solvents. It displayed 92%, 109%, and 88% of its control (i.e., absence of organic solvents) activity in the presence of 25% (v/v) xylene, octane, and methanol, respectively [20]. Due to the tolerance for usually toxic organic solvents, a simpler method for purifying *Pseudomonas* sp. AMS8 lipase has been developed [34]. The method consists of a two-step (from aqueous phase to an organic phase and back to an aqueous phase) liquid−liquid extraction using a mixture of toluene and Triton X-100, a non-ionic surfactant, as organic phase. The extraction recovered 43% of the enzymatic activity when performed at 10°C—for comparison purposes, gel-filtration chromatography recovers 23% of activity. This extraction method dispenses the need of onerous chromatographic steps, making purification more suitable for industrial settings.

20.2.1.4 Enzymes for pharmaceuticals and cosmetics production

As discussed earlier, Antarctic environment acts as pressure to produce biomolecules that enable organisms' survival in that extreme environment. In the case of UV light, its incidence in Antarctic region is more intense due to ozone layer depletion [2]. Photolyase is a class of enzymes with the ability of repairing UV-damaged DNA [7]. UV lights induced the formation of pyrimidine dimers, impairing the transcription process by RNA polymerase and ultimately leading to skin cancer [7]. A photolyase gene has been identified in genome of lake bacterium *Hymenobacter* sp. UV-11 [7]. Heterologous expression of this gene in *Escherichia coli* allowed the purification of the recombinant enzyme preserving its UV-photoprotective activity. Recombinant photolyase could remove pyrimidine dimers of UV-irradiated DNA and repair UV-induced DNA damage in CHO and HaCat cells. The application of the Antarctic photolyase in the dermatological formulations could generate valuable product with skin cancer preventive action.

A leucine dehydrogenase from the Antarctic sea-ice bacterial strain *Pseudoalteromonas* sp. ANT178 was purified after heterologous expression in an *E. coli* DE3 vector [8]. This enzyme catalyzes the conversion of branched chain amino acids (with the highest specificity for leucine), to their corresponding α-ketoacids by oxidative deamination. This type of catalysis is important for pharmaceutical industry because the conversion products (e.g., L-tert-leucine) are used as active ingredients in pharmaceutical industry [8]. The cold-active leucine dehydrogenase obtained from *Pseudoalteromonas* sp. ANT178 showed a maximum activity at 30°C and pH 9. However, the enzyme retained 40% of its activity at 0°C and 65% at 15°C. The most prominent example of L-tert-leucine derivative is atazanavir, one of most prescribed antiretroviral drugs for the treatment of HIV infection [35].

20.2.1.5 Enzymes for agriculture and brewing

N-Acylhomoserine-lactones are a group of signaling molecules used in quorum-sensing of bacterial communities [9]. The Antarctic bacterium *Planococcus versutus* L10.15 is known to produce the enzyme *N*-acylhomoserine-lactonase, which degrades homoserine-lactones at high rates [9]. The optimum degrading activity is at 28°C, but the enzyme retains 60% of this activity at 18°C. Thus *P. versutus N*-acylhomoserine-lactone might be used in quorum-quenching (i.e., interrupting quorum-sensing communication between bacteria) for inhibiting some plant diseases. Soft-rot disease in cabbage is caused by phytopathogen *Pectobacterium carotovorum*, the phytopathogeny mechanism of which relies on homoserine-lactones-based quorum-sensing. In one experiment, *P. versutus N*-acylhomoserine-lactone was able to inhibit rotting of Chinese cabbage caused by *P. carotovorum*. This inhibition was due to quorum-quenching, which attenuated plant-tissue degradation by the phytopathogen [9]. In another approach, enzymes from Antarctica

microorganisms have been used in the brewing process optimization. Amylases are responsible for the degradation of starch into mono- and oligosaccharides and are of value for different industries, including brewing and baking [30]. Two of most important enzymes of this class are α-amylases, which break down α-(1,4) links within polysaccharide chain, and glucoamylases, which cleave nonreducing ends of starch chains, releasing glucose [30,36]. Beer production demands enzymes as adjuncts for brewing processes and amylases may be employed at various steps of brewing process and they improve fermentability properties of wort [36]. As brewing fermentation processes take place at relatively low temperatures: lagers at 10°C−15°C and ales at 15°C−20°C, the use of cold-adapted enzymes becomes beneficial. A cold-active α-amylase was obtained from the actinomycete *Nocardiopsis* sp. 7326, which was isolated from Antarctic deep-sea sediment [22]. While α-amylase activity maximum occurs in 35°C, more than 70% of that is maintained at 20°C and 35% at 0°C. In addition, a cold-adapted glucoamylase was isolated from Antarctic soil yeast *Tetracladium* sp. through heterologous expression [23]. Activity of this enzyme was optimum at 30°C, retaining more than 50% of this activity at 22°C. As most glucoamylases present enzymatic optimum at 45°C−50°C, Antarctic glucoamylase would provide high catalytic activity in industrial process with low-temperature requirements.

20.2.1.6 Immobilization of Antarctic-derived enzymes

As discussed throughout this section, Antarctic enzymes are excellent catalysts at low and moderate temperatures, with promising industrial applications. However, industrial processes require high-yielding biocatalysts to be reused and this is achieved by immobilization techniques [37]. Immobilization improves physical−chemical stability, allowing enzymes to remain active after multiple cycles [37]. Immobilization of cold-active enzymes could improve feasibility of low-temperature processes by dispensing energy consumption and recovering usually expensive biocatalysts. An α-amylase from *Geomyces pannorum*, a psychrotolerant fungus isolated from continental Antarctica, was covalently immobilized onto iron-oxide magnetic nanoparticles, resulting in an evident stability enhancement [24]. Both soluble and immobilized amylase displayed an activity optimum at 40°C. When immobilized, the enzyme retained more than 40% of its optimal activity at 20°C and 70°C, while soluble enzyme activity was below 25% in either case. In addition, 90% of its activity was retained after three cycles and 60% was retained after eight cycles of reutilization. In another case, chitosan beads were used as support for covalent immobilization of β-galactosidase from *Pseudoalteromonas* sp. 22b, isolated from the digestive system of Antarctic krill *Thysanoessa macrura* [11,26]. Retention of enzyme activity after immobilization was 53%, with lactose hydrolysis being carried at 4°C for 48 h. From that a recycling system for continuous lactose hydrolysis (1 mL/min) was developed with a column packed with enzyme-functionalized beads. The system reached a steady efficiency of 93% of lactose hydrolysis at 18 h of operation. The activity of continuous lactose hydrolysis lasted for 40 days at 15°C.

20.2.2 Drug discovery

20.2.2.1 Antimicrobial drug discovery

Antarctica's extreme environments with different abiotic characteristics is home to a large variety of microbial species [3]. This combination makes Antarctica a promising site for obtention of bioactive compounds due to the diversity of metabolic pathways resulting from evolutionary adaptation to cold and nutrient-limited environments [38]. Production of extracellular antimicrobial compounds as secondary metabolites is assumed to be an adaption strategy by conferring producing microorganisms a competitive advantage. In one study, fungal strains isolated from marine environments showed production of metabolites with antimicrobial action against important human pathogens [39]. Cultivation of isolated strains at low temperatures positively influenced the production of antimicrobial substances: *Atradidymella* sp. showed higher production at 4°C, while *Pseudogymnoascus* sp. and *Penicillium flavigenum* more intense production at 15°C. This finding highlights the adaptative ability in producing and excreting antimicrobials at polar environments and the role of temperature in regulating production of these bioactive compounds. Table 20.2 summarizes antimicrobial activities of compounds isolated from Antarctic microbiota and Fig. 20.4 depicts the structures of these compounds.

As most identified antimicrobial molecules are excreted during microbial growth, preliminary characterization on their biological activity is performed using cell-free fermentation media containing metabolic products. Using this approach, a search of antimicrobial-producing strains from Antarctic permafrost identified six *Bacillus* sp. strains with relevant antimicrobial activity against pathogenic bacteria [5]. Among them, *Bacillus safensis* showed strong inhibition of multidrug-resistant *Pseudomonas aeruginosa* ATCC 27853 and *Staphylococcus aureus* INA 00761. Fermentation broth of halophilic bacterium *Nocardioides* sp. A1 isolated from soil samples from Antarctica also showed strong activity against *Bacillus subtilis* and rice-phytopathogen *Xanthomonas oryzae* [46]. Purification, structural characterization,

TABLE 20.2 Antimicrobial and antiviral components derived from Antarctic microorganisms.

Source microorganism	Component(s)	Test microorganism(s)	Activity measure	Values (μg/mL)	Reference
Pseudomonas sp. BTN1	Rhamnolipids C1 and C2	*Burkholderia cenocepacia*	MIC	3.12 (C1 and C2)	Tedesco et al. [40]
		Staphylococcus aureus		1.56 (C1) and 3.12 (C2)	
Aequorivita sp.	Aminolipids	Methycilin-resistant *S. aureus*	IC_{50}	22	Chianese et al. [41]
Penicillium sp. SCSIO 05705	Questiomycin A	*Mycobacterium tuberculosis*	MIC	0.83	Wang et al. [42]
Streptomyces griseus	Frigocyclinone	*Bacillus subtilis* DSM 10	MIC	4.6	Bruntner et al. [43]
		S. aureus		15.3	
Spiromastix sp.	Spiromastixone J	Methycilin-resistant *S. aureus*	IC_{50}	1.0	Niu et al. [44]
		Methycilin-resistant *Staphylococcus epidermidis*		0.5	
		Vancomycin-resistant *Enterococcus faecalis*		2.0	
Aspergillus ochraceopetaliformis	Ochraceopone A (oa), asteltoxin (as) and isoasteltoxin (ia)	H1N1	IC_{50}	0.10 (as) and 0.23 (ia)	Wang et al. [45]
		H3N3		5.5 (oa), 0.28 (as), and 0.35 (ia)	

Their activity against selected test strain is listed as minimal inhibitory concentration (MIC) or IC_{50} as available from the respective reference.

and further studies of bioactivities of isolated compounds may then proceed in the case of confirmed positive activity in those preliminary tests. Partial characterization of organic extract of *Nocardioides* sp. A1 growth medium revealed active substances consisted mainly of glycolipids and/or lipopeptides [46]. This discovery is in accordance with the described fact antimicrobial activities of lipidic compounds from natural sources [47].

Different antimicrobial lipid−based substances from Antarctic microorganisms have been isolated. Rhamnolipids, a particular class of bacterial lipids, are structurally composed by a rhamnose sugar moiety bound to a 10- to 12-carbon long lipid chain [40]. Rhamnolipids named C1 and C2 have been purified from the marine-sediment bacterium *Pseudomonas* sp. BTN1 obtained from Antarctica samples and displayed antibacterial activity against *Burkholderia cenocepacia* isolated from patients with cystic fibrosis and a standard strain of *S. aureus* [40]. Aminolipids are another special class of microbial lipids. Their structural skeleton comprises a fatty acid amide chain esterified with a second fatty acid chain through their C3 hydroxy groups [41]. Three aminolipids bearing an N-terminal glycine residue were isolated from shallow-sea-sediment bacterium *Aequorivita* sp. [41]. These three compounds were effective against methycilin-resistant *S. aureus* (MRSA).

Apart from lipids, a variety of compounds have also been described from Antarctic microorganisms with potential to be used in treatments of bacterial infections of great public health concern, including in cases of antibiotic resistance. Alkaloids questiomycin A from soil *Penicillium* strain SCSIO 05705 displayed potent antituberculosis activity [42]. Antibacterial activity H37Ra strain of *Mycobacterium tuberculosis* was close to that of antituberculosis antibiotic isoniazid, used as positive control [42]. Frigocyclinone, an antibiotic, the structure of which consists of a four-ring moiety attached to an aminodeoxysugar through a C-glycosidic linkage to an aminodeoxysugar, was isolated from the soil actinomycete *Streptomyces griseus* strain NTK 97 [43]. It has been described as a good inhibitor of *B. subtilis* DSM 10 and *S. aureus* DSM 20231.

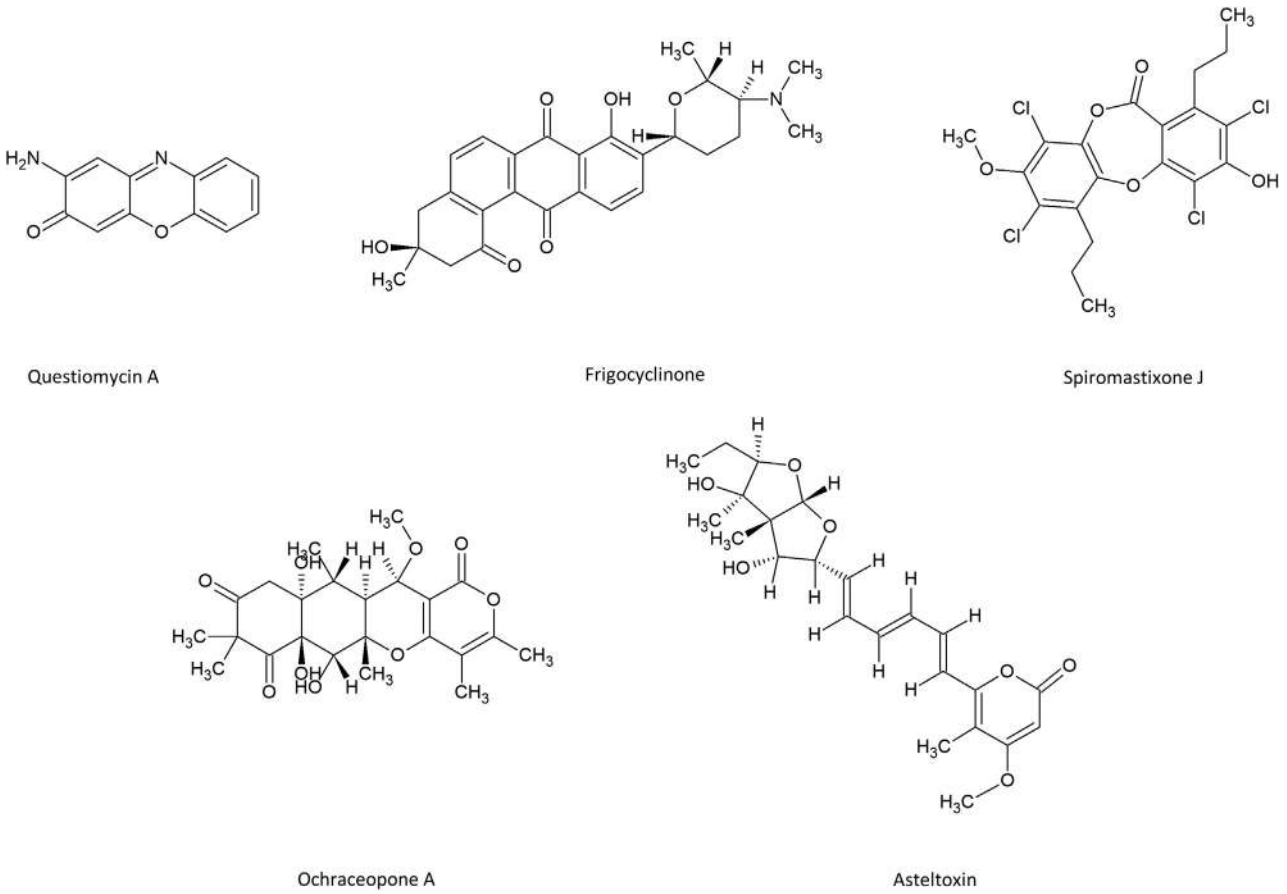

FIGURE 20.4 Structure of selected antimicrobial metabolites isolated from Antarctic microorganisms.

Spiromastix sp. fungus from deep-sea sediment produces spiromastixones, the skeleton of which consists of two chlorinated benzene rings linked through an ester and an ether bridges [44]. Structurally related spiromastixones A−O present variable degree of antimicrobial activity against multidrug-resistant clinical strains [44]. Among them, spiromastixone J is the most promising of isolated compounds with a 16-fold more potent inhibition of MRSA and 4-fold better activity against methycilin-resistant *Staphylococcus epidermidis* than the control antibiotic levofloxacin. While spiromastixone J also resulted in strong inhibition of two vancomycin-resistant *Enterococcus* sp. isolates, levofloxacin, had minor effect. Antarctic bioactive molecules are effective to pathogens other than bacteria. Three compounds with antiviral activity were extracted from fermentation broth of *Aspergillus ochraceopetaliformis* SCSIO05702 isolated from an Antarctica's soil sample [45]. These compounds, sequiterpenoids ochraceopone A, asteltoxin, and isoasteltoxin, were more potent against H1N1 and H3N3 viruses than antiviral drug oseltamivir [45].

As we described here, Antarctic microbiome is a source of structurally diverse compounds. Harsh conditions in that continent drives genetic-level evolutionary adaptations leading to diversified metabolic pathways [38]. The drug-synthetizing property of psychrophiles constitutes a biotechnological potential to transpose the ability to eliminate competitors in natural habitats to generate more efficient medicines to inhibit/kill human pathogens, especially when treatments no longer respond to available therapies.

20.2.2.2 Anticancer drug discovery

Screening of antibiotics from natural sources has led to discovery of efficient drugs for treatment of cancers [48]. Commonly, antibiotics that made their ways to cancer chemotherapy present DNA-binding action interfere with transcription or replication of DNA and block cell replication [48]. For that reason, microbial secondary metabolites from environmental samples have inhibitory cross action against cancer cells. Thus, metabolite-producing Antarctic microorganisms become good candidates for anticancer drug search. Table 20.3 summarizes anticancer activities of compounds isolated from Antarctic microbiota and Fig. 20.5 depicts the structures of these compounds.

TABLE 20.3 Components derived from Antarctic microorganisms and their IC_{50} against selected cell lines.

Source microorganism	Component(s)	Cell line(s)	IC_{50} (μg/mL)	Reference
Botryidiopsidaceae sp. (microalga)	Ethanolic extract	Hs578T (breast cancer)	~7[a]	Suh et al. [49]
		HeLa (breast cancer)	~5[a]	
		A375 (melanoma)	~14[a]	
Penicillium sp. PR19N-1	1-Chloro-3β-acetoxy-7-hydroxy-trinoreremophil-1,6,9-trien-8-one	HL60 (leukemia)	3.34 ± 0.05	Wu et al. [50]
		A549 (lung carcinoma)	3.45 ± 0.03	
Streptomyces sp. SCO736	Antartin	A549	4.45	Kim et al. [51]
		U87 (brain cancer)	8.06	
Penicillium sp. SCSIO 05705	Meleagrin	K562 (myelogenous leukemia)	1.54 ± 0.21	Wang et al. [42]
		U937 (lymphoma)	1.18 ± 0.22	
	Neoxaline	K562	1.73 ± 0.13	
		U937	2.13 ± 0.14	
Oidiodendron truncatum GW3-13	Chetracin B	HCT8	0.009 ± 0.04	Li et al. [52]
		Bel-7402	0.002 ± 0.03	
	Melinacidin IV	HCT8	0.038 ± 0.05	
		Bel-7402	0.004 ± 0.02	
Bacillus sp. N11-8	PBN11-8 (polypeptide)	Bel-7402	1.56	Zheng et al. [53]
		HepG2 (liver cancer)	1.57	
		Panc-28 (pancreatic cancer)	1.73	

[a]*Approximately calculated from data available on paper.*

In vitro studies against cancer cell lines have demonstrated the anticancer potential of metabolites present in cell lysates and extracts as well as in culture supernatants of Antarctic microorganisms. In a screening study [54], fermentation broths from cultivation of seven microbial strains isolated from Antarctic seawaters were tested in cytotoxicity assays against several cell cancer lines. The most promising results of this screening were inhibitions between 35% and 68% of viability of human hepatocellular carcinoma cells from Bel7402 line [54].

Although most studies describe antitumoral metabolites from fungi and bacteria, Antarctic microalgae are also promising sources of these compounds. Dried biomass of Antarctic freshwater microalga *Botryidiopsidaceae* sp. was submitted to extraction of bioactive compounds with ethanol as extractive solvent [49]. The microalgal extract displayed a selective antiproliferative action (i.e., no effect observed on noncancerous cell lines) against different human cancer cell lines. The most evident results were against Hs578T and HeLa (breast cancer) and A375 (human melanoma) cell lines, which were inhibited in a concentration- and time-dependent manner. The anticancer activity of this extract is at least partially due to induction of apoptosis. Treatment of HeLa cells increased expression of p53 and caspase-3 (proapoptotic proteins) and decreased expression of Bcl-2 (antiapoptotic protein) [49]. In addition, it was observed an impaired invasion and migration capacities through basement membrane [49].

Sesquiterpenes are a class of natural products of 15-carbon skeleton synthesized by biochemical pathways in plants and marine organisms [55]. These small molecules are of great interest for drug discovery because of their varied

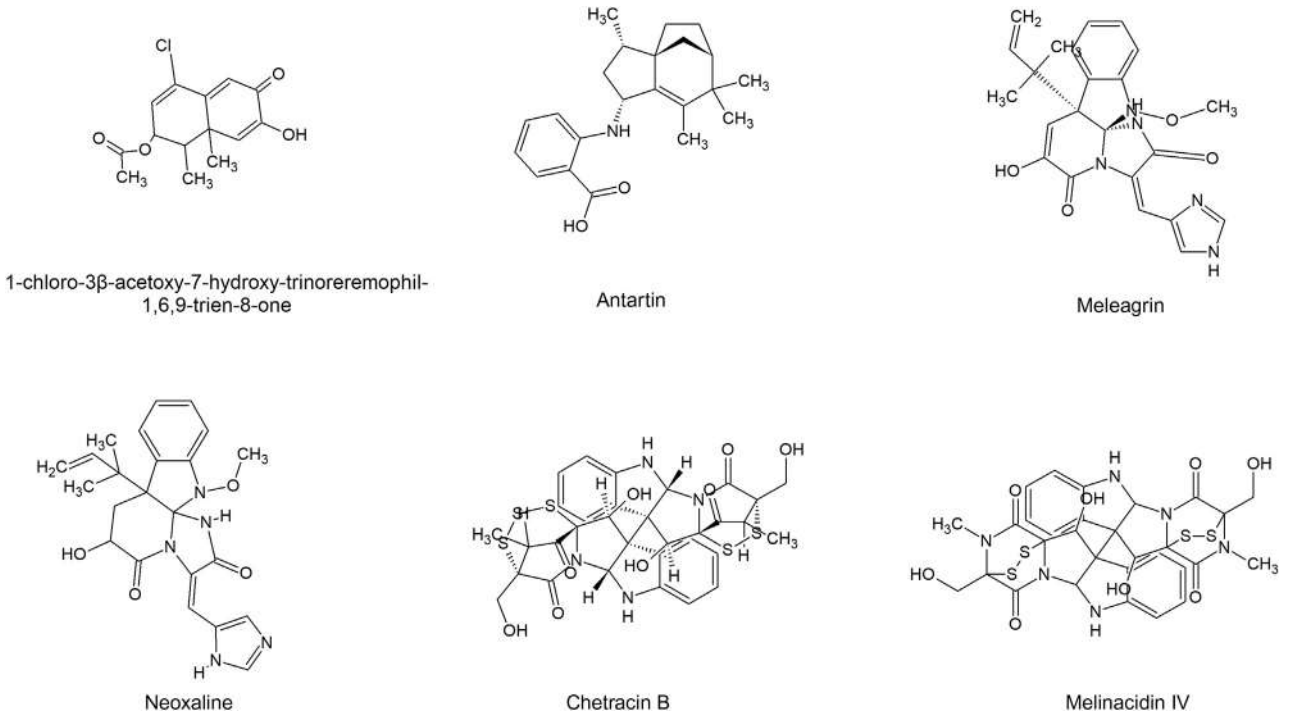

FIGURE 20.5 Structures of compounds isolated from Antarctic microorganism with described anticancer activity.

biological activities, with good potential for cancer treatment, and availability from natural sources [56]. Isolation and identification of excreted secondary metabolites belonging to sesquiterpenoid class was achieved for deep-sea-sediment fungus *Penicillium* sp. PR19N-1 [50]. Among identified metabolites, a novel chlororinated eremophilane-type sesquiterpene 1-chloro-3β-acetoxy-7-hydroxy-trinoreremophil-1,6,9-trien-8-one (molecular formula $C_{14}H_{15}ClO_4$) was the only one with cancer-inhibiting property. HL60 (human leukemia) and A549 (human lung carcinoma) cell lines suffered moderate inhibition when treated with that compound [50]. Another anticancer compound, Antartin, a zizaane-type sesquiterpene, was purified from *Streptomyces* sp. SCO736 fermentation broth [51]. Treatment of cells from A549 and H1299 (lung cancer) and U87 (brain cancer) lines with 10 μg/mL antartin led to almost complete proliferation inhibition. For lung cancer lines the formation of tumorigenic foci was prevented, indicating reversal of capacity of cells to aggregate into tumors. Anticancer activity of antartin against lung cancer is underpinned by the suppressed expression of Ki-67 (proliferation marker) and cyclins and cyclin-dependent kinases (cell-cycle-regulation factors) [51].

Microbial anticancer compounds of other classes have also been identified microorganisms isolated from Antarctica's samples. Alkaloids meleagrin and neoxaline from soil *Penicillium* strain SCSIO 05705 displayed potent cytotoxic activity against U937 (lymphoma) and K562 (myelogenous leukemia) [42]. Chetracin B and melinacidin IV, belonging to epipolythiodioxopiperazine class, were isolated from soil fungus *Oidiodendron truncatum* GW3-13 [52]. Chetracin B showed cytotoxic activity against HCT-8 (human colorectal tumor) and Bel-7402 (hepatocellular carcinoma), while melinacidin IV inhibited Bel-7402 cells at nanomolar concentrations. Activities of both *Penicillium* and *O. truncatum* metabolites were more potent than that of classic chemotherapy drug paclitaxel, which was used as a positive control in proliferation assays.

An extracellular polypeptide was identified from fermentation broth of marine *Bacillus* sp. N11-8 [53]. The peptide PBN11-8 displayed significant cytotoxicity against Bel-7402, HepG2 (liver cancer), and Panc-28 (pancreatic cancer). Bel-7402 inhibition was further studied and a reduction in the migration and invasion abilities of tested cells was observed. The expression of integrin β1, an important mediator of cell survival, proliferation, differentiation, and migration in cancer [57], was also downregulated in the presence of PBN11-8. The peptide also hindered the expression of matrix metalloproteinases, which participate in metastasis process by degrading extracellular matrix [53].

20.2.3 Ice-binding proteins

One adaptive mechanism for survival in extremely cold regions is the synthesis of molecules that inhibits ice formation inside cells [58]. Ice-binding proteins (IBPs) have the unique capacity to interact with ice surface and prevent growth of

ice crystals [58,59]. In polar marine environments, water temperature is commonly under 0°C as salinity decreases seawater freezing point. In order to survive in such cold environments, IBPs are synthetized, which is essential for keeping tissue integrity in Arctic and Antarctic fishes as ice crystal formation could cause cell disruption [58]. Due to this ability, these proteins have potential for application in process where freezing damage is undesirable such as food preservation and cell storage [58].

Despite more commonly described in fishes, antifreezing proteins may also be isolated from Antarctic psychrophile microorganisms. Here, we describe some of microbial sources of these antifreezing agents and discuss some potential applications. Cold-induced IBP expression has been observed in the Antarctic yeast *Glaciozyma antarctica* [60]. A set of nine different genes coding for IBPs were overexpressed as temperature decreased from 15°C to −12°C.

Structural analysis of IBPs from bacteria that survived a freezing−thawing selection test revealed ice-binding regions contains multiple and regularly spaced threonine residues [59]. IBPs from *Sphingomonas* GU1.7.1, *Plantibacter* GU3.1.1, and *Pseudomonas* AFP5.1 were isolated and used as cryopreservatives of cucumber and zucchini. The fruits were treated with IBPs in a concentration of 0.1 mg/mL and frozen at −20°C for 16 h. While disrupted cell walls and dead cells were observed in nontreated fruits, IBP-treated tissues retained cell viability and cell wall integrity.

In another approach, an IBP from *Flavobacterium frigoris* was supplemented in freezing medium along with DMSO for preservation of microalga *Isochrysis galbana* [61]. Cells viability after thawing was greater in comparison to DMSO used as the only cryopreservative. Thermal hysteresis (TH) is the parameter used for measurement of cryoprotective activity and corresponds to the difference between freezing and melting points. IBPs from marine flagellate *Pyramimonas gelidicola* [62] and diatom *Chaetoceros neogracile* [63] have close TH values, which are also similar to fish IBPs. Ice crystals formed in the presence of IBPs from all microorganisms presented here showed a hexagonal shape, which is related to antifreezing activity. These results reinforce the potential of IBP to be used as cryoprotective agents for food preservation and cell culture purposes.

20.3 Nanoparticles

Besides organic molecules, some microorganisms are excellent producers of inorganic nanoparticles through biomineralization processes [64]. Application of nanoparticles is present in diverse fields in technology. Microbial synthesis of nanoparticles is considered green chemistry because it does not use expensive and toxic chemicals, which are often necessary for synthetic production [64]. Quantities of produced nanoparticles may be increased by scaling up cultivation from lab flasks to 100-L bioreactors [64]. Despite underexplored, Antarctic biomineralizing microorganisms have been described and constitute a promising platform for the synthesis of these nanomaterials [64].

20.3.1 Cadmium nanoparticles

Peroxide-resistant psychrophile strains of *Pseudomonas* spp. were grown from Antarctic samples through cultivation under in oxidative stress conditions [65]. These bacteria synthetize semiconductor cadmium sulfide (CdS) nanoparticles when cultured at 15°C in a medium supplemented with H_2O_2 and $CdCl_2$. Two tellurium-resistant *Pseudomonas* sp. and one *Psychrobacter* sp. that also produce CdS nanoparticles were isolated through tellurite enrichment [66]. For these strains, production is better achieved at 28°C. The uptake of Cd ions from environments at relatively low temperatures characterizes these microorganisms as excellent candidates for bioremediation of heavy-metal-contaminated waters and soils in polar and subpolar regions [66]. In addition to removal of these pollutants, minerals formed from captured metals can be recovered as these microorganisms accumulate these components in form of nanoparticles. These nanostructures range in size from 10 to 40 nm as measured in observation of producing cells by transmission electron microscopy. Semiconductor nanoparticles from Antarctic bacteria have emission peaks between 500 and 600 nm when excited at 400 nm [65]. The fluorescence properties of CdS enable nanoparticles to be used as quantum dots in medical image diagnostics.

20.3.2 Iron-oxide nanoparticles

A peculiar group of iron-mineralizing prokaryotes has been identified in extreme aquatic environments, including Antarctica [67]. The so-called magnetotactic bacteria synthetize iron-oxide nanoparticles, either magnetite (Fe_3O_4) or greigite (Fe_3S_4) depending on the biomineralizing species. These structures, known as magnetosomes, are disposed in a single or multiple chain along bacterial cell long axis [67]. The iron mineral is in the nanoparticle core and is surrounded by a biological membrane, possibly derived from cell's inner membrane [68]. Magnetotactic bacteria constitute

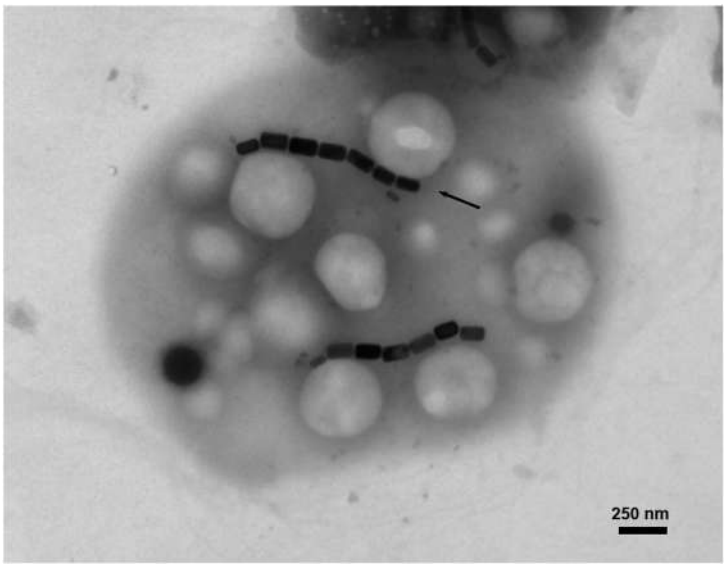

FIGURE 20.6 Transmission electron microscopy of a magnetotactic coccus from marine sediments from Monsiment Cove, King George Island. Arrow indicates one of the magnetosome chains.

a morphologic, phylogenetically and metabolically diverse group. Phylogenetic analyses based on the gene sequence encoding the 16S rRNA have led to the identification of magnetotatic bacteria in the phylum Proteobacteria (classes Alpha-, Delta-, Gamma- and, more recently, Beta- and Zetaproteobacteria), in the phylum Nitrospirae, in the superphylum Planctomycetes−Verrucomicrobia−Chlamydiae and possibly in the candidate phylum Latescibacteria [69]. Magnetotactic cocci (Fig. 20.6) from Antarctica marine sediments belong to the Alphaproteobacteria class and produce elongated magnetite magnetosomes disposed in two or four chains or nonorganized in chains [70]. Dimensions of aligned magnetosomes ranged between 117−102 nm in length and 67−72 nm in width. Unlike chemical synthesis processes (i.e., iron precipitation), microbial production of magnetite yields nanoparticles with finely controlled size, morphology, and chemical purity [68]. These unique characteristics are result of a genetically controlled biomineralization process and enable magnetosomes to be used in a variety of applications [1]. Purified magnetosomes have been employed as support for enzyme immobilization, nanoformulations for magnetically driven drug delivery, alternating magnetic field−induced hyperthermia agents for cancer treatments, contrast agents for magnetic resonance imaging, among others [1].

20.4 Conclusion and future directions

This brief review about Antarctica's microbial metabolic content/products showed the inestimable value of this extreme environment as a scientific preserve and biotechnological repository. Hopefully, future studies on psychrophilic/psychrotolerant microorganisms and their enzymes will allow the development of new technologies, processes, and products. In this sense, future research should focus on the upscaling of cultivation of psychrophiles, high-yield purification of bioactive products, and genetic engineering for an optimized production of Antarctic biotechnological products.

References

[1] Vargas G, Cypriano J, Correa T, Leão P, Bazylinski DA, Abreu F. Applications of magnetotactic bacteria, magnetosomes and magnetosome crystals in biotechnology and nanotechnology: mini-review. Molecules 2018;23. Available from: https://doi.org/10.3390/molecules23102438.

[2] Hughes KA, Lawley B, Newsham KK. Solar UV-B radiation inhibits the growth of Antarctic terrestrial fungi. Appl Environ Microbiol 2003;69:1488−91. Available from: https://doi.org/10.1128/AEM.69.3.1488-1491.2003.

[3] Wilkins D, Yau S, Williams TJ, Allen MA, Brown MV, Demaere MZ, et al. Key microbial drivers in Antarctic aquatic environments. FEMS Microbiol Rev 2013;37:303−35. Available from: https://doi.org/10.1111/1574-6976.12007.

[4] Yarzábal LA. Antarctic psychrophilic microorganisms and biotechnology: history, current trends, applications, and challenges. In: Castro-Sowinski S, editor. Microbial models: from environmental to industrial sustainability. Singapore: Springer Singapore; 2016. p. 83−118. <https://doi.org/10.1007/978-981-10-2555-6>.

[5] Efimenko TA, Efremenkova OV, Demkina EV, Petrova MA, Sumarukova IG, Vasilyeva BF, et al. Bacteria isolated from Antarctic permafrost are efficient antibiotic producers. Microbiology 2018;87:692−8. Available from: https://doi.org/10.1134/S0026261718050089.

[6] Sarmiento F, Peralta R, Blamey JM. Cold and hot extremozymes: industrial relevance and current trends. Front Bioeng Biotechnol 2015;3:243−54. Available from: https://doi.org/10.3389/fbioe.2015.00148.

[7] Marizcurrena JJ, Martínez-López W, Ma H, Lamparter T, Castro-Sowinski S. A highly efficient and cost-effective recombinant production of a bacterial photolyase from the Antarctic isolate *Hymenobacter* sp. UV11. Extremophiles 2018;. Available from: https://doi.org/10.1007/s00792-018-1059-y.

[8] Wang Y, Hou Y, Wang Y, Zheng L, Xu X, Pan K, et al. A novel cold-adapted leucine dehydrogenase from Antarctic sea-ice bacterium *Pseudoalteromonas* sp. ANT178. Mar Drugs 2018;16. Available from: https://doi.org/10.3390/md16100359.

[9] See-Too WS, Convey P, Pearce DA, Chan KG. Characterization of a novel *N*-acylhomoserine lactonase, AidP, from Antarctic *Planococcus* sp. Microb Cell Fact 2018;17:179. Available from: https://doi.org/10.1186/s12934-018-1024-6.

[10] Laye VJ, Karan R, Kim J-M, Pecher WT, DasSarma P, DasSarma S. Key amino acid residues conferring enhanced enzyme activity at cold temperatures in an Antarctic polyextremophilic β-galactosidase. Proc Natl Acad Sci USA 2017;114:201711542. Available from: https://doi.org/10.1073/pnas.1711542114.

[11] Turkiewicz M, Białkowska A, Kalinowska H, Bielecki S. Antarctic marine bacterium *Pseudoalteromonas* sp. 22b as a source of cold-adapted b-galactosidase. Biomol Eng 2003;20:317−24. Available from: https://doi.org/10.1016/S1389-0344(03)00039-X.

[12] Gul-Guven R, Guven K, Poli A, Nicolaus B. Purification and some properties of a β-galactosidase from the thermoacidophilic *Alicyclobacillus acidocaldarius* subsp. *rittmannii* isolated from Antarctica. Enzyme Microb Technol 2007;40:1570−7. Available from: https://doi.org/10.1016/j.enzmictec.2006.11.006.

[13] Araújo LS, Kagohara E, Garcia TP, Pellizari VH, Andrade LH. Screening of microorganisms producing cold-active oxidoreductases to be applied in enantioselective alcohol oxidation. An Antarctic survey. Mar Drugs 2011;9:889−905. Available from: https://doi.org/10.3390/md9050889.

[14] Guthrie E, Davis T, Benner J. Overexpression, purification and characterization of a thermolabile phosphatase. US7319014B2. 2008.

[15] Pereira JQ, Lopes FC, Petry MV, Medina LFDC, Brandelli A. Isolation of three novel Antarctic psychrotolerant feather-degrading bacteria and partial purification of keratinolytic enzyme from *Lysobacter* sp. A03. Int Biodeterior Biodegrad 2014;88:1−7. Available from: https://doi.org/10.1016/j.ibiod.2013.11.012.

[16] Barghini P, Moscatelli D, Garzillo AMV, Crognale S, Fenice M. High production of cold-tolerant chitinases on shrimp wastes in bench-top bioreactor by the Antarctic fungus *Lecanicillium muscarium* CCFEE 5003: bioprocess optimization and characterization of two main enzymes. Enzyme Microb Technol 2013;53:331−8. Available from: https://doi.org/10.1016/j.enzmictec.2013.07.005.

[17] Park HJ, Kim D, Kim IH, Lee C-E, Kim I-C, Kim JY, et al. Characteristics of cold-adaptive endochitinase from Antarctic bacterium *Sanguibacter antarcticus* KOPRI 21702. Enzyme Microb Technol 2009;45:391−6. Available from: https://doi.org/10.1016/j.enzmictec.2009.07.002.

[18] Gil-Durán C, Ravanal MC, Ubilla P, Vaca I, Chávez R. Heterologous expression, purification and characterization of a highly thermolabile endoxylanase from the Antarctic fungus *Cladosporium* sp. Fungal Biol 2018;122:875−82. Available from: https://doi.org/10.1016/j.funbio.2018.05.002.

[19] Castilla A, Panizza P, Rodríguez D, Bonino L, Díaz P, Irazoqui G, et al. A novel thermophilic and halophilic esterase from *Janibacter* sp. R02, the first member of a new lipase family (Family XVII). Enzyme Microb Technol 2017;98:86−95. Available from: https://doi.org/10.1016/j.enzmictec.2016.12.010.

[20] Ganasen M, Yaacob N, Rahman RNZRA, Leow ATC, Basri M, Salleh AB, et al. Cold-adapted organic solvent tolerant alkalophilic family I.3 lipase from an Antarctic *Pseudomonas*. Int J Biol Macromol 2016;92:1266−76. Available from: https://doi.org/10.1016/j.ijbiomac.2016.06.095.

[21] Florczak T, Daroch M, Wilkinson MC, Białkowska A, Bates AD, Turkiewicz M, et al. Purification, characterisation and expression in *Saccharomyces cerevisiae* of LipG7 an enantioselective, cold-adapted lipase from the Antarctic filamentous fungus Geomyces sp. P7 with unusual thermostability characteristics. Enzyme Microb Technol 2013;53:18−24. Available from: https://doi.org/10.1016/j.enzmictec.2013.03.021.

[22] Zhang JW, Zeng RY. Purification and characterization of a cold-adapted α-amylase produced by *Nocardiopsis* sp. 7326 isolated from Prydz Bay, Antarctic. Mar Biotechnol 2008;10:75−82. Available from: https://doi.org/10.1007/s10126-007-9035-z.

[23] Carrasco M, Alcaíno J, Cifuentes V, Baeza M. Purification and characterization of a novel cold adapted fungal glucoamylase. Microb Cell Fact 2017;16:1−10. Available from: https://doi.org/10.1186/s12934-017-0693-x.

[24] He L, Mao Y, Zhang L, Wang H, Alias SA, Gao B, et al. Functional expression of a novel α-amylase from Antarctic psychrotolerant fungus for baking industry and its magnetic immobilization. BMC Biotechnol 2017;17:1−13. Available from: https://doi.org/10.1186/s12896-017-0343-8.

[25] Martínez-Rosales C, Castro-Sowinski S. Antarctic bacterial isolates that produce cold-active extracellular proteases at low temperature but are active and stable at high temperature. Polar Res 2011;30. Available from: https://doi.org/10.3402/polar.v30i0.7123.

[26] Martinez A, Cavello I, Garmendia G, Rufo C, Cavalitto S, Vero S. Yeasts from sub-Antarctic region: biodiversity, enzymatic activities and their potential as oleaginous microorganisms. Extremophiles 2016;20:759−69. Available from: https://doi.org/10.1007/s00792-016-0865-3.

[27] Cavicchioli R, Charlton T, Ertan H, Omar SM, Siddiqui KS, Williams TJ. Biotechnological uses of enzymes from psychrophiles. Microb Biotechnol 2011;4:449−60. Available from: https://doi.org/10.1111/j.1751-7915.2011.00258.x.

[28] Makowski K, Białkowska A, Szczęsna-Antczak M, Kalinowska H, Kur J, Cieśliński H, et al. Immobilized preparation of cold-adapted and halotolerant Antarctic β-galactosidase as a highly stable catalyst in lactose hydrolysis. FEMS Microbiol Ecol 2007;59:535–42. Available from: https://doi.org/10.1111/j.1574-6941.2006.00208.x.

[29] Laye VJ, DasSarma S. An Antarctic extreme halophile and its polyextremophilic enzyme: effects of perchlorate salts. Astrobiology 2017;18. Available from: https://doi.org/10.1089/ast.2017.1766 ast.2017.1766.

[30] Aehle W. Enzymes in industry: production and applications. 3rd ed. Wiley-VCH; 2007.

[31] Kurita K. Chitin and chitosan: functional biopolymers from marine crustaceans. Mar Biotechnol 2006;8:203–26. Available from: https://doi.org/10.1007/s10126-005-0097-5.

[32] Walia A, Guleria S, Mehta P, Chauhan A, Parkash J. Microbial xylanases and their industrial application in pulp and paper biobleaching: a review. 3 Biotech 2017;7:1–12. Available from: https://doi.org/10.1007/s13205-016-0584-6.

[33] Yücel S, Terziolu P, Zime D. Lipase applications in biodiesel production. Biodiesel—feedstocks, production and applications.. InTech; 2012. <https://doi.org/10.5772/52662>.

[34] Jalil F, Rahman RA, Salleh R, Mohamad A. Optimization and in silico analysis of a cold-adapted lipase from an Antarctic *Pseudomonas* sp. strain AMS8 reaction in triton X-100 reverse micelles. Catalysts 2018;8:289. Available from: https://doi.org/10.3390/catal8070289.

[35] Grayson I, Kessler C. Modern applications of amino acids and dipeptides in pharmaceuticals and biopharmaceuticals. Chim Oggi/Chem Today 2015;33:46–51.

[36] Briggs D, Brookes C, Stevens R. Brewing science and practice. Woodhead Publishing; 2004.

[37] Mateo C, Palomo JM, Fernandez-Lorente G, Guisan JM, Fernandez-Lafuente R. Improvement of enzyme activity, stability and selectivity via immobilization techniques. Enzyme Microb Technol 2007;40:1451–63. Available from: https://doi.org/10.1016/j.enzmictec.2007.01.018.

[38] Núñez-Montero K, Barrientos L. Advances in Antarctic research for antimicrobial discovery: a comprehensive narrative review of bacteria from Antarctic environments as potential sources of novel antibiotic compounds against human pathogens and microorganisms of industrial importance. Antibiotics 2018;7:90. Available from: https://doi.org/10.3390/antibiotics7040090.

[39] Ulaganathan Y, Weber J-FF, Convey P, Rizman-Idid M, Alias SA. Antimicrobial properties and the influence of temperature on secondary metabolite production in cold environment soil fungi. Polar Sci 2017;14:60–7. Available from: https://doi.org/10.1016/j.polar.2017.09.005.

[40] Tedesco P, Maida I, Esposito FP, Tortorella E, Subko K, Ezeofor CC, et al. Antimicrobial activity of monoramnholipids produced by bacterial strains isolated from the Ross Sea (Antarctica). Mar Drugs 2016;14. Available from: https://doi.org/10.3390/md14050083.

[41] Chianese G, Esposito FP, Parrot D, Ingham C, de Pascale D, Tasdemir D. Linear aminolipids with moderate antimicrobial activity from the Antarctic gram-negative bacterium *Aequorivita* sp. Mar Drugs 2018;16. Available from: https://doi.org/10.3390/md16060187.

[42] Wang J, He W, Qin X, Wei X, Tian X, Liao L, et al. Three new indolyl diketopiperazine metabolites from the Antarctic soil-derived fungus *Penicillium* sp. SCSIO 05705. RSC Adv 2015;5:68736–42. Available from: https://doi.org/10.1039/c5ra10828d.

[43] Bruntner C, Binder T, Pathom-Aree W, Goodfellow M, Bull AT, Potterat O, et al. Frigocyclinone, a novel angucyclinone antibiotic produced by a *Streptomyces griseus* strain from Antarctica. J Antibiot (Tokyo) 2005;58:346–9. Available from: https://doi.org/10.1038/ja.2005.43.

[44] Niu S, Liu D, Hu X, Proksch P, Shao Z, Lin W. Spiromastixones A-O, antibacterial chlorodepsidones from a deep-sea-derived *Spiromastix* sp. fungus. J Nat Prod 2014;77:1021–30. Available from: https://doi.org/10.1021/np5000457.

[45] Wang J, Wei X, Qin X, Tian X, Liao L, Li K, et al. Antiviral merosesquiterpenoids produced by the Antarctic fungus *Aspergillus ochraceopetaliformis* SCSIO 05702. J Nat Prod 2016;79:59–65. Available from: https://doi.org/10.1021/acs.jnatprod.5b00650.

[46] Gesheva V, Vasileva-Tonkova E. Production of enzymes and antimicrobial compounds by halophilic Antarctic *Nocardioides* sp. grown on different carbon sources. World J Microbiol Biotechnol 2012;28:2069–76. Available from: https://doi.org/10.1007/s11274-012-1009-2.

[47] Thormar H. Lipids and essential oils as antimicrobial agents, <https://doi.org/10.1002/9780470976623>; 2010.

[48] Katzung BG, Masters SB, Trevor AJ. Basic and clinical pharmacology. 11th ed. McGraw-Hill Lange; 2009.

[49] Suh SS, Kim SM, Kim JE, Hong JM, Lee SG, Youn UJ, et al. Anticancer activities of ethanol extract from the Antarctic freshwater microalga, *Botryidiopsidaceae* sp. BMC Complement Altern Med 2017;17:1–9. Available from: https://doi.org/10.1186/s12906-017-1991-x.

[50] Wu G, Lin A, Gu Q, Zhu T, Li D. Four new chloro-eremophilane sesquiterpenes from an Antarctic deep-sea derived fungus, *Penicillium* sp. PR19N-1. Mar Drugs 2013;11:1399–408. Available from: https://doi.org/10.3390/md11041399.

[51] Kim D, Lee EJ, Lee J, Leutou AS, Shin YH, Choi B, et al. Antartin, a cytotoxic zizaane-type sesquiterpenoid from a *Streptomyces* sp. Isolated from an Antarctic marine sediment. Mar Drugs 2018;16:1–10. Available from: https://doi.org/10.3390/md16040130.

[52] Li L, Li D, Luan Y, Gu Q, Zhu T. Cytotoxic metabolites from the Antarctic psychrophilic fungus *Oidiodendron truncatum*. J Nat Prod 2012;75:920–7. Available from: https://doi.org/10.1021/np3000443.

[53] Zheng L, Zhu X, Yang K, Zhu M, Farooqi A, Kang D, et al. PBN11-8, a cytotoxic polypeptide purified from marine *Bacillus*, suppresses invasion and migration of human hepatocellular carcinoma cells by targeting focal adhesion kinase pathways. Polymers (Basel) 2018;10:1043. Available from: https://doi.org/10.3390/polym10091043.

[54] Zheng L, Yang K, Liu J, Sun M, Zhu J, Lv M, et al. Screening of microorganisms from Antarctic surface water and cytotoxicity metabolites from Antarctic microorganisms. Food Sci Nutr 2016;4:198–206. Available from: https://doi.org/10.1002/fsn3.273.

[55] Dewick PM. Medicinal natural products: a biosynthetic approach. 3rd ed. Wiley; 2009.

[56] Modzelewska A, Sur S, Kumar S, Khan S. Sesquiterpenes: natural products that decrease cancer growth. Curr Med Chem Agents 2005;5:477–99. Available from: https://doi.org/10.2174/1568011054866973.

[57] Lu X, Lu D, Scully M, Kakkar V. The role of integrins in cancer and the development of anti-integrin therapeutic agents for cancer therapy. Perspect Med Chem 2008;2008:57–73.

[58] Bang JK, Lee JH, Murugan RN, Lee SG, Do H, Koh HY, et al. Antifreeze peptides and glycopeptides, and their derivatives: potential uses in biotechnology. Mar Drugs 2013;11:2013−41. Available from: https://doi.org/10.3390/md11062013.

[59] Muñoz PA, Márquez SL, González-Nilo FD, Márquez-Miranda V, Blamey JM. Structure and application of antifreeze proteins from Antarctic bacteria. Microb Cell Fact 2017;16:1−13. Available from: https://doi.org/10.1186/s12934-017-0737-2.

[60] Firdaus-Raih M, Hashim NHF, Bharudin I, Bakar MFA, Huang KK, Alias H, et al. The *Glaciozyma antarctica* genome reveals an array of systems that provide sustained responses towards temperature variations in a persistently cold habitat. PLoS One 2018;13:1−18. Available from: https://doi.org/10.1371/journal.pone.0189947.

[61] Kim HJ, Koo BW, Kim D, Seo YS, Nam YK. Effect of marine-derived ice-binding proteins on the cryopreservation of marine microalgae. Mar Drugs 2017;15:13−15. Available from: https://doi.org/10.3390/md15120372.

[62] Jung W, Gwak Y, Davies PL, Kim HJ, Jin ES. Isolation and characterization of antifreeze proteins from the Antarctic marine microalga *Pyramimonas gelidicola*. Mar Biotechnol 2014;16:502−12. Available from: https://doi.org/10.1007/s10126-014-9567-y.

[63] Gwak IG, sic Jung W, Kim HJ, Kang SH, Jin ES. Antifreeze protein in Antarctic marine diatom, *Chaetoceros neogracile*. Mar Biotechnol 2010;12:630−9. Available from: https://doi.org/10.1007/s10126-009-9250-x.

[64] Lloyd JR, Byrne JM, Coker VS. Biotechnological synthesis of functional nanomaterials. Curr Opin Biotechnol 2011;22:509−15. Available from: https://doi.org/10.1016/j.copbio.2011.06.008.

[65] Gallardo C, Monrás JP, Plaza DO, Collao B, Saona LA, Durán-Toro V, et al. Low-temperature biosynthesis of fluorescent semiconductor nanoparticles (CdS) by oxidative stress resistant Antarctic bacteria. J Biotechnol 2014;187:108−15. Available from: https://doi.org/10.1016/j.jbiotec.2014.07.017.

[66] Plaza DO, Gallardo C, Straub YD, Bravo D, Pérez-Donoso JM. Biological synthesis of fluorescent nanoparticles by cadmium and tellurite resistant Antarctic bacteria: exploring novel natural nanofactories. Microb Cell Fact 2016;15:1−11. Available from: https://doi.org/10.1186/s12934-016-0477-8.

[67] Bazylinski D, Lefèvre C. Magnetotactic bacteria from extreme environments. Life 2013;3:295−307. Available from: https://doi.org/10.3390/life3020295.

[68] Uebe R, Schüler D. Magnetosome biogenesis in magnetotactic bacteria. Nat Rev Microbiol 2016;14:621−37. Available from: https://doi.org/10.1038/nrmicro.2016.99.

[69] Lin W, Zhang W, Zhao X, Roberts AP, Paterson GA, Bazylinski DA, et al. Genomic expansion of magnetotactic bacteria reveals an early common origin of magnetotaxis with lineage-specific evolution. ISME J 2018;12:1508−19. Available from: https://doi.org/10.1038/s41396-018-0098-9.

[70] Abreu F, Carolina A, Araujo V, Leão P, Silva KT, Carvalho FM, et al. Culture-independent characterization of novel psychrophilic magnetotactic cocci from Antarctic marine sediments. Environ Microbiol 2016;18:4426−41. Available from: https://doi.org/10.1111/1462-2920.13388.

Chapter

Biomineralization of Magnetosomes: Billion-Year Evolution Shaping Modern Nanotools

Tarcisio Nascimento Correa, Igor Nunes Taveira, Rogerio Presciliano de Souza Filho and Fernanda de Avila Abreu

Abstract

Biomineralization in the microbial realm usually gives origin to finely structured inorganic nanomaterials. Perhaps, one of the most elegant bioinorganic processes found in nature is the iron biomineralization into magnetosomes, which is performed by magnetotactic bacteria. A magnetosome gene cluster within the bacterial genome precisely regulates the mineral synthesis. The spread and evolution of this ability among bacteria are thought to be a 2,7-billion-year process mediated by horizontal gene transfers. The produced magnetite or greigite nanocrystals coated by a biological membrane have a narrow diameter dispersibility, a highly precise morphology, and a permanent magnetic dipole due to the molecular level control. Approaches inspired by this bacterial biomineralization mechanism can imitate some of the biogenic nanomagnets characteristics in the chemical synthesis of iron oxide nanoparticles. Thus, this chapter will give a concise overview of magnetosome synthesis's main steps, some hypotheses about the evolution of magnetosomes' biomineralization, and approaches used to mimic this biological phenomenon *in vitro*.

Keywords: magnetotactic bacteria, magnetosomes, magnetic nanoparticles, magnetite, magnetosome gene cluster, horizontal gene transfer, biomimetics

1. Introduction

Among everything that is known in Microbiology, magnetotactic bacteria (MTB) are known to perform one of the finest examples of a controlled biomineralization process. MTB were first observed in the late 1950s, by the medical Doctor Salvatore Bellini in the Italian city of Pavia and later described in Massachusetts by Richard Blakemore in the 1970s [1, 2]. MTB are known to align its motility axis to the geomagnetic field and use it for orientation. When observed under the light microscope, MTB present unidirectional swimming to the North or South Magnetic Poles from an applied external magnetic field (a magnet); this behavior is called magnetotaxis [3]. This behavior occurs due to the presence of magnetic

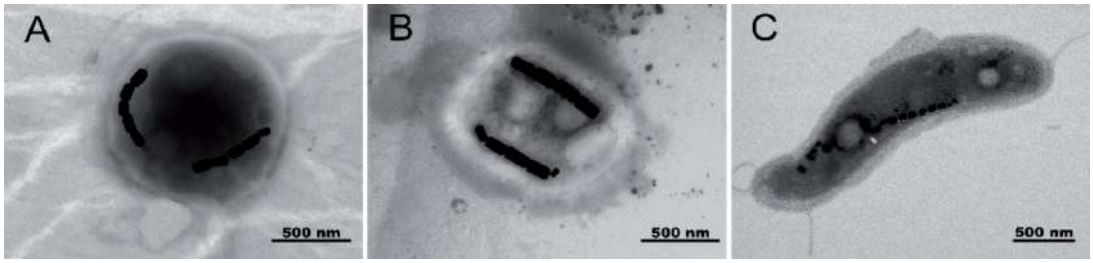

Figure 1.
Transmission electron microscopy of: (A) uncultured coccoid magnetotactic bacteria from Monsimet Cove, Antarctica. (B) Uncultured coccoid magnetotactic bacteria from Punta Ullman, Antarctica. (C) Magnetovibrio blakemorei strain MV-1^{T}.

nanocrystals—the magnetosomes—, usually aligned in single or multiple chains within the bacterial cytoplasm (**Figure 1**), and flagellar propulsion guided by chemotaxis [3]. In a simple way, chemotaxis in MTB is assisted by bacterial orientation along Earth's magnetic field (magnetotaxis). Therefore, magnetotaxis allows MTB to find the optimum position for survival and growth in a chemically stratified water column, seeking for an optimum environment where proton motive driving force reaches maximum potential. For MTB, which are frequently microaerophilic or anaerobic microrganisms, this environment is near the oxic/anoxic interface [4].

Magnetosomes are composed of a magnetic nanoparticle in most cases composed of magnetite (Fe_3O_4) and sometimes greigite (Fe_3S_4) with species specific shapes and sizes, and enveloped by a phospholipid bilayer with associated proteins, which constitutes the magnetosome membrane (MM) [3]. The gene regulation of magnetosome biomineralization (MB) and organization within the cell will be discussed in more detail in the sections ahead. Based on the total iron amount within a magnetotactic bacterium cell, MTB appear to play a major role in the biogeochemical cycling of iron [5]. MTB through magnetosome synthesis,

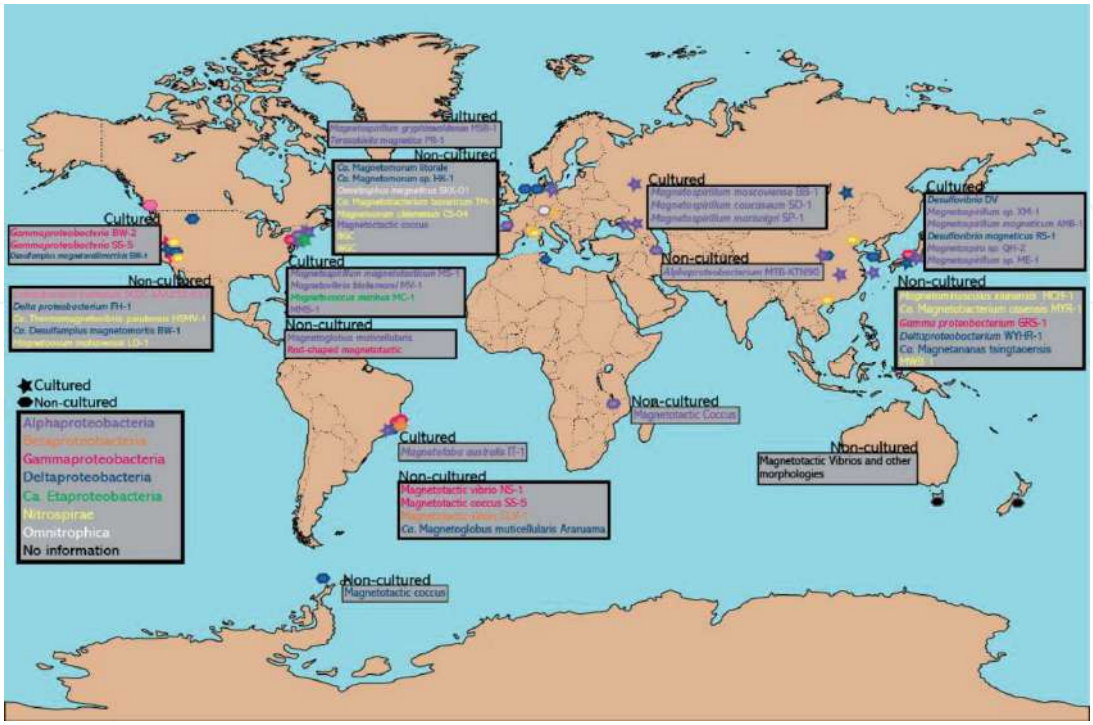

Figure 2.
Map of the distribution of known cultured and non-cultured magnetotactic bacteria across de world by phylogenetic group (see the correspondence between taxa and colors on the bottom left corner of the image).

assimilate the iron solubilized in the environment to an inorganic crystal. After cell lysis, the magnetosome is deposited in the sediment, forming what is known as magnetofossils [6]. Besides, MTB can be ingested by protozoans, and the iron from magnetosomes is, then, incorporated in the food chain [7]. Apart from iron and based on their physiology, MTB seem to have relevant roles in other biogeochemical cycles of sulfur, nitrogen, and carbon [8].

MTB are an extremely diverse group of Gram-negative bacteria with a variety of morphotypes (i.e., rods, vibrios, spirilla, coccoid, and ovoid) and species affiliated to Proteobacteria (Alpha-, Beta-, Gamma-, Delta-, and *Ca.* Etaproteobacteria class), Omnitrophica and Nitrospirae phyla [9]. MTB affiliation to other taxa have been proposed based on metagenomics studies, but observation of the magnetosomes was not performed to confirm this matter. This great diversity is reflected in MTB ubiquity in almost all aquatic habitats across the Earth (**Figure 2**), including extreme environments such as thermal trenches and saline-alkaline lakes [6, 10]. More than being interesting species for their unique evolutionary process and ecological importance, MTB are also proving to be of interest for biotechnological applications. Their unique physiology makes MTB potential bioremediators of heavy metals and magnetosomes can be extracted and used as nanotools for magnetic controlled drug targeting, contrast agents for magnetic resonance imaging, enzyme immobilization and many more industrial and biomedical applications [11].

2. Steps of magnetosome biomineralization in MTB

MB is highly regulated at the genetic level [12]. Magnetosome gene clusters (MGCs) [13], structured as *operons*, are responsible for MB in MTB. MTB genomes contain: (i) conserved *mam* genes, encountered in all MTB; and (ii) restricted genes encountered in some phylogenetic groups of MTB [14]. Examples of genes restricted to certain MTB are: (i) *mms* (from magnetosome membrane specific) genes found in magnetotactic Proteobacteria; (ii) *mad* (from magnetosome associated Deltaproteobacteria), which were first reported in magnetotactic deltaproteobacteria [15] and recently encountered in MTB affiliated to Omnitrophica and Nitrospirae phyla [9]; and (iii) *man* (from magnetosome genes in Nitrospirae), which are genes reported in MTB affiliated to Nitrospirae phylum [16]. Comprehension of MB were inferred by *mam* and *mms* genes deletion in the cultured magnetotactic alphaproteobacteria *Magnetospirillum magneticum* strain AMB-1 and *Magnetospirillum gryphiswaldense* strain MSR-1 [14]. Precise *man* and *mad* genes roles in MB remain unclear as they were studied in uncultured MTB [16], thus genetic systems to test gene function is not available.

As previously described, MTB are capable of biomineralizing magnetosomes, an organelle with a ferrimagnetic mineral core surrounded by a biological membrane [3]. A series of complex mechanisms occur in order to transform the environmental bioavailable iron into a complete and fully functional magnetic organelle. MB process involves different steps such as iron uptake, magnetosome vesicle formation, specific protein recruiting, crystal nucleation, redox balance, and pH control in magnetosome vesicle, size and crystalline morphology control and magnetosome vesicle docking in the bacterial cytoskeleton [3].

Mam and Mms proteins involved in MB belong to different protein families including: TPR proteins (from Tetratrico Peptide Repeat; MamA) [17], CDF transporters (Cation Diffusion Facilitators: MamB and MamM) [14, 18], serine proteases HtrA-like (MamE, MamP, and MamO) [14], actine-like proteins (MamK) [19], liposome tubulation protein (MamY) [20], generic transporters (MamH and MamN) [14, 21] and MTB specific proteins without prior homology in other non-magnetotactic microrganisms

(MamG, MamF, MamD, MamC, MamJ, MamW, MamX, MamY, Mms6, MtxA) [3]. MB involves four major steps as they are: (i) MM formation (participation of MamI, MamL and MamAB proteins) [3, 14]; (ii) crystal nucleation (which include MamE, Mms6, MamB and MamM) [3, 14]; (iii) crystal maturation (participation of MamE, MmsF, MamGFDC and Mam P, S, T) [3, 14]; and (iv) magnetosome chain alignment within cell body (participation of MamJ, MamK and MamY) [14, 20]. Mam and Mms protein functions involved in MB are described in **Table 1** and **Figure 3**.

Protein	*Operon*	Function	MTB strain	Reference
MamA	*mam*AB	Protein recruitment	AMB-1	[23]
MamB	*mam*AB	Membrane invagination and iron uptake	AMB-1/ MSR-1	[14, 18]
MamC	*mam*GFDC	Size and morphology control	AMB-1	[24]
MamD	*mam*GFDC	Size and morphology control	AMB-1	[24]
MamE	*mam*AB	Protein targeting and redox control	AMB-1	[14]
MamF	*mam*GFDC	Size control	AMB-1	[24]
MamG	*mam*GFDC	Size and morphology control	AMB-1	[24]
MamH	*mam*AB	Iron uptake	AMB-1/ MSR-1	[14, 21]
MamI	*mam*AB	Membrane invagination	AMB-1	[14]
MamJ	*mam*AB	Magnetosome alignment	MSR-1	[25]
MamK	*mam*AB	Magnetosome alignment	MSR-1	[19]
MamL	*mam*AB	Membrane invagination	AMB-1	[14]
MamM	*mam*AB	Iron uptake	AMB-1/ MSR-1	[14, 18]
MamN	*mam*AB	pH control	AMB-1	[14]
MamO	*mam*AB	Crystal nucleation	AMB-1/ MSR-1	[14, 26]
MamP	*mam*AB	Redox control	AMB-1	[14]
MamQ	*mam*AB	Membrane invagination	AMB-1	[14]
MamR	*mam*AB	Size and morphology control	AMB-1	[14]
MamS	*mam*AB	Size and morphology control	AMB-1	[14]
MamT	*mam*AB	Size e morphology control and redox control	AMB-1	[27]
MamU	*mam*AB	Not defined	AMB-1	[14]
MamV	*mam*AB	Not defined	MSR-1	[18]
MamW	*mam*AB	Magnetosome alignment	MSR-1	[28]
MamX	*mam*XY	Redox control	MSR-1	[21]
MamY	*mam*XY	Membrane invagination and magnetosome alignment	AMB-1/ MSR-1	[20, 29]
MamZ	*mam*XY	Iron uptake and redox control	MSR-1	[21]
Mms6	*mms6*	Size and morphology control	AMB-1	[30]
MmsF	*mms6*	Size and morphology control	AMB-1	[31]

Table 1.
Mam and Mms protein functions inferred by mutant construction in the cultured magnetotactic alphapreoteobacteria Ms. magneticum strain AMB-1 and Ms. gryphiswaldense strain MSR-1.

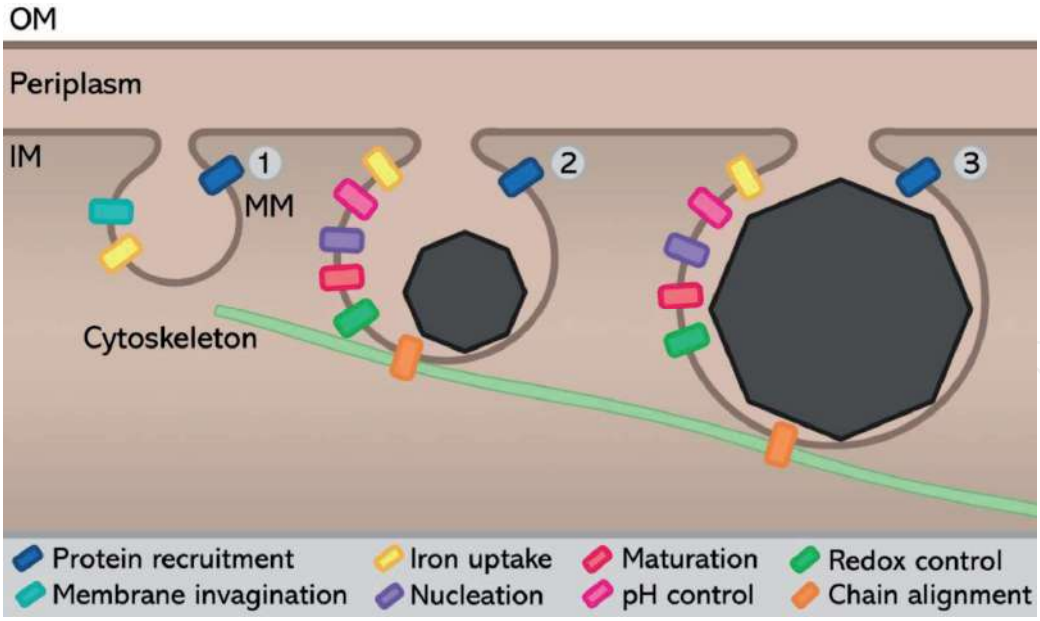

Figure 3.
Three major steps of MB in MTB. 1st step: protein recruitment initiating the biomineralization process while forming the invagination of the magnetosome membrane (MM) and iron uptake. 2nd step: Crystal nucleation, characterized by the incorporation of iron and oxygen for magnetite biomineralization. Interestingly, oxygen for the synthesis of magnetite is derived from water [22]. So far, the sulfur source for the synthesis of greigite has not been clarified. Magnetosome begins to grow in size while morphology, pH and redox balance are strictly regulated. Magnetosomes are aligned in chains within the cell's cytoskeleton. 3rd step: Magnetosomes continue to grow under strict regulation until de crystal maturation is complete. OM: outer membrane; IM: inner membrane, meaning the cytoplasmic membrane.

The advances of molecular biology techniques provided a much greater understanding of the MB mechanism over the last years as cultured and environmental MTB had their genomes sequenced. Magnetite MGCs and magnetite magnetosomes were studied in magnetotactic proteobacteria affiliated to the classes Alpha- [32–36], Beta- [37], Gamma- [38, 39], Delta- [40–43], *Ca.* Eta- [9, 32, 44, 45], *Ca.* Lambda- [9] and Zetaproteobacteria [9] and MTB affiliated to Nitrospirae [13, 16, 46–50] and Omnitrophica [49] phyla. Greigite MGC and greigite magnetosomes were characterized in magnetotactic deltaproteobacteria [51, 52] and MTB affiliated to *Ca.* Latescibacteria [8] and Planctomycetes [9] phyla. Culturing environmental MTB and mutant constructs different from the already known magnetotactic alphaproteobacteria *Ms. magneticum* strain AMB-1 and *Ms. gryphiswaldense* strain MSR-1 may provide a greater comprehension of the MB mechanism.

3. Evolutionary history of MGCs within Bacteria domain

MGC origin and evolution within the Bacteria domain is a constantly discussed topic in the literature. The scattering of MGCs and the magnetotactic behavior raises questions as MTB encompasses high diversity regarding their ecology, metabolism, and phylogeny. The first proposed hypothesis was the polyphyletic origin of magnetite and greigite MB [53]. According to this hypothesis, biomineralization of greigite and magnetite magnetosomes would have evolved without sharing a last universal common ancestor of magnetotactic bacteria (LUCA MTB). At that time MGCs were not discovered. Thus, this assumption relied on the information that the biochemical and nutritional parameters for greigite and magnetite biomineralization are different. Likewise, all known MTB affiliated to Alphaproteobacteria synthesized magnetite magnetosomes, while the ones affiliated to Deltaproteobacteria

synthesized greigite magnetosomes, thus permitting the inference the polyphyletic hypothesis. Years later, after the discovery of MGCs, similarities between *mam* genes of magnetite and greigite MTB showed a common ancestor for both minerals synthesis in MTB [54]. It is speculated that greigite MGCs originated after events of duplication and divergence from magnetite MGCs in sulfate-reducing bacteria like the multicellular magnetotactic prokaryote (MMP) *Ca.* Magnetoglobus multicellularis strain Araruama affiliated to Deltaproteobacteria [54].

On behalf of that, Lefèvre and colleges [55] hypothesized a monophyletic origin of MGCs concerning magnetotactic proteobacteria. The comparison of 16S rRNA gene and conserved Mam proteins evolution showed a convergence of both phylogenetic inferences. It was suggested that MTB affiliated to Proteobacteria phyla shared a LUCA MTB and over time, some proteobacteria would have lost the MGC, resulting in the inability of biomineralizing magnetosomes [55].

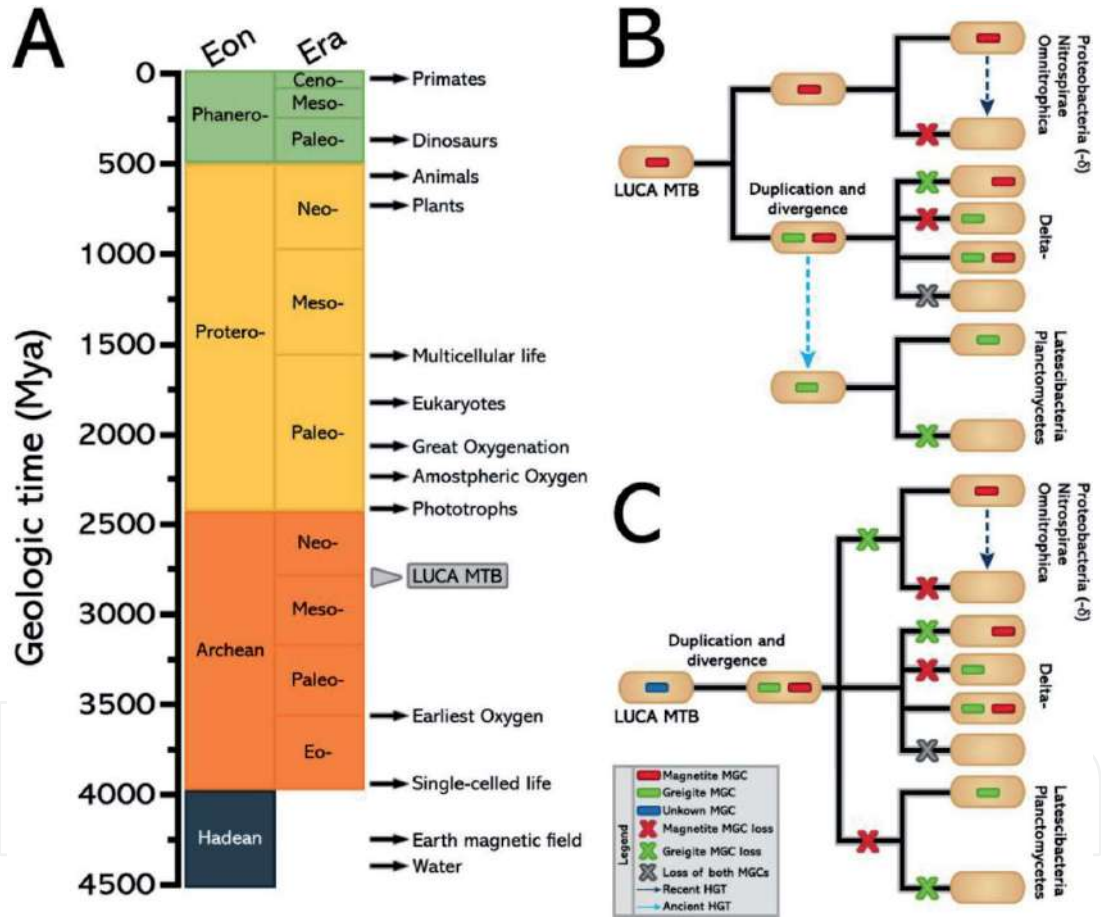

Figure 4.
Geologic time and evolution model proposed for MGC and magnetotaxis evolution. (A) Geologic rule in million years ago (Mya). LUCA MTB origin (gray arrowhead) is estimated 2.7 billion years ago during the Archean eon. The first single-celled form of life originated ~4 billion years ago and the origin of phototrophs, that permitted great oxygenation in earth, only happened ~2.4 billion years ago. (B and C) Two models for MGC and magnetotaxis evolution adapted from [9]. (B) LUCA MTB containing magnetite MGC branched two MTB lineages: (i) MTB affiliated to Proteobacteria (without Delta-), Nitrospirae and Omnitrophica phyla with recent HGT events responsible for MGC scattering; and (ii) MTB affiliated to Deltaproteobacteria class that after events of duplication and divergence hosted microbes with magnetite, greigite or both MGCs. Ancient HGT events would have been responsible for greigite MGC acquaintance in Plantomycetes and Ca. Lastescibacteria phyla. Adapted from [9]. (C) LUCA MTB containing an unknown MGC after events of duplication and divergence gave origin for both magnetite and greigite MGC. A monophyletic origin is proposed for MTB affiliated to Proteobacteria (without Delta- class), Nitrospirae, Omnitrophica, Planctomycetes and Ca. Latescibacteria phyla and Deltaproteobacteria class. Recent HGT events originating from MTB affiliated to Proteobacteria (without Delta- class), Nitrospirae, Omnitrophica could have been responsible for the scattering of MGC and magnetotactic behavior. Adapted from [9].

Opposing all previous statements, a considerable number of authors proposed the importance and influence of horizontal gene transfer (HGT) events on the evolution and scatter of MGC in Bacteria domain [9, 13, 56–59]. In light of these events, different non-MTB would have received MGCs by HGT, granting them the capacity of biomineralizing magnetosomes [9].

The origin of MB was dated, by molecular Bayesian clock, before the divergence of the Nitrospirae and Proteobacteria phyla during the Archean eon [13]. The divergence happened 2.7 billion years ago before the appearance of phototrophs and Great Oxygenation at the time of Paleoproterozoic on the Proterozoic eon (**Figure 4**). This hypothesis is supported by: (i) low pressure or absence of O_2 in the atmosphere and anoxic oceans in Archean [60]; (ii) abundant dissolved Fe^{2+} as concentrations of 40 to 120 μmol/L [61]; (iii) presence of primary electron donors of Earth early ecosystems such as H_2, H_2S, S^0, Fe^{2+}, CH_4, NH_4^+ and CH_2O [62]; and (iv) presence of primary electron acceptors of Earth early ecosystems such as CO_2, CO, SO_4^{2-}, NO, NO_2^- and NO_3^- [62]. These conditions favored the survival and growth of MTB [13]. Known examples of such conditions that are in accordance with available resources of primitive Earth are: (i) microaerophilic or anaerobic respiration in all known MTB; (ii) chemolithoautotrophy as MTB are capable of CO_2 fixation by Calvin–Benson–Bassham cycle, the reverse tricarboxylic acid cycle, or the reductive acetyl-CoA pathway [63]; (iii) capacity of denitrification of NO, NO_2^- and NO_3^- [16, 49]; (iv) capacity of oxidizing H_2S via sulfur oxidation pathway [16, 49]; (v) water temperature ranging from 26 to 85°C [64, 65] compatible with MTB growth as there are psychrophilic [66], mesophilic [8] and moderately thermophilic MTB [47]. Alongside these conditions, Earth's magnetic field originated 4.2 billion years ago enduring several inversions until the present time [67]. Considering this panorama, it is plausible that MTB and the geomagnetic fields have coevolved selecting the ones capable of undergoing all the continuous biotic and abiotic variations [13].

Large scale metagenome approach of MTB diversity demonstrated two possible routes concerning MGC evolution over time [9]. It is hypothesized that a LUCA MTB contained magnetite or an unknown MGC followed by events of MGC duplication, divergence, and loss combined with ancient and recent HGT events could explain the scattering of the magnetotactic behavior in the Bacteria domain [9] (**Figure 4**). The unending studies regarding MTB diversity and ecology are indispensable for an accurate decipherment of MGC evolution in the Bacteria domain.

4. Influence of the medium on biomineralization

The fact that related magnetotactic strains synthesize magnetosomes with significant differences in sizes and elongation is a clue that, despite a rigorous genetic control, environmental factors may influence the characteristics of the biomineralized nanocrystals [68]. Extensive experiments performed in cultures of MTB have pointed out temperature, pH, iron concentration, oxygen concentration, external magnetic fields, and nutrient concentrations as important factors driving physical changes in magnetosomes [69].

Ferric iron concentrations exert an important influence on the magnetic properties of *Magnetospirillum magnetotacticum* strain MS-1 cells due to alterations within biogenic magnetite [70]. The coercive force (H_C), probably the most important criterion in the selection of magnetic nanoparticles for technological applications, is significantly affected [70]. The H_C was increased from 216 Oe when cells were cultured at 12 μM Fe^{3+} to 238 Oe at 68 μM [70].

In another study, it was shown that reducing conditions leads to an increase in magnetosomes crystals of *Ms. magneticum* strain AMB-1 in culture [71]. An oxidoreduction

potential of 0 mV (neutral condition) led to a crystal diameter of 31.5 ± 1.3 nm, which augmented to 37.2 ± 0.6 nm when the culture was carried out at -500 mV (reducing condition) [71]. The reducing condition also caused an increase in the total magnetite mass per cell as 9.1 ± 1.9 magnetosomes were observed per μm (cell length), in contrast to 5.48 ± 1.3 in neutral condition.

The evidence that characteristics of biogenic magnetite can be modified is of great interest for practical applications because certain purposes may require specific particle properties. Therefore, the knowledge of the interplay between environmental conditions and process regulation by biomolecules in biomineralization can help develop methods for the *in vitro* biomimetic preparation of magnetic nanoparticles with tunable properties.

5. Microbes inspire chemistry: biomimetic synthesis of artificial nanoparticles

Understanding MB is key not only for the in-depth learning of microbial physiological phenomena, but it can teach us valuable insights for the fabrication of technological materials. Magnetic nanoparticles have emerged as functional materials since the 1940s, when iron oxide powders, with crystals ranging from 60 nm to 1 μm, were used to impregnate recording tapes [72]. In that media, recorded information was engraved through changes in magnetization of the impregnated nanoparticles. Similarly, the biogenic magnetosomes can carry paleomagnetic signals, which can be detected, for instance, through the measurement of their magnetic properties in marine sediments [73]. The roles of bacterial magnetite as magnetofossils is only possible due to their stable single magnetic domain, caused by their controlled size range (20–100 nm) [73, 74]. This magnetic property also permits the utilization of biogenic nanomagnets in research on anticancer and antimicrobial therapy—as drug carriers, contrast agents, and hyperthermal agents—, enzyme immobilization—as recyclable supports—, cell labeling and other applications [11].

Biological materials are precisely arranged at the nanoscale. Hence, biomimetics, which is the art of imitating biological process to architecture novel materials, is proving profitable for nanotechnology industries [75]. One of the foundations of biomimetics is the biodiscovery and bioengineering of surface-binding proteins and peptides [76]. The regular structures present in such biomolecules enables the recognition and the interaction with atomic patterns on the surface of synthetic polymers, semiconductors, and metal oxide crystals [76]. In the case of metal oxides, these interactions occur basically via non-covalent weak bindings like hydrogen bonds and electrostatic dipoles.

In chemical syntheses, the shape- and size-controlled nanoparticles generally are obtained with high temperatures and organic solvents [74]. These consumptions are related to high production costs and environmental impacts during the life cycle of the nanoparticles [74]. One of the simplest and widely utilized techniques for making iron oxide nanoparticles is coprecipitation [74]. In this technique, ferrous and ferric salts are dissolved, and the cations are precipitated in an alkaline aqueous medium. For the synthesis of magnetite, a fixed molar proportion of 2:1 (Fe^{3+}/Fe^{2+}), is precipitated, following the stoichiometry:

$$2Fe^{3+} + Fe^{2+} + 8OH^{-} \rightarrow Fe_3O_4 + 4H_2O$$

This molar proportion is mandatory because it is the same ferrous/ferric ratio within magnetite [77]. In MTB, iron is accumulated inside the magnetosome vesicle

in it ferrous form before being oxidized to ferric ion by magnetochromes—oxidizing domains of MamP, MamX, MamT and MamE [77]. This is an example of naturally occurring partial oxidation of ferrous ion. Partial oxidation is also used to obtain artificial, biomimetic magnetite [78]. In this case, the ferrous cation is precipitated to form ferrous hydroxide ($Fe(OH)_2$). After that, a strong oxidizing agent, usually nitrate, partially transform Fe^{2+} to Fe^{3+}, leading to magnetite:

$$Fe^{2+} + 2OH^- \rightarrow Fe(OH)_2$$

$$3Fe(OH)_2 + NO_3^- \rightarrow Fe_3O_4 + 3H_2O + NO_2^-$$

While coprecipitation leads to nanoparticles of an irregular shape, partial oxidation magnetite has a well-defined faceted morphology and a larger size [78]. Due to its low solubility, $Fe(OH)_2$ tends to form larger precipitates. This is not the case for the coprecipitation of Fe^{3+} and Fe^{2+}, which tends to form multiple, smaller precipitates [78].

Complementary to oxidation control, the surface interaction of the forming magnetic crystal with biomolecules is the main strategy for synthesizing magnetosome-like nanoparticles. A summary of biomolecule-supplemented chemical syntheses of magnetic nanoparticles is in **Table 2**.

MamC protein from *Magnetococcus marinus* strain MC-1 has an effect of enlarging magnetite precipitates [79, 84]. Due to its effect over synthesis, this protein has been expressed for use in different biomimetics studies (**Figure 5**). Different coprecipitation experiments have shown an increase from ~10-25 nm, in control synthesis, to ~30-40 nm, when recombinant MamC from strain MC-1 is added in concentrations over 10 μg/mL [79, 84].

In another study, *Ms. magneticum* strain AMB-1-derived Mms6 displays a negative effect on average particle size – 20 nm length down from 32 nm in the control experiment – in partial oxidation and coprecipitation-derived magnetite [80]. Instead, its addition to the reactional medium narrows size distribution regardless of the chemical route. The presence of recombinant Mms6 derived from strain AMB-1 imprints the cubo-octahedral morphology of the naturally occurring magnetosomes onto chemically precipitated crystals. From experiments using mutant clones of strain AMB-1, it has been demonstrated that the anionic residues Asp123, Glu124, and Glu125 effectively participate as key residues of Mms6 for defining crystal morphology are in the protein binding to magnetite [88]. The interactions between these C-terminal side-groups and the magnetite surface ultimately respond for the strong morphology and size controlling character of Mms6 either in biologic or biomimetic mineralization [89].

To modulate/improve magnetite chemical synthesis by the use MB proteins, magnetite-interacting components (MICs) of three magnetite-associated proteins (MamC, Mms6, and Mms7) have been subjected to NMR studies to investigate their affinity and binding to the ferrous ion during coprecipitation [81]. In all cases, it has been a clear role of aspartate and glutamate residues to the affinity to the cation [81]. The strong binding of ferrous cation to four anionic residues is related to confinement of iron by Mms6- and Mms7- MICs and, consequently, to the initiation of magnetite nucleation by these proteins. Besides ferrous ion, Mms6 glutamate residues positions 44, 50, and 55 at C-terminal region shows a strong binding affinity to ferric ion [90]. MamC-MIC, in turn, displays a weaker iron-binding but a stronger effect on magnetite size [81]. Thus, the ionotropic (i.e. iron-affinity) effect of MamC does not give sufficient ground for the role of this protein in

Additive(s)	Synthesis	Size (nm)	Shape	Ms (emu/g)	References
Magnetosomal proteins					
MamC	CP	30–40	Rhomboid	—	[79]
Mms6	PO	20.2 ± 4.0	Cubo-octahedral	—	[80]
MamC-MIC	CP	26.1 ± 0.61	Cuboid	—	[81]
Mms6-MIC		19.9 ± 0.36	Rhomboid	—	
Mms7-MIC		18.54 ± 0.29	Cuboid	—	
MmsF	CP	36	Rounded	129	[82]
MamF		25	Irregular	44	
Active loop of MmsF	CP	50 ± 13	Cuboidal	90	[83]
Active loop of Mms13		34 ± 12	Irregular	93	
MamC + Mms6	CP	30 ± 10	Rhomboid	—	[84]
Aminoacids					
Lysine (0.1 to 10 mM)	CP	21 ± 7 to 29 ± 7	Rhomboid	67 (for 10 mM Lys)	[85]
Arginine (0.1 to 10 mM)		16 ± 7 to 19 ± 6	—	36 (for 10 mM Arg)	
Polyaminoacids and polypeptides					
Polyarginine	CP	35 ± 5	Irregular	—	[86]
Polyaspartate	PO	7.6 ± 1.5	Rounded	78	[78]
14-mer peptide (magnetite-binding domain + ovarian cancer target) + ginger extract	CP	7.35 ± 3.7	Irregular	48.9	[87]

M_s = magnetization saturation at 300 K; CP = coprecipitation; PO = partial oxidation; MIC = magnetite-interacting component.

Table 2.
Summary of methods for chemical synthesis of biomimetic magnetic nanoparticles.

biomineralization [84, 91, 92]. MamC must exert a template effect in magnetite formation [84]. In the MM, MamC is constituted by two transmembrane domains connected by alpha-helical looping, which contacts the forming magnetite within the magnetosome vesicle lumen [92]. The distance between iron-interacting residues Glu66 and Asp70 of the alpha-helical looping matches the iron interatomic distance within the magnetite surface plane. The alpha-helical conformation of the MamC-MIC ensures the proper positioning of the points of interaction with iron [91]. The complementary roles of MamC and Mms6 can be combined in a biomimetic synthesis, yielding large magnetosomes (30 ± 10 nm) with well-defined crystal faces [84].

Other MM proteins are also good candidates for use in biomimetics. MamF controls the size monodispersity of nanocrystals. In aqueous solution, this protein forms a self-aggregative proteinosome of approximately 36 nm [82]. When used as an additive in coprecipitation, homogeneously sized nanocrystals are obtained. As in MamC, Mms13 and MmsF have their active loops located between the two transmembrane domains [83]. These active loops were expressed in a chimeric coiled-coil scaffold protein, which was called Mms13cc and MmsFcc. The MmsFcc construct regulated the cuboidal morphology of the produced nanocrystals.

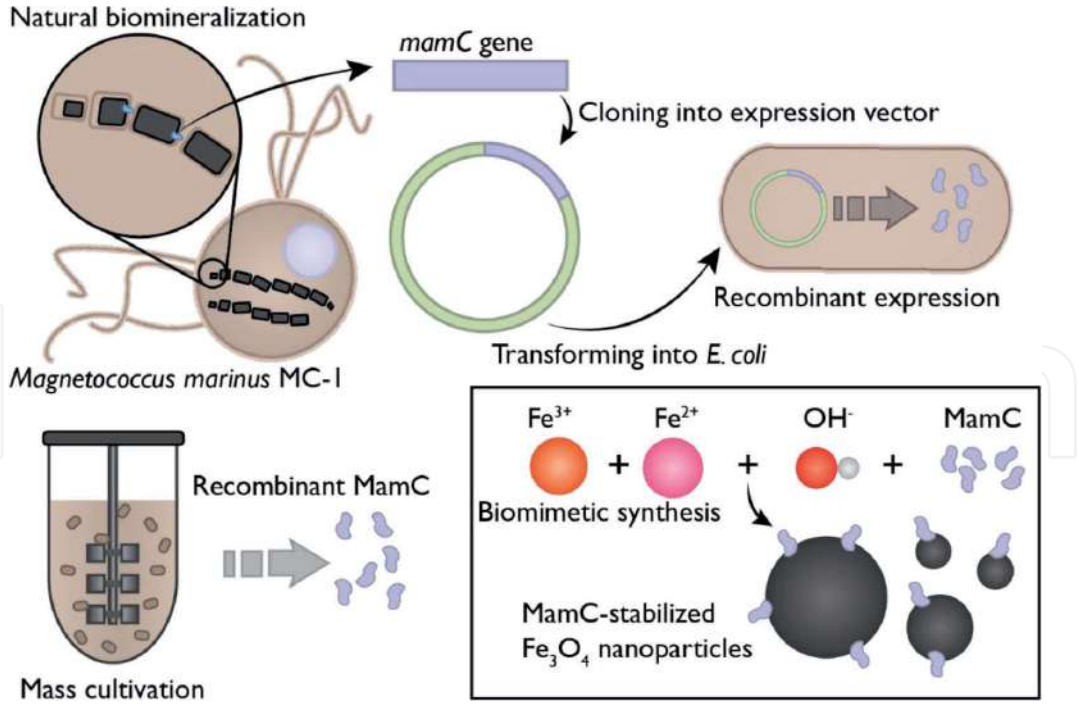

Figure 5.
Biomimetic route for making size- and shape-controlled magnetite nanoparticles [79]. MamC is a 12.4 kDa magnetite-interacting transmembrane protein found in different species of MTB. The gene encoding this protein in Mc. marinus strain MC-1 (mamC) was cloned in a pTrcHis-TOPO plasmidial expression vector. It was, then, transformed into Escherichia coli TOP10. The transforming E. coli can be cultivated in a large-volume (1–10 L) bioreactor and express the recombinant MamC. After mass-cultivation, expressed MamC, which is found in intracellular inclusion bodies, is recovered and then purified. MamC can be used as an additive for the coprecipitation of iron to synthesize nanometric magnetite. In this synthesis, MamC binds and stabilizes crescent magnetite nuclei. This interaction ultimately results in nanocrystals of narrowly distributed size and uniform morphology.

Taking the inspiration of the interaction between anionic residues and nascent magnetite, the addition of acidic polypeptides is an alternative to recombinant proteins [78]. In the presence of poly-aspartate, partial oxidation synthesis resulted in narrower size distribution of nanocrystals [78]. Using a classical partial oxidation synthesis, 65% of magnetite nanoparticles assumed a facetted shape with a size distribution between 20 and 60 nm. When the synthesis was supplemented with poly-aspartate, a drastic change of the morphology occurred, with 85% of the nanoparticles showing a more rounded shape. However, the size distribution became significantly narrower, with most particles ranging 15-30 nm.

As discussed, biomimetic synthesis of magnetite with recombinant magnetosome proteins involves electrostatic interaction between anionic aminoacids with iron cations. Nevertheless, the use of cationic polymers and aminoacids also has been proven successful in imitating characteristics of magnetosomes into artificial magnetite. In those cases, the one accepted chemical mechanism is the dipole stabilization of the negatively charged surface of magnetite crystals by positive side groups, namely amino and guanidine, present in alkaline aminoacids [85, 86]. This phenomenon is supported by the phosphatidylethanolamine composition of the magnetosome vesicle, which exposed positively charged amino groups to the nucleation sites [86, 93].

In one experiment performed at the Max Planck Institute of Colloids and Interfaces, Germany, a wide array of randomly-generated peptides was expressed in phage display and had their binding capacity tested against a magnetite powder [86]. The primary structure of magnetite adhering peptides was then compared to the proteomes of several MTB species, but no significant similarity was spotted.

However, of the five magnetite-interacting peptides identified in that study, three had arginine as half the residues in the sequence. The cationic poly-arginine was used as an additive to the iron precipitation. The resulting nanoparticles possessed a fine size distribution (30-40 nm), reproducible – despite irregular – morphologies and colloidal stability. These characteristics were not achieved in the control of conventional precipitation. Poly-arginine also improves the tuneability of the biomimetic synthesis. In the presence of the additive, the average diameters of the magnetite precipitates could be adjusted from 10 to 40 nm when the reaction occurred in pHs from 9 to 11, respectively [94].

As polyaminoacids, single aminoacids can promote control over magnetic nanoparticle syntheses [85]. When arginine and lysine were tested for that purpose, the latter was able to control the particle size according to its concentration (**Table 2**) [85]. The side-chain amino group in lysine can perform a steadier stabilization of the anionic oxyhydroxide precursor of magnetite. Then, further growth of lysine-stabilized nuclei enables a larger crystal size with a better-defined hexahedral shape. The control over size and shape also reflects in the magnetic properties of the nanomaterial. The obtained nanoparticles displayed a superparamagnetic behavior, with a large magnetic moment and magnetization saturation (67 emu/g).

Not only is the size dispersity and morphology better controlled in biomimetic synthesis, but the colloidal stability of bioinspired nanomagnets is generally improved. The magnetic core of bare nanomagnets exerts an attractive force, possibly leading to instability to the colloidal suspension [78, 85]. When peptides are added to the precipitation media, functional groups of the same charge become exposed on the nanoparticle surface and counterbalance the attractive force with electrostatic repulsion [78, 85]. Due to the interaction of cationic amino groups with magnetite, carboxyl groups become exposed during coprecipitation with lysine [85]. Thus, the zeta-potential of those nanoparticles was -31 mV at physiological pH, while the control nanoparticles showed a 0 value. The synthesis of magnetite supplemented with poly-aspartate led to nanoparticles with surface-exposed carboxyl groups [78]. Therefore, the measured zeta potential was approximately -30 mV. Because suspension stability in aqueous media is crucial for biomedical applications, the colloidal stability obtained in biomimetic nanoparticles is a fundamental property.

The knowledge gained from biomimetic approaches was used to construct a double-stimuli-responsive nanoformulation consisting of a nanomagnet bound to the antiproliferative drug oxaliplatin [95]. The nanocrystal was synthesized by co-precipitation of iron ions in the presence of recombinant MamC. The magnetite-oxaliplatin bond was stable at pH 7.2. In acidic pH, the release of oxaliplatin was triggered. This release was further boosted by the application of an alternating magnetic field and the cytotoxicity against colorectal cancer cells was improved [95]. The responsive to alternating magnetic fields also enables MamC-derived magnetic nanoparticles to be used in hyperthermia treatments [96]. A 25 mg/mL suspension of the biomimetic nanoparticles exposed to an alternating field of 226 Oe at a 280 kHz frequency can cause a temperature increase of 16.7 °C (specific absorption rate = 47 W/g).

Another functional magnetic nanoparticle was coprecipitated in the presence of a bifunctional polypeptide and ginger extract [87]. The fourteen-residue-long polypeptide was designed from two heptapeptides: a magnetite binding domain and a cell-targeting domain with specificity to ovarian carcinoma cells. The metal-reducing and chelating activity of the ginger extract leads to nanoparticles averaging 10 nm in length and 48.9 emu/g of magnetization saturation. When different cell lines – A2780 (ovarian carcinoma) and L929 (mouse fibroblast) – were treated with the functional nanoparticle, the first group exhibited a particle uptake almost 5 times more intense.

6. Conclusion

In this chapter, we have summarized how the basic-science knowledge gained through molecular biology, phylogenetics, and metagenomics of MTB can be translated into tools of technological interest. Although the authors had not the pretentiousness of gathering extensive information available on the topic, the chapter evidences how cross-disciplinary research is crucial for understanding and applying such a complex biological phenomenon. This is especially true in a field in which intriguing discoveries are made at a fast pace.

Acknowledgements

We thank Unidade de Microscopia Multiusuário Souto-Padrón & Lins (UniMicro, UFRJ, Brazil) for the use of their microscopy facility.

This research was funded by Brazilian agencies CNPq, CAPES and FAPERJ.

Conflict of interest

The authors declare no conflicts of interest.

Author details

Tarcisio Nascimento Correa, Igor Nunes Taveira, Rogerio Presciliano de Souza Filho and Fernanda de Avila Abreu*
Universidade Federal do Rio de Janeiro, Rio de Janeiro, Brazil

*Address all correspondence to: fernandaaabreu@micro.ufrj.br

References

[1] Blakemore R. Magnetotactic bacteria. Science. 1975;**190**(4212):377-379. DOI: 10.1126/science.170679

[2] Bellini S. On a unique behavior of freshwater bacteria. Chinese Journal of Oceanology and Limnology. 2009;**27**(1):3-5. DOI: 10.1007/s00343-009-0003-5

[3] Uebe R, Schüler D. Magnetosome biogenesis in magnetotactic bacteria. Nature Reviews Microbiology. 2016;**14**(10):621-637. DOI: 10.1038/nrmicro.2016.99

[4] Lefèvre CT, Bazylinski DA. Ecology, diversity, and evolution of magnetotactic bacteria. Microbiology and Molecular Biology Reviews. 2013;**77**(3):497-526. DOI: 10.1128/MMBR.00021-13

[5] Amor M, Tharaud M, Gélabert A, Komeili A. Single-cell determination of iron content in magnetotactic bacteria: Implications for the iron biogeochemical cycle. Environmental Microbiology. 2020;**22**(3):823-831. DOI: 10.1111/1462-2920.14708

[6] Lin W, Bazylinski DA, Xiao T, Wu LF, Pan Y. Life with compass: Diversity and biogeography of magnetotactic bacteria. Environmental Microbiology. 2014;**16**(9):2646-2658. DOI: 10.1111/1462-2920.12313

[7] Martins JL, Silveira TS, Abreu F, Silva KT, da Silva-Neto ID, Lins U. Grazing protozoa and magnetosome dissolution in magnetotactic bacteria. Environmental Microbiology. 2007;**9**(11):2775-2781. DOI: 10.1111/j.1462-2920.2007.01389.x

[8] Lin W, Pan Y, Bazylinski DA. Diversity and ecology of and biomineralization by magnetotactic bacteria. Environmental Microbiology Reports. 2017;**9**(4):345-356. DOI: 10.1111/1758-2229.12550

[9] Lin W, Zhang W, Zhao X, Roberts AP, Paterson GA, Bazylinski DA, et al. Genomic expansion of magnetotactic bacteria reveals an early common origin of magnetotaxis with lineage-specific evolution. ISME Journal. 2018;**12**(6):1508-1519. DOI: 10.1038/s41396-018-0098-9

[10] Bazylinski D, Lefèvre C. Magnetotactic bacteria from extreme environments. Life. 2013;**3**(2):295-307. DOI: 10.3390/life3020295

[11] Vargas G, Cypriano J, Correa T, Leão P, Bazylinski D, Abreu F. Applications of magnetotactic bacteria, magnetosomes and magnetosome crystals in biotechnology and nanotechnology: Mini-review. Molecules. 2018;**23**(10):1-25. DOI: 10.3390/molecules23102438

[12] Bazylinski DA, Frankel RB. Magnetosome formation in prokaryotes. Nature Reviews Microbiology. 2004;**2**(3):217-230. DOI: 10.1038/nrmicro842

[13] Lin W, Paterson GA, Zhu Q, Wang Y, Kopylova E, Li Y, et al. Origin of microbial biomineralization and magnetotaxis during the Archean. Proceedings of the National Academy of Sciences of the United States of America. 2017;**114**(9):2171-2176. DOI: 10.1073/pnas.1614654114

[14] Murat D, Quinlan A, Vali H, Komeili A. Comprehensive genetic dissection of the magnetosome gene island reveals the step-wise assembly of a prokaryotic organelle. Proceedings of the National Academy of Sciences of the United States of America. 2010;**107**(12):5593-5598. DOI: 10.1073/pnas.0914439107

[15] Lefèvre CT, Trubitsyn D, Abreu F, Kolinko S, Jogler C, de Almeida LGP, et al. Comparative genomic analysis of magnetotactic bacteria from the Deltaproteobacteria provides new insights into magnetite and greigite magnetosome genes required for magnetotaxis. Environmental Microbiology. 2013;**15**(10):2712-2735. DOI: 10.1111/1462-2920.12128

[16] Lin W, Deng A, Wang Z, Li Y, Wen T, Wu LF, et al. Genomic insights into the uncultured genus "Candidatus Magnetobacterium" in the phylum Nitrospirae. ISME Journal. 2014;**8**(12):2463-2477. DOI: 10.1038/ismej.2014.94

[17] Zeytuni N, Ozyamak E, Ben-Harush K, Davidov G, Levin M, Gat Y, et al. Self-recognition mechanism of mamA, a magnetosome-associated TPR-containing protein. promotes complex assembly. Proceedings of the National Academy of Sciences of the United States of America. 2011;**108**(33):480-487. DOI: 10.1073/pnas.1103367108

[18] Uebe R, Junge K, Henn V, Poxleitner G, Katzmann E, Plitzko JM, et al. The cation diffusion facilitator proteins MamB and MamM of *Magnetospirillum gryphiswaldense* have distinct and complex functions, and are involved in magnetite biomineralization and magnetosome membrane assembly. Molecular Microbiology. 2011;**82**(4):818-835. DOI: 10.1111/j.1365-2958.2011.07863.x

[19] Komeili A, Li Z, Newman DK, Jensen GJ. Magnetosomes are cell membrane invaginations organized by the actin-like protein MamK. Science . 2006 Jan 13 [cited 2012 Nov 15];311(5758):242-5. DOI: 10.1126/science.1123231

[20] Toro-Nahuelpan M, Giacomelli G, Raschdorf O, Borg S, Plitzko JM, Bramkamp M, et al. MamY is a membrane-bound protein that aligns magnetosomes and the motility axis of helical magnetotactic bacteria. Nature Microbiology. 2019;**4**(11):1978-1989. DOI: 10.1038/s41564-019-0512-8

[21] Raschdorf O, Müller FD, Pósfai M, Plitzko JM, Schüler D. The magnetosome proteins MamX, MamZ and MamH are involved in redox control of magnetite biomineralization in *Magnetospirillum gryphiswaldense*. Molecular Microbiology. 2013;**89**(5):872-886. DOI: 10.1111/mmi.12317

[22] Mandernack KW, Bazylinski DA, Shanks WC, Bullen TD. Oxygen and iron isotope studies of magnetite produced by magnetotactic bacteria. Science. 1999;**285**(5435):1892-1896. DOI: 10.1126/science.285.5435.1892

[23] Komeili A, Vali H, Beveridge TJ, Newman DK. Magnetosome vesicles are present before magnetite formation, and MamA is required for their activation. Proceedings of the National Academy of Sciences of the United States of America. 2004;**101**(11):3839-3844. DOI: 10.1073/pnas.0400391101

[24] Scheffel A, Gärdes A, Grünberg K, Wanner G, Schüler D. The major magnetosome proteins MamGFDC are not essential for magnetite biomineralization in *Magnetospirillum gryphiswaldense* but regulate the size of magnetosome crystals. Journal of Bacteriology. 2008;**190**(1):377-386. DOI: 10.1128/JB.01371-07

[25] Scheffel A, Gruska M, Faivre D, Linaroudis A, Plitzko JM, Schüler D. An acidic protein aligns magnetosomes along a filamentous structure in magnetotactic bacteria. Nature. 2006;**440**(7080):110-114. DOI: 10.1038/nature04382

[26] Yang W, Li R, Peng T, Zhang Y, Jiang W, Li Y, et al. mamO and mamE genes are essential for magnetosome

crystal biomineralization in *Magnetospirillum gryphiswaldense* MSR-1. Research in Microbiology. 2010;**161**(8):701-705. DOI: 10.1016/j.resmic.2010.07.002

[27] Siponen MI, Adryanczyk G, Ginet N, Arnoux P, Pignol D. Magnetochrome: A c-type cytochrome domain specific to magnetotatic bacteria. Biochemical Society Transactions. 2012;**40**(6):1319-1323. DOI: 10.1042/BST20120104

[28] Lohsse A, Ullrich S, Katzmann E, Borg S, Wanner G, Richter M, et al. Functional analysis of the magnetosome island in *Magnetospirillum gryphiswaldense*: The mamAB operon is sufficient for magnetite biomineralization. PLoS One. 2011;**6**(10):e25561. DOI: 10.1371/journal.pone.0025561

[29] Tanaka M, Arakaki A, Matsunaga T. Identification and functional characterization of liposome tubulation protein from magnetotactic bacteria. Molecular Microbiology. 2010;**76**(2):480-488. DOI: 10.1111/j.1365-2958.2010.07117.x

[30] Tanaka M, Mazuyama E, Arakaki A, Matsunaga T. Mmm6 protein regulates crystal morphology during nano-sized magnetite biomineralization in vivo. Journal of Biological Chemistry. 2011;**286**(8):6386-6392. DOI: 10.1074/jbc.M110.183434

[31] Murat D, Falahati V, Bertinetti L, Csencsits R, Körnig A, Downing K, et al. The magnetosome membrane protein, MmsF, is a major regulator of magnetite biomineralization in *Magnetospirillum magneticum* AMB-1. Molecular Microbiology. 2012;**85**(4):684-699. DOI: 10.1111/j.1365-2958.2012.08132.x

[32] Bazylinski DA, Williams TJ, Lefèvre CT, Berg RJ, Zhang CL, Bowser SS, et al. *Magnetococcus marinus* gen. nov., sp. nov., a marine, magnetotactic bacterium that represents a novel lineage (Magnetococcaceae fam. nov., Magnetococcales ord. nov.) at the base of the Alphaproteobacteria. Internationl Journal of Systematic and Evolutionary Microbiology. 2013;**63**(3):801-808. DOI: 10.1099/ijs.0.038927-0

[33] Matsunaga T, Okamura Y, Fukuda Y, Wahyudi AT, Murase Y, Takeyama H. Complete genome sequence of the facultative anaerobic magnetotactic bacterium *Magnetospirillum* sp. strain AMB-1. DNA Research. 2005;**12**(3):157-166. DOI: 10.1093/dnares/dsi002

[34] Wang Y, Lin W, Pana Y. High diversity of magnetotactic Deltaproteobacteria in a freshwater Niche. Applied Environmental Microbiology. 2013;**79**(8):2813-2817. DOI: 10.1128/AEM.03635-12

[35] Ji B, Da ZS, Arnoux P, Rouy Z, Alberto F, Philippe N, et al. Comparative genomic analysis provides insights into the evolution and niche adaptation of marine *Magnetospira* sp. QH-2 strain. Environmental Microbiology. 2014;**16**(2):525-544. DOI: 10.1111/1462-2920.12180

[36] Monteil CL, Perrière G, Menguy N, Ginet N, Alonso B, Waisbord N, et al. Genomic study of a novel magnetotactic Alphaproteobacteria uncovers the multiple ancestry of magnetotaxis. Environmental Microbiology. 2018;**20**(12):4415-4430. DOI: 10.1111/1462-2920.14364

[37] Abreu F, Leão P, Vargas G, Cypriano J, Figueiredo V, Enrich-Prast A, et al. Culture-independent characterization of a novel magnetotactic member affiliated to the Beta class of the Proteobacteria phylum from an acidic lagoon. Environmental Microbiology. 2018;**20**(7):2615-2624. DOI: 10.1111/1462-2920.14286

[38] Lefèvre CT, Viloria N, Schmidt ML, Pósfai M, Frankel RB, Bazylinski DA.

Novel magnetite-producing magnetotactic bacteria belonging to the Gammaproteobacteria. ISME Journal. 2012;**6**(2):440-450. DOI: 10.1038/ismej.2011.97

[39] Leão P, Teixeira LCRS, Cypriano J, Farina M, Abreu F, Bazylinski DA, et al. North-seeking magnetotactic gammaproteobacteria in the southern hemisphere. Appl Environmental Microbiology. 2016;**82**(18):5595-5602. DOI: 10.1128/AEM.01545-16

[40] Nakazawa H, Arakaki A, Narita-Yamada S, Yashiro I, Jinno K, Aoki N, et al. Whole genome sequence of *Desulfovibrio magneticus* strain RS-1 revealed common gene clusters in magnetotactic bacteria. Genome Research. 2009;**19**(10):1801-1808. DOI: 10.1101/gr.088906.108

[41] Lefèvre CT, Frankel RB, Pósfai M, Prozorov T, Bazylinski DA. Isolation of obligately alkaliphilic magnetotactic bacteria from extremely alkaline environments. Environmental Microbiology. 2011;**13**(8):2342-2350. DOI: 10.1111/j.1462-2920.2011.02505.x

[42] Zhou K, Zhang WY, Yu-Zhang K, Pan HM, Da ZS, Zhang WJ, et al. A novel genus of multicellular magnetotactic prokaryotes from the Yellow Sea. Environmental Microbiology. 2012;**14**(2):405-413. DOI: 10.1111/j.1462-2920.2011.02590.x

[43] Abreu F, Morillo V, Nascimento FF, Werneck C, Cantão ME, Ciapina LP, et al. Deciphering unusual uncultured magnetotactic multicellular prokaryotes through genomics. ISME Journal. 2014;**8**(5):1055-1068. DOI: 10.1038/ismej.2013.203

[44] Lefèvre CT, Bernadac A, Yu-Zhang K, Pradel N, Wu LF. Isolation and characterization of a magnetotactic bacterial culture from the Mediterranean Sea. Environmental Microbiology. 2009;**11**(7):1646-1657. DOI: 10.1111/j.1462-2920.2009.01887.x

[45] Morillo V, Abreu F, Araujo AC, De Almeida LGP, Enrich-Prast A, Farina M, et al. Isolation, cultivation and genomic analysis of magnetosome biomineralization genes of a new genus of south-seeking magnetotactic cocci within the Alphaproteobacteria. Frontiers in Microbiology. 2014;**5**(72):1-12. DOI: 10.3389/fmicb.2014.00072

[46] Jogler C, Wanner G, Kolinko S, Niebler M, Amann R, Petersen N, et al. Conservation of proteobacterial magnetosome genes and structures in an uncultivated member of the deep-branching Nitrospira phylum. Proceedings of the National Academy of Sciences of the United States of America. 2011;**108**(3):1134-1139. DOI: 10.1073/pnas.1012694108

[47] Lefèvre CT, Abreu F, Schmidt ML, Lins U, Frankel RB, Hedlund BP, et al. Moderately thermophilic magnetotactic bacteria from hot springs in Nevada. Applied Environmental Microbiology. 2010;**76**(11):3740-3743. DOI: 10.1128/AEM.03018-09

[48] Lefèvre CT, Frankel RB, Abreu F, Lins U, Bazylinski DA. Culture-independent characterization of a novel, uncultivated magnetotactic member of the Nitrospirae phylum. Environmental Microbiology. 2011;**13**(2):538-549. DOI: 10.1111/j.1462-2920.2010.02361.x

[49] Kolinko S, Richter M, Glöckner FO, Brachmann A, Schüler D. Single-cell genomics of uncultivated deep-branching magnetotactic bacteria reveals a conserved set of magnetosome genes. Environmental Microbiology. 2016;**18**(1):21-37. DOI: 10.1111/1462-2920.12907

[50] Qian XX, Liu J, Menguy N, Li J, Alberto F, Teng Z, et al. Identification of novel species of marine magnetotactic bacteria affiliated with Nitrospirae phylum. Environmental Microbiology Reports. 2019;**11**(3):330-337. DOI: 10.1111/1758-2229.12755

[51] Lins U, Keim C, Evans F, Farina M, Buseck P. Magnetite (Fe_3O_4) and greigite (Fe_3S_4) crystals in multicellular magnetotactic prokaryotes. Geomicrobiology Journal. 2007;**24**(1):43-50. DOI: 10.1080/01490450601134317

[52] Lefèvre CT, Menguy N, Abreu F, Lins U, Pósfai M, Prozorov T, et al. A cultured greigite-producing magnetotactic bacterium in a novel group of sulfate-reducing bacteria. Science. 2011;**334**(6063):1720-1723. DOI: 10.1126/science.1212596

[53] DeLong EF, Frankel RB, Bazylinski DA. Multiple evolutionary origins of magnetotaxis in bacteria. Science. 1993;**259**(5096):803-806. DOI: 10.1126/science.259.5096.803

[54] Abreu F, Cantão ME, Nicolás MF, Barcellos FG, Morillo V, Almeida LGP, et al. Common ancestry of iron oxide- and iron-sulfide-based biomineralization in magnetotactic bacteria. ISME Journal. 2011;**5**(10):1634-1640. DOI: 10.1038/ismej.2011.35

[55] Lefèvre CT, Trubitsyn D, Abreu F, Kolinko S, de Almeida LGP, de Vasconcelos ATR, et al. Monophyletic origin of magnetotaxis and the first magnetosomes. Environmental Microbiology. 2013;**15**(8):2267-2274. DOI: 10.1111/1462-2920.12097

[56] Schübbe S, Kube M, Wawer C, Heyen U, Meyerdierks A, Madkour MH, et al. Characterization of a spontaneous nonmagnetic mutant of *Magnetospirillum gryphiswaldense* reveals a large deletion comprising a putative magnetosome island. Journal of Bacteriology. 2003;**185**(19):5779-5790. DOI: 10.1128/JB.185.19

[57] Richter M, Kube M, Bazylinski DA, Lombardot T, Glöckner FO, Reinhardt R, et al. Comparative genome analysis of four magnetotactic bacteria reveals a complex set of group-specific genes implicated in magnetosome biomineralization and function. Journal of Bacteriology. 2007;**189**(13):4899-4910. DOI: 10.1128/JB.00119-07

[58] Jogler C, Kube M, Schübbe S, Ullrich S, Teeling H, Bazylinski DA, et al. Comparative analysis of magnetosome gene clusters in magnetotactic bacteria provides further evidence for horizontal gene transfer. Environmental Microbiology. 2009;**11**(5):1267-1277. DOI: 10.1111/j.1462-2920.2009.01854.x

[59] Jogler C, Schüler D. Genomics, genetics, and cell biology of magnetosome formation. Annual Reviews of Microbiology. 2009;**63**:501-521. DOI: 10.1146/annurev.micro.62.081307.162908

[60] Canfield DE. The early history of atmospheric oxygen: Homage to Robert M. Garrels. Annual Reviews of Earth and Planetary Sciences. 2005;**33**:1-36. DOI: 10.1146/annurev.earth.33.092203.122711

[61] Rouxel OJ, Bekker A, Edwards KJ. Iron isotope constraints on the Archean and Paleoproterozoic Ocean redox state. Science. 2005;**307**(5712):1088-1091. DOI: 10.1126/science.1105692

[62] Canfield DE, Rosing MT, Bjerrum C. Early anaerobic metabolisms. Philosophical Transactions of the Royal Society B: Biological Sciences. 2006;**361**(1474):1819-1834. DOI: 10.1098/rstb.2006.1906

[63] Williams TJ, Zhang CL, Scott JH, Bazylinski DA. Evidence for autotrophy via the reverse tricarboxylic acid cycle in the marine magnetotactic coccus strain MC-1. Applied Environmental Microbiology. 2006;**72**(2):1322-1329. DOI: 10.1128/AEM.72.2.1322

[64] Blake RE, Chang SJ, Lepland A. Phosphate oxygen isotopic evidence for a temperate and biologically active Archaean Ocean. Nature. 2010;**464**(7291):1029-1032. DOI: 10.1038/nature08952

[65] Knauth LP. Temperature and salinity history of the Precambrian Ocean: Implications for the course of microbial evolution. Palaeogeography, Palaeoclimatology, Palaeoecology. 2005;**219**(1-2):53-69. DOI: 10.1016/j.palaeo.2004.10.014

[66] Abreu F, Carolina A, Araujo V, Leão P, Silva KT, de CFM, et al. Culture-independent characterization of novel psychrophilic magnetotactic cocci from Antarctic marine sediments. Environmental Microbiology. 2016;**18**(12):4426-4441. DOI: 10.1111/1462-2920.13388

[67] Tarduno JA, Cottrell RD, Davis WJ, Nimmo F, Bono RK. A hadean to Paleoarchean geodynamo recorded by single zircon crystals. Science. 2015;**349**(6247):521-524. DOI: 10.1126/science.aaa9114

[68] Pósfai M, Lefèvre CT, Trubitsyn D, Bazylinski DA, Frankel RB. Phylogenetic significance of composition and crystal morphology of magnetosome minerals. Frontiers in Microbiology. 2013;**4**:1-15. DOI: 10.3389/fmicb.2013.00344

[69] Moisescu C, Ardelean II, Benning LG. The effect and role of environmental conditions on magnetosome synthesis. Frontiers in Microbiology. 2014;**5**:1-12. DOI: 10.3389/fmicb.2014.00049

[70] Yiriletu IT. Magnetic properties of magnetite synthesized by *Magnetospirillum magnetotacticum* MS-1 cultured with different concentrations of ferric iron. Biotechnology Letters. 2015;**37**(12):2427-2433. DOI: 10.1007/s10529-015-1928-8

[71] Olszewska-Widdrat A, Schiro G, Reichel VE, Faivre D. Reducing conditions favor magnetosome production in magnetospirillum magneticum AMB-1. Frontiers in Microbiology. 2019;**10**(582):1-10. DOI: 10.3389/fmicb.2019.00582

[72] Mee CD. Magnetic tape recording materials. IEEE Transactions on Communication and Electronics. 1964;**83**(73):399-408. DOI: 10.1109/tcome.1964.6541245

[73] Amor M, Busigny V, Durand-Dubief M, Tharaud M, Ona-Nguema G, Gélabert A, et al. Chemical signature of magnetotactic bacteria. Proceedings of the National Academy of Sciences of the United States of America. 2015;**112**(6):1699-1703. DOI: 10.1073/pnas.1414112112

[74] Mirabello G, Lenders JJM, Sommerdijk NAJM. Bioinspired synthesis of magnetite nanoparticles. Chemical Society Reviews. 2016;**45**(18):5085-5106. DOI: 10.1039/C6CS00432F

[75] Bhushan B. Bioinspired materials and surfaces for green science and technology (part 3). Philosophical Transactions of the Royal Society A: Mathematical, Physical and Engineering Sciences. 2020;**378**(2167):2-3. DOI: 10.1098/rsta.2019.0439

[76] Sawada T, Serizawa T. Peptides as smart biomolecular tools: Utilization of their molecular recognition for materials engineering. In: Ito Y, Chen X, Kang I-K, editors. Advances in Bioinspired and Biomedical Materials. Washington, D.C.: American Chemical Society; 2017. pp. 31-48. DOI: 10.1021/bk-2017-1252.ch003

[77] Barber-Zucker S, Zarivach R. A look into the biochemistry of magnetosome biosynthesis in magnetotactic bacteria. ACS Chemical Biology. 2017;**12**(1):13-22. DOI: 10.1021/acschembio.6b01000

[78] Altan CL, Lenders JJM, Bomans PHH, De With G, Friedrich H, Bucak S, et al. Partial oxidation as a rational approach to kinetic control in bioinspired magnetite synthesis. Chemistry - A European Journal. 2015;**21**(16):6150-6156. DOI: 10.1002/chem.201405973

[79] Valverde-Tercedor C, Montalbán-López M, Perez-Gonzalez T, Sanchez-Quesada MS, Prozorov T, Pineda-Molina E, et al. Size control of in vitro synthesized magnetite crystals by the MamC protein of *Magnetococcus marinus* strain MC-1. Applied Microbiology and Biotechnology. 2015;**99**(12):5109-5121. DOI: 10.1007/s00253-014-6326-y

[80] Amemiya Y, Arakaki A, Staniland SS, Tanaka T, Matsunaga T. Controlled formation of magnetite crystal by partial oxidation of ferrous hydroxide in the presence of recombinant magnetotactic bacterial protein Mms6. Biomaterials. 2007;**28**(35):5381-5389. DOI: 10.1016/j.biomaterials.2007.07.051

[81] Nudelman H, Lee YZ, Hung YL, Kolusheva S, Upcher A, Chen YC, et al. Understanding the biomineralization role of magnetite-interacting components (MICs) from magnetotactic bacteria. Frontiers in Microbiology. 2018;**9**(2480):1-14. DOI: 10.3389/fmicb.2018.02480

[82] Rawlings AE, Bramble JP, Walker R, Bain J, Galloway JM, Staniland SS. Self-assembled MmsF proteinosomes control magnetite nanoparticle formation in vitro. Proceedings of the National Academy of Sciences of the United States of America. 2014;**111**(45):19094-19099. DOI: 10.1073/pnas.1409256111

[83] Rawlings AE, Somner LA, Fitzpatrick-Milton M, Roebuck TP, Gwyn C, Liravi P, et al. Artificial coiled coil biomineralisation protein for the synthesis of magnetic nanoparticles. Nature Communications. 2019;**10**(1):1-9. DOI: 10.1038/s41467-019-10578-2

[84] Peigneux A, Jabalera Y, Vivas MAF, Casares S, Azuaga AI, Jimenez-Lopez C. Tuning properties of biomimetic magnetic nanoparticles by combining magnetosome associated proteins. Scientific Reports. 2019;**9**(1):1-11. DOI: 10.1038/s41598-019-45219-7

[85] Contreras-Montoya R, Jabalera Y, Blanco V, Cuerva JM, Jimenez-Lopez C, Alvarez de Cienfuegos L. Lysine as size-control additive in a bioinspired synthesis of pure superparamagnetic magnetite nanoparticles. Crystal Growth & Design. 2020;**20**(2):533-542. DOI: 10.1021/acs.cgd.9b00169

[86] Baumgartner J, Antonietta Carillo M, Eckes KM, Werner P, Faivre D. Biomimetic magnetite formation: From biocombinatorial approaches to mineralization effects. Langmuir. 2014;**30**(8):2129-2136. DOI: 10.1021/la404290c

[87] Liu L, Pu X, Yin G, Chen X, Yin J, Wu Y. Biomimetic mineralization of magnetic iron oxide nanoparticles mediated by bi-functional copolypeptides. Molecules. 2019;**24**(7):16. DOI: 10.3390/molecules24071401

[88] Yamagishi A, Narumiya K, Tanaka M, Matsunaga T, Arakaki A. Core amino acid residues in the morphology-regulating protein, Mms6, for intracellular magnetite biomineralization. Scientific Reports. 2016;**6**(35670):1-10. DOI: 10.1038/srep35670

[89] Yamagishi A, Tanaka M, Lenders JJM, Thiesbrummel J, Sommerdijk NAJM, Matsunaga T,

et al. Control of magnetite nanocrystal morphology in magnetotactic bacteria by regulation of mms7 gene expression. Scientific Reports. 2016;**6**:1-11. DOI: 10.1038/srep29785

[90] Rawlings AE, Liravi P, Corbett S, Holehouse AS, Staniland SS. Investigating the ferric ion binding site of magnetite biomineralisation protein Mms6. PLoS One. 2020;**15**(2):1-16. DOI: 10.1371/journal.pone.0228708

[91] Nudelman H, Perez Gonzalez T, Kolushiva S, Widdrat M, Reichel V, Peigneux A, et al. The importance of the helical structure of a MamC-derived magnetite-interacting peptide for its function in magnetite formation. Acta Crystallographica Section D: Structural Biology. 2018;**74**:10-20. DOI: 10.1107/S2059798317017491

[92] Ubago-Rodríguez A, Casares Atienza S, Fernández-Vivas A, Peigneux A, Jabalera Y, De La Cuesta-Rivero M, et al. Structure-function of MamC loop and its effect on the in vitro precipitation of biomimetic magnetite nanoparticles. Crystal Growth & Design. 2019;**19**(5):2927-2935. DOI: 10.1021/acs.cgd.9b00150

[93] Grünberg K, Müller E-C, Otto A, Reszka R, Linder D, Kube M, et al. Biochemical and proteomic analysis of the magnetosome membrane in *Magnetospirillum gryphiswaldense*. Applied Environmental Microbiology. 2004;**70**(2):1040-1050. DOI: 10.1128/AEM.70.2.1040-1050.2004

[94] Kuhrts L, Macías-Sánchez E, Tarakina NV, Hirt AM, Faivre D. Shaping magnetite with poly-l-arginine and pH: From small single crystals to large mesocrystals. Journal of Physical Chemistry Letters. 2019;**10**(18):5514-5518. DOI: 10.1021/acs.jpclett.9b01771

[95] Jabalera Y, Garcia-Pinel B, Ortiz R, Iglesias G, Cabeza L, Prados J, et al. Oxaliplatin–biomimetic magnetic nanoparticle assemblies for colon cancer-targeted chemotherapy: An in vitro study. Pharmaceutics. 2019;**11**(8):4-6. DOI: 10.3390/pharmaceutics11080395

[96] Iglesias GR, Jabalera Y, Peigneux A, Fernández BLC, Delgado ÁV, Jimenez-Lopez C. Enhancement of magnetic hyperthermia by mixing synthetic inorganic and biomimetic magnetic nanoparticles. Pharmaceutics. 2019;**11**(6):16. DOI: 10.3390/pharmaceutics11060273